ANL-7417

ENP

ANL-7417

Argonne National Laboratory

ANNUAL PROGRESS REPORT FOR 1967 METALLURGY DIVISION

Printed in the United States of America
Available from
Clearinghouse for Federal Scientific and Technical Information
National Bureau of Standards, U. S. Department of Commerce
Springfield, Virginia 22151
Price: Printed Copy $3.00; Microfiche $0.65

ARGONNE NATIONAL LABORATORY
9700 South Cass Avenue
Argonne, Illinois 60439

ANNUAL PROGRESS REPORT FOR 1967
METALLURGY DIVISION

Michael V. Nevitt, Director

Paul G. Shewmon, Associate Director

The last three Annual Reports

ANL-7000 1964
ANL-7155 1965
ANL-7299 1966

TABLE OF CONTENTS

PART I
ENGINEERING METALLURGY

PART II
BASIC METALLURGY

Part I

Engineering Metallurgy

FAST-REACTOR FUEL-ELEMENT DEVELOPMENT AND FABRICATION

Metal-Fuel Development

ALLOY PREPARATION

Development of Uranium-Plutonium-Zirconium Alloys *(H. F. Jelinek and G. B. O'Keeffe)*

The fabrication of irradiation specimens containing alloys of uranium-zirconium and uranium-plutonium-zirconium requires methods for making master alloys with high-melting temperatures. One ideal method is arc melting in conjunction with a water-cooled copper mold. During 1967 an arc-melting furnace was designed and fabricated for glovebox use. The furnace is presently being tested prior to installation in a glovebox.

Crucible and Mold Development *(H. F. Jelinek and D. E. White)*

A study was initiated to find a container material suitable for U-Zr and U-Pu-Zr alloy melts. Previous experience indicated that these alloys react with containers of Al_2O_3, MgO, and graphite. Some success was obtained with zirconia crucibles, although oxygen contamination was evident.

A series of tests is being made to obtain quantitative information on the effects of melting and alloying U-Zr and U-Pu-Zr. Yttria, gadolinia, and dysprosia appear to be most resistant to chemical reaction with the U-Zr alloy. Tests are in progress to evaluate these materials as protective coatings in graphite crucibles. Alloys of U-15 wt% Pu-12 wt% Zr are being prepared for the next series of tests.

FABRICATION AND ASSEMBLY OF FUEL ELEMENTS

Fabrication of Group M-4 Fuel Elements *(H. F. Jelinek and D. A. Kraft)*

Forty Group M-4 fuel elements are being fabricated for irradiation experiments. The fuel is a U-15 wt% Pu-12 wt% Zr alloy contained in jackets of either Type 304 or Type 316 stainless steel, or nickel- or vanadium-base alloys. A triple indent in each jacket is being used to restrain the fuel pin below the sodium surface.

A total of 47 acceptable fuel pins have been fabricated in two steps: A binary alloy of U-14.5 wt% Zr (93.2% enriched) was made by gravity casting. Plutonium was then added and the material was injection cast into glass molds 0.169-in. ID by 18 in. long. Nineteen fuel elements have been assembled and examined.

Fabrication of EBR-II, Mark-II Fuel Elements *(A. G. Hins and J. R. Summers)*

Sixty-seven experimental fuel elements of the EBR-II, Mark-II design were assembled and inspected for use in studies of irradiation performance. The fuel pins, 0.130-in.-diam by 14.22 in. long, were injection-cast right cylinders of U-5 wt% Fs alloy that were sodium bonded in jacket tubes of Type 304L stainless steel. Three types of restrainers were installed: the slotted ferrule, the cylindrical ferrule, and the recently developed triple indent. The sodium bond was inspected by both point-probe and encircling-coil eddy-current test equipment. The elements were shipped to the Engineering Irradiation Group for secondary encapsulation and for irradiation testing in EBR-II.

Fabrication of Controlled-Density Fuels *(D. E. Walker)*

Since gaseous fission products promote swelling in nuclear fuels, and since the pressure within the fuel body can force the fuel outward against the jacket and cause a jacket failure, controlled-density fuel bodies with interconnected porosity are being developed to allow the fission gases produced to diffuse rapidly to the annulus and then to the plenum chamber provided for gas accumulation. Uranium-2 wt% zirconium alloy powder was selected as a suitable model for the U-15 wt% Pu-12 wt% Zr alloy of interest as a fuel. Several disks (0.40-in.-diam and 0.18 in. high) with a density of 73% of theoretical were made by pressing the powder isostatically at 25,000 psi and then sintering at 950°C in vacuum.

Studies of Fuel-Element Assembly and Liquid-Metal Bonding *(A. G. Hins and D. C. Carpenter)*

Rapid heat transfer from the fuel pin to the jacket is a requirement of metallic fuel elements in an LMFBR. To facilitate heat transfer, the sodium annulus should be free of gas bubbles and the surfaces of the pin and jacket should be completely wetted by the sodium. In practice, a perfect annular bond has been difficult to achieve. Although bond defects can often be removed by subjecting the elements to axial impaction at 500°C, reject rates from specific bonding batches may vary from less than 5% to more than 19%.

A bonding study has been initiated to evaluate the characteristics of bond defects and to improve methods of eliminating these defects. Recently, fuel elements have been produced by methods that are designed to minimize the

formation of bond defects. Sixty-seven EBR-II experimental driver fuel elements (described previously) were assembled by inserting the fuel pin into the jacket and loading the sodium wire above the pin. The elements were evacuated to 100 μ, heated to 150°C, and pressurized to 10 psig to force the molten sodium downward into the annulus. The elements were soaked at 500°C for 2 hr but were not impacted. No bond defects were evident in 17 of the elements, and 9 elements contained defects smaller than the maximum allowable size. Although impact bonding was required to reclaim elements with bond defects, 26 (39%) of the 67 elements were accepted without impaction.

Forty-seven experimental M-4 fuel elements (described previously) were assembled by the same procedure (loading, evacuating, heating, and pressurizing) as that used for the driver elements. Of the 19 elements examined to date, 13 elements contained a void-free bond before impaction; apparently impaction is not required for void-free sodium bonds.

PHYSICAL METALLURGY OF METALLIC FUELS

Phase Studies of Uranium-Plutonium-Zirconium Alloys *(D. R. O'Boyle)*

In order to establish the phases in equilibrium at reactor operating temperatures, a series of high-purity U-Pu-Zr alloys that contain a constant uranium-to-plutonium ratio of 4:1 has been arc melted, homogenized, heat treated at temperatures between 590 and 700°C, and examined metallographically. The heat-treat conditions were selected so that the two- and three-phase regions in the isoplethal section through the ternary system could be defined by means of electron-probe microanalysis. The oxygen-stabilized alpha-zirconium phase previously identified[1,2] in cast and heat-treated U-Pu-Zr alloys was examined by microanalysis and was found to contain approximately 6 wt% oxygen. Previous work on a series of alloys with varying amounts of oxygen (in the range from 100 to 1200 ppm) had established that the volume fraction of the stabilized alpha-zirconium phase is proportional to the oxygen content of the alloy.

To study surface-corrosion layers that may form on U-Pu-Zr alloys during compatibility tests or during fabrication into fuel elements, alloys in the composition range of interest as fast-reactor fuels were heat treated in NaK and also in a helium atmosphere for 2 to 168 hr at temperatures between 700 and 800°C. Commercial-quality NaK and helium were used in these experiments. The structure and composition of the surface layers were examined by metallographic methods and by electron-probe microanalysis. Characteristic x-ray photographs and linear x-ray traces were recorded to establish the variation of concentrations of uranium, plutonium, and zirconium in the surface layers and in the fuel adjacent to the surface. Plutonium-rich surface layers formed on alloys heat treated in NaK consisted of multiphase layers of plutonium oxide and an oxynitride of uranium and plutonium. Multiphase surface layers, rich in plutonium and zirconium, were also formed on the U-Pu-Zr alloys heat treated in helium.

To characterize the structure of injection-cast U-Pu-Zr alloys, four pins prepared for irradiation in EBR-II were examined by means of metallography, microhardness measurements, and electron-probe analysis. Samples from these pins are being annealed at temperatures between 350 and 700°C for 60 and 300 days to study the effect of heat treatment on the cast structure. Results of this investigation will be published after both exposures are completed.

Compatibility of U-5 wt% Fs Alloy with Type 304 Stainless Steel *(S. T. Zegler)*

Compatibility studies have shown that U-5 wt% Fs alloy and Type 304 stainless steel react to form a liquid phase at a temperature of 715 ±5°C. The liquid phase is formed from the reaction of compounds primarily composed of U_6Fe and UFe_2 with a gamma-uranium phase that is enriched with molybdenum. During an anneal of 1000 hr at temperatures of 550, 600, and 650°C, the depths to which diffusing elements penetrate the fuel and steel are consistent with the penetration depth obtained from an extrapolation of earlier data[3] for times up to 840 hr. The compatibility of U-5 wt% Fs alloy with Type 304 stainless steel at temperatures to 700°C is unaffected by the presence of iron in the fissium alloy in amounts ranging from 500 to 1000 ppm by weight. The presence of 1100 ppm of aluminum and 800 ppm of silicon also does not affect compatibility for times up to 1000 hr at 700°C.

Compatibility of Uranium-Plutonium-Zirconium Alloys with Potential Jacket Materials *(S. T. Zegler)*

The progress made through 1967 in the development of compatible fuel-jacket combinations for fast-reactor application has been summarized in a recent paper;[4] data are

[1] S. T. Zegler, D. R. O'Boyle, B. Blumenthal, C. M. Walter, and H. V. Rhude, Annual Progress Report for 1965, Metallurgy Division, ANL-7155, pp. 14-18.

[2] D. R. O'Boyle, "Discussion on Alloy Systems–2," *Plutonium 1965*, Proc. Third Intl. Conf. on Plutonium, London, England, 1965, A. E. Kay and M. B. Waldron, eds. Chapman and Hall, London, 1967, pp. 532-534.

[3] C. M. Walter, USAEC Report ANL-6816, Argonne National Laboratory, 1964.

[4] S. T. Zegler and C. M. Walter, *Compatibility Between Metallic U-Pu-Base Fuels and Potential Cladding Materials*, Proc. 1967 Nucl. Met. Symp., Scottsdale, Arizona, October 4-6, 1967, K. E. Horton, R. E. Macherey, and R. J. Allio, eds, IMD-AIME (to be published).

presented that pertain to the out-of-reactor compatibility of U-Pu-Zr, U-Pu-Ti, U-Pu-Fz, and U-Zr alloys with various iron-, nickel-, and vanadium-base jacket materials. Additional study was directed to the compatibility of U-Pu-Zr alloys that contain from 15 to 18 wt% plutonium and from 10 to 14 wt% zirconium with iron-base materials.

Unlike austenitic alloys (e.g., Type 304 stainless steel), ferritic alloys, specifically Type 440 stainless steel, Fe-18 wt% Cr-5 wt% Ni, and Fe-5 wt% Ni, react with U-18 wt% Pu-14 wt% Zr to form a liquid phase during an annealing of 7 days at 750°C. This strongly indicates that the higher nickel content and absence of ferrite are major factors that contribute to the good compatibility of austenitic alloys up to 800°C. The results of other work[5] have shown that an increase in the nickel content from 8 to 20 wt% in iron alloys containing 18 wt% chromium enhances the compatibility.

Results of a previous investigation[6] noted that only solid-state reactions occur between the U-18 wt% Pu-14 wt% Zr alloy and Type 304 stainless steel during an anneal of up to 1000 hr at temperatures up to 800°C. During an anneal of 5000 hr, liquid reactions have been observed at 750°C but not at 700 and 800°C. From results of electron-probe analyses, the compatibility at 800°C results from the formation in diffusion layers of zirconium-rich phases that are stabilized by oxygen.

The U-18 wt% Pu-14 wt% Zr alloy is compatible with Types 309 and 310 stainless steel for times up to 5000 hr at 750°C. Penetration of the fuel into the Type 309 stainless steel is less than 8 μ; penetration into the Type 310 stainless steel ranged from 30 to 44 μ. The fact that no liquid-phase reactions occur, as had been observed with Type 304 stainless steel, is believed to be due to the higher nickel and chromium contents of Types 309 and 310 stainless steel.

FUEL-ELEMENT PERFORMANCE OF URANIUM-PLUTONIUM-ZIRCONIUM ALLOYS *(W. F. Murphy and L. A. Neimark)*

During the past year, progress was made in the postirradiation examination of 16 prototypal fuel elements (U-15 wt% Pu-8 to 12 wt% Zr alloy) irradiated to a burnup level of 4.5 at.% in EBR-II.[7] The examination consisted of measurements of released fission gas, metallographic studies, chemical analyses, and density measurements of fuel sections.

Eight elements have been punctured for gas-release measurements. The gas recovered ranged from 55 to 71% of the theoretical yields. Calculated fuel volumes of these elements indicated that the fuel had swelled from 32 to 46%. Data from prior experiments with U-Fs and U-Pu-Fs alloys[8] showed that the fission-gas release increased rapidly as fuel swelling increased in the range from 20 to 40%; gas release began to level off above 40% swelling. The data from the eight U-Pu-Zr elements are in good agreement with the prior data.

Metallographic examination of four elements confirmed that the fuel had expanded to the cladding. A reaction zone on the inside of the cladding has been found, and work is in progress to verify the existence of a corresponding reaction zone on the outside of the fuel. Three major annular zones were found in transversal sections from the upper three-fourths of the fuel length. The central and outer zones were more porous than the middle zone. The major concentric zones in the fuel are thought to be related to both the distribution of phases during irradiation and the temperature distribution. A number of smaller annular zones were present in these larger zones.

Beta-gamma autoradiographs showed high radioactivity in the center zone, relatively low activity in the middle zone, and moderate activity in the outer zone. Toward the bottom of the fuel column, where the zone structure fades, less beta-gamma activity was found at the center than toward the outside of the fuel.

Samples from each of the three zones (from the same fuel element) were analyzed for the fission product technetium and for zirconium. The atomic ratios, Tc/(U+Pu), determined for the three zones were based on the original composition: center, 2.0×10^{-3}; middle, 1.1×10^{-3}; and outer, 2.8×10^{-3}. The weight percent of zirconium (originally 9%) in the three zones was: center, 22; middle, 3; and outer, 10. Technetium and zirconium apparently had migrated from the middle zone.

Immersion densities of samples (from three fuel elements) of each of the three major zones showed that the center zones were from 46 to 64% of the density of the original material; the middle zones were from 93 to 104%, and the outer zones were from 69 to 84%. The high density of the middle zone is partially attributable to the lower zirconium content.

Metallographic evidence of a structural change was observed on the inside surface of the claddings of the elements examined. Both Hastelloy-X and Type 304 stainless steel showed maximum reaction zones of about 5 mils.

[5] S. T. Zegler, unpublished data.

[6] S. T. Zegler, Annual Progress Report for 1966, Metallurgy Division, ANL-7299, pp. 22-23.

[7] W. N. Beck, F. L. Brown, W. F. Murphy, and C. C. Crothers, Annual Progress Report for 1966, Metallurgy Division, ANL-7299, pp. 23-24.

[8] W. N. Beck, Annual Progress Report for 1966, Metallurgy Division, ANL-7299, Figure 21, p. 33.

Type 316 stainless steel showed the smallest reaction zone, about 0.8 mil. The reaction zone of the Type 304 stainless steel was examined with an electron microanalyzer, and it was found that the nickel concentration–normally about 10 wt% in the steel–had dropped to about 1% in the reaction zone. No uranium, plutonium, or zirconium was detected. X-ray spectral profiles showed the presence of a number of fission products (i.e., cerium and lanthanum) in the reaction zone.

In other phases of this program, duplicate pairs of encapsulated U-15 wt% Pu-10 wt% Zr and U-15 wt% Pu-10 wt% Ti fuel pins with V-20 wt% Ti cladding were irradiated in EBR-II. One pair was removed after 5 at.% burnup. Neutron radiographic examination of the elements in their capsules showed that the claddings were intact. The U-Pu-Zr and U-Pu-Ti alloy fuel pins had elongated 3.6 and 8.8%, respectively. The second pair has accumulated 85% of the target burnup of 7.5 at.%.

Fifteen U-15 wt% Pu-10 wt% Zr fuel elements (Group M-3) were inserted into EBR-II for irradiation at a linear power rating of 10 kW/ft. The elements have accumulated 0.25 at.% burnup at a maximum cladding temperature of 625°C. They are similar to the elements irradiated to 4.5 at.% burnup in subassembly XA07 except that the target burnup is 10 at.% with interim examinations scheduled at 5 and 7.5 at.%. Also, the gas plenums are smaller in the M-3 elements and operating pressures are higher.

The M-4 group of experimental U-15 wt% Pu-12 wt% Zr fuel elements has been designed to determine fuel behavior at higher power ratings and to chart the course of this behavior at burnups of from 1 to 10 at.%. The linear power rating will be 14 kW/ft. The claddings to be used are Types 304, 316, and 318 stainless steel; V-15 wt% Ti-7.5 wt% Cr; and V-15 wt% Cr-5 wt% Ti. Fabrication is under way.

Oxide-Fuel Development

ELECTRON-PROBE STUDIES OF IRRADIATED OXIDE FUEL *(D. R. O'Boyle)*

A UO_2-20 wt% PuO_2 fuel pin irradiated in EBR-II to 5.6 x 10^{20} fissions/cc was examined by means of electron-probe microanalysis. Two separate types of solid fission-product inclusions were identified: (1) white metallic inclusions, located in the equiaxed and in the columnar grain regions, that contained the fission products molybdenum, technetium, ruthenium, rhodium, and palladium; and (2) a gray phase, located in the equiaxed grain region, that contained strontium, barium, and cerium. The concentrations of molybdenum, technetium, and ruthenium were measured in 42 white metallic inclusions in the columnar grain region, and the results are shown in Figure 1. The observed partition of solid fission products between the oxide matrix and the inclusions is in agreement with predictions based on the free energy of formation of fission-product oxides and the balance of oxygen between that liberated by the fission process and that required to form stable fission-product oxides. Measurements made of the radial distribution of uranium and plutonium confirmed the migration of plutonium up the temperature gradient. The results of this experiment have been discussed in detail elsewhere.[9,10]

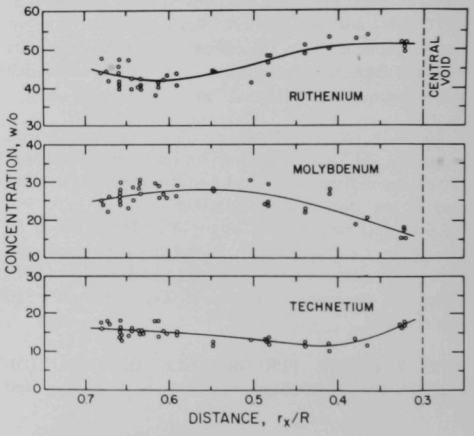

Fig. 1. Radial Variation in Ruthenium, Molybdenum, and Technetium Content of Metallic Fission-product Inclusions in the Columnar Grain Region of UO_2-20 wt% PuO_2 Irradiated to 5.6 x 10^{20} fissions/cc. Concentration of each element was measured simultaneously by using three independent spectrometers.

FUEL-ELEMENT PERFORMANCE OF URANIUM-PLUTONIUM OXIDES *(F. L. Brown, R. F. Janninck, and L. A. Neimark)*

The experimental fuel elements contained vibratorily compacted, slightly hyperstoichiometric UO_2-PuO_2 powder made by pneumatic impaction.* Compacted densities were

[9] D. R. O'Boyle, F. L. Brown, and J. E. Sanecki, Trans. Am. Nucl. Soc. *10*(2), 462-463 (November 1967).

[10] D. R. O'Boyle, F. L. Brown, and J. E. Sanecki, *Solid Fission Product Behavior in Uranium-Plutonium Oxide Fuel Irradiated in a Fast Neutron Flux*, J. Nucl. Mater. (to be published).

*Material supplied by Pacific Northwest Laboratory, Richland, Washington.

from 77 to 86% of theoretical. Cladding materials were Type 304 stainless steel, Hastelloy-X, and V-20 wt% Ti alloy.

Elements SOV-5 and SOV-6, both clad in Type 304 stainless steel (0.021-in. thick), were examined after burnups of 2.6 and 2.7 at.% at linear heat ratings of 16.3 and 17.0 kW/ft, respectively.[11] The appearance of both elements was excellent, and dimensional changes were insignificant. Only element SOV-6 has been destructively examined. Fission-gas release was 58% of the theoretical yield, which correlates approximately with the development of columnar grains across 54% of the fuel volume. The columnar grains surrounded the common central cavity. The cavity was straight over the length of the fuel, except at the upper end of the fuel column where a slight enlargement was caused by an initially low fuel density in this region. The columnar grains contained numerous small metallic inclusions. From the columnar grains outward to the cladding, the microstructure consisted of a transition zone of sintered particles and equiaxed grains, a gray phase in grain boundaries along the inner edge of the transition zone, and lightly sintered particles at the fuel surface.

Electron-probe analysis showed that the metallic inclusions in the columnar grains contained molybdenum, ruthenium, technetium, rhodium, and palladium.[9] The same elements were found in larger "ingots" that were deposited at the base of the central cavity. These ingots initially were found in both SOV-5 and SOV-6 by neutron radiography. The gray phase adjacent to the columnar grains contained the fission products barium, strontium, and cerium.

Electron-probe microanalysis also indicated plutonium migration up the temperature gradient toward the central void, although migration was not indicated by alpha autoradiography. The autoradiographs did show clearly that homogenization of the PuO_2 and UO_2 fraction occurred in the columnar grain zone. Before irradiation, some areas of high UO_2 concentration were present because of particle agglomeration during the ball-milling operation that precedes pneumatic impaction; these areas were still evident in the lightly sintered area next to the cladding.

The remaining seven mixed-oxide fuel elements had a nominal target burnup of 5 at.%; however, an indication of fission-product release to the reactor coolant was identified as coming from the subassembly (XO11) that contained these elements, and the experiment was temporarily terminated after an accumulated burnup of about 3.5 at.%.

Neutron radiographic examination indicated that the cladding of two elements (HOV-4 and HOV-10) had failed inside their irradiation capsules. Both specimens had Hastelloy-X cladding and had operated at approximately 23 kW/ft. The leaking capsule has been tentatively identified as HOV-4. This capsule lost weight equivalent to the weight of sodium bond, and an indication of escaping ^{85}Kr was obtained during leak tests.

Neutron radiography indicated probable melting of the fuel in HOV-4. Melting was deduced from the irregular central axial cavity and a meniscus-shape break in the fuel column. In spite of the probable melting, no gross fuel slumping was found, but there were two large breaks in the fuel column. Although evidence of fuel melting in HOV-10 was not as conclusive, irregularity was found in the central cavity, and a few minor breaks were observed in the fuel column.

Axial gamma scans disclosed that the distribution of fission products in the two elements differed markedly. Concentrated fission products were found only near the bottom of HOV-4, but in several places along the length of HOV-10.

Attempts to withdraw the elements from the irradiation capsules were unsuccessful because of the severity of the failures. Sectioning was begun with the elements still in the capsules.

Carbide-Fuel Development

FABRICATION OF (U,Pu)C FUEL FROM MIXED-CARBIDE POWDERS *(N. J. Carson and E. J. Petkus)*

Effort during the past year was directed toward the development of a simple method to incorporate $(U_{0.85}Pu_{0.15})C$ powders into fuel elements by the development of a process to produce carbide granules, and the construction of a larger-scale facility for vibratory compaction. The granule-making process chosen for development consists of three main steps: (1) powders are pressed into tablets, (2) tablets are pushed through a screen to make granules, and (3) granules are sintered. The facility established for the process is PF-21, a glovebox with a capacity of 192 ft^3. The glovebox was readied, the desired atmosphere was established, and the purification system was tested during the first half of 1967.

Dies for the tableting process were constructed, tested, and installed in the glovebox press. The sintering furnace was operated at 2000°C and the cooling system, which uses negative water pressure, was tested. A graphite-boronated graphite control thermocouple was installed and calibrated

[11] F. L. Brown, L. A. Neimark, B. J. Koprowski, J. E. Ayer, and J. H. Kittel, Trans. Am. Nucl. Soc. *10*(1), 101-102 (June 1967). Summary

against an optical pyrometer. The equipment was given a final performance test, and handling techniques were developed during tests with depleted uranium carbide; suitable techniques for adding and removing binders were also established.

The decision to scale-up the vibratory compaction process also included a decision to install another glovebox (PF-16). Glovebox PF-16 has been completed, leak rated, and is being used to make oxide fuel elements. The glovebox will also be used to make carbide elements.

COMPATIBILITY STUDIES

Reaction of (U,Pu)C with Potential Cladding Materials *(T. W. Latimer)*

The reaction of three carbide compositions (each with a uranium-to-plutonium ratio of 4:1) with various jacket materials has been studied to determine the changes that occur at elevated temperatures for extended periods of time. The carbon contents studied were 4.83 wt% equivalent carbon (single-phase (U,Pu)C), 5.25 wt% equivalent carbon (approximately 20 vol% $(U,Pu)_2C_3$), and 6.75 wt% equivalent carbon (approximately 90 vol% $(U,Pu)_2C_3$). The (U,Pu)C composition can only be obtained as single-phase material, if the nonmetal atom content (carbon, oxygen, and nitrogen) does not exceed 50 at.%. The assemblies used for the compatibility tests have been described previously.[12]

Iron- and nickel-base alloys: After tests of various commercial iron- and nickel-base alloys with (U,Pu)C and $(U,Pu)_2C_3$, the following observations were made:

1. In three cladding alloys containing more than 30 wt% nickel (Incoloy 800,* Hastelloy-X,** and Inconel 625†), intermetallic phases containing uranium, plutonium, nickel, and iron were formed on the fuel side of the interface accompanied by the release of carbon to the cladding.

2. In six alloys containing 25 wt% nickel or less, no intermetallic phases were formed. Metallographic evidence did indicate a transfer of a small amount of carbon to the cladding, which resulted in some chromium- and/or molybdenum-rich carbide precipitates.

3. In all tests, hyperstoichiometric (U,Pu)C containing $(U,Pu)_2C_3$ as a dispersed second phase changed the magnitude of the cladding effects only slightly, or not at all, when compared with the effects of (U,Pu)C.

A more complete discussion of these compatibility effects was presented previously.[13]

Vanadium-base alloys: Six vanadium-base alloys were tested at 800°C for 1000 hr with hyperstoichiometric $(U_{0.8}Pu_{0.2})C$ (5.25 wt% equivalent carbon). Four of the alloys were developed at Argonne National Laboratory: V-20 wt% Ti, V-15 wt% Ti-7.5 wt% Cr, V-15 wt% Cr-5 wt% Ti, and V-10 wt% Cr. Two other alloys were developed at Westinghouse Advanced Reactor Division: HSV-207 (approximately V-9 wt% Cr-3 wt% Fe) and HSV-208 (approximately V-8 wt% Cr-10 wt% Ta).

The matrices of the two alloys containing 15 wt% or more titanium were carburized to an average depth of 75 μ. The matrices of the two alloys containing no titanium or tantalum were unaffected, but grain-boundary precipitation was found to an average depth of 90 μ in HSV-207 and 250 μ in V-10 wt% Cr. The two alloys that were unaffected by hyperstoichiometric (U,Pu)C were V-15 wt% Cr-5 wt% Ti and HSV-208 (representing 5.3 at.% Ti and 3.0 at.% Ta, respectively). Thus the amount of strong carbide formers, such as titanium and tantalum, appears to play an important role in determining the overall compatibility of vanadium-base alloys with (U,Pu)C.

Reaction of Uranium Sulfide and Uranium Phosphide with Selected Cladding Materials *(T. W. Latimer)*

No effects were observed metallographically in any of four austenitic alloys (Type 304 stainless steel, Incoloy 800, Hastelloy-X, and Inconel 625) after contact with US for 1000 hr at 800°C. The only evidence of fuel-cladding interaction was a small (3-6 μ) gray band observed on the fuel side of the interface in each specimen. Electron-probe examination of this band revealed that the two major layers, observed optically in a similar but larger band that formed at 900°C, were UOS and U_2S_3.

Couples containing UP in contact with either Type 304 stainless steel or Hastelloy-X have been examined by metallographic and electron-probe techniques. In both metals, diffusion of iron and nickel from the cladding alloy into the UP had occurred, which resulted in well-defined zones of reasonably constant composition on each side of the fuel-cladding interface. The depths of these zones are

[12] T. W. Latimer, C. M. Walter, and W. R. Jacoby, Annual Progress Report for 1965, Metallurgy Division, ANL-7155, pp. 25-29.

*The approximate composition of Incoloy 800, in wt%, is 32.0 Ni, 20.5 Cr, 46.0 Fe, 0.75 Mn, 0.35 Si, 0.30 Cu, 0.30 Ti, and 0.30 Al.

**The approximate composition of Hastelloy-X, in wt%, is ~59.0 Ni, 22.0 Cr, 18.5 Fe, 0.5 Mn, 0.5 Si, and 0.6 W.

†The approximate composition of Inconel 625, in wt%, is 62.0 Ni, 0.05 C, 22.0 Cr, 3.0 Fe, 4.0 Nb, and 9.0 Mo.

[13] T. W. Latimer and W. R. Jacoby, *Compatibility of (U,Pu) Carbides with Potential Jacketing Materials*, Proc. 1967 Nucl. Met. Symp., Scottsdale, Arizona, October 4-6, 1967, K. E. Horton, R. E. Macherey, and R. J. Allio, eds, IMD-AIME (to be published).

listed in Table 1. The nickel content in the affected cladding zone was reduced to 25% or less of the original content. No uranium or phosphorus was found in the cladding alloys. In the affected fuel zone, the combined nickel and iron concentration was between 35 and 40 at.%; the uranium-to-plutonium ratio remained at 1:1.

TABLE 1. Extent of Interaction between UP and Two Potential Cladding Alloys after 1000 hr at 800°C

	Type 304 Stainless Steel		Hastelloy-X	
Zones	Average Depth, μ	Maximum Depth, μ	Average Depth, μ	Maximum Depth, μ
Fuel	18	21	50	55
Cladding	22	25	20	26

FUEL-ELEMENT PERFORMANCE *(F. L. Brown and L. A. Neimark)*

Studies are being conducted to establish models that will realistically predict the behavior and lifetime of carbide fuel elements in the complex LMFBR environment. Initial irradiation results indicate the relative behavior of Vipac and pellet rods, and of solid-solution powder and physically mixed powders of UC and PuC.

Three fuel elements irradiated in EBR-II were examined in the Alpha-Gamma Hot Cell Facility[14] during the past year, and 15 other elements continued under irradiation. The initial phase of the examination was by means of optical metallography. The three elements maintained cladding integrity during irradiation. Additional examinations of the three fuel elements will include electron microscopy and electron-probe analyses.

Element SMP-1 contained slightly hyperstoichiometric (~4.8 wt% carbon) helium-bonded pellets of $(U_{0.8}Pu_{0.2})C$ with a smear density of 81.4%. The cladding was Type 316 stainless steel, 0.024-in. thick. The element achieved a maximum burnup of 1.9 at.% at a linear heat rating of 15.9 kW/ft. Calculated maximum fuel and cladding temperatures were ~1300 and ~565°C, respectively.

Although there were no measurable changes in the linear dimensions of the element, a change of 0.32% in volume was measured. Fission-gas release was 4.3% of the theoretical yield. Only minor changes in the fuel structure were noted. What appeared to be dicarbide needles in the preirradiated structure were not present after irradiation. Finely distributed particles (or small bubbles) of a phase, were found in the grain boundaries; the particles increased in quantity and size toward the center of the fuel. Autoradiography disclosed no evidence of plutonium migration in the hottest section of the element, but slight depletion of fission products radially from the center of the element was indicated. A reaction zone 8 μ thick was noted in the cladding.

Element VMV-1 contained vibratorily compacted powder of slightly hyperstoichiometric $(U_{0.8}Pu_{0.2})C$ with a smear density of 85.9% of theoretical. The cladding was 0.024-in.-thick unalloyed vanadium. The element achieved a maximum burnup of 3.0 at.% at a linear heat rating of 25.8 kW/ft. Calculated maximum fuel and cladding temperatures were ~1800 and ~645°C, respectively.

The element exhibited a maximum diametral increase of 0.83%, a length increase of 0.31%, and a volume increase of 1.48%. In comparison with the findings on the other two elements, these changes reflect both the relatively low strength of unalloyed vanadium (compared with stainless steel) and the higher operating power level. Fission-gas release was 8.6% of the theoretical yield. Structurally, the fuel sintered over 65% of the diameter; the estimated temperature at the edge of the sintered area is about 1500°C. Autoradiography indicated slight plutonium movement from the center and some fission-product depletion from the sintered area. The reaction layer found in the vanadium cladding was 8 μ thick.

Element SMV-1 contained a physical mixture of 80% UC and 20% PuC powders vibratorily compacted to 80% of theoretical density. The cladding was Type 316 stainless steel, 0.024-in. thick. The element achieved a maximum burnup of 2.6 at.% at a linear heat rating of 21.3 kW/ft. Calculated maximum fuel and cladding temperatures were ~1750 and ~630°C.

Macrosintering and homogenization of the UC and PuC phases were not apparent in the fuel structure. The PuC fraction appeared either to melt or to move fluidly (in the solid state) into the center region and encompass the UC phase. In peripheral regions, the PuC that occupied void space around the UC phase sintered and swelled. Evidence also was found of PuC penetration into the grain boundaries of the large UC particles.

Although this element operated at less than the maximum power rating of the three elements examined, it had the greatest apparent outward radial migration of plutonium and fission products. A reaction layer 12 μ thick was found in the cladding.

BEHAVIOR OF GASEOUS FISSION PRODUCTS IN CARBIDE FUELS *(L. C. Michels)*

Experiments are being conducted to determine the swelling and fission-gas release behavior of carbide fuels

[14] F. L. Brown, L. A. Neimark, B. J. Koprowski, J. H. Kittel, J. E. Ayer, and O. L. Kruger, Trans. Am. Nucl. Soc. *10*(2), 473-474 (November 1967). Abstract

during irradiation to burnups up to 10 at.% at maximum cladding-surface temperatures that range from 625 to 1000°C. Specimens of vibratorily compacted PuC powders and mixed UC and PuC powders are being used.

Specimens have been irradiated to estimated burnups of 0.3 and 5-6 at.% at maximum cladding-surface temperatures of 860 and 700°C, respectively. The former group of specimens was originally intended to achieve a burnup of 2 at.% at a maximum cladding temperature of 1000°C, but was removed from MTR after one reactor cycle because of a capsule malfunction. Irradiations are continuing on fuel specimens intended to achieve burnups of 10 at.% at maximum cladding-surface temperatures of 600°C. These specimens have achieved estimated burnups of from 9.1 to 9.6 at.% at maximum cladding temperatures of from 500 to 700°C.

Postirradiation examination of eight specimens irradiated to nominal burnups of 0.3 and 5-6 at.% is in progress. Gamma scanning and leak testing, as well as diameter, length, weight, and density measurements have been completed.

One specimen that contained PuC failed prior to removal from MTR at an estimated burnup of 6.2 at.%. Several longitudinal cracks of varying lengths and widths were observed in the Nb-1 wt% Zr cladding. The largest crack observed was near the bottom of the specimen; the top of the crack had the appearance of a ductile fracture, while the bottom portion had the appearance of a brittle fracture. The cause of the cladding failure is most likely related to fuel swelling ($\Delta D \cong 6.2\%$).

The remaining seven specimens were all intact. No leaks were detected in the cladding during leak tests performed in liquid nitrogen and alcohol. No significant diametral or volume changes were found.

Neutron radiographs taken after irradiation indicate that the fuel density in two specimens decreased in the bottom portion of the pins. Gamma scans of these pins support the data obtained with neutron radiography. The cause of this apparent fuel redistribution is not known.

Fast-Reactor Cladding Development

DRAWING OF COMPOSITE RODS *(J. J. Rechtien and J. E. Flinn)*

Publication

J. E. Flinn and J. J. Rechtien, J. Nucl. Eng. and Design *6*, 217-222 (October 1967).

A short project to investigate the stress and strain considerations for composite-rod drawing was completed during the past year; experimental and phenomenological approaches were used. Tubes of Type 304 stainless steel were drawn to various reductions with cores of copper, aluminum, and Type 304 stainless steel at constant die angles and coefficients of friction at the die-tube interface. When frictional effects at the core-tube interface were neglected (an assumption that was experimentally justified), the analysis showed that the draw stress should follow the standard rod equation with a composite yield criterion. The draw-stress data are in good agreement with this theory, with the exception of pure sinking (no core).

An experiment was performed to determine whether the neglect of frictional forces at the tube-core interface could be justified. A comparison of draw forces was made between tubes with and without a lubricant at the interface. The draw forces were identical, and equivalent dimensional changes were obtained. Although the results support the contention that frictional forces at the interface can be neglected, the observation that slippage occurred at the unlubricated interface makes the validity of our contention suprising.

CORROSION OF CLADDING MATERIALS IN SODIUM

Interactions of Vanadium Alloys with Impure Sodium *(W. E. Ruther, D. J. Dorman, C. F. Cheng, and Sherman Greenberg)*

The kinetics of the interactions between selected alloys and the impurities in sodium have been studied as a function of test temperature (450-700°C), cold-trap temperature (~110 and 175°C), and alloy composition. The tests were performed in refreshed static autoclaves and in a dynamic sodium system at a velocity of 6.1 m/sec. Relative corrosion rates were determined by weight and dimensional changes.

The V-20 wt% Ti alloy was the most corrosion-resistant alloy tested (except at 700°C) under static conditions with a cold-trap setting of about 175°C. Following in order were V-15 wt% Ti-7.5 wt% Cr, V-10 wt% Cr, V-15 wt% Cr-5 wt% Ti, and V. At 700°C, V-10 wt% Cr and V-20 wt% Ti showed the best and poorest resistance to corrosion, respectively.

Much less corrosion was encountered in static

experiments that used the 110°C cold-trap temperature, but no obvious ranking of the alloys was evident in terms of corrosion resistance.

The weight changes of specimens subjected to dynamic tests (6.1 m/sec sodium velocity and 110°C cold-trap temperature) were always smaller and sample appearance always better than in corresponding static tests. Corrosion rates in the dynamic tests were low enough to indicate satisfactory performance of vanadium alloys, particularly V-5 wt% Cr or V-10 wt% Cr, in well cold-trapped sodium systems. The lack of dimensional changes in the specimens (measured to 10^{-4} in.) confirmed the implications of low weight gains.

Chemical analyses of the corroded dynamic test specimens showed that oxygen was the major impurity gained. Additional carbon was detected also, but the hydrogen and nitrogen levels did not increase during sodium exposure.

The x-ray analysis of samples exposed to sodium cold-trapped at 110°C indicated that gamma vanadium carbide ($VC_{0.4\text{-}0.5}O_{0\text{-}0.1}$) was the major corrosion product.

Under all conditions of out-of-pile exposure to sodium, V alloys that contained titanium developed a subsurface hardened zone of from 2 to 100 μ thick, depending on temperature, time, sodium-oxygen level, and titanium content. Unalloyed vanadium and V-Cr alloys did not develop this hardened band during exposures to sodium cold-trapped at 110°C.

Vanadium, V-20 wt% Ti, and V-40 wt% Ti were exposed in EBR-II at full power for 119 days at temperatures of 510 and 530°C.[15] The V-20 wt% Ti and V-40 wt% Ti specimens showed small weight losses and no subsurface-hardened zone; unalloyed vanadium suffered nearly 50% weight loss.

Interactions of Type 304 Stainless Steel with Impure Sodium *(W. E. Ruther, R. R. Schlueter, D. J. Dorman, Sherman Greenberg, R. A. Noland, and Steve Matras)*

As a consequence of the discovery of copper deposits in an EBR-II heat exchanger, the possibility of the penetration of Type 304 stainless steel by copper dissolved in sodium was examined. A metallurgical examination of specimens from this heat exchanger showed no copper penetration. This study was augmented by the examination of stainless steel tubing upon which copper was deposited during deliberate exposure to copper-bearing sodium in a recirculating loop experiment. The copper deposits generated in the EBR-II heat exchanger and in the test loop were dendritic and discontinuous. No penetration was observed metallographically or with the aid of an electron probe.

Sections of the Type 304 stainless steel encapsulation tubes of EBR-II subassembly XO09 were examined for penetration of tin or bismuth. The subassembly was in the reactor from March 24 to November 15, 1966, a period during which the tin and the bismuth content of the reactor sodium was unusually high. Unfortunately, any compounds on the exterior surface of the capsule wall would have been exposed to water during the normal fuel-assembly cleaning procedure and at least partially lost. Anhydrous polishing techniques were employed to prevent any further aqueous reaction and subsequent loss of any tin-sodium or bismuth-sodium compounds in the transverse section. Electron-probe analysis of the transverse section showed no trace of tin or of bismuth. This result is not unexpected. If tin and bismuth had penetrated the surface of the thin-walled stainless steel tubing, degradation of the mechanical properties could reasonably be expected. None has been observed.

In cooperation with E. L. Kimont and F. A. Smith of the Reactor Engineering Division, an effort was made to elucidate some of the earlier observations of these investigators concerning the interaction of Type 304 stainless steel with sodium. Exposure of tube specimens to cold-trapped (120°C) sodium at 650°C in Metallurgy Division equipment was followed by Strauss testing in Reactor Engineering. The results indicated no effect of sodium exposure when compared with similar specimens heated at 650°C in vacuum for the same period. The conclusion is tentatively drawn that the earlier observations of severe effects of sodium exposure on subsequent Strauss testing were due to one or more impurities, yet to be identified, in the sodium of the Reactor Engineering Division test loop.

Another hypothesis, derived from earlier Reactor Engineering Division exposures, was that sodium penetrated the grain boundaries of stainless steel to a depth of at least 6×10^{-3} in. Recent experiments in the Metallurgy Division have not supported the hypothesis. Careful experiments on thin-wall ($4\text{-}5 \times 10^{-3}$ in.) stainless-steel capsules showed no detectable penetration of sodium through the thin wall after a one-week exposure at 650°C. Sensitivity of the detection method was of the order of 6×10^{-10} g Na/cm^2. Subsequent Strauss testing of the capsules (one sodium filled, one helium filled) by Kimont and Smith confirmed the previous Metallurgy Division experience and showed no effect of sodium exposure.

Rods of Type 304 stainless steel were carefully machined, exposed in Reactor Engineering Division sodium for one week at 650°C, and various layers then machined

[15] S. Greenberg, C. F. Cheng, and W. E. Ruther, *In-Reactor Sodium Corrosion of Vanadium and Vanadium-Titanium Alloys*, Nucl. Appl. (to be published).

off for chemical analysis. Surface layers, to a depth of about 4×10^{-3} in., had carbon concentrations of about 0.070 wt%. Specimen layers from 6×10^{-3} to 12×10^{-3} in. deep showed gradually reduced carbon content, from 0.056 to 0.052 wt%. Strauss testing of sodium-exposed specimens (Reactor Engineering), from which the surface layers have been removed in steps, has been started by Kimont and Smith to learn if the rapid Strauss-attack region coincides with the carbon-enriched region.

Interactions of Nickel-Base Alloys with Impure Sodium *(C. F. Cheng, J. C. Tezak, and Sherman Greenberg)*

Commercially available nickel-base (>35 wt% Ni) alloys may be useful as fuel cladding and as structural materials for LMFBR applications. With respect to use in a sodium environment, the most important question relevant to these alloys concerns mass transfer of nickel under a temperature gradient.

A pumped sodium loop has been constructed for a study of mass-transfer of nickel and nickel-base alloys. This loop has a unique feature: the test section for high-temperature sodium (≥350°C) is constructed of essentially inert refractory material, while the components in contact with low-temperature sodium (<350°C) are made of Type 304 stainless steel.

A preliminary test of specimens of Nickel 200* in purified sodium flowing at 0.5 gpm and at 8.7 cm/sec velocity resulted in the exceptionally small weight loss of 0.44 mg/cm² in 48 days (equivalent to approximately 0.15 mil/year by linear extrapolation).

Creep tests of Nimonic 80A** were conducted at 650°C in zirconium-gettered sodium (<5 ppm oxygen) and in vacuum for comparison. At a stress of 46.2 kg/mm², the Nimonic sample exposed in sodium prematurely ruptured in 212 hr with a true strain of 1.2%; in vacuum a similarly treated specimen ruptured in 765 hr with a true strain of 4.6%. The true strain rate diminished in the third stage of creep in sodium as compared with vacuum exposure, while the corresponding rates were similar in the first and second stages of creep.

Samples of Type 304 stainless steel (included in all tests as a control), Inconel 600,† Incoloy 800, and Hastelloy-X alloys were exposed to sodium in the core of EBR-II for a time equivalent to 4 months at full power (7 months total) at temperatures of 510 and 530°C and at a sodium velocity of 3.8 m/sec.[15] No weight or dimensional changes occurred in any of the samples. Detailed metallographic examination indicated no intergranular corrosion. Although the temperatures of exposure (510 and 530°C) were relatively low, the surface area of the nickel alloy samples to the volume of sodium was favorable for accelerated thermal-gradient mass transfer. Electron-probe analysis of the specimen surface revealed selective dissolution of chromium and iron in Incoloy 800 and of nickel and chromium in Inconel 600. No change of surface composition occurred for Type 304 stainless steel and Hastelloy-X. The significance of the results regarding Type 304 stainless steel and Hastelloy-X is enhanced, in spite of the relatively low temperature, by the fact that selective dissolution did take place in the case of Inconel 600 and Incoloy 800.

MECHANICAL PROPERTIES OF FUEL CLADDING ALLOYS

Tensile Properties of Vanadium and Vanadium-Base Alloys at Constant Strain Rate *(F. L. Yaggee and A. R. Brown)*

The short-term tensile properties of vanadium, V-10 wt% Ti, V-20 wt% Ti, and V-40 wt% Ti sheet specimens were determined at a strain rate of 2×10^{-4} sec^{-1} and at temperatures between 25 and 800°C. The materials tested contained interstitials (carbon, oxygen, nitrogen, and hydrogen) in the amount of 1100-1300 ppm by weight. All specimens were vacuum annealed for 1 hr at the following temperatures before testing: vanadium at 1250°C, V-10 wt% Ti at 1250 and 1000°C, V-20 wt% Ti at 1000 and 900°C, and V-40 wt% Ti at 1250 and 900°C.

The tensile strength and yield stress of these alloys, as a group, decreased about 85% in the range of temperatures between 25 and 800°C; Young's modulus decreased about 10% over the same temperature range. The total elongation decreased by about 45% between 25 and 600°C, and then increased between 600 and 800°C. At 800°C the value of elongation was about 20% greater than the value at 25°C. The sharpest changes in mechanical properties of these alloys occurred between 650 and 800°C. At 600°C the ranges of property values obtained for these alloys are as follows: tensile strength from 16 to 56 $kg\text{-}mm^{-2}$ (23,000-80,100 psi), yield stress from 8 to 45 $kg\text{-}mm^{-2}$ (11,400-64,300 psi), Young's modulus from 8 to 12.4 $\times 10^3$ $kg\text{-}mm^{-2}$ (11.4×10^6-17.7×10^6 psi), and total elongation from 13 to 45%. The uniform elongation varies between 7 and 13%. In general, the variation in tensile properties of these alloys as a function of temperature is similar to that previously reported for V-15 wt% Ti-7.5 wt%

*The approximate composition of Nickel 200, in wt%, is 99.0 Ni and about 0.25 each of Mn, Si, Fe, and Cu.

**The approximate composition of Nimonic 80A, in wt%, is ~75.0 Ni, 19.5 Cr, 2.5 Ti, 1.3 Nb + Ta, 0.7 Si, and 0.4 Fe.

†The approximate composition of Inconel 600, in wt%, is 72.0 (minimum) Ni, 14.0-17.0 Cr, 6.0-10.0 Fe, 1.0 Mn, 0.5 Si, and 0.5 Cu.

Cr.[16] However, the specific values of the V-15 wt% Ti-7.5 wt% Cr alloy are somewhat higher.

At temperatures below 400°C, the addition of titanium to vanadium tends to increase the values of the short-term tensile properties of the V-Ti alloys for titanium concentrations of up to 40 wt%. Above 400°C the maximum values of the short-term tensile properties of V-Ti alloys are realized at 20 wt% titanium.

Creep in Unalloyed Vanadium *(F. L. Yaggee)*

The activation energy for creep in V-15 wt% Ti-7.5 wt% Cr containing 1300 ppm total interstitial impurities (carbon, oxygen, nitrogen, and hydrogen) was previously reported as 89,000 cal-g mole^{-1} in the test temperature range between 500 and 850°C and at stresses of from 15 to 60 kg-mm^{-2} (21,400-85,800 psi).[17] In the same temperature range, two activation energies were determined for the creep of unalloyed vanadium. An activation of 72,000 cal-g mole^{-1} was found at stresses between 5 and 10 kg-mm^{-2} (7100-14,300 psi), and an activation energy of 56,000 cal-g mole^{-1} was found at a stress of 15 kg-mm^{-2} (~21,400 psi). These values are in good agreement with the 72,000 cal-g mole^{-1} reported by Peart[18] and the 61,000 cal-g mole^{-1} reported by Lundy[19] respectively, for vanadium self-diffusion.

Surface Defects as Failure Sites in Type 304 Stainless Steel *(F. L. Yaggee)*

Biaxial creep tests conducted on artificially defected Type 304 stainless steel seamless tubing show that defects penetrating to a depth equal to 5% of the wall thickness are the failure sites. The biaxial creep tests (using internal gas pressure) were conducted in vacuum at 650°C and stresses between 15 and 25 kg-mm^{-2} (21,400-35,700 psi). Defects located on the inside surface of the tube are more detrimental than those located on the outside tube surface and can decrease the strain at fracture by more than 70%.

Thermal Expansivities of Vanadium-Base Alloys and Type 304 Stainless Steel *(F. L. Yaggee)*

An analysis of previously reported data on the thermal expansivity of vanadium-base alloys and Type 304 stainless steel[20] reveals the following information regarding the potential of vanadium alloys as fuel cladding materials in a fast-breeder reactor system. At temperatures between 25 and 1000°C, the fractional expansion of V, V-Ti, V-Ti-Cr, and Type 304 stainless steel can be defined by a quadratic polynomial. In this temperature range the expansivities of the V-Ti and V-Ti-Cr alloys are about one-half that of Type 304 stainless steel, and the thermal conductivities of the vanadium alloys are approximately one-third greater than that of Type 304 stainless steel.

A simple expression has been developed[21] that relates the instantaneous expansion coefficient and the mean expansion coefficient; the expansion yields calculated values for the instantaneous expansion coefficient that are within 1% of the experimentally determined values. By using this expression and a graphical construction, the fractional expansion curve can be reconstructed from two known values of the mean expansion coefficient.

IRRADIATION OF FAST-REACTOR CLADDING MATERIALS *(Richard Carlander)*

Specimens of promising alloys (selected on the basis of optimum preirradiation strength, corrosion resistance, and fuel compatibility characteristics) are being irradiated at elevated temperatures. The alloy compositions that exhibit improved mechanical properties in comparison with austenitic stainless steel and nickel-base cladding alloys irradiated and tested under identical conditions are then selected for further investigation.

The tube-burst properties at 550°C of V-15 wt% Ti-7.5 wt% Cr, Type 304 stainless steel, Hastelloy-X, and Inconel 625 were measured after these alloys were irradiated in EBR-II to a fluence of ~5 x 10^{21} n/cm^2 at 600 ±100°C. The maximum changes in strength and ductility for all of the alloys did not necessarily occur in the region of highest fluence, but appeared to be dependent on both irradiation temperature and fluence. The maximum changes in burst properties of the alloys are compared in Table 2. Also listed in the table are the changes in burst properties of V-15 wt% Ti-7.5 wt% Cr and Type 304 stainless steel irradiated at approximately equivalent conditions.

---

[16] F. L. Yaggee, E. R. Gilbert, J. E. Flinn, and A. R. Brown, Annual Progress Report for 1966, Metallurgy Division, ANL-7299, pp. 79-80.

[17] F. L. Yaggee, E. R. Gilbert, and A. R. Brown, Annual Progress Report for 1966, Metallurgy Division, ANL-7299, pp. 80-81.

[18] R. F. Peart, J. Phys. Chem. Solids *26*, 1853-1861 (1965).

[19] T. S. Lundy, USAEC Report ORNL-3617, Oak Ridge National Laboratory, June 1964.

[20] F. L. Yaggee, E. R. Gilbert, and J. W. Styles, *Thermal Expansivities, Thermal Conductivities, and Densities of Vanadium, Titanium, Chromium, and Some Vanadium-Base Alloys (A Comparison with Austenitic Stainless Steel)*, J. Less-Common Metals (to be published).

[21] F. L. Yaggee and F. G. Foote, *A Method for the Reconstruction of a Thermal Expansion Curve from Two Values of the Mean Expansion Coefficient*, Proc. Symp. on Thermal Expansion of Solids, National Bureau of Standards, Gaithersburg, Maryland (to be published).

TABLE 2. Tube-Burst Properties of Irradiated Cladding Alloys Tested at 550°C

Material	Maximum Change in Property, %	
	Rupture Strength	Tangential Ductility
V-15 wt% Ti-7.5 wt% Cr	+32	-70
Type 304 Stainless Steel	+16	-74
Hastelloy-X	+22	-78
Inconel-625	+56	-73
	Property Change at Equivalent Irradiation Conditions, %	
V-15 wt% Ti-7.5 wt% Cr	+32	-26
Type 304 Stainless Steel	+16	-74

The tensile properties of V-20 wt% Cr, Type 304 stainless steel, and Hastelloy-X were measured at test temperatures between 400 and 650°C after irradiation in EBR-II to a fluence of ~5 x 10^{22} at 600 ±100°C. Comparison of the changes in tensile properties at 550°C of the vanadium alloys and the iron- and nickel-base alloys is given in Table 3. Although the increases in irradiation strength of all four alloys were approximately the same, the loss in ductility, as measured by total elongation, was less for the vanadium alloys.

The effect on irradiation performance that could result from increases in the preirradiation grain size of the vanadium alloys was also investigated. The results indicated that an increase in grain size from 10 to 35 μ did not degrade nor improve the postirradiation tensile properties at test temperatures between 400 and 650°C after irradiation to 5 x 10^{21} n/cm^2.

Irradiation of V-20 wt% Ti alloy to ~3 x 10^{22} n/cm^2 resulted in an increase in maximum strength of 27% at test temperatures below 650°C; however, this fluence level had little effect on ductility over the test-temperature range from 400 to 650°C.

TABLE 3. Tensile Properties of Cladding Alloys Tested at 550°C

Alloy	Change in Property, %	
	Yield Strength	Total Elongation
V-20 wt% Ti	+43	-21
V-15 wt% Ti-7.5 wt% Cr	+50	-14
Type 304 Stainless Steel	+44	-33
Hastelloy-X	+64	-24

Zero-Power Fuels and Fuel Elements

DEVELOPMENT OF OXIDE-ROD FUEL ELEMENTS

(J. E. Ayer and F. D. McCuaig)

During fiscal year 1969 Reactor Physics studies will commence on simulations of oxide-fueled reactors of 2000, 3500, and 5000 liter sizes in ZPPR. The fuel elements required for these studies will be commercially procured to specifications and designs generated under this task. The required Type 304L stainless steel tubing (reactor grade) with a 0.385-in. OD and a 0.012-in. wall was received and drawn down to a 0.351-in. ID. The tubing was nondestructively tested and sampled for metallographic inspection. Thirty jacket tubes were prepared from the inspected tubing. End caps were made from Type 304 stainless steel, and the bottom end caps welded into the jackets. The end-cap design, shown in Figure 2, has been proved with respect to our ability to make a girth weld with minimum protrusion beyond the outside diameter of the jacket. The shape of the end cap was chosen to conform to the requirements of the Reactor Physics and Metallurgy Divisions of (1) a fixed length, (2) a minimum clearance between rod and collandria tube, (3) a bearing surface apart from the weld, and (4) a weld that is relatively insensitive to welding parameters. The techniques for loading plutonium-containing pellets into close-fitting jackets have been developed.

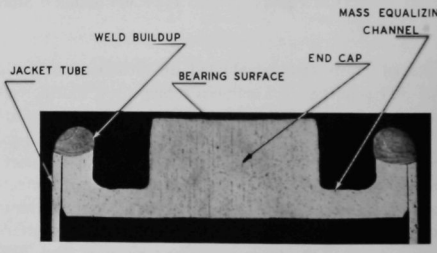

350-1020

Fig. 2. Welded End-Cap Section.

A testing apparatus to thermal cycle sample jackets has been built and is in operation. Three of the thirty assembled fuel jackets are in the process of being tested. One sample has been cycled over 2000 times in air at temperatures between 100 and 600°C. The time at 600°C was on the order of seconds. The purpose of this test was to obtain a quick assessment of the adherence of the oxide layer on the jacket surface. A second assembled jacket was cycled 200 times and held at 600°C for 4 hr. Upon completion of thermal cycling tests, the weight gain or loss of each sample will be determined, as well as any

dimensional changes that may have occurred during testing. Each jacket will then be sectioned and examined metallographically to ascertain the extent of corrosion.

FABRICATION OF SPECIAL PURPOSE FUEL ELEMENTS

Instrument-Traverse Fuel Elements *(J. E. Ayer and F. D. McCuaig)*

The ZPPR series of Reactor Physics experiments will require the fabrication, in 1969, of about 250 instrument-traverse elements. These elements provide a means to achieve fine-flux mapping of the reactor core.

An approved design of the traverse element has been achieved, and the jackets for 50 traverse elements have been fabricated. Figure 3 shows the standard ZPPR jackets with a ferrule welded into the sides. Core plates for the traverse elements will be made from standard ZPPR core plates and from elements submitted to Argonne National Laboratory by commercial vendors as evidence of their readiness to begin full-scale production of standard ZPPR elements. A sufficient number of plates are presently on hand to fabricate 50 instrument-traverse elements. A die to accomplish a simultaneous punching and shearing operation has been designed and constructed. A loading fixture has been designed to permit the loading of halves of core plates into each end of a traverse-element jacket and maintain an alpha-free exterior.

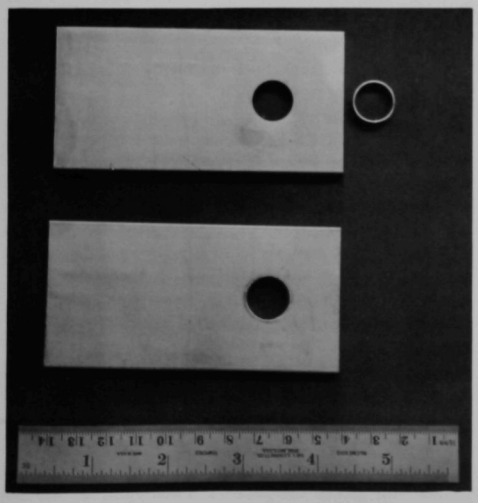

350-990

Fig. 3. Standard ZPPR Jackets with a Ferrule Welded into the Sides.

Oxide-Plate Fuel Elements *(G. D. White, J. T. Dusek, and C. T. de Freitas)*

Fabrication of a large number of $(U_{0.8}Pu_{0.2})O_2$ fuel plates for use in ZPPR requires the development of a process and the establishment of specifications for the mixed-oxide fuel. The two manufacturing procedures being investigated are cold pressing and sintering, and hot pressing.

Cold pressing: Cold-pressed specimens were made by ball milling a mixture of depleted UO_2 and PuO_2 powders, cold pressing, and then sintering for 4 hr at 1650°C in either vacuum, helium, or helium-6% hydrogen. Table 4 lists data for the three sintering atmospheres.

TABLE 4. Data on $(U_{0.8}Pu_{0.2})O_2$ Reacted and Sintered for 4 hr at 1650°C in Vacuum, Helium, and Helium-6% Hydrogen

Atmosphere	a_0, Å	Oxygen-to-Metal Atom Ratio	
		Oxidation-Reduction	Chemical Analysis
Vacuum (10^{-6} Torr)	5.459	1.977	1.982
Helium-6% hydrogen	5.460	1.972	1.976
Helium	5.457	1.985	1.992

The x-ray diffraction patterns were sharp with clean $K\alpha_1$-$K\alpha_2$ separation at high angles. The high-angle reflections of the specimens heated in helium-6% hydrogen were somewhat broader than the reflections for the specimens heated in vacuum and in helium. The unit-cell parameters in Table 4 were determined by the Nelson-Riley method. The oxygen-to-metal atom ratios were determined by oxidizing material in helium-2% oxygen for 2 hr at 850°C, followed by a reduction in CO-CO_2 at 850°C for 3 hr. Stoichiometry was determined from the weight changes. The chemical technique used was the inert gas-fusion method. Metallographic examinations of these specimens have been made, but the grain boundaries were not well delineated when the normal etchant for UO_2 was used.

The sintered specimens had densities that ranged from 94 to 96% of theoretical, which is higher than the density required for the ZPPR oxide plates (85-87%). Lowering the sintering temperature to 1500°C lowered the specimen density to about 91% of theoretical.

Hot pressing: Since a hot press was not available in the plutonium fabrication facilities, initial experiments were carried out on UO_2. A graphite die with graphite separators was used to press several plates at one time. As many as 11 plates were simultaneously pressed; however, for convenience this number was reduced to five. Pressings at 1400, 1500, and 1625°C gave average densities (% of theoretical) of 76.21, 81.40, and 88.88%, respectively.

Since the diameter of each specimen was determined by the die, very little variation of this dimension was observed. The thickness of the plates, a function of powder weight, uniformity of loading, and ultimate density, varied by a standard deviation of ~0.009 cm for stacks of five specimens.

Chemical analyses for carbon were made with specimens pressed at 1500 and 1625°C. Both as-pressed and hydrogen-treated specimens were sampled from the top and middle of the stacks. The results are listed in Table 5.

TABLE 5. Carbon Analyses of UO_2 Specimens

Specimen Position	Temperature, °C	Carbon Content, ppm	
		As-pressed	Hydrogen-Treated
Top	1625	193	25
	1625	221	26
	1500	508	35
Middle	1625	212	44
	1625	165	32
	1500	357	30

Uranium-Plutonium-Molybdenum Test Elements *(N. J. Carson)*

The reference fuel alloy for ZPPR is a uranium-plutonium-molybdenum alloy containing 25 wt% fissionable plutonium ($^{239}Pu + {}^{241}Pu$) plus molybdenum to suppress the formation of a zeta phase. The plutonium that was used has approximately 89% fissionable atoms which makes the total plutonium content of the alloy about 28 wt% and the amount of molybdenum about 2.5 wt%.

As part of the program to obtain information on alloys with higher plutonium contents, two U-Pu-Mo alloy melts were made. Melt R-418 was a U-36 wt% Pu-2.5 wt% Mo alloy and melt R-420 was a U-36 wt% Pu-3.7 wt% Mo alloy. The casting procedures developed for ZPPR were followed.[22] No obvious differences were found in melting and casting the two alloys.

The castings were parted on a mill with slitting saws. No differences in machinability were apparent, which was somewhat surprising since an increased amount of zeta phase was expected in the low-molybdenum alloy. After the samples were removed, sufficient material remained to make three ZPPR core plates 4 in. long. The plates were machined, inspected, and jacketed as an exercise for the ZPPR resident inspectors now being trained in Building 350.

[22]A. B. Shuck, H. F. Jelinek, A. G. Hins, N. J. Carson, Jr., A. A. Denst, and T. A. Steele, USAEC Report ANL-7313, Argonne National Laboratory, August 1967.

Metallographic examination showed the major phase in the as-cast structure of both alloys to be zeta U-Pu and retained gamma. The increase in molybdenum content from 2.5 to 3.7 wt% had the following effect: the amount of retained gamma phase was increased, and the structure was changed from predominantly Widmanstätten zeta U-Pu to an equiaxed structure of retained gamma in a matrix of finely transformed zeta U-Pu. The microhardness of the alloys was about the same. One polished specimen of each alloy was exposed to a glovebox atmosphere of dry nitrogen for about two weeks. The surface discoloration was more severe in the alloy of lower molybdenum content.

Reactivity Coefficient Fuel Elements *(N. J. Carson)*

Ninety-five of 218 plate-type fuel elements required for zero-power reactor experiments were manufactured during 1967. The elements were fabricated by a conventional technique that included the following operations: casting of billets, rolling billets into strips, blanking core plates from the rolled strips, loading core plates into stainless steel jackets, and welding.

The operations that comprise the fabrication process were chosen to reduce the amount of handling required, since it was predicted, by means of a computer program, that a technician could tolerate only 30 minutes per week of direct handling time. Reduced handling time, close monitoring of personnel exposure, and rotation of personnel between jobs allowed the fabrication to be completed with only minimal use of shielding.

Doppler Coefficient Fuel Elements *(J. E. Ayer, C. F. Konicek, and E. W. Kay)*

Doppler coefficient fuel elements have been fabricated for Reactor Physics experiments in ZPPR. Approximately 15 kg of depleted UO_2 was granulated and then vibratorily compacted into 200 tubes 0.635 cm in diameter and 4 tubes 1.27 cm in diameter. The packed density of the oxide was found to be 77 ±2% of theoretical. The loaded fuel tubes were tested by radiographic techniques to detect nonuniformity of density in the packed column. The ends of the fuel tubes were closed to complete the fabrication.

During 1967 the fuel material necessary to fabricate the 32 additional doppler coefficient elements[23] requested by the Reactor Physics Division has been obtained, blended where necessary, and converted to unfired granules. The $^{233}UO_2$ and 100% PuO_2 granules have been fired and loaded into jacket components. Twenty-one of the elements were assembled, welded, inspected, and accepted.

[23]J. E. Ayer, Annual Progress Report for 1966, Metallurgy Division, ANL-7299, pp. 60-61.

Danger Coefficient Fuel Elements *(F. D. McCuaig)*

Twenty-four danger coefficient elements were made during 1967. Twenty are plate-type elements that have core plates made of either Pu-1.1 wt% Al alloy or ^{233}U enclosed in stainless steel jackets. Four are dummy elements that do not contain fuel. Core plates of both materials were cast to thicknesses of 0.200, 0.080, and 0.050 in. In addition, 0.030 and 0.015-in.-thick foils of Pu-1.1 wt% Al alloy were made by hot rolling. The jackets were manufactured by a process similar to the one developed to manufacture the jackets for ZPPR elements.

The surface dose rate for the ^{233}U metal ran as high as 15 R/hr, which is more than sufficient to cause a handling problem and was the basis for the decision to produce the core plates by precision casting. Operations were designed to minimize the time of exposure of the workers. Where practical, 0.125- or 0.25-in.-thick lead shields were hung on glovebox walls to reduce body exposure. Leaded aprons were worn by personnel whose work required lengthy fuel handling. Fuel was transferred between stations in lead-lined cans. The accumulated radiation exposures during a one-month period were well under maximum permissible levels.

Homogeneous Drawer Fuel Elements *(D. E. White)*

Eight homogeneous fuel blocks, individually composed of UC; UC and Type 304 stainless steel; UC and sodium; or UC, Type 304 stainless steel, and sodium have been fabricated for use by the Reactor Physics Division to compare the effects of plate and rod geometry on reactivity with homogeneous samples of the same composition.

The eight blocks were made from Type 304L stainless steel fuel cans (4.95 by 4.70 by 4.55 cm) vibratorily compacted with particles of UC (250-450 μ) or with a blend of UC and 7.5 wt% Type 304L stainless steel particles. The UC consisted of both depleted and 12.75% enriched material. Four of the cans were backfilled with sodium before sealing.

Thirty-six additional fuel cans containing urania of various enrichments have been requested by Reactor Physics. Thirty-two of these cans will have urania with additions of iron and Type 304 stainless steel, and 26 of these will also be backfilled with liquid sodium.

Capture-to-Fission Fuel Elements *(F. D. McCuaig and A. G. Hins)*

As a means of determining the capture-to-fission ratio of ^{239}Pu and ^{241}Pu, 30 "shoe" assemblies of the type shown in Figure 4 were fabricated. Each "shoe" contained high-purity ^{239}Pu or ^{241}Pu. Four "shoe" assemblies were placed in a cluster on the specimen holder. The clusters were then irradiated in EBWR.

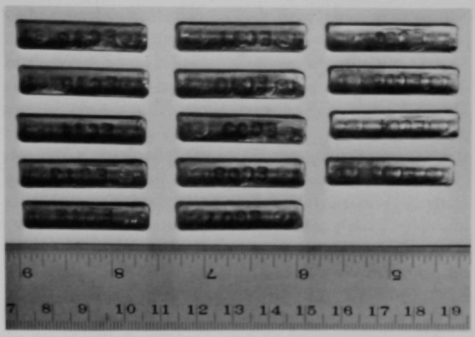

350-1004

Fig. 4. Shoe Assemblies.

PROPERTIES OF ZERO-POWER URANIUM-PLUTONIUM METAL FUELS *(H. V. Rhude and D. R. O'Boyle)*

The fuel alloy selected for the Zero-Power Plutonium Reactor (ZPPR) is a U-Pu-Mo alloy containing 36 wt% plutonium (25 wt% fissionable $^{239,241}Pu$, remainder ^{240}Pu). Previous studies[24] established that the addition of 2.5 wt% molybdenum to U-Pu alloys containing up to 30 wt% plutonium will adequately improve the mechanical and physical properties and corrosion resistance of the highly pyrophoric U-Pu alloys. Since little information was available for alloys containing more than 30 wt% plutonium, tests were conducted to determine the properties of the 36 wt% plutonium alloys.

Two compositions of ternary U-Pu-Mo, U-36 wt% Pu-2.5 wt% Mo and U-36 wt% Pu-3.7 wt% Mo, were examined by means of x-ray diffraction and metallography; microhardness and dilatometric measurements were also made. The x-ray diffraction studies indicated that both alloys are predominantly zeta U-Pu and the 3.7 wt% molybdenum alloy contains more retained gamma than the 2.5 wt% molybdenum alloy. A comparison of the corrosion resistance of the ternary (U-Pu-Mo) alloys and the binary (U-Pu) alloys suggests that some molybdenum is soluble in the zeta phase, which reduces the susceptibility of this phase to air corrosion and intergranular cracking.

[24] L. R. Kelman, H. V. Rhude, J. G. Schnizlein, and H. Savage, "Metallic Plutonium Alloys for Fast Critical Experiments," *Plutonium 1965*, Proc. Third Intl. Conf. on Plutonium, London, England, 1965, A. E. Kay and M. B. Waldron, eds. Chapman and Hall, London, 1967, pp. 510-524.

Corrosion tests with the 2.5 wt% molybdenum alloy resulted in a slight amount of surface powdering after a 30-day exposure to an air atmosphere and only slight additional surface powdering after a six-month exposure. The 3.7 wt% molybdenum alloy exhibited no surface powdering after an exposure of six months to an air atmosphere. During the six-month test both alloys developed a black surface layer, but showed no signs of cracking or disintegration. Both alloys showed a weight gain of approximately 0.09% during the first five weeks of the air-corrosion test, but gained no further weight during the next 20 weeks.

The following results were obtained from studies of the mechanical and physical properties of both alloys: (1) microhardness readings of as-cast plates varied between 380 and 405 DPH. These values agree with the microhardness of zeta U-Pu in the as-cast condition, as Ellinger[25] has determined, (2) thermal expansion measurements gave expansion characteristics comparable to those of alloys with lower plutonium contents, and (3) increased plutonium content resulted in an unexpected improvement in the machinability of the alloys.

In summary, the corrosion resistance and other properties of both U-Pu-Mo alloys are adequate for use in ZPPR. The alloy with the lower molybdenum content (U-36 wt% Pu-2.5 wt% Mo) has been selected for use in ZPPR because of a greater density of fissionable atoms. Compression tests with the two alloys are scheduled for 1968.

EBR-II Research and Development

SWELLING BEHAVIOR OF MARK-IA FUEL ELEMENTS

(F. G. Foote, K. F. Smith, and R. J. Fousek)

Experiments were made to determine the cause of the variable swelling behavior of Mark-IA fuel elements.[26] The swelling results are summarized in Figure 5. The study has determined that the effect of impurity elements is a primary source of variable swelling.

Extensive analyses for the impurities carbon, silicon, aluminum, and iron have been made, and a good correlation between swelling behavior and silicon content was obtained. As shown in Figure 6, silicon in amounts exceeding

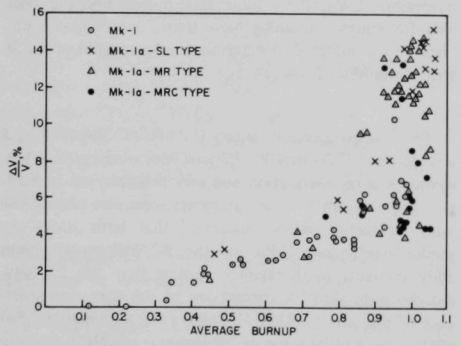

106-9758

Fig. 5. Swelling of EBR-II Driver Fuel as a Function of Average Burnup.

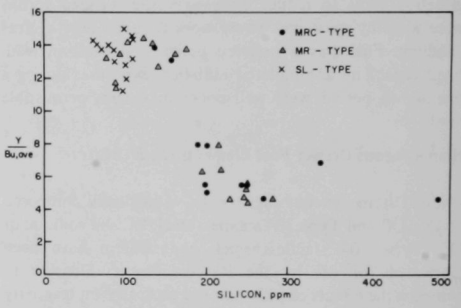

51638

Fig. 6. Unit Swelling of Mark-IA Fuel as a Function of Silicon Content.

about 200 ppm by weight is beneficial and, if not already present, should be added to all melts in amounts of from 250 to 500 ppm; thus, silicon is now considered a vital alloying element rather than an impurity. The other trace elements (carbon, aluminum, and iron) apparently have little effect upon swelling behavior.

Since the Mark-IA design can accept at least 15% fuel swelling without jacket failure, and since fuel alloys with higher silicon content swell only about 5% at the presently established average burnup limit of 1.05 at.%, extension of the burnup of silicon-containing alloys well beyond this limit is now possible. Irradiation tests are under way to establish swelling behavior at higher burnups and to study the effect of silicon at the 500 to 1000 ppm level.

Tests to evaluate the effect of several other factors upon fuel swelling have also been carried out. Variables such as

[25] F. H. Ellinger, R. O. Elliott, and E. M. Cramer, J. Nucl. Mater. *3*, 233-243 (1959).

[26] F. G. Foote, Annual Progress Report for 1966, Metallurgy Division, ANL-7299, pp. 102-113.

change in fuel-element design from Mark-I to Mark-IA, increase in enrichment from 48 to 52%, position of the pin in the casting bundle, and orientation of the fuel pin in the fuel element (top of cast pin at top or at bottom of the fuel element) had no significant effect upon fuel-pin swelling. An increase in the gas-plenum pressure from 50 to 330 psi decreased fuel swelling by about a factor of two. But, since these results were obtained with samples that swelled from 70 to 80% at the lower pressure, an improvement of the same magnitude probably could not be obtained if the maximum swelling had been only the 15% acceptable for the Mark-IA fuel-element design. Preirradiation heat treatment also affects the swelling behavior to some extent. The lowest swelling values were obtained with material in the as-cast condition and as-quenched from the high-gamma region (900-980°C). After aging for 1 hr at 500°C, the swelling was about 1.25 times greater than the lowest swelling values. Unfortunately, all fuel used in EBR-II receives this aging treatment as part of the sodium-bonding operation.

Microstructures of Unirradiated Fuel Pins *(S. T. Zegler and H. V. Rhude)*

Comprehensive studies were made of the microstructure of a number of U-5 wt% Fs alloy driver fuel pins that were prepared for the EBR-II, Mark-I, and Mark-IA (SL*-series) cores. The purpose of the study was to determine microstructural features that may have affected the rates at which the two materials swell during irradiation; Mark-I pins apparently swell at more moderate rates than the Mark-IA pins.

The studies were limited to one or two pins from each of 10 melts for the Mark-I core (a total of 150 melts were prepared) and to one pin from each of 10 melts for the Mark-IA core (50-melt total). The compositions of all the pins were approximately the same; the main difference was the concentration of ruthenium and impurity elements. The major impurities were those normally found in reactor-grade uranium, which include carbon, oxygen, nitrogen, silicon, copper, aluminum, iron, and nickel. Of these, the concentrations of carbon and oxygen varied over the widest range (from <100 to a maximum of 300 ppm by weight). Silicon, iron, and nickel contents were as high as 200 ppm; nitrogen, copper, and aluminum concentrations generally were less than 100 ppm.

Numerous microstructural variations were noted in the pins, but none were unique or consistent for either of the two types of materials. "As-injection-cast" microstructures consist essentially of alpha uranium and retained gamma, as well as phases based on U_2Ru, delta (UMo), UC, and UO_2. When less than 150 ppm each of carbon and oxygen are present, the latter two phases occur generally in very small amounts (less than 1 vol%) uniformly distributed throughout the lengths of the pins. When the maximum concentrations of carbon and oxygen are present (300 ppm), both the UC and UO_2 phases occur in a highly segregated manner and are often associated with shrinkage voids. When the remaining impurity elements are present in the maximum cited amounts, no phases that contain these elements are clearly discernible in the microstructures. However, the results of other work[27] have shown that a silicide (composed mainly of U_3Si_2) containing some molybdenum does occur when the silicon content is increased from 200 to 400 ppm. This is significant because a number of Mark-I pins (from melts that were not included in the present work) contain silicon in amounts as high as 1000 ppm. The generally more moderate swelling of the Mark-I pins may be related to the presence of the silicide. We have also demonstrated that the compounds U_6Fe and UAl_2 occur in the fissium alloy when iron and aluminum are present in amounts greater than 500 ppm.[27]

The sodium-bonding treatment, to which all pins are subjected during processing and which involves a thermal treatment of approximately 1 hr at 500°C, has two major effects upon microstructure: the complete transformation of gamma-to-alpha with an attendant increase in density, and the precipitation of extremely fine secondary-phase particles (~400Å diam) with an attendent marked increase in hardness. The precipitation occurs largely at the center of equiaxed parent gamma-grains rather than at the grain boundaries where precipitation of U_2Ru and U_2Mo usually occurs prior to the bonding treatment, i.e., during cooling from the melt.

The subsequent storage of the pins in the EBR-II reactor vessel involves a thermal treatment of approximately two to four weeks at 370°C, and has little effect on the microstructures caused by bonding or the related hardness and density.

The as-cast microstructures of all the pins are characterized by extensive coring, which generally is more pronounced at the midlengths of the pins than at the top and bottom ends. Coring reflects a concentration gradient of fissium from the center to the edge of gamma grains formed upon solidification; the fissium content is minimum at the centers of the grains and maximum at the grain boundaries. Because of the high content of fissium at the boundaries, U_2Ru particles are readily formed during cooling in the solid state, and are often in a highly

*SL–fuel pins (shorter in length than the original Mark-I pins) cast from virgin metal.

[27]S. T. Zegler and H. V. Rhude, unpublished data.

coalescent state. Subsequent sodium bonding and storage of the pins has little effect on homogenizing the cast structure. The effect of coring on swelling behavior has not been resolved. The problem is currently being investigated in irradiation tests in CP-5.

The parent gamma grain size, which depends on the cooling rate at high gamma temperature, above 720°C, is also highly variant in all the pins. Generally, grain size is largest at the bottom of the pins, which are cooled slowly, and smallest at the top, which are cooled more rapidly. Average grain diameters range from 0.01 to 0.10 mm. The effect of gamma grain size on swelling is also being investigated in irradiation tests in CP-5.

Hot-Laboratory Examination of Irradiated Fuel Pins
(D. R. O'Boyle)

The microstructure of U-5 wt% Fs fuel irradiated in EBR-II has been examined to determine (1) the swelling mechanism responsible for volume changes during irradiation, (2) the microstructural differences caused by manufacturing variables,* and (3) the phases in equilibrium in the fuel during irradiation. Samples from irradiated pins of each fuel type were examined by optical and electron metallography, x-ray diffraction, and electron-probe microanalysis; density and dimensional measurements were also made. Fuel swelling was calculated from dimensional measurements that were made along the length of a bare fuel pin. The plot of fuel swelling versus temperature during irradiation suggested that the controlling swelling mechanism is mechanical tearing similar to that reported by Angerman[28] and by Leggett[29] for uranium and dilute uranium alloys. To confirm this hypothesis, 19 irradiated specimens were submitted to Pacific Northwest Laboratories (PNL) for detailed examination by means of electron microscopy and x-ray diffraction; density measurements were also made. Electron microscopy revealed extremely small mechanical tears (0.1-1.0 μ in length) in the three types of fuel. The number of tears per unit volume of fuel varied with temperature and burnup; as the irradiation temperature increased the number of microtears per unit volume generally increased. At a fixed temperature the number of microtears per unit volume increased with burnup. A typical distribution of microtears in U-5 wt% Fs irradiated at 550°C is shown in Figure 7. The microtears

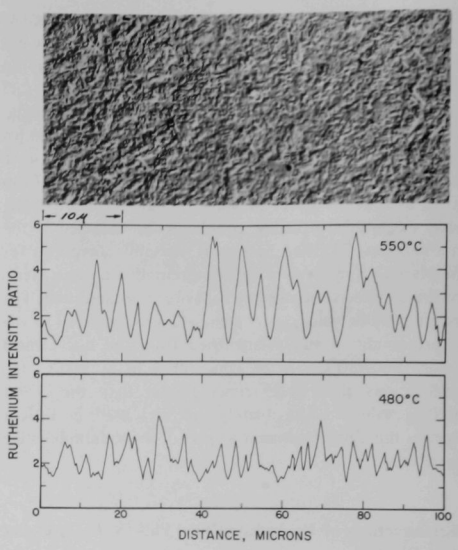

48195
Top 51854

Fig. 7. Fuel Structure and Variation in Ruthenium Concentration in U-5 wt% Fs Irradiated in EBR-II to 0.76 at.% Burnup. The electron micrograph shows microtears that develop in U-5 wt% Fs during irradiation. Electron probe x-ray traces show the variation in ruthenium concentration at the center (irradiated at 550°C) and near the edge (irradiated at 480°C) of the fuel pin.

appear as black areas that are irregular in shape and are distinguishable by the shadow cast toward the lower right of the illustration. In the temperature range from 450 to 550°C, inert-gas bubbles approximately 200Å in diam were visible in the three fuel types. A high concentration of bubbles was visible in certain grains in fuel irradiated above 560°C.

The phases in equilibrium in the fuel during irradiation were determined by electron-probe microanalysis of a complete cross section of a pin irradiated to 0.76 at.% burnup. The variation in ruthenium, molybdenum, and uranium concentration was measured near the circumference of the fuel (irradiated at 480°C) and near the centerline of the fuel (irradiated at 550°C). The linear variation in ruthenium at these two locations is shown in Figure 7. Even though large variations in ruthenium occur in the fuel, which corresponds to the precipitation of U_2Ru, the precipitates could not be identified after either electrolytic or cathodic etching of the irradiated fuel. An analysis of the probe results shows that during irradiation the intermediate phases (U_2Ru and U_2Mo) precipitate in the alpha-uranium matrix, and their rate of growth is

*These variables consist of three fabrication procedures: MR–melt-refined, recycled fuel pins, MR-C–melt-refined, recycled fuel pins containing considerable amounts of reject pins and pin ends from previous castings, and SL–fuel pins (shorter in length than the original Mark-I pins) cast from virgin metal.

[28]C. L. Angerman and G. R. Caskey, Jr., J. Nucl. Mater. *13*(2), 182-196 (1964).

[29]R. D. Leggett, T. K. Birerlein, B. Mastel, and H. A. Taylor, USAEC Report BNWL-SA-154, Battelle Northwest Laboratory, 1967.

controlled by the irradiation temperatures. At 550°C the intermediate phases have grown larger than when irradiated at 480°C (Figure 7). The electron-probe microanalysis also showed evidence of the heavy precipitation of molybdenum and ruthenium that occurs at gamma grain boundaries in the original casting. The microanalysis of the carbides in the irradiated fuel showed that they are uranium-zirconium carbides with no iron, silicon, or aluminum present.

In summary, we conclude that (a) the mechanism that controls the swelling of U-5 wt% Fs driver fuel irradiated at temperatures less than 560°C is microtearing and is not due to the formation and agglomeration of inert-gas bubbles. The microtears responsible for swelling are visible only at high magnification (>2000X). (b) The SL-, MR-, and MR-C-type fuels show little microstructural difference after irradiation. (c) During irradiation of U-5 wt% Fs at temperatures less than 550°C, the phases in equilibrium in the fuel are alpha uranium, U_2Ru, and U_2Mo. (d) The intermediate phases, U_2Ru and U_2Mo, precipitate and grow as a function of temperature and time at approximately the same rate as in unirradiated U-5 wt% Fs.

DEVELOPMENT OF MARK-II DRIVER FUEL ELEMENTS *(W. N. Beck, M. A. Pugacz, and J. H. Kittel)*

The EBR-II Mark-I series of driver fuel elements offers limited possibility for improvement of achievable burnup levels. At present, allowable peak burnup is 1.2 at.% at a reactor power level of 45 MW. While peak burnup will be increased as a result of work now in progress on Mark-IA fuel elements, the allowable burnup level at the proposed reactor power levels of 50 and 62.5 MW will remain under 2 at.%. The anticipated reduction of allowable burnup would result from the increased fuel swelling rates and weaker cladding strengths that are associated with the higher fuel-element temperatures at increased power levels. The lower fuel burnups will, in turn, correspond to increased consumption rates of fuel subassemblies. Subassembly consumption rates will be increased further when the reactor plant factor is increased to 50 or 70%, as projected. Clearly, a more advanced design of driver fuel element is required that incorporates performance goals which will permit burnups of at least 3 at.% at a reactor power level of 62.5 MW.

The design of an advanced fuel element is predicated on the experimentally observed fact that if metallic fuel is permitted to swell sufficiently within the cladding, interconnection of voids within the fuel permits escape of enough fission gas to enable the cladding to restrain further swelling. Irradiations under the LMFBR program have shown that experimental metallic fuel elements designed on this basis can be irradiated to a burnup of at least 4.6 at.% without cladding failure. The results indicated that development of an advanced (Mark-II) fuel-element design using U-5 wt% Fs alloy is feasible and should be undertaken without delay.

With these observations in mind, a reference design for the Mark-II element has been established. The fuel is U-5 wt% Fs alloy, sodium-bonded to Types 304 or 316 stainless steel cladding. The dimensions of the Mark-II fuel element are listed in Table 6. The dimensions of the Mark-I and Mark-IA designs are included for comparison.

TABLE 6. Dimensions of Fuel Elements

	Mark-I	Mark-IA	Mark-II
Fuel-pin diam, in.	0.144	0.144	0.130
Fuel-pin length, in.	14.2	13.5	14.2
Sodium-bond thickness, in.	0.006	0.006	0.010
Cladding thickness, in.	0.009	0.009	0.012
Cladding ID, in.	0.156	0.156	0.150
Cladding OD, in.	0.174	0.174	0.174
Fuel-pin restrainer gap, in.	0.40	0.40	0.70
Plenum length, in.	2.2	2.9	10.3
Fuel-element length, in.	18	18	26

In order to determine the effect of variations in design parameters on fuel-element performance, a total of 62 Mark-II fuel elements, individually encapsulated, will be irradiated in a special Type B-37 subassembly in EBR-II. Thirty-seven capsules will constitute a subassembly, and 25 additional capsules will be used as substitutes at predetermined burnup intervals of 1, 2, 3, 4, and 5 at.%. Postirradiation examinations are scheduled at these projected burnup levels. Both 80 and 93% enriched fuel will be used so that simulations of reactor operation at 50 and 62.5 MW can be obtained.

The irradiations will evaluate the relative performance of a 24-in.-long Mark-II element and the preferred element length of 26 in. Thus, different gas plenum volumes will be tested to evaluate the effects of a wide range of pressures and burnup levels. The sodium levels in the two fuel elements will be adjusted to control the pressure. The irradiations will also determine the relative performance of three axial fuel-restrainer designs.

A total of 67 injection-cast fuel pins (clad in Type 304L stainless steel tubes of 0.174-in. OD by 0.150-in. ID, sodium bonded, and sealed) were received from the Plutonium Fabrication Facility. Of this total, 35 fuel pins were clad in tubes 26 in. in length and the remaining 32 in tubes 24 in. in length. The sodium levels were ~0.21 and ~0.71 in. above the top of the pins for the 24- and 26-in.-long elements, respectively.

The fuel elements were placed in secondary containment capsules that contained a predetermined amount of sodium for heat conduction from the fuel element to the EBR-II coolant sodium. The capsules were sealed (welded in an atmosphere of helium), leak tested, and finally sodium bonded by an impact vibrator while held at a temperature of 500°C for 3 hr. This step was considered necessary to promote wetting of all the surfaces; thus, voids or gas bubbles, which could cause hot spots, were eliminated. The sealed capsules were examined for sodium-bond defects by radiography and pulsed electromagnetic inspection techniques. After successful completion of these tests, extensions with identification numbers were welded to the ends, and the capsules were shipped to Idaho for assembly into a Type B-37 experimental subassembly.

The objective of the irradiations of Mark-II driver fuel subassemblies is to test the performance of the complete subassemblies. The irradiations will also establish confidence levels relating to Mark-II fuel-element performance under conditions amenable to statistical treatment.

This second-phase evaluation of the Mark-II element consists of irradiations of unencapsulated elements in complete Mark-II, 91-element subassemblies. These subassemblies will, therefore, function in EBR-II as driver fuel subassemblies. They will be exposed to sodium flow so that any effects due to the primary coolant can be determined.

A total of five subassemblies are scheduled for irradiation. The burnup levels will range up to 5 at.%. The insertion of each subassembly will be timed to occur after the removal and examination (at the predetermined burnup levels of 1, 2, 3, 4, and 5 at.%) of the encapsulated elements.

Selection of the preferred axial fuel-restrainer design and the gas plenum volume for the subassembly irradiations will be based on examination results of the encapsulated irradiations at 1 and 2 at.% burnup.

The necessary hardware for the assembly of the elements has been purchased or manufactured. Both Type 304L and Type 316 stainless steel tubing, which will be used for fuel cladding, has been received and nondestructively examined. Sufficient quantity of each type of tubing is available to fabricate 1000 Mark-II elements. The end plugs for these elements have been fabricated.

Arrangements are being made for the casting of the pins and assembly of the elements in the Idaho-FCF cold line. One thousand Vycor molds have been transferred from Illinois to the Idaho site for injection casting of the Mark-II pins.

The EBR-II Irradiation Evaluation Committee has approved, in principle, the irradiation of the five Mark-II subassemblies. Final Mark-II element and subassembly drawings have been completed. An evaluation of the Mark-II-subassembly design is being conducted preparatory to final submission for approval by AEC-RDT.

FABRICATION OF OXIDE-ROD FUEL ELEMENTS

(N. J. Carson)

Thirty-eight $(U_{0.8}Pu_{0.2})O_2$ pellet-fueled elements were fabricated in mid-1967 for irradiation in EBR-II followed by destructive testing in TREAT. The elements fit a standard B-37 irradiation assembly in EBR-II. Each element has an 18-in.-long fuel section that can be cut out and used in TREAT following irradiation in EBR-II. The elements will be used to introduce the variable of burnup into studies of failure mechanisms and thresholds.

Each jacket subassembly was fitted with a loading funnel and covered with shrinkable electrical insulation. This completely enclosed assembly was loaded inside the glove-box without any contamination to the outside portions of the jacket.

The length, diameter, and weight of each pellet was measured before loading. A tantalum disk was added, and the distance between the disk and the top of the jacket was measured with a depth gage. This measurement was used to insure that the pellets were at the correct depth and to determine the required length of the restrainer spring.

The ends of the jacket tube were sealed with plugs attached by TIG welding. Welding conditions were determined beforehand by metallography, and quality control was based on x-radiography. All fuel sections were checked for contamination, first by counting wipes, then by direct counting. All materials leaving Building 350 read less than 10 dis/min of loose contamination and less than 500 dis/min of fixed contamination.

All fuel sections were leak tested with a leak detector (helium mass spectrometer) calibrated with a standard leak of 3.7×10^{-8} standard cm^3/sec. No element with a leak indication greater than that of the standard leak was accepted. Each completed fuel section was subjected to x-ray so that the overall position of the pellets within the fuel tube could be determined.

EVAPORATION OF PuO_{2-x} *(D. R. Messier)*

A study of the evaporation behavior of compositions of oxygen-deficient plutonium dioxide has been concluded. Figure 8 shows the results of a preliminary series of tests of the kinetics of evaporation in vacuo at 2090°K of a $PuO_{2.00}$ pellet contained in a rhenium wire coil. The data, obtained by reoxidizing and rerunning the same specimen several times, show the large preferential loss of oxygen that occurs during the initial evaporation period. The weight loss probably originates from a complex process that involves the diffusion of oxygen from a phase of continuously varying composition.

The preliminary kinetic results showed that the rate of loss of oxygen and, thus, the rate of approach to the congruently evaporating composition, was extremely slow. Specimens that were used for subsequent Knudsen-cell runs were, therefore, prereduced to low O/Pu ratios by heat treatment in dry hydrogen.

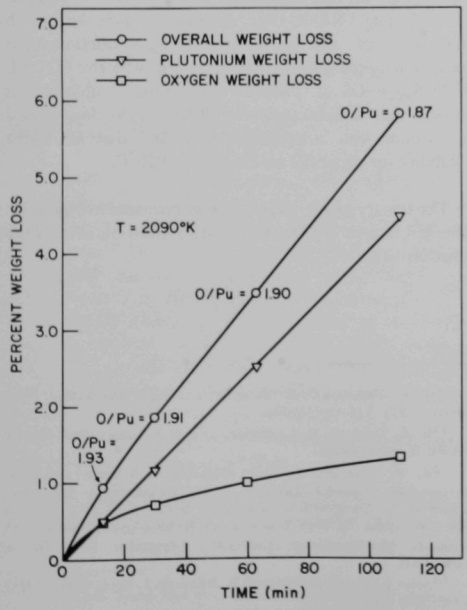

106-9714

Fig. 8. Evaporation of a PuO_2 Pellet at 2090°K.

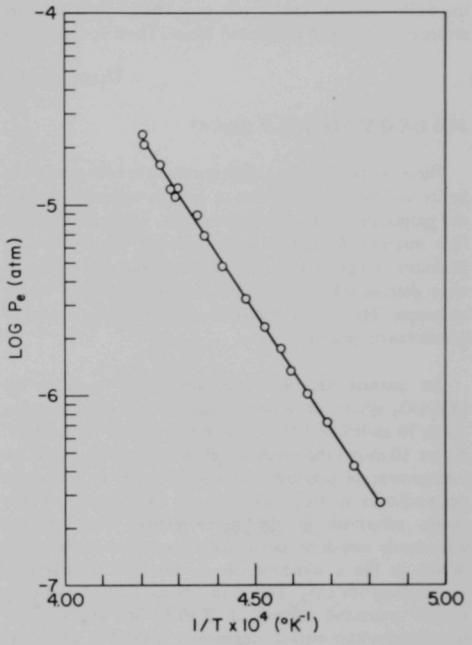

106-9718

Fig. 9. Vapor Pressure versus Temperature for the Evaporation of $PuO_{1.83}$ over the Temperature Range from 2070 to 2380°K.

The results of a series of tests with tungsten Knudsen cells on a specimen of initial O/Pu ratio of 1.83 are presented in Figure 9. The tests were made in the temperature range from 2070 to 2380°K. The equation best fitting the data is

$$\log_{10} P_e \text{ (atm)} = 8.38(\pm 0.11) - \frac{30.97(\pm 0.25) \times 10^3}{T} \quad (1)$$

where P_e is the pressure assuming that the vapor is entirely PuO_2(g). During the entire series of tests, about 5% of a 1.4 g specimen was evaporated, and the O/Pu ratio changed only from 1.83 to 1.81. This small change in the O/Pu ratio indicates that the ratio for the congruent composition must be close to 1.82 in the temperature range investigated (2070-2380°K).

Additional experiments with the Knudsen cell were made on compositions with O/Pu ratios of 1.56 and 1.62 at

temperatures of 2240 and 2380°K. The evaporation of the $PuO_{1.56}$ composition was univariant at both temperatures, which indicates the existence of two condensed phases. The evaporation of the $PuO_{1.62}$ composition was bivariant; i.e., the O/Pu ratio increased with time, which indicates the presence of a single condensed phase. These results are in accord with the proposed phase diagram for the plutonium-oxygen systems,[30,31] which shows that the boundary of the PuO_{2-x} phase remains fixed at $PuO_{1.61}$ at temperatures up to the liquidus. Ohse and Ciani[32] also observed similar evaporation behavior at temperatures up to 2200°K.

Uranium-Mixed Anion Systems

THE U-S-O SYSTEM *(P. D. Shalek)*

Phase relations in the U-S-O system have been studied to better understand the effects of oxygen contamination on the properties of uranium monosulfide, a potential reactor fuel material. Compacts were thermally equilibrated in individual tungsten cells, and liquidus and solidus curves were determined by using a modified Mendenhall wedge technique. The general approach was to examine a series of pseudobinary systems.

An unusual structural relationship was found in the UOS-UO_2 system, in which, contrary to substitution rules, up to 70 mole% of UO_2 was soluble in the UOS structure. Figure 10 shows the similarity of the two structures in the arrangement of uranium and oxygen atoms in the planes perpendicular to the c axis. As the 28% smaller oxygen atoms substitute in the sulfur double layer, a predominantly one-dimensional accommodation of the strain occurs in the c direction, as c_0 for UOS contracts to approach a_0 for UO_2. The 70 mole% solid solution of UO_2 showed peritectic melting at 2090°C, and the stoichiometric oxysulfide melted congruently at 1880°C. There was no detectable solubility of UOS in UO_2.

A simple eutectic was found for the US-UO_2 system which showed no indication that the region of liquid immiscibility reported for the U-UO_2 system[33] extends to this portion of the U-S-O ternary system. The eutectic occurs at about 44 mole% UO_2 and at a temperature of 1985°C; the melting points of US and UO_2 were determined to be 2451 and 2843°C, respectively. By applying the Clausius-Clapeyron equation to the liquidus data, the heats and entropies of fusion for US and UO_2 are calculated to be 28.6 kcal/mole and 9.18 cal/°C mole, and 20.8 kcal/mole and 7.68 cal/°C mole, respectively.

The pseudobinary systems US-UOS and U_2S_3-UOS were eutectic in nature with melting-point minimums occurring at 1675 and 1625°C, respectively. The U_2S_3 phase, however, showed peritectic melting at 1810°C.

Selected ternary observations confirmed the eutectic nature of the US-UOS-U_2S_3 subsystem, which can be represented by the equation L = US + UOS + U_2S_3 at 1590°C. The US-UOS-UO_2 subsystem, which was much more complex, can be represented by a reaction intermediate between eutectic and peritectic, whereby UO_2 + L = UOS_{ss} + US at 1730°C. Other ternary observations showed that liquids containing UOS or U_2S_3 decomposed in vacuum with a net sulfur loss, and that US had a solubility for about 0.7 mole% UO at 1950°C.

The ternary phase relations are summarized in Figure 11. The U-US and U-UO_2 binary data were obtained from other investigators.[34,35]

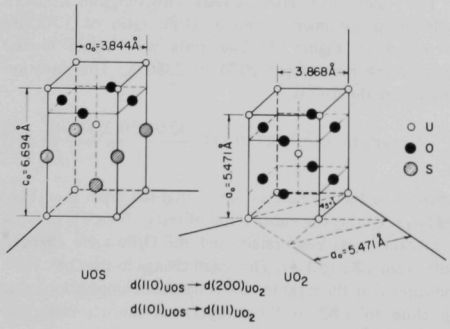

Fig. 10. Relationship between the UOS (PbFCl) and $UO_2(CaF_2)$ Structures.

30T. D. Chikalla, C. E. McNeilly, and R. E. Skavdahl, J. Nucl. Mater. *12*(2), 131-141 (1964).

31E. R. Gardner, T. L. Markin, and R. S. Street, Brit. Report, AERE-R 4602 (1964).

32R. W. Ohse and V. Ciani, *Evaporation Behavior and High-Temperature Thermal Analysis of Substoichiometric Plutonium Oxide in the Composition Range from O/Pu = 1.51 to 2.00*, Proc. 3rd Intl. Symp. on High Temperature Technology, Asilomar Conf. Grounds, Pacific Grove, California, September 1967 (to be published).

33Allan E. Martin and Russell K. Edwards, J. Phys. Chem. *69*(5), 1788 (May 1965).

34O. Kubaschewski, Trans. Brit. Ceram. Soc. *60*, 67-83 (1961).

35Chemical Engineering Division Research Highlights, May 1964-April 1965, ANL-7020, pp. 163-164.

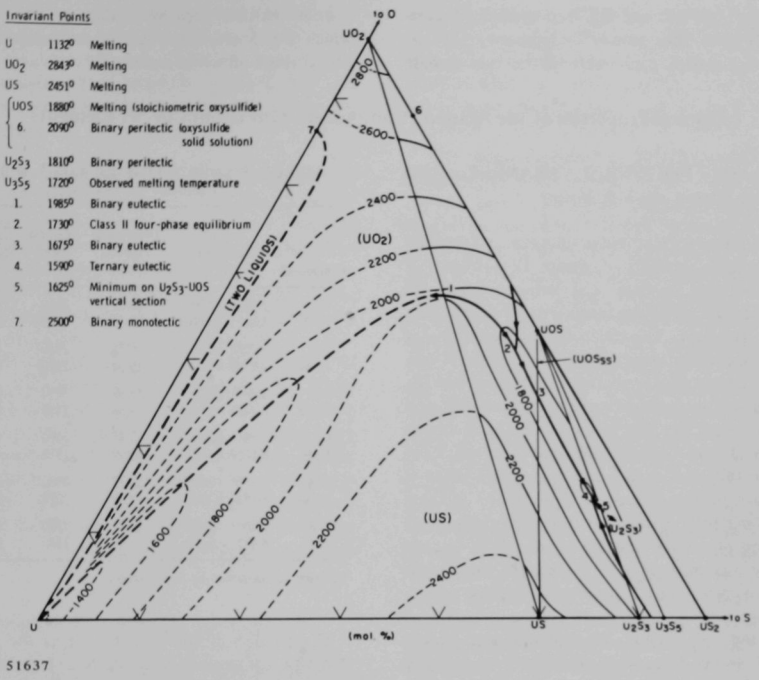

Fig. 11. Phase Diagram for the U-US_2-UO_2 Portion of the U-S-O System at Equilibrium Vapor Pressure.

THE UP-US SYSTEM *(Yehuda Baskin)*

The NaCl-type compounds UP and US exhibit complete mutual solubility, and the lattice parameters of the two compounds show a slight positive deviation from Vegard's relationship.[36] The existence of a maximum in the liquidus temperature was reported previously for specimens that melted under a dynamic atmosphere of helium gas.[37,38] The maximum, which occured at a temperature of 2670°C, and an initial composition of approximately $U(P_{0.67}S_{0.33})$, was 100°C higher than the melting temperature of UP under identical conditions. However, x-ray analyses of the melted specimens revealed the presence of metallic uranium and indicated that substantial dissociation occurred under a helium atmosphere.

In this study, the pellets were encapsulated in tungsten crucibles, and dissociation was prevented because the samples were in equilibrium with their vapor at elevated temperatures; x-ray and metallographic examinations of the samples did not show the presence of metallic uranium. A melting temperature maximum at the same initial composition $[U(P_{0.67}S_{0.33})]$ was again observed, but, by preventing dissociation, the liquidus temperatures of the UP-rich compositions were 100°C higher than the temperatures of samples melted under helium. However, metallographic analyses revealed that the melted samples contained varying amounts of dissolved tungsten that ranged from 60 at.% in UP to less than 1 at.% in US. Metallographic examination also indicated that tungsten formed eutectics with UP and with UP-rich solid solutions; with the exception of US, eutectic temperatures probably were observed rather than true melting-point or liquidus temperatures.

Thus, the observed phenomenon of a melting temperature maximum appears to be related to the formation of eutectics with tungsten and occurs because the W-$U(P_{0.67}S_{0.33})$ eutectic temperature is higher than either the W-UP eutectic temperature or the US melting point. The smooth shape and positive deviation of the UP-US lattice parameter curve makes it highly unlikely that a real melting maximum exists in this system similar to maxima

[36] Y. Baskin, Trans. Met. Soc. AIME *239*, 1708-1712 (1967).

[37] Y. Baskin and P. D. Shalek, Annual Report for 1963, Metallurgy Division ANL-6868, pp. 156-157.

[38] Y. Baskin, Annual Progress Report for 1965, Metallurgy Division, ANL-7155, pp. 127-128.

reported for the ZrC-TaC and HfC-TaC systems,[39] especially since Norton and Mowry[40] reported that the room-temperature lattice parameters of the two carbide systems exhibit negative deviations from Vegard's law, which are most pronounced in the compositional regions that correspond to the maxima.

Physical Properties of the Actinide Compounds with Groups IV-VI Elements

COMPOUNDS OF PLUTONIUM, URANIUM, AND THORIUM *(O. L. Kruger and J. B. Moser)*

The actinide elements plutonium, uranium, and thorium and the nonmetallic elements of groups IV (carbon), V (nitrogen, phosphorus, arsenic, and antimony) and VI (sulfur, selenium, and tellurium) form compounds that have the NaCl-type structure. The electronic configurations of these compounds are extremely complex because of variations in the energy-state distribution of electrons and the changes in degree of mixed bonding (metallic, covalent, and ionic) that can occur. Because of the interest in monocarbides, mononitrides, monophosphides, and monosulfides as constituents in fast reactor fuels, an appreciable effort is being made to determine the physical properties of these compounds. Since little is known of the other compounds of uranium and plutonium and the nonmetals of Groups IV-VI, a study was undertaken to prepare the compounds and to measure their lattice constants and melting points.

Uranium and plutonium monophosphides, monoarsenides, and monosulfides were synthesized by reaction of the decomposed metal hydride with phosphine, arsine, or hydrogen sulfide gas.[41,42] The antimonides, selenides, and tellurides were prepared by arc-fusion of the elements. High-purity uranium and plutonium and nonmetal elements with a minimum purity of 99.999 wt% were used in this study. Compositions of 50, 53, and 55 at.% nonmetal were prepared to determine the lattice constants of the binary phases in equilibrium with phases of higher nonmetal content.

The results of chemical analyses for oxygen and nitrogen, and of the determinations of lattice constants and melting points of the various compounds are given in Table 7. Although some of these compounds have nonmetal defect structures and exist over a range of compositions, only the maximum value of the lattice constants are reported.

TABLE 7. Properties and Chemical Analyses of Uranium and Plutonium VA-VIA Compounds

Compound	Lattice Constant, Å	Theoretical Density, g/cm³	Melting Point, °C	Chemical Analyses	
				Oxygen, wt%	Nitrogen, wt%
UP	5.5888 ±0.0001	10.22	2610	0.04	0.06
PuP	5.6613 ±0.0001	9.89	2600[a]	0.05	0.02
UAs	5.7788 ±0.0001	10.77	2540[a]	0.07	0.005
PuAs	5.8586 ±0.0001	10.34	2420[a]	0.08	0.006
USb	6.2091 ±0.0001	9.98	1850	0.06	0.03
PuSb	6.2411 ±0.0004	9.86	1980	0.02	0.01
US	5.4847 ±0.0001	10.87	2480	0.04	0.01
PuS	5.5412 ±0.0001	10.59	2350	0.03	0.01
USe	5.7399 ±0.0003	11.13	2080	0.09	0.03
PuSe	5.7934 ±0.0001	10.86	2075	0.02	0.02
UTe	6.150 ±0.001	10.55	1720	0.08	0.04
PuTe	6.183 ±0.001	10.31	1870	0.02	0.02

[a]Melting accompanied by vaporization.

Comparison of the data for all of the actinide group IVA-VIA compounds with the NaCl-type structure shows that the lattice constants generally increase with the number of electrons in the inner shell of the nonmetal element. In the same period, however, this spacing decreases as the number of electrons in the valence shell of the nonmetal increases.

Thorium monotelluride was reported to have the CsCl-type structure[43] with a lattice constant of 3.827Å and to decompose below 1000°C in vacuo. In view of the unexpected structure reported, compositions of ThTe and $ThTe_{1.1}$ were prepared by arc-fusion and examined. The CsCl-type structure was confirmed, and the lattice constant of ThTe in equilibrium with a phase of higher tellurium content was 3.8319 ±0.0001Å. The melting point of ThTe was 1680°C.

The melting points of the actinide compounds generally decrease as the number of electrons in the inner shells of the nonmetal atoms increase. Comparison of the melting points of the actinide monocarbides shows that PuC has a much lower melting point (1660°C) than expected. The instability of this compound compared with that of ThC and UC suggests the presence of metallic bonds not present

[39]C. Agte and H. Alterthun, Z. Techn. Physik 11, *182* (1930).

[40]John T. Norton and A. L. Mowry, Trans. Met. Soc. AIME *185*, 133-136 (February 1949).

[41]O. L. Kruger and J. B. Moser, J. Inorg. Nucl. Chem. *28*(3), 825-832 (March 1966).

[42]O. L. Kruger and J. B. Moser, J. Phys. Chem. Solids *28*, 2321-2325 (1967).

[43]R.W.M. D'Eye and P. G. Sellman, J. Chem. Soc. (London), 3760 (1954).

in the other two carbides. All other compounds of plutonium and the more ionic group V and VI nonmetals have melting points similar to those of thorium and uranium compounds. This behavior indicates that the additional electrons in the uranium and plutonium compounds are shielded.

When elements in the same period are compared, the actinides in combination with the group V nonmetals have higher bonding energies (as indicated by their melting points) than compounds with the nonmetals from the other two groups. For example, the mononitrides in period two are more stable than the monocarbides, and the monophosphides in period three are more stable than the monosulfides. The same is true for the group V monoarsenides and monoantimonides compared with the monoselenides and monotellurides of group VI. The monoantimonide and monotelluride of plutonium have melting points 130 and 150°C higher than the corresponding uranium compounds, and thorium monotelluride has the CsCl-type crystal structure. In the compounds with period-five nonmetals, the large nonmetal radius apparently changes the bonding to lower the stability of the NaCl-type structure as the atomic number of the actinide component decreases.

THE US-PuS SYSTEM *(O. L. Kruger and J. B. Moser)*

The US-PuS system was investigated as part of a program to determine the phase relationships in potential fuel materials for fast breeder reactors. Melting points and lattice constants were measured and microstructures were examined to gain information regarding phase relationships in this system.

Melting points of the pure compounds and various solid-solution compositions were found to decrease uniformly from the melting point of US to the melting point of PuS. The solid-solution compositions did not melt abruptly; therefore, the exact temperature of melting could not be determined. The melting point of 2480 ±30°C for US is in excellent agreement with the value obtained by previous investigators.[44]

One objective of this study was to determine the lattice constants for the US and PuS phases. Although these data could not be determined as a function of composition because of the limited accuracy of the sulfur analysis, precise lattice constants were determined for compositions at the sulfur-rich and sulfur-deficient phase boundaries. The maximum lattice constant of US_{1+x}* was found to be 5.4847Å, whereas US_{1-y}* had a value of 5.4810Å. These limits were established from a number of samples that were cooled at various rates from temperatures of 1600 to 1800°C. There was no indication of a change in lattice constant with cooling rate.

The lattice parameter of PuS had a maximum value of 5.5412Å in compacts cooled at various rates from 1600 to 1800°C after annealing for periods of from 2 to 24 hr. A lattice constant of 5.531Å was observed for PuS_{1-y} cooled slowly from 1000°C. The low accuracy of this measurement was the result of interpreting blurred doublets in the x-ray diffraction pattern. This behavior indicated that equilibrium was not attained by slow cooling because of a shift (in the phase boundary) to increase sulfur solubility at low temperatures. Similar results have been observed for PuC_{1-x}, which has an extensive range of solubility for carbon and considerable curvature of the low-carbon phase boundary. Sulfur-rich compositions retained about the same lattice constant whether these compositions were slow cooled or quenched from 1800°C. This comparison shows that the sulfur-rich phase boundary has little curvature below this temperature. Significant increases were observed in the lattice constants of the PuS_{1+x} composition quenched from 2000°C; consequently, there is an apparent shift in the sulfur-rich phase boundary toward higher sulfur solubility above 1800°C. The width of the PuS phase field was estimated from these measurements to be about twice that of the US phase field at 1700°C.

A $(U,Pu)_2S_3$ phase that is isostructural with Pu_2S_3-Pu_3S_4 was found in the sulfur-rich compositions containing 40, 60, and 80 mole% PuS. The U_2S_3 phase was found in the US_{1+x} and $(U,10Pu)S_{1+x}$ compositions. Since the Pu_2S_3 phase is cubic and the U_2S_3 phase has the orthorhombic crystal structure, a transformation to the U_2S_3 structure was expected in compositions with low plutonium contents. Metallographic examination revealed the presence of two sesquisulfide phases in the microstructure of the $(U,10Pu)S_{1+x}$ compositions. The lattice constants of the $(U,Pu)_2S_3$ phase in the other compositions remain close to the value of 8.4211Å, even though the uranium-to-plutonium ratio in this compound changes appreciably. This behavior was expected because the bonding in the sesquisulfide phase is thought to have appreciable ionic character, and substitution of a uranium atom for a plutonium atom would result in an insignificant change in the lattice constant where the ionic radii have almost the same values. The electron probe will be used for further study of this system.

[44] E. David Cater, Paul W. Gilles, and R. J. Thorn, J. Chem. Phys. *35*, 608 (1961).

*The subscript 1+x designates the composition at the sulfur-rich phase boundary and 1-y is used for the composition at the sulfur-deficient phase boundary because "x" could have a negative value. For simplicity, the same terminology has been used for both uranium and plutonium monosulfides.

Structures and Properties of Advanced Fuel Materials

FABRICATION OF CERAMIC FUELS FOR PROPERTY MEASUREMENTS *(O. L. Kruger and J. B. Moser)*

The hot-pressing characteristics of UC, UP, and US powders have recently been investigated because high-density specimens that are needed for thermal property measurements can be obtained by the hot-pressing method of fabrication. Materials densified by this process usually have a fine grain size because grain growth does not occur at the relatively low temperatures and short times used. The densification-rate data were analyzed according to the expression of Rossi and Fulrath[45] who assumed that the strain rate for creep as expressed by the Nabarro-Herring relationship is proportional to the shrinkage rate of the pressure-sintered specimen. A stress-correction factor that takes into account the influence of die-wall constraint on the creep rate and the effect of porosity on applied pressure is included in the expression of Rossi and Fulrath. It is noteworthy that their equation and the one derived from the Mackenzie-Shuttleworth model[46] differ only by a slight change in numerical constant and the correction factors normally used with the latter expression.

Curves of density as a function of time were obtained for pressure-sintered UC, UP, and US from 1200 to 1400°C. The results indicate that a wider temperature range and longer exposure times are needed to obtain a better analysis of the pressure-sintering process. At 1400°C, the UC specimen attained a maximum density of 87% of theoretical in 1-1/2 hr; however, the final density at 1300°C was 81%, and the density at 1200°C was 63% of theoretical. Riley[47] has shown that densities of about 94% of theoretical can be obtained at 1400°C in 30 min with finely divided UC (<4-μ diam particle size). Uranium monophosphide with a particle size of about 5 μ was hot-pressed to a density of about 90% of theoretical in 1 hr at 1200°C; whereas, the same material with an average particle diameter of about 7 μ attained a density of only 85% of theoretical at the same pressure and temperature. These data show that, all other factors being equal, the densification rate increases with decreasing particle size. This behavior suggests a diffusion-controlled process and adds emphasis to the efforts of more recent investigators to invoke diffusion theory for the analysis of the hot-pressing data.

The diffusion coefficients calculated from the hot-pressing data for UC were in excellent agreement with creep-diffusion coefficients calculated by Lee and Barrett.[48] Their calculations were based on measurements of compressive creep rates of UC by Norreys.[49] The latter values were closer to the diffusion coefficients of carbon than to those of uranium. The use of any reasonable correction factor for stress for the hot-pressing data would still leave present measurements in close agreement with the creep data. The diffusion coefficients[50] for UP and US were of the same order of magnitude as the value for UC at 1400°C; therefore, the compounds should have about the same plasticity at this temperature.

Since no end-point density was reached, the data are consistent with a diffusion model for densification. The change in slope of the curves at densities greater than 90 to 95% of theoretical can be attributed to gas entrapped within the closed pores. Further densification would depend on the diffusion rate of the gas from the pores. This process has been described by Coble[51] for pressureless-sintered Al_2O_3. The densification rate above about 95% of theoretical density would probably be extremely slow for pressure-sintering in argon. The curvatures of the plots of density versus time are consistent with this predicted behavior; however, very fine powder of UC has been hot-pressed to a density greater than 98% of theoretical in the short time of 30 min.[47] These results suggest that in argon the densification rate in the closed-pore stage is dependent on the pore distribution and perhaps on the pore configuration. Additional hot-pressing data in vacuum and in argon are needed to clarify the effect of entrapped gas on the end-point density.

FABRICATION OF TANTALUM CARBIDE CONTAINERS *(J. T. Dusek)*

Tantalum carbide powder has been hot-pressed to form a container for the measurement of the thermal expansion of uranium carbide. Tantalum carbide was chosen as the container material since negligible reaction occurs with liquid uranium carbide. The fabricated apparatus consisted of a crucible to contain the uranium carbide, a pedestal to support the crucible in the furnace, and a tantalum-tipped sensing rod to determine the expansion of the uranium carbide.

[45] Ronald C. Rossi and Richard M. Fulrath, J. Am. Ceram. Soc. *48*, 558 (1965).

[46] J. K. Mackenzie and R. Shuttleworth, Proc. Phys. Soc. (London) *62*, 833 (1949).

[47] B. Riley, Brit. Report, AERE-R 4154 (1962).

[48] H. M. Lee and L. R. Barrett, Proc. Brit. Ceram. Soc. 7, 159 (1967).

[49] J. Norreys, "The Compressive-Creep of Uranium Monocarbide," *Carbides in Nuclear Energy* (Macmillan and Co., Ltd., 1964), Vol. I, p. 435.

[50] O. L. Kruger and J. B. Moser, *Densification Processes of Actinide IVA-VIA Compounds*, Proc. Brit. Ceram. Soc. (to be published).

[51] R. L. Coble, J. Am. Ceram. Soc. *45*, 123 (1962).

THERMAL CONDUCTIVITY AND HEAT CAPACITY OF PLUTONIUM MONOPHOSPHIDE AND MONOSULFIDE

(J. B. Moser and O. L. Kruger)

The thermal properties of plutonium monophosphide (PuP) and plutonium monosulfide (PuS) have been measured from room temperature to 650°C by a previously described heat-pulse technique.[52] Disk-shape specimens made by cold-pressing and sintering were used for these measurements. Thermal conductivity was calculated from the product of two measured properties the thermal diffusivity, and the volumetric heat capacity. The data were corrected to theoretical density. The result of a least-squares computer analysis is shown in Table 8, and the heat capacities of the two compounds are shown in Table 9.

TABLE 8. Thermal Conductivity[a] of Plutonium Monophosphide and Plutonium Monosulfide

Temperature, °C	PuP, cal/cm °C sec	PuS-I, cal/cm °C sec	PuS-II, cal/cm °C sec
25	0.0145	0.0233	0.0177
100	0.0148	0.0203	0.0166
200	0.0153	0.0190	0.0162
300	0.0158	0.0202	0.0179
400	0.0165	0.0234	0.0226
500	0.0173	0.0283	0.0281
600	0.0184	0.0344	0.0342
650	0.0189	0.0377	0.0373

[a]Data corrected to theoretical density by means of the Maxwell equation $K_T = (2 + P/2 - 2P)K_M$, and accurate to the third decimal.

TABLE 9. Heat Capacity[a] of Plutonium Monophosphide and Plutonium Monosulfide

Temperature, °C	PuP, cal/g °C	PuS, cal/g °C	Temperature, °C	PuP, cal/g °C	PuS, cal/g °C
25	0.0550	0.0540	400	0.0558	0.0568
100	0.0553	0.0546	500	0.0560	0.0575
200	0.0555	0.0554	600	0.0561	0.0580
300	0.0557	0.0560	650	0.0561	0.0582

[a]Data accurate to the third decimal.

The heat capacity as a function of temperature was essentially constant; therefore, the trend of the calculated values of thermal conductivity of PuP and PuS generally followed that of the measured thermal diffusivity. The thermal conductivity of PuP increased from 0.014 cal/cm °C sec at room temperature to 0.019 cal/cm °C sec at 650°C. Over the same temperature range, PuS changed from 0.023 (batch I) and 0.018 (batch II) to 0.037 cal/cm °C sec, with a minimum observed at 200°C.

[52]J. B. Moser and O. L. Kruger, Annual Progress Report for 1966, Metallurgy Division, ANL-7299, pp. 130-133.

Measurements of electrical conductivity[53] were used to calculate the electronic component of the thermal conductivity of both PuP and PuS. These data were then used to calculate the lattice component, which was found to be equal to 0.01 cal/cm °C sec. The lattice contribution was similar to that of the corresponding uranium compounds, which varied between 0.01 and 0.02 cal/cm °C sec.[52] The total thermal conductivity of PuP is only about 50% that of UP; therefore, the electronic contribution decreases substantially when plutonium is substituted for uranium in the monophosphide. The same comparison, however, cannot be made for the monosulfide because of the pseudometallic behavior of US in contrast to the semiconductor nature of PuS.

Plutonium monophosphide had a heat capacity of 0.055 cal/g °C at room temperature and 0.056 cal/g °C at 650°C. For PuS, the increase with temperature was slightly higher, from 0.054 cal/g °C at room temperature to 0.058 cal/g °C at 650°C.

The heat capacities of the plutonium compounds were approximately 20% higher than those of the corresponding uranium compounds previously studied.[52] This increase is attributed to the difference in specific heat between plutonium and uranium, a difference of 22% at room temperature.[54,55] Values calculated by use of the Kopp-Neumann rule were 6% below the experimental room-temperature determinations.

THERMAL PROPERTIES OF VIBRATORILY COMPACTED CERAMIC FUELS *(N. H. Schilmoeller* and D. E. White)*

An apparatus has been built to study the feasibility of a system to measure the thermal conductivity and thermal diffusivity of vibratorily compacted nuclear ceramic materials. Vibratory compaction of plutonium and plutonium-uranium fuel materials offers some advantages in economy and ease of fabrication over conventional methods of cold pressing and sintering. Thermal-property values for such fuel systems are necessary for the proper design of new elements.

The method of thermal-property measurement described by Harmathy[56] was used as a model. The test system consisted of a container fabricated of 0.90-mm-thick Type

[53]O. L. Kruger and J. B. Moser, J. Chem. Phys. *46*, 891 (1967).

[54]A. E. Kay and R. G. Loasby, Phil. Mag. *9*, 37 (1964).

[55]K. K. Kelly and E. G. King, *CONTRIBUTIONS TO THE DATA ON THEORETICAL METALLURGY, XIV. Entropies of the Elements and Inorganic Compounds*, U. S. Bureau of Mines, Bull. 592 (1961).

*Consultant, Metallurgy Division, from University of Illinois, Urbana, Illinois.

[56]T. Z. Harmathy, J. Appl. Phys. *35*, 1190 (1964).

304 stainless steel, 7.62 cm square and 20.32 cm high. End fixtures held a constantan heating foil in place. The power dissipated by the foil was determined by measuring the current and the voltage drop across the foil. The temperature of the sample was monitored, at selected time intervals, with an iron constantan-foil thermocouple at a distance of 1 cm from the foil heater. The overall test time ranged from 10 to 25 min.

The mathematical model used to describe the heat flow in an infinite solid with a constant heat flux in the x = 0 plane[57] is represented by the following equations:

$$\partial T/\partial t = \alpha(\partial^2 T/\partial x^2) \quad (1)$$

in the range

$$-\infty < x < 0$$

and

$$0 < x < \infty.$$

The following additional boundary conditions are assumed for the model

$$q/2 = k\,(\partial T/\partial x), \quad (2)$$

when

$$x = 0,\ t > 0,\ T = 0 \text{ for}$$

$$-\infty < x < \infty,\ T = 0.$$

The solution to these equations by the curve-fitting technique was given by Carslaw and Jaeger.[57] For a point selected at x = 1, the dimensionless form of Equation (1) is

$$kTe/q\ell = (\alpha t/\ell^2)^{1/2}\ \text{ierfc}\ 1/2\,(\ell^2/\alpha t)^{1/2} \text{ at } x = 0 \quad (3)$$

and

$$T_0 = (q/k)(\alpha t/\pi)^{1/2} \quad (4)$$

It also follows from Equation (4) that

$$\frac{T\ell(2t)}{T\ell(t)} = \frac{\sqrt{2}\ \text{ierfc}\,(1/2\sqrt{2})(\ell^2/\alpha t)^{1/2}}{\text{ierfc}\ 1/2\,(\ell^2/\alpha t)^{1/2}}, \quad (5)$$

where

T = temperature, °C,

q = heat flux, cal/cm² sec,

ℓ = distance between the plane of the hot junction of the thermocouples and the plane of heat supply, cm,

k = thermal conductivity, cal/cm °C sec,

α = thermal diffusivity, cm²/sec,

t = time, sec, and

ierfc = an error function.

With the plots of Equations (3) and (5) and the temperature history of a point at x = 1 in an infinite solid, the thermal diffusivity and thermal conductivity can be determined. If the density is known or can be measured, the specific heat can also be calculated.

Four tests were carried out with UO_2 in three groups of particle sizes. Angular particles of two average sizes, 1.68 mm and 125 μ, were used in two of the tests. The third test was made with 125-μ spherical particles, and the fourth test was run on 1.68-mm angular material infiltrated with 125-μ angular particles. Densities of the packed systems are shown in Table 10. These tests were run in air at room temperature and atmospheric pressure. Table 11 lists the

TABLE 10. Density of Vibratorily Compacted UO_2

Particle Grouping	Weight of UO_2 Used, kg	Measured Density, g/cc	Theoretical Density, %
125 μ Spherical	5.2	6.7	61
125 μ Angular	5.6	6.8	62
1.68 mm Angular	5.35	6.5	59
1.68 mm and 125 μ Angular	6.93	8.2-8.5	75-78

TABLE 11. Measured Thermal Properties of UO_2 in Air

Material	Thermal Diffusivity $\alpha \times 10^{-3}$, cm/sec	Thermal Conductivity $k \times 10^{-4}$, cal/cm °C sec
125 μ Spherical	1.4	4.4
125 μ Angular	1.4	4.7
1.68 mm Angular	2.9	9.7
1.68 mm and 125 μ Angular	The results of these tests are not yet available.	

[57] H. S. Carslaw and J. C. Jaeger, *Conduction of Heat in Solids* (Oxford University Press, London, 1959), 2nd ed.

experimental values of thermal conductivity and thermal diffusivity for the UO_2 measured in air.

THERMAL DIFFUSIVITY OF URANIUM AND PLUTONIUM CARBIDES *(J. B. Moser and O. L. Kruger)*

The thermal diffusivities of UC, PuC, and $(U_{0.8}Pu_{0.2})C$ were measured from 500 to 1500°C by using the flash technique with a lead-sulfide detector.[52] The specimen characteristics are given in Table 12 and the results of the investigation are shown in Figure 12.

TABLE 12. Specimen Characteristics

Material	UC Arc-cast	UC Sintered at 1800°C	$(U_{0.8}Pu_{0.2})C$ Sintered at 1800°C	PuC Sintered at 1400°C
Density, % of Theoretical	99.0	78.8	74.8	83.8
Carbon, wt%	4.93	4.69	4.66	4.12
Oxygen, wt%	0.0117	0.106	0.202	0.567
Nitrogen, wt%	0.0021	0.0228	0.0206	0.0440
Equivalent Carbon,[a] wt%	4.94	4.79	4.83	4.58
Equivalent Carbon, at.%	50.8	49.9	50.2	48.9

[a]Equivalent carbon wt% = wt% C + 12-16 wt% O + 12-14 wt% N.

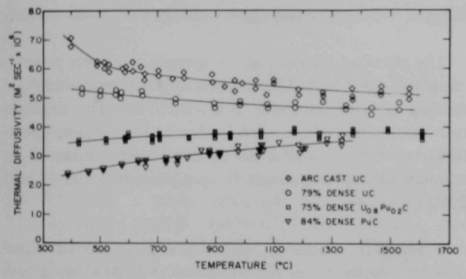

47742

Fig. 12. Thermal Diffusivity of Uranium and Plutonium Monocarbides.

The major impurities (oxygen and nitrogen) were converted to equivalent carbon content since they dissolve in the monocarbides to a considerable extent. Uranium monocarbide and $(U_{0.8}Pu_{0.2})C$ can be obtained only as single-phase material, if the nonmetal atom content does not exceed 50 at.%; for PuC the upper limit for single-phase material is 46.5 at.%.

The arc-cast uranium carbide had an equivalent carbon content of 50.8 at.%, and a small amount of a second phase consisting of UC_2 was observed in the microstructure. The sintered uranium carbide specimen contained more oxygen, but less carbon, than the arc-cast material and had an equivalent carbon content of 49.9 at.%. No second phase was observed. Compounds containing plutonium generally have a greater affinity for oxygen, and the increase in oxygen with increasing plutonium content is shown in Table 12. The mixed carbide contained 0.2 wt% oxygen. The calculated equivalent carbon content of this material was 50.2 at.%, and no significant amounts of any second phase were observed. The equivalent carbon content of the plutonium monocarbide was 48.9 at.% with approximately 10% plutonium sesquicarbide (Pu_2C_3) phase present.

Since the values are not available for the heat capacity of carbides containing appreciable oxygen and nitrogen, a calculation of the thermal conductivity is unrealistic. For this reason we decided to analyze the data directly in terms of the experimentally determined diffusivity. The rank of the curves in Figure 12 has been reported by Leary and co-workers,[58] who measured the thermal conductivity of UC, PuC, and $(U_{0.8}Pu_{0.2})C$ from 200 to 400°C. Considerable work has been done on electrical conductivity measurements,[53,58,59] and a comparison of the data shows that the same rank is followed in electrical conductivity.

The thermal conductivity of chemically stoichiometric UC with a carbon content of 4.8 wt% but with various impurity contents was investigated by Hayes and DeCrescente,[59] who used a radial heat-flow method. The results of this work generally fall within the range of the Laboratory UC data over the temperature span from 1000 to 1500°C.

The lower thermal diffusivity of PuC compared with UC is probably due to PuC being a defect structure. The difference in thermal diffusivity between the three compounds studied decreases as the temperature increases. At 1300°C the diffusivity of PuC becomes approximately equal to that of $(U_{0.8}Pu_{0.2})C$.

HEATS OF FORMATION OF NaCl-TYPE URANIUM COMPOUNDS *(Yehuda Baskin)*

A program was initiated in 1967 to measure the relative heats of formation (ΔH) of the compounds US, UP, UAs, USe, UTe, USb, and UBi by means of reaction calorimetry. This information and the available ΔH data on UC and UN will be utilized to assess the relative stability of the NaCl-type compounds, and to provide a basis for the prediction of their high-temperature compatibility with various metals and alloys.

Measurements of the enthalpy of formation were

[58]J. A. Leary, R. L. Thomas, A. E. Ogard, and G. C. Wonn, "Thermal Conductivity and Electrical Resistivity of UC, (UPu)C, and PuC," *Carbides in Nuclear Energy* (Macmillan and Co., Ltd., 1964) Vol. I, p. 365.

[59]B. A. Hayes and M. A. DeCrescente, Pratt and Whitney Report PWAC-480, 1965.

obtained by the direct-reaction calorimetric method similar to that described by Kubaschewski and Densch[60] A twin calorimeter[61] that operates at 425°C was employed for this investigation. A preliminary value of the heat of formation of US has been measured in the calorimeter; the value, an average of three determinations, is 70.4 ±3.5 kcal/mole. The presence of a total of 2 to 3% elemental uranium and uranium sesquisulfide, revealed by x-ray and metallographic examinations, undoubtedly affected the ΔH value. Nevertheless, this value is in closer agreement with the value of ΔH obtained by fluorine bomb calorimetry[62] (-73.2 kcal/mole) than by the vapor-effusion method[44] (-94.5 kcal/mole). The heats of formation derived from vapor pressure measurements tend to be of low accuracy[63] because small errors in the temperature dependence of the vapor pressure yield large errors in the heat of formation. Additional experiments are planned with US in order to refine the measured value of ΔH.

Irradiation Behavior of Advanced Ceramic Materials

IRRADIATION OF URANIUM SULFIDE

(L. C. Michels)

Experiments are being made to characterize the irradiation behavior of uranium sulfide; swelling, fission-gas release, and macro- and microstructural changes are of primary interest.

Two temperature-controlled capsules that contain eight specimens of uranium-sulfide pellets clad in Nb-1 wt% Zr continued under irradiation in MTR during the year. These specimens have achieved estimated burnups that range from 6.6 to 9.8 at.% at maximum cladding-surface temperatures of from 380 to 750°C. They will be discharged after target exposures of 10 at.%.

Mechanical Properties of Uranium Compounds

PROPERTIES OF URANIUM MONOSULFIDE AND MONOPHOSPHIDE *(R. J. Beals)*

The mechanical behavior of materials is generally investigated by tests characterized by the use of a specific stress system such as tension, compression, torsion, bending, or a combination of these, as well as by the time rate of application of stresses and the total time under load. Bending tests have been conducted with US and UP because these tests are the simplest to perform on brittle ceramic materials. This loading produces failure in the tensile face of the specimen.

The uranium monosulfide powders used in this investigation were prepared by the gas-solid reaction. Two materials were used: one containing approximately 1.5 wt% UOS as an impurity (with no detectable UO_2) and the second containing approximately 2.3 wt% UO_2 and 0.3 wt% UOS. The prepared powders were homogenized at 1850°C in flowing argon, crushed, sieved, and ball milled. Test bars were cold pressed and then sintered in vacuo at 1850°C for 2 hr. The sintered density of the specimens varied between 88 and 98% of theoretical.

The uranium monophosphide was also prepared by the gas-solid reaction. The monophosphide powders were homogenized at 1400°C in the flowing argon and ground to an average particle size of from 1 to 5 μ. Test specimens were dry pressed and sintered at 1800°C in vacuo for 2 hr. The sintered density was approximately 95% of theoretical.

The principal variables in this investigation were temperature and strain rate. All cross-bending tests were made in a vacuum of approximately 2×10^{-5} Torr. The uranium monosulfide specimens were loaded to failure at temperatures between 25 and 1750°C; tests were conducted on uranium monophosphide at temperatures between 25 and 2050°C.

Uranium monosulfide with UOS as a second phase showed a brittle-to-ductile transition at 1000°C, as shown in Figure 13. The material with a 93% theoretical density was stronger at this temperature than was the more dense material, and the strength of the monosulfide material was greater at 1000°C than at room temperature. Above 1000°C, a substantial increase in deflection was realized with each temperature increase. The specimen containing UO_2 as the major impurity was brittle to 1250°C. Above this temperature, the plasticity increased markedly to 1500°C.

At 1750°C, the US(UOS) tested at the fast strain rate failed with practically no load application. Cracks formed on the tensile face at this very low load by a separation along grain boundaries. We expect, however, that uranium

[60] O. Kubaschewski and W. A. Densch, Acta Met. *3*(7), 339 (1955).

[61] J. B. Darby, Jr., R. Kleb, and O. J. Kleppa, Rev. Sci. Instr. *37*(2), 164 (1966).

[62] P.G.G. O'Hare, J. L. Settle, H. M. Feder, and W. N. Hubbard, *Thermodynamics of Nuclear Materials*, Proc. IAEA Symp., Vienna, 1967 (in press).

[63] P. M. Robinson and M. B. Bever, *Intermetallic Compounds*, J. H. Westbrook, ed. (John Wiley and Sons, Inc., New York, 1967), p. 38.

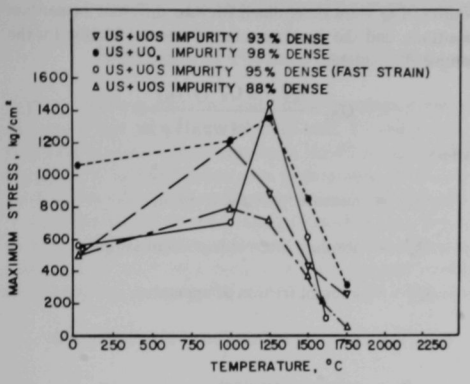

47485

Fig. 13. The Effect of Temperature and Strain upon the Maximum Fiber Stress of Uranium Monosulfide.

monosulfide has other slip systems available, or that the presence of UO_2 affects the deformation mechanisms, because US with no UOS at the grain boundaries was highly plastic at 1250°C.

The load-deflection curves for uranium monophosphide resemble those of uranium dioxide[64] at all test temperatures. Figure 14 shows an increase over the room-temperature values when the monophosphide (with approximately 1% UO_2 as a second phase) was tested at 1000°C. Only a slight deflection was recorded below 1250°C. Above 1000°C, the rate of load application had little effect upon the maximum fiber stress. The plasticity of UP, greater than that of uranium dioxide,[64] increased steadily in a manner similar to that of US as the test temperature was raised.

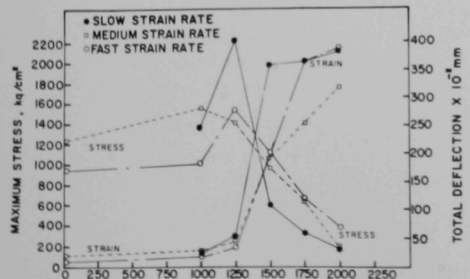

47484

Fig. 14. The Effect of Temperature and Strain upon the Maximum Fiber Stress in Uranium Monophosphide.

Examination of the microstructure of the monophosphide after testing showed the formation of enlarged pores that could promote intergranular crack propagation similar to that observed in UO_2.[64] At higher temperatures, intergranular cracking appeared to be the cause of some of the deformation; however, because of the high total plasticity, slip within the grains of the uranium monophosphide probably occurred.

ELASTIC AND ANELASTIC PROPERTIES IN UO_2-PuO_2 POLYCRYSTALLINE SYSTEM *(A. W. Nutt)*

The macroscopic elastic properties of polycrystalline oxide fuels with randomly oriented, equiaxed grains are isotropic.[65] Isotropic elastic and anelastic behavior can be characterized best by first determining a standard set of property values for fully dense oxide at a reference temperature (25°C), and then correcting these values for the effects of porosity, grain size, stoichiometry, temperature, composition, and other variables by appropriate empirical or theoretical expressions. This approach is being used in the investigation of elastic and anelastic properties of the UO_2-PuO_2 mixed-oxide fuels.

The installation of equipment for the resonance testing of mixed-oxide fuel specimens is near completion. The internal friction and Young's modulus of the UO_2-PuO_2 compositions will be measured by using the Förster method of free-free flexural vibration.[66] Techniques are being developed for the fabrication of UO_2-PuO_2 specimens of controlled density, porosity, and stoichiometry.

The equation for the calculation of Young's modulus, as reported by Hasselman,[67] is

$$E = 0.94645 \frac{Cmf_r^2}{D} \qquad (1)$$

where

E = Young's modulus,

C = constant as given by Hasselman,[67]

m = mass of specimen,

---

[64] R. J. Beals, J. H. Handwerk, and G. M. Dragel, *High Temperature Mechanical Properties of Uranium Compounds*, Proc. 3rd Intl. Symp. on High Temperature Technology, Asilomar Conf. Grounds, Pacific Grove, California, September 1967 (to be published).

[65] R. A. Wolfe and S. F. Kaufman, Westinghouse Electric Corporation Report WAPD-TM-587, October 1967.

[66] F. Förster, Z. Metallkunde 29, 116 (1937).

[67] D.P.H. Hasselman, *Tables for the Computation of the Shear Modulus and Young's Modulus of Elasticity from the Resonant Frequencies of Rectangular Prisms*, Applied Research Branch, Research and Development Division, The Carborundum Company, Niagara Falls, New York, 1961.

f_r = flexural resonance frequency, and

D = dimension of cross section perpendicular to the direction of vibration.

The internal friction is calculated by using the free-decay method and the suspension damping correction of Wachtman and Tefft:[68]

$$Q^{-1} = \frac{\ln 2A_0/2A_1}{\pi f_r \Delta t}, \qquad (2)$$

where

Q^{-1} = internal friction of specimen,

A_0 = amplitude at t = 0 (as measured from decay trace on the storage oscilloscope),

A_1 = amplitude at t = t, and

Δt = time differential between amplitude measurements.

Values of Q^{-1} are determined for two different suspension positions, and the absolute value of internal friction for the sample is calculated:

$$Q_m^{-1} = \frac{Q_s^{-1} + k\,Q_a^{-1}\,(y/y_0)^2}{1 + k\,(y/y_0)^2}, \qquad (3)$$

where

Q_m^{-1} = measured internal friction,

Q_s^{-1} = absolute internal friction of sample,

Q_a^{-1} = internal friction of apparatus,

(y/y_0) = constant as function of suspension, and

k = specimen constant.

The reliability and reproducibility of the equipment was demonstrated by tests made on a single crystal of sapphire. Young's modulus of polycrystalline UO_2 was also measured, and the data corroborated the data of Forlano, et al.[69]

[68] J. B. Wachtman, Jr. and W. E. Tefft, Rev. Sci. Instr. 29, 517 (1958).

[69] R. J. Forlano, A. W. Allen, and R. J. Beals, USAEC Report ANL-7101, Argonne National Laboratory, 1965.

DEVELOPMENT OF THORIUM-URANIUM-PLUTONIUM FUELS

Irradiation of Thorium-Uranium-Plutonium Fuel Alloys *(W. N. Beck and R. J. Fousek)*

Two thorium-uranium and four thorium-uranium-plutonium fuel alloys clad in V-20 wt% Ti tubing were irradiated in instrumented capsules in the CP-5 reactor. The objectives of the experiment were to determine the relative swelling behavior of the fuels, the restraint characteristics of the cladding, and the maximum attainable burnup before cladding failure. When the specimens had reached a maximum of 28.6 at.% burnup, a thermocouple in the irradiation capsule indicated the possibility of a cladding failure. The capsule was then neutron radiographed. The results indicated that if cladding failure occurred, the extent of the failure was not severe. The capsule will be destructively examined. Observations of fuel-length change show that the Th-20 wt% U fuel pins had not elongated; while the Th-10 wt% Pu-20 wt% U and the Th-10 wt% Pu-10 wt% U pins elongated an average of 8%. Table 13 summarizes design details and irradiation variables for these metal-fuel experiments.

TABLE 13. Summary of Information for Thorium-Uranium and Thorium-Uranium-Plutonium Specimens Irradiated in Capsule CP-50

Specimen Number	Fuel Composition, wt%	Effective Density, %	Maximum kW/ft	Maximum Cladding Temperature, °C	Burnup		Fuel Length Change, %
					U + Pu, at.%	fiss/cc x 10^{-20}[a]	
1N16	Th-20 U	74.7	8.7	610	25.1	12.1	-0.9
4N19	Th-20 U	74.0	8.7	610	25.1	12.1	0
2N17	Th-10 Pu-10 U	74.1	9.2	630	28.6	13.5	7.8
5N20	Th-10 Pu-10 U	73.0	9.2	630	28.6	13.5	8.2
3N18	Th-10 Pu-20 U	73.5	8.7	630	17.0	12.4	7.9
6N21	Th-10 Pu-20 U	73.5	8.7	610	17.0	12.4	8.2

[a]Based on effective density.

Fundamentals of Corrosion in Liquid Metals

DISSOLUTION KINETICS IN LIQUID-METAL SYSTEMS *(T. F. Kassner, D. L. Smith, D. L. Rink, and R. H. Lee)*

Results of the investigations of the dissolution kinetics of tantalum in liquid tin, and of Type 304 stainless steel in the bismuth-tin eutectic alloy have been reported recently.[70,71] These studies were undertaken to test the applicability of the convective-diffusion model[72] for mass transport from rotating disk samples in high-temperature liquid-metal systems.

Having demonstrated the ability to deduce the rate-controlling step of the corrosion process in these experiments, we have constructed and successfully tested an apparatus in which disk-shape sample geometry will be used to investigate corrosion processes in metal-sodium systems that contain impurities.

A number of processes are possible in a metal-sodium system when additional components such as oxygen, nitrogen, carbon, and hydrogen are present at low concentrations. Therefore, in systems of interest, it is necessary first to identify the reaction process and the range of experimental conditions over which the process is operative; and secondly, to determine the effect of variables such as temperature, flow, and impurity concentration on the kinetics of the process.

Phase equilibria calculations in the Ta-O-Na and Nb-O-Na systems have been reported.[73] The conditions of temperature and oxygen concentration in sodium over which the phases Ta, Ta_2O_5 and Nb, NbO, and NbO_2 are thermodynamically stable in sodium have been predicted. In addition, the kinetics of oxygen solution in tantalum and in niobium that were exposed to sodium with low oxygen content have been examined as a function of temperature, oxygen concentration in sodium, and initial oxygen concentration in the refractory metals.

Experimental measurements of the distribution of oxygen between the group 5B refractory metals and liquid sodium are in progress. Internal-friction techniques and standard methods of analysis have been used to measure the oxygen concentration in the refractory-metal wires. The measurements have been correlated with the cold-trap temperature of sodium and vacuum distillation analyses for oxygen in sodium. These studies will provide experimental confirmation of the metal-metal oxide-liquid sodium phase equilibria and will reveal any deviation from Raoult's law in the metal-oxygen solid solutions. Similar experiments involving nitrogen and carbon are also in progress.

The results will be used in the design and interpretation of corrosion experiments in these systems.

CORROSION INHIBITION BY DISSOLVED GETTERS IN LIQUID-SODIUM ENVIRONMENT *(C. A. Youngdahl, Sherman Greenberg, and W. D. McFall)*

Coupons of V-20 wt% Ti and V-15 wt% Cr-5 wt% Ti have been tested for 7.5 days at 650°C in flowing sodium solution that contained 100 wt ppm magnesium. The samples were not visibly affected. Small weight gains of about 0.3 mg/cm^2 were observed. Hardened surface layers of the order of 10 μ in thickness were found.

The substances that caused the weight gain and surface hardening are being identified by chemical analysis. Internal friction analysis applied to a vanadium wire included in the test tentatively indicated an available oxygen concentration in sodium of about 0.1 ppm and relatively small amounts of available nitrogen.

LITHIUM CORROSION STUDIES AT ELEVATED TEMPERATURES *(J. Y. N. Wang and K. G. Figlik)*

The inhibition of lithium corrosion of tantalum has been accomplished by dissolving silicon in the lithium.[74,75]

The study was expanded to include the lithium-iridium-tantalum system. Our work showed that iridium is readily soluble in lithium at 1200°C (a necessary condition for inhibition). At this temperature, a solution of 1.5 at.% iridium in lithium formed an intermetallic compound on the surface of a tantalum sample. The layer, formed over a period of 9 days, was about 50 μ deep and protected the tantalum from penetrating lithium attack.

Electron-probe microanalysis indicates this diffusion zone is made up of three compounds. X-ray analyses

[70] T. F. Kassner, J. Electrochem. Soc. *114*, 689 (1967).

[71] T. F. Kassner, Trans. Met. Soc. AIME *239*, 1643 (1967).

[72] V. G. Levich, *Physiochemical Hydrodynamics* (Prentice-Hall, Inc., Englewood Cliffs, New Jersey, 1962), 2nd ed., p. 60.

[73] T. F. Kassner and D. L. Smith, USAEC Report ANL-7335, Argonne National Laboratory, April 1967.

[74] James Y. N. Wang and Walter D. McFall, Annual Progress Report for 1965, Metallurgy Division, ANL-7155, pp. 143-145.

[75] J.Y.N. Wang, W. D. McFall, and J. W. Schlamer, Annual Progress Report for 1966, Metallurgy Division, ANL-7299, pp. 168-172.

indicated that the surface layer is predominately $TaIr_3$. A band, which appears gray in color, exists between the outer layer and the tantalum-base metal. The composition of the intermediate layer of the gray band corresponds to TaIr, while that of the innermost layer adjacent to the tantalum corresponds to Ta_3Ir.

The compounds Ta_3Ir and $TaIr_3$ have been reported by other investigators. The existence of a tetragonal sigma phase (Ta_3Ir) was first reported by Nevitt and Downey[76] and later confirmed by Knapton.[77] The lattice parameter of $TaIr_3$ (determined in our work) is $a_0 = 3.88Å$, which agrees with Dwight and Beck.[78] The TaIr phase has not been reported in the literature.

[76] M. Nevitt and J. Downey, J. Metals 9, 1072 (1957).

[77] A. G. Knapton, J. Less-Common Metals *2*, 113 (1960).

[78] A. E. Dwight and P. A. Beck, Trans. Met. Soc. AIME *215*, 976 (1959).

ULTRASONIC TECHNIQUES

Development of an Electrodynamic Ultrasonic Transducer *(R. A. di Novi)*

One of the disadvantages inherent in piezoelectric ultrasonic transducers is the degradation of physical and mechanical properties in a radioactive environment. A new method of ultrasound generation has been developed that may eliminate this difficulty. The electrodynamic method of sound generation involves the induction of mechanical vibrations in a material by the force produced when an electric current flows perpendicular to a magnetic field. When current flows over the end of a bar-shape sample, the same end of which is in a magnetic field oriented perpendicular to the axis of the bar, a mechanical force is exerted along the axis of the bar. A pulsed, oscillatory current produces a force that is pulsed and oscillatory; a pulse of some frequency is generated down the bar, which produces the "motor effect." The reverse "generator effect" is also possible when a pulse of mechanical vibration, propagated in a conducting medium, enters a magnetic field (current source attached at the end opposite the magnet). The resulting electric current can be detected.

The electrodynamic effect (both motor and generator) has been demonstrated at a frequency of 5 MHz with a signal-to-noise ratio of 10:1.

Development of an Ultrasonic Instrument and Transducer *(R. H. Selner)*

Porous metals are being investigated for use as backing members for ultrasonic transducer probes. Backing media should provide an acoustical impedance match with the piezoelectric element for maximum transfer of energy in the rear direction, and should also effectively attenuate ultrasound to prevent interference with the signals generated in the forward direction. The evaluation of Type 316 stainless steel has been reported previously.[79]

A study of porous tungsten has also been made. In the range of theoretical densities from 50 to 80%, tungsten is an adequate backing member for such piezoelectric elements as barium titanate, lead zirconate-titanate, and lead metaniobate. Ultrasonic attenuation can be increased if a cone is added on the rear face of a tungsten backing member. An evaluation of cone angle (defined as the angle formed by a line drawn perpendicular to the tip) shows that 30° is the optimum angle for most applications.

Passive Ultrasonic Techniques *(R. H. Selner)*

The use of acoustical techniques is being investigated as a method of detecting coolant boiling in an LMFBR. Numerous investigators have studied the feasibility of applying acoustical techniques to the detection of boiling in a liquid.[80-83] Such techniques can generally be classified into two categories: (1) Sonic or ultrasonic energy is generated externally and directed into the liquid, and some property (e.g., power required to produce cavitation) is measured. (2) Sonic or ultrasonic energy is generated internally in the system and is detected.

The latter method of acoustical detection will be used in this program. A high-temperature piezoelectric transducer probe (>650°C operating capability) will be immersed in liquid metal to detect internally generated sonic or ultrasonic energy. Boiling detection is based on the premise that noise generated by boiling can be separated from other noises in the reactor system.

The basic probe design consists of a Type 304 stainless steel capsule, a piezoelectric transducer, a porous tungsten backing, and signal leads. Lithium niobate and tourmaline, both of which have Curie temperatures (that temperature at which piezoelectric effects disappear) above 650°C, have been selected as the piezoelectric materials to be studied. Methods of joining a piezoelectric element to a capsule and to a backing member are being evaluated.

Determination of Elastic Constants of High-Temperature Materials *(Allen Sather)*

The ultrasonic pulse-echo technique for the measurement of high-temperature dynamic moduli has been described by Dunegan[84] and by Peterson.[85] One section of the rod

[79] R. H. Selner, Annual Progress Report for 1966, Metallurgy Division, ANL-7299, pp. 183-184.

[80] C. F. DePrisco, H. Kartluke, N. Maropis, and W. B. Tarpley, USAEC Report NYO-10010, New York Operations, March 1962.

[81] Technological University of Eindhoven, EURAEC-366, United States-Euratom Joint Research and Development Program, February 1962.

[82] I. D. Macleod, TRG Report 1205(R), United Kingdom Atomic Energy Authority, 1966.

[83] T. J. Ledwidge, Nucl. Sc. Abst. *21*(12), 2290 (1967).

[84] H. L. Dunegan, Mater. Eval. *22*(6), 266-276 (1966).

[85] R. G. Peterson, USAEC Report ANL-7119, Argonne National Laboratory, 1966.

specimen is placed in the hot zone of a furnace, and the other end is outside the furnace at room temperature; ultrasound is coupled with the cold end. One disadvantage of this technique is the requirement of a long specimen, part of which serves as a buffer for ultrasonic coupling. Since many of the new alloys being developed for potential reactor use are costly, scarce, and difficult to fabricate, long specimens are often difficult to obtain.

A new technique[86] has been developed that enables ultrasound to be transmitted from a separate buffer rod to a short specimen. Since only the index region of the rod is of importance for ultrasonic measurements, the long specimen rod is replaced by a short index section of the material under test and by a long buffer rod of some inexpensive, easily machined material that has a low ultrasonic attenuation. The buffer rod and specimen are joined by a threaded (mechanical) coupler. The test specimen is reduced to a length of 7.5 cm or less.

A good high-temperature ultrasonic bond is achieved by making a superior mechanical bond between the buffer rod and specimen. The ends of the buffer rod and specimen are made parallel and flat to within 0.1 mm and then polished with diamond paste. The threaded ends of the buffer rod and specimen are screwed into a coupler and tightened with a force of 87.5 x 10^6 dynes/cm^2. The final tightening of the coupler brings the two surfaces into contact intimately enough to transmit ultrasound.

This technique has been employed in the measurement of the elastic moduli of Types 304 and 316 stainless steel at temperatures up to 1200°C.

NEUTRON RADIOGRAPHIC TECHNIQUES

Neutron Image Intensifier *(Harry Berger)*

The development of the first-generation neutron image intensifier tube is complete. Several useful tubes have been designed, constructed, and tested,[87] and a useful tube life in excess of a year has been demonstrated.

Consideration has been given to the development of a second-generation detection tube that would provide an order-of-magnitude improved resolution and an improved neutron-to-gamma response ratio. The improved response ratio might reduce neutron sensitivity. One possible approach is an image-intensifier tube that has a metal input target such as ^{235}U. Incident neutrons would produce fission and release electrons. The electrons could be voltage accelerated to a storage target, the output of which could be read by an electron scanning beam. Some preliminary experiments with this type of neutron detection tube are planned.

Integrating Neutron-Image Detection Methods *(Harry Berger)*

Two methods of neutron-image detection have been investigated during the past year.[88] One method involves a thermoluminescent technique.[89] The detector, a thin (1 mm) layer of thermoluminescent ^{6}LiF, is exposed to the thermal neutron image long enough to obtain a useful result. The second detection method is the track-etch detector.[90] Tracks of radiation damage left by the passage of heavy nuclear particles through insulating materials can be selectively attacked by chemical agents to reveal a visible track. Cellulose nitrate films, exposed to the neutron beam with a ^{235}U foil, have been evaluated as a detector for neutron images. Each method is capable of integrating neutron-image information for long periods, which should ease some of the limitations of low neutron-intensity detection relative to transfer detection. Each of the methods also shows some improvement in neutron-gamma response when compared with direct-exposure film methods. Both types of detectors require total neutron exposures of ~10^9 neutrons/cm^2, and both display contrasts of about 10%. Better detection materials may lead to sensitivity improvements. Methods of enhancing image contrast are presently under study. More complete accounts of the present capabilities of these detection methods have been presented elsewhere.[88-90]

Studies have also been made to determine the improvement obtainable by using individual gadolinium isotopes as detectors for direct-exposure neutron radiography. The study was made with pellets of oxide powder used as a back screen. Natural gadolinium, ^{155}Gd, and ^{157}Gd were used.

As expected, ^{157}Gd (the isotope of highest cross section) yielded an improvement in speed of about a factor of two over the other two materials. An unanticipated result was some improvement in contrast capability with radiographs produced with ^{157}Gd. The improvement is probably the result of less gamma interference on the radiographs because the required exposure time is shorter. Comparisons of resolution were inconclusive, possibly because of the powdered nature of the conversion screens.

86A. Sather, J. Acoust. Soc. Am. (to be published).

87H. Berger, P. Dolon, and W. F. Niklas, IEEE Trans. on Nuclear Science *14*(1), 428-432 (February 1967).

88H. Berger, Brit. J. Non-Destructive Testing (to be published).

89J. Kastner, H. Berger, and I. R. Kraska, *A Thermoluminescent Image Detection Method for Neutron Radiography*, 5th Intl. Conf. on Nondestructive Testing, Montreal, Canada, May 1967 (to be published).

90H. Berger and I. R. Kraska, Trans. Am. Nucl. Soc. *10*(1), 72-73 (1967).

Effects of Scatter on Neutron Radiographic Quality *(I. R. Kraska and Harry Berger)*

Investigations are being made to determine the effects of neutron-scatter factors (ratios of scattered neutrons to directly transmitted neutrons) on neutron radiographic examinations of lead, steel, and natural uranium. The scatter factor is important because it influences the radiographic quality that can be achieved. Results of the study[91] indicate that neutron-scatter factors increase with increasing sample thickness, and reach a peak at a direct beam attenuation of between 50 to 100; above this attenuation, the scatter factor begins to decrease. The effect is particularly pronounced with steel, but has also been observed with lead and natural uranium samples. The effect can be observed as a change in radiographic quality. Further confirmation of the effect is under study. Possible reasons for this unusual scatter factor peak are being considered, but the effect is as yet unexplained. Beam spectrum and filtration effects are being studied in particular. Attempts are being made to perform similar studies with a neutron beam of higher intensity so that additional data points beyond the peak can be obtained.

Development of Nonreactor Neutron Sources *(J. P. Barton and Harry Berger)*

Studies have been initiated to determine the usefulness of radioactive Am-Cm-Be as a neutron source for neutron radiography. The investigation will also check a computer program used by the ANL Idaho Division[92] to predict thermal neutron intensity and cadmium ratio information for fast neutron sources in various moderators. If the predicted computer results are obtained experimentally, then the computer could be used with some degree of confidence to predict optimum moderator arrangements for many potentially useful fast neutron sources. Water and BeO moderators are now undergoing experimental evaluation.

SCATTER RADIOGRAPHY BY X-RAY TECHNIQUES *(N. P. Lapinski)*

Scattered x radiation is normally to be avoided because the increase in background radiation decreases radiographic contrast. On occasion, scattered x radiation can be useful, for example, the use of a scatter x radiograph to determine sodium levels in reactor fuel rods.[93] The determination was complicated by the fact that an internal spring tended to mask the indication of sodium level on a normal transmission radiograph. Scatter techniques solved the masking problem.

Scatter methods appear generally useful for the location and characterization of material of low atomic number near the surface of material of high atomic number. The technique also shows promise for crack detection, particularly near-surface cracks in rod material. These advantages depend on the fact that the scattered radiation is generated in the center of the sample, and that the radiation is emitted isotropically. The scattered radiation is also of lower energy than the primary radiation and, therefore, offers more contrast for light materials.

The intensity of x radiation scattered from a known type of inspection sample is being studied to experimentally determine what types of useful inspection information can be obtained from this method. The source of radiation is generated from a 140 kV industrial x-ray unit that has a 2.0 mm^2 effective focal spot. The beam of radiation is collimated to 0.95 cm. Provisions are made to insert disks, with various size apertures, at the exposure port of the collimator. The insertion of the disks will restrict the size of the beam entering a sample to any desired diameter.

Experimental efforts in the x-ray scatter studies have been limited to the inspection of 1.27-cm-diam aluminum rods with holes drilled into the end face to simulate internal voids. An effective method of obtaining an image of the simulated internal voids in an aluminum sample consists of placing x-ray sensitive film around the circumference of the sample and holding the film in close contact by wrapping tightly with 0.127-mm-thick lead foil. The sample is oriented so that the longitudinal axis is in line with the center x-ray beam and then radiographed. The beam of radiation is collimated to 0.63 cm and is directed at the end of the sample that has the drilled holes. An x-ray energy of 100 kV is found to be most effective for these specimens.

The information assembled thus far shows some promise; however, the usefulness of scatter radiography as a meaningful test still must be determined. Future studies will include the use of materials other than aluminum, and will endeavor to improve the present methods of generating scatter radiographs.

SUPPRESSION AND REDUCTION OF NOISE IN ELECTROMAGNETIC TEST SYSTEMS *(C. J. Renken)*

The central problem of the electromagnetic test method is the suppression and reduction of noise. Two promising approaches to noise reduction are under study. One is related to the transducer and the other deals with the signal

[91] I. R. Kraska and H. Berger, Mater. Eval. (to be published).

[92] D. C. Cutforth, Argonne National Laboratory, Idaho Falls, Idaho, private communication, 1966.

[93] N. S. Beyer, N. P. Lapinski, and R. B. Perry, J. Nondestructive Testing *19*, 408-409 (1961).

processing and readout equipment. In addition, we are investigating the nature of pulsed current diffusion in good conductors for basic information relative to the noise problem.

The problem of noise response in electromagnetic test systems is closely related to transducer resolution. Since the causes of specimen noise usually exist over much greater specimen volumes than the volume affected by a typical defect, improvements in transducer resolution will produce an improved signal-to-noise ratio. The term "resolution," as applied to electromagnetic transducers, has no universally accepted definition. If a transducer is considered as a type of filter, the broader the frequency response of the filter the better the transducer resolution. The frequency response of the "transducer-filter" can be calculated if the time domain response to a hypothetical "impulse defect" is known. The impulse defect is defined as a discontinuity in the permeability or resistivity of the test specimens that occurs over an infinitely small volume. If the transducer produces a signal AB(x) at the system output when responding to such a defect, the spectral response of the transducer can be calculated by means of the ordinary Fourier integral.

$$\Omega(\omega) = A\int_{-\infty}^{\infty} B(x)e^{-j\omega x}dx, \qquad (1)$$

where B(x) gives the spectral response function of the transducer with respect to distance x, and the magnitude of A indicates the strength of the impulse. If a real defect could be synthesized by the proper arrangement of a sequence of impulse defects of the proper strength, the response of the transducer to this defect could be calculated by use of the superposition integral

$$g(x') = \int_{-\infty}^{x'} B(x)f(x' - x)dx, \qquad (2)$$

where x' is a particular value of x, and $f(x' - x)$ is a function that expresses the variations in the defect strength as a function of position.

The use of Equation (2) to calculate transducer response is very difficult because most transducer responses are complicated three-dimensional functions of defect position and of time. Nevertheless, reasonable experimental approximations of impulse defects are easily made for any transducer; thus, the impulse response provides a means of comparing one transducer with another. By comparing functions of transducer spectral response with the calculated power-density functions of various defects, a reasonable idea can be obtained of how effectively a given transducer will detect a certain type of defect. The impulse response of a transducer to various paths of the impulse defect through the field can lead to the construction of approximate field maps that provide useful information of transducer design.

Signal-processing techniques have been studied to improve the signal-to-noise ratio of the system. Specimen noise as a class is unique, but usually can be considered ergodic, stationary, and rather limited in bandwidth. Often, because of the manufacturing process, noise signals are concentrated in a few discrete frequency lines. For this reason, simple filtering in the frequency domain often has provided means of enhancing the signal-to-noise ratio. For more complicated causes of noise, additional processing is necessary, such as matched filtering, autocorrelation, cross correlation between sample-point channels, decision theory, and pattern recognition. Cross correlation seems to offer one of the easiest ways of improving the signal-to-noise ratio. The inspection of several important types of fuel-element jacket materials is now possible to a 5% defect level (defects greater than 5% of the wall thickness) at a confidence level of 75%. This result was impossible several years ago even at the 10% defect level.

The long-term improvement in pulsed electromagnetic methods is dependent upon a useful theory of the diffusion of pulsed electromagnetic fields of limited area into conductors of various shapes. Recent work shows that the direction of the magnetic field inside the metal relative to the direction of propagation of the wave has no effect on the field attenuation. This observation has led to the conclusion that the present divergence between theoretical and experimental values of field attenuation is a result of faults in the assumed boundary conditions of the analysis rather than incorrect assumptions about field directions in the metal.

NONDESTRUCTIVE TESTS OF FAST-REACTOR COMPONENTS

Examination of Fuel Elements and Subassemblies

(N. P. Lapinski, C. J. Renken, Allen Sather, I. R. Kraska, and M. F. Klozar)

Inspections of a large number of fuel elements and subassemblies were completed. These included x-ray inspections of the fuel and welds of the jacket end cap, x-ray and pulsed eddy-current tests to determine the quality of sodium bonds, and neutron radiographic examinations of irradiated material at various stages during the irradiation tests.

The x-ray inspection of sodium bonds was designed to simulate the reactor environment of EBR-II irradiation capsules to determine sodium-bond integrity after successive heating and freezing cycles. The sodium in each capsule was examined by x ray in the frozen and molten

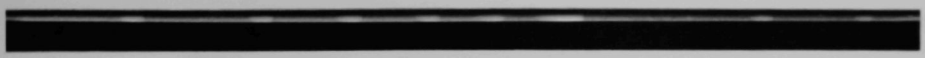

Fig. 15. A Radiograph of an Irradiation Capsule that Shows the Condition of the Sodium Bond in the Molten State. No indications of voids were found in the sodium bond. The light gray horizontal line constitutes the area of the sodium.

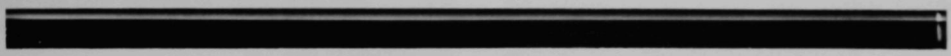

Fig. 16. A Radiograph that Shows the Condition of the Sodium Bond When the Sodium Is Frozen. The oval-shape areas of lesser density are shrinkage voids in the sodium bond.

states. Four views were taken of each capsule, and after each exposure, the capsule was rotated axially 30°. The capsules were examined while the sodium was molten, then cooled from the top down in order to cause the greatest number and largest size of shrinkage voids in the bond sodium. After each of five cycles on four typical capsules, radiographs showed that shrinkage voids were present in the frozen state and that the sodium bonds remained free of voids when returned to the molten state. These conditions are shown in Figures 15 and 16. This demonstration indicates there will be no deterioration of the bond quality from phase changes in the sodium.

In-Cave Testing of Sodium Bonds of Irradiated Capsules *(C. J. Renken)*

Electromagnetic test equipment has been designed to test the quality of the sodium bonds of irradiated capsules that have been withdrawn from EBR-II for interim inspection. The electromagnetic test is considered to be the most feasible method of testing the heat-transfer capabilities of the bond layer after irradiation. The electromagnetic determination of sodium-bond quality is based on the expectation that heat will flow freely through any interface that conducts current well (although the converse may not be true).

The electronic system now under construction makes use of a 25 μsec current pulse with a peak power of about 500 watts and a repetition rate of 300 Hz. The reflected field, which is detected by a shielded transducer, is sampled at four time intervals (2, 5, 50, and 80 μsec) after the initiation of the field pulse. The resultant four-dimensional signal should permit the extraction of sufficient information to unambiguously determine the depth and size of the defect. The first application of the new test system will probably be with the capsules from subassembly XO11.

Tests with prototype equipment indicate that, in the Mark-A capsules, voids with a volume equivalent to a 1.6 mm diameter sphere can be detected under a sodium layer of 0.76 mm. A good indication of depth of the void in the annulus is obtained independent of void size. Simulated tests indicate that annular gaps between sodium and jacket of less than 0.0025 mm are clearly detectable, if the gaps extend around the jacket circumference at least 90° and along the capsule longitudinal axis for at least 1 mm. The prototype equipment appears to provide a satisfactory test for voids in the Mark-A capsules.

The Mark-B-19, Mark-B-37, and Mark-B-61 types of irradiation capsules have a spiral spacer wire attached to the outside of the jacket. The spacer wire will seriously complicate the application of the electromagnetic test, and may make the test impractical. When samples of these types of capsules can be obtained, the seriousness of the spacer-wire problem will be determined.

Measurement of Thermal Conductivity of Irradiated Fuel as a Function of Burnup and Temperature *(R. A. di Novi)*

The thermal-pulse method[94] is being used to measure the thermal properties of irradiated EBR-II fuel materials. A vacuum furnace with associated equipment was installed in a cave area, and measurements were initiated on three types (MR,* MR-C,** and SL†) of U-5 wt% Fs driver fuel. Fuel pins were sectioned into transverse (measurements in the axial direction) and longitudinal specimens (measurements in the radial direction); sectioned specimens were 1-mm thick. The specimens were cut from the bottom (cool end), middle, and top (hot end) of the fuel pins.

For each of these specimens the burnup, swelling, and irradiation temperatures of the outer surface, geometric center, and center of mass have been calculated so that the

---

[94] W. J. Parker, R. J. Jenkins, C. P. Butler, and G. L. Abbot, J. Appl. Phys. *32*(9), 1679-1684 (1961).

*MR—melt refined, recycled fuel pins.

**MR-C—melt refined, recycled fuel pins containing considerable amounts of reject pins and pin ends from previous castings.

†SL—fuel pins (shorter in length than the original Mark-I pins) cast from virgin metals.

effects of these parameters on the postirradiation value of the thermal conductivity could be evaluated.

A relationship was found between the percentage decrease in conductivity after irradiation and the swelling. This relationship involves the three types of EBR-II driver fuel, and indicates that, despite the different swelling characteristics of the three, the postirradiation thermal properties of the alloy U-5 wt% Fs can be predicted from the swelling. The dependence of conductivity on swelling means that the loss in conductivity will be greatest at the region where the center-of-mass irradiation temperature of the fuel was about 515°C (rather than at the region where burnup was greatest).

Type SL fuel had the largest losses of conductivity. A 30% loss of conductivity was accompanied by 14.1% swelling at a burnup of 0.8958 at.% and a center-of-mass irradiation temperature of 517°C. A specimen of Type MR-C fuel had a 10% loss of conductivity for swelling of 4% at a burnup of 0.803 at.% and a center-of-mass irradiation temperature of 484°C.

The porosity volume was calculated for each specimen, and the conductivity was calculated by means of several porosity-corrected formulas. Reasonably good agreement with the experimental results was achieved with a modified Maxwell-Eucken equation,[95]

$$K_p = K_{100}\frac{(1 - p)}{(1 + \beta)p}, \qquad (1)$$

where K_p = conductivity of material with pores, K_{100} = conductivity of solid material, p = pore volume, and β is an empirical constant that is dependent on pore shape (β can vary from 0.5 to 1.5). Metallographic examination of the specimens will assist in the selection of β; present calculations were based on the maximum and minimum values of β.

Development of Techniques and Equipment for Alpha-Gamma Hot Cell

INERT ATMOSPHERE SYSTEM *(B. J. Koprowski and W. H. Livernash)*

An inert atmosphere is necessary if toxic and pyrophoric materials such as plutonium, sodium, or potassium are to be examined safely. A system that provides an atmosphere of nitrogen gas in the main working area of the Alpha-Gamma Hot Cell was included in the original construction of the cell for the postirradiation examination of reactor fuel elements.[96] As part of a plan to provide additional space in the hot cell for experimental work, the use of the nitrogen-atmosphere system has been extended to include parts of the cell that were formerly air-ventilated storage areas.

SHIELDED METALLOGRAPH *(B. J. Koprowski and M. F. Adam)*

Optical metallography is one of the primary tools used to study the effects of irradiation on fuel materials. In order to satisfy the increasing demand for this type of examination, a second metallograph has been purchased for installation in the Alpha-Gamma Hot Cell.

Since fuel specimens that contain irradiated plutonium will be examined with this metallograph, special safety features were incorporated into the design of the instrument.[97] The metallograph, glovebox, and front portion of shielding were mounted on a movable base that permits separation from the gamma shield; thus, the sealed and shielded parts of the instrument are accessible for maintenance.

AUTORADIOGRAPHY *(B. J. Koprowski)*

Autoradiography is being used to determine fission-product distribution in irradiated fuel materials.[98] Beta-gamma autoradiographs have been produced in the Alpha-Gamma Hot Cell by placing a polished metallographic fuel specimen in contact with a sealed envelope that contains a Kodak high-resolution film plate wrapped in aluminum foil.

There are three disadvantages to the film-plate technique: (1) special transfer methods are necessary to remove the film packet from the contaminated interior of the hot cell; (2) the sealed envelope, which is also contaminated, requires special handling methods to remove the film plate; and (3) the thick separation between the film and specimen, which is caused by the sealed envelope and film wrapper, results in poor definition in the final print of the autoradiograph.

In an attempt to eliminate these disadvantages, an autoradiographic "camera" was designed and installed in the glove wall of the hot cell. Some preliminary work with

[95] J. Belle, R. M. Berman, W. F. Bourgeois, I. Cohen, and R. C. Daniel, USAEC Report WAPD-TM-586, Bettis Atomic Power Laboratory, 1967.

[96] B. J. Koprowski, W. H. Livernash, and F. L. Brown, Proc. 12th Conf. on Remote Systems Technology, San Francisco, California, November 30-December 3, 1964, Am. Nucl. Soc., Hinsdale, Illinois, 1964, p. 315.

[97] R. Carlander, Annual Progress Report for 1966, Metallurgy Division, ANL-7299, pp. 190-192.

[98] B. J. Koprowski, F. L. Brown, and C. H. Gebo, Annual Progress Report for 1966, Metallurgy Division, ANL-7299, p. 192.

this equipment indicates that all the disadvantages of the original method have been eliminated.

SHIELDED ELECTRON-PROBE MICROANALYZER

(B. J. Koprowski, Y. K. Yoon, and R. J. Neisius)

Electron-probe microanalysis is a fairly recent development for qualitative and for quantitative analysis of samples as small as 10^{-11} g. In this technique electromagnetic lenses are used to focus an electron beam to a diameter of approximately 1 μ. The interaction of the electron beam with the specimen produces x rays that can be analyzed by an x-ray spectrometer; the characteristic x rays identify the elements, while the intensity of the x rays is related to the concentration of each element. The real advantage of this technique is the ability to determine spatial distribution of elements in larger specimens. The results obtained by optical microscopy can be correlated with the distribution of elemental components obtained by electron-probe microanalysis. This will be the primary use for the instrument in the Alpha-Gamma Hot Cell.

Electron-probe microanalysis of irradiated fuel elements that contain plutonium generates certain other related problems; the instrument must be capable of being sealed and shielded, and a system is required that can transfer highly radioactive samples between the hot cell and the instrument. The instrument selected is a Materials Analysis Company Model 450 microanalyzer that has been modified by the addition of sufficient shielding for safe operation. A specimen with an activity level of 100 Ci can be examined. The transfer system, designed at ANL, is a pneumatic system that will propel the specimen from the hot cell to a sealed and shielded cubicle adjacent to the microprobe, a distance of approximately 30 ft.

Part II

Basic Metallurgy

Contribution to a Statistical Theory of Fatigue *(P. O. Kettunen and U. F. Kocks)*

Introduction: In a theoretical study of the phenomenon of fatigue, the nonregular distribution of the relevant obstacles was linked to dislocation motion in the specimen. The obstacles may be other dislocations, solute atoms, precipitates, or inclusions. In actual specimens the obstacles are never arranged in a regular lattice, although such an assumption is implicit in many flow stress theories. The hypothetical case that the obstacle distribution is entirely random has been investigated.[99-102] In this case, some areas will be essentially free of obstacles into which dislocations could penetrate at very low stresses. The larger the stress, the larger the mean free-slip areas until, at a critical stress corresponding to the asymptotic macroscopic flow stress, the mean free-slip areas join to form a continuous area through which any dislocation can penetrate indefinitely.

Cyclic Hardening: If the specimen is cycled between two stress limits, the flow stress continuously increases. The increase of the flow stress can be established qualitatively by observing that the plastic strain amplitude continuously decreases, and can be measured quantitatively by interposing tensile tests after a varying number of cycles (Figure 17). If the applied stress amplitude σ remains constant and the flow stress τ increases, the ratio σ/τ continuously decreases. According to the conclusions from the statistical theory of flow stress,[101] the mean free-slip area should also continuously decrease. After an initial hardening stage of some hundreds or thousands of cycles, the flow stress reaches a saturation value τ_S. The mean free-slip area also should reach a steady-state value that will be available for the to-and-fro movement of the dislocations during the remaining major part of the fatigue life of the specimen.

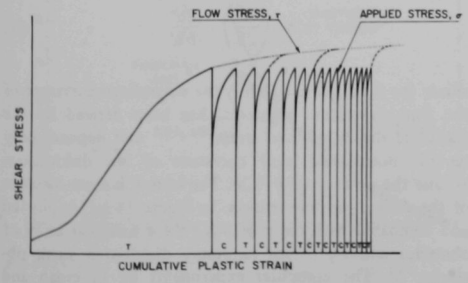

106-9462

Fig. 17. Schematic Diagram of Shear Stress versus the Cumulative Magnitudes of the Shear Strain in Tension T and Compression C for a Fatigue Test at Constant Stress Amplitude σ, with Interposed Tensile Tests (---) Defining the Locus (·····) of Flow Stresses τ.

Endurance Limit: The central thought of the present contribution is that fatigue failure can occur only if there is some probability that structural changes occur during every cycle.[103] If, however, the mean free-slip area during saturation is of the same order of magnitude as the area per obstacle in the slip plane, the dislocations will merely bow out without tearing loose from, or intersecting, any obstacle. Some energy dissipation is possible in such a process, but structural changes are not. Thus, a specimen cannot fail in fatigue if the rate of cyclic hardening in the initial stage is large so that the value of σ/τ_S will be lower than some critical value. The critical value should be of the order of 0.6, according to the present status of the statistical theory.[101] It is speculated that a high rate of cyclic hardening may be correlated with a high rate of work hardening, and the endurance limit may be correlated with a critical value of the work-hardening coefficient. If this value is lower than θ_{II}, a rough correlation between the endurance limit and τ_{III} should be expected, as is observed.[104] While simultaneous operation of hardening and softening mechanisms[105] is necessary to reach such a low value of the net hardening coefficient, the softening mechanism does not necessarily have to be identified with the cross-slip of individual screw dislocations.[106]

Surface Effects: Structural changes should occur in the entire specimen when the mean free-slip area is large enough; thus, fatigue could potentially be a bulk phenomenon. On the other hand, the strong influence of surface conditions on fatigue properties is quite compatible with our model. In many cases, the flow stress[107] and the dislocation content[108] in plastically deformed specimens are lower near the surface than in the interior. The mean free-slip area and the rate of structural change would be larger near the surface. Whether an initiation of fatigue failure near the surface will lead to failure of the entire specimen is a question related to macroscopic crack

---

[99] U. F. Kocks, Annual Progress Report for 1966, Metallurgy Division, ANL-7299, pp. 229-231.

[100] U. F. Kocks, Phil. Mag. *13*, 541 (1966).

[101] U. F. Kocks, Can. J. Phys. *45*, 737 (1967).

[102] U. F. Kocks, *Thermal Analysis for an Obstacle Controlled Flow Stress*, Proc. Intl. Conf. on The Strength of Metals and Alloys, Tokyo, Japan, September 4-8, 1967, Supp. Trans. Japan Inst. of Metals (to be published).

[103] P. O. Kettunen and U. F. Kocks, Scripta Met. *1*, 13 (1967).

[104] R. K. Ham and T. Broom, Phil. Mag. *7*, 95 (1962).

[105] S. Weissmann, A. Shrier, and V. Greenhut, Trans. ASM *59*, 709 (1966).

[106] P. Feltham, Proc. Roy. Soc. *A242*, 158 (1957).

[107] J. T. Fourie, Can. J. Phys. *45*, 777 (1967).

[108] P. R. Swann, Acta Met. *14*, 900 (1966).

propagation. For hardened surface layers, our model would predict fatigue crack generation in the interior of the specimen.

S-N Curve: We should like to postulate[109] that failure occurs after a given amount of structural change, and that structural change is directly proportional to the total number of intersections of obstacles by the moving dislocations. This number is proportional to the number of cycles N, and to the ratio of the mean free-slip area at saturation a_S to the mean area per obstacle point a_0:

$$N \cdot \frac{a_S}{a_0} = C(\sigma). \tag{1}$$

The given amount of damage C that leads to failure may, of course, depend on the stress in such a way as to decrease when the stress gets larger, by virtue of some crack nucleation or propagation mechanism. When this dependence is known, Equation (1) is the equation of the *S-N* curve. The ratio a_S/a_0 is given by the statistical theory as a function of the ratio σ/τ_S, and this ratio depends on the most important material characteristic for fatigue tests: the rate of cyclic hardening. Very little is known about this rate, and comprehensive measurements of τ as a function of σ, orientation, stacking fault energy, and other parameters are in progress.

Saturation Strain: The plastic strain amplitude at saturation γ_S is related to the mean free-slip area at saturation a_S by

$$a_S = \frac{\gamma_S}{b \cdot n(\sigma)}, \tag{2}$$

where $n(\sigma)$ is the number of mobile dislocations, and b is the amount of the Burgers vector. On the other hand, the mean area per obstacle in the slip plane a_0 is inversely proportional to the square of the flow stress. If, for this purpose, the difference between flow stress and applied stress amplitude is neglected, we can replace the ratio of a_S/a_0 in Equation (1) by a term that is proportional to $\gamma_S \cdot \sigma^2$. We would then have

$$\gamma_S \sigma^2 N = C'(\sigma) \tag{3}$$

as an approximate form of the *S-N* curve for comparison with experiments in which τ_S was not measured. We have analyzed experiments on polycrystalline copper, nickel, and titanium by Coffin[110] and found that they are in agreement with Equation (3), if $C'(\sigma)$ is roughly proportional to $1/\sigma$. This is not an unreasonable relation.

Summary: The hypothesis that the possibility of fatigue failure increases as the rate of structural change increases, independent of what particular structural change is used for a fatigue mechanism, has led, by application of the statistical theory of hardening, to the prediction of an endurance limit and an *S-N* curve in terms of the rate of cyclic hardening in the first few hundred cycles. For an experimental test of this theory, the applied stress amplitude must be kept constant from the first cycle, and the flow stress must be measured in an interposed tensile test after saturation has been reached. If this theory is correct, the boundary conditions during the first few hundred cycles are very important and long-range predictions can be made on the basis of tests performed after this initial stage.

Statistical Theory of Precipitation Hardening *(U. F. Kocks and C. Y. Cheng)*

Introduction: If a precipitate exerts a force F on a dislocation that is in the process of cutting through the precipitate, this force is linked to the local stress σ acting on a dislocation segment of length r by

$$\sigma = \frac{F}{br}, \tag{1}$$

where b is the amount of the Burgers vector. The macroscopic flow stress τ is then related to F by

$$\tau = \frac{F}{b\lambda}, \tag{2}$$

where λ is the effective obstacle spacing at the macroscopic flow stress. The spacing λ is not equal to, but is proportional to, the average obstacle spacing ℓ; since, however, the proportionality factor depends upon the interaction strength F, the flow stress relation may be written as

$$\tau = s\left(\frac{F}{2E}\right) \cdot \frac{2E}{b\ell}, \tag{3}$$

where the function s, which is the normalized curvature of the free dislocation segments, has been derived by the statistical theory of flow stress[101,102] and depends only on the normalized local curvature of the dislocations around the obstacles $f \equiv F/2E$. The term E is some measure of the dislocation line tension. In Figure 18 $s(f)$ is plotted and compared with the relations $s=f$ for a regular array of obstacles and $s=f^{3/2}$ for randomly distributed weak obstacles.[111] The computer experiments by Foreman and

[109] U. F. Kocks and P. O. Kettunen, Abst. Bull. IMD-AIME 2(2), 4 (1967).

[110] L. F. Coffin, Jr., *Internal Stresses and Fatigue in Metals*, G. M. Rassweiler and W. L. Grube, eds (Elsevier, Amsterdam, 1959).

[111] J. Friedel, *Dislocations* (Addison-Wesley Publishing Co., Inc., Reading, Massachusetts, 1964) p. 224.

Makin[112] and our calculations[101] did not incorporate the interaction of neighboring branches of the dislocation near each obstacle. This effect has been taken into account in a qualitative manner[102] in the solid curve of Figure 18; it leads to a jump in stress at a critical force. The curve could, in principle, be verified experimentally by measuring the flow stress in precipitation-hardened alloys as a function of the diameter of the precipitates, which should be directly related to the interaction strength f. Before such experimental comparisons can be made, one must define more precisely the "measure of the dislocation line tension" E. This definition has become important only since $s(f)$ is no longer a linear function.

Screw versus Edge Dislocations: It is inherent in the statistical model of the macroscopic flow stress that those dislocations which are harder to move in the slip plane have to be able to move indefinitely.[100] Since screw dislocations are harder to bow out, they should be responsible for the Orowan stress that corresponds to the plateau in Figure 18. When the obstacles are weaker, screw dislocations are, of course, still harder to bow out between two obstacles; on the other hand, they also exert less force on an obstacle at a given included angle between neighboring branches of the dislocation. Equation (3) shows that, when $s(f)$ is stronger than linear, the latter effect predominates, and the dislocations with the *smaller* value of E are harder to move. Figure 18 shows that this is the case for all obstacles, except those strong enough to demand the Orowan stress.

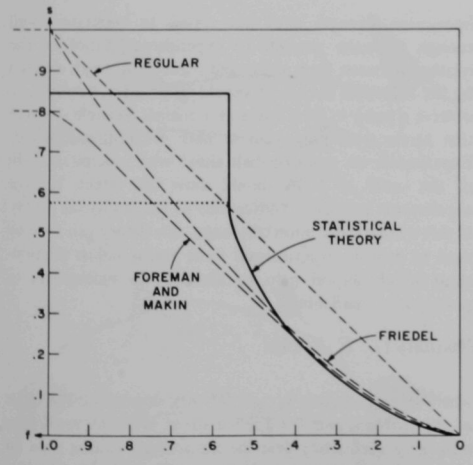

106-9546 R-2

Fig. 18. The Relation between the Normalized Flow Stress $s \equiv \tau b\ell/2E$ and the Normalized Interaction Force $f \equiv F/2E$, for a Regular Array of Obstacles and for a Random Arrangement According to the Statistical Theory,[102] According to Friedel,[111] and According to Foreman and Makin[112] and Our Previous Version.[101]

If the interaction strength F between the dislocation and the obstacle is the same for screw and edge, one should expect the edges to be the controlling dislocations for all such obstacles. When specific interactions between dislocations and obstacles are compared, the interaction involving edge dislocations usually is as strong or stronger than the interaction with screw dislocations. This comparison reinforces the contention that the energy to bow out an *edge* dislocation to the critical angle should be used to determine E in all cases outside the Orowan regime.

Line Energy versus Line Tension: If the equilibrium shape of a free dislocation loop is assumed to be an ellipse[113] the ratio of the length of a screw segment to that of an edge segment (both of which bow out under the same applied stress to cover the same area) is equal to the ratio of the principal axes of the ellipse, i.e., to the ratio of the line energies (not line tensions[101,102]) of edge and screw. Conversely, a comparison of screw and edge segments of the same length (with the same area covered), demands applied stresses in the same ratio. Thus, the value to be inserted for E is the line energy of the edge dislocation if screws are controlling (such as in the Orowan regime), and the line energy of the screw dislocation if edges are controlling (such as presumably in all other cases).

The line energy of the edge can be determined experimentally in a material that clearly yields by the Orowan mechanism, such as copper single crystals with dispersed spheres of amorphous silica.[114] From these data, using Equation (3) and $s_0 = 0.85$, we obtain $2E_e/b^2 = 6620$ kg/mm^2. The ratio E_s/E_e may be assumed to be equal to the ratio K_s/K_e of the normalized line energies derived for copper by deWit and Koehler,[115] giving $2E_s/b^2 = 3760$ kg/mm^2. In the case of aluminum, we have assumed the material to be isotropic with $G = \sqrt{c_{44}(c_{12} - c_{12})/2}$ (values from Reference 116), and $E_s/(Gb^2/2) = E_s/K_s = E_e/K_e = 0.87$ as in copper above, giving $2E_s/b^2 = 2300$ kg/mm^2.

Precipitation Hardening: In hardening by spherical precipitates of a radius R, their average spacing ℓ in the slip plane is determined from

$$\frac{1}{\ell} = \frac{\sqrt{c}}{R} \cdot \sqrt{\frac{3}{2\pi}} \qquad (4)$$

---

[112] A.J.E. Foreman and M. J. Makin, Phil. Mag. *14*, 911 (1966).

[113] J.C.M. Li and G.C.T. Liu, *Strengthening Effects of Curved Dislocations*, Proc. Intl. Conf. on The Strength of Metals and Alloys, Tokyo, Japan, September 4-8, 1967, Supp. Trans. Japan Inst. of Metals (to be published).

[114] M. F. Ashby, in *Oxide Dispersion Strengthening*, Gordon and Breach, in press.

[115] G. deWit and J. S. Koehler, Phys. Rev. *116*, 113 (1959).

[116] H. B. Huntington, in *Solid State Physics* 7, 274 (1958).

where c is the volume fraction. The measured values of the increase in flow stress τ should be multiplied by ℓ/b and divided by the relevant G' to obtain the normalized flow stress s. From our relation $s(f)$ (Figure 18), the normalized interaction force f can be determined and plotted versus $R/b(b = 2.55$ Å$)$. Figure 19 shows two such plots for data on aluminum-zinc single crystals[117,118] of random orientations and for data on copper-cobalt polycrystals[119] (taking the average orientation factor to be 3.06). Since in both cases the Orowan stress was not reached, we have assumed that the edge dislocations are controlling and thus we have inserted the line energy of the screws. We do not believe that uncertainties in our relation $s(f)$ can be responsible for the general deviation from linearity of the plot of f versus R. This belief is based on the fact that, in the case of aluminum-zinc, the linearity is definitely not obeyed even in the range of obstacle strengths that corresponds to the Friedel[111] regime which we have to regard as well established. In the case of copper cobalt, the highest stress reached lies, in fact, in the range of stresses corresponding to the jump in Figure 18. If all our assumptions are exact, the highest stress should correspond precisely to the critical value of the precipitate radius. It is quite likely that it in fact corresponds to a value somewhat lower than this and that our relation $s(f)$ will have to be adjusted in this range.

A linearity between strength and obstacle radius is frequently assumed in mechanistic calculations, notably those based on coherency strains.[117] We have to conclude that these do not adequately describe the process. Calculations based on the generation of new surface area between precipitates and matrix[118] generally give a relation roughly like $f \propto \sqrt{R}$. Figure 19 appears to fit this relation better in a qualitative fashion, but this has not been borne out by plotting f versus $\sqrt{R}$. Finally, R is not as yet a well-defined quantity. The values given by Gerold and Haberkorn[117] correspond,[118] in terms of the moments of a log-normal distribution, to $\sqrt{\langle R^7\rangle/\langle R^5\rangle}$; those given by Harkness[118] correspond to $\sqrt{\langle R^3\rangle/\langle R\rangle}$. Neither is likely to be the correct average for a nonuniform distribution of particle radii.

Conclusions: The relation between precipitate radius and interaction strength does not appear to be known well enough to make possible an experimental proof of the relation between flow stress and obstacle strength derived by the statistical theory. It should be possible, however, to observe a jump in flow stress at a critical obstacle strength that agrees with prediction in both location and height. Experiments on copper-cobalt alloys with precipitate radii of the order of 150Å should show this effect. If such experiments provide modifications to the statistical theory in this theoretically uncertain range, this theory can then be used to provide experimental force versus radius relationships which should help to identify the mechanism of precipitation hardening.

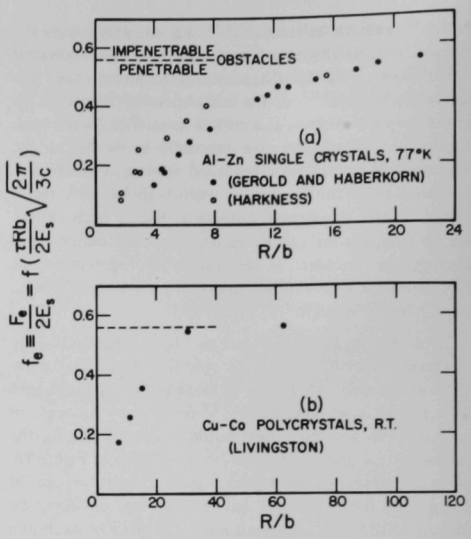

106-9744

Fig. 19. Normalized Interaction Force f_e between Edge Dislocation and Precipitate, as Derived According to the Statistical Theory from the Observed Increase in Flow Stress τ at a Given Volume Fraction c and Particle Radius R: (a) in aluminum-zinc alloys,[117,118] (b) in copper-cobalt alloys.[119]

The Arrhenius Equation in Plasticity *(U. F. Kocks)*

The dependence of the plastic strain rate $\dot{\gamma}$ on the temperature T is often described by an equation of the form

$$\dot{\gamma} = \dot{\gamma}_0 \cdot \exp(-H^*/kT), \qquad (1)$$

where the parameters $\dot{\gamma}_0$ and H^* may depend on the state of the material and the applied stress. While an Arrhenius term may adequately describe the average waiting time an individual dislocation spends at an individual obstacle, it is by no means evident that the same should hold for the macroscopic average over many dislocations and many obstacles, as expressed in Equation (1). For example, such an equation does not hold when more than one kind of obstacle to dislocation motion is involved, or when more

[117] V. Gerold and H. Haberkorn, phys. stat. sol. *16*, 675 (1966).

[118] S. Harkness, Ph.D. Thesis, University of Florida (1967).

[119] J. D. Livingston, Trans. Met. Soc. AIME *215*, 566 (1959).

than one interaction process between dislocations and a particular obstacle is involved. Furthermore, one might assume that the different spacings and angles to be expected between individual obstacles throughout a specimen constitute sufficient heterogeneity to invalidate Equation (1).

A recent paper[102] has shown that such suspicions concerning the validity of the Arrhenius equation are groundless, in many cases. First let us, however, review two cases in which Equation (1) is obviously violated. One is a competition between two processes in parallel, such as the cutting of obstacles in planar slip and their surrounding by cross-slip. *The strain rates resulting from the two processes are additive* and each may have a different activation energy H^* and preexponential term $\dot{\gamma}_0$. Only if one process predominated, would Equation (1) hold.

The second case involves two processes in series, such as the production of a jog and the subsequent generation of vacancies by the same jog, which lead to an additivity of waiting times, i.e., of the inverses of the exponential in Equation (1). Only if one process predominated, would Equation (1) hold, as is illustrated in Figure 20(a). Since the same neighboring obstacles are involved, *the force on the two successive obstacle parts is the same* at the same applied stress. The waiting times will, in general, be different, and the relative importance of the two obstacle parts may change with temperature, as is shown.

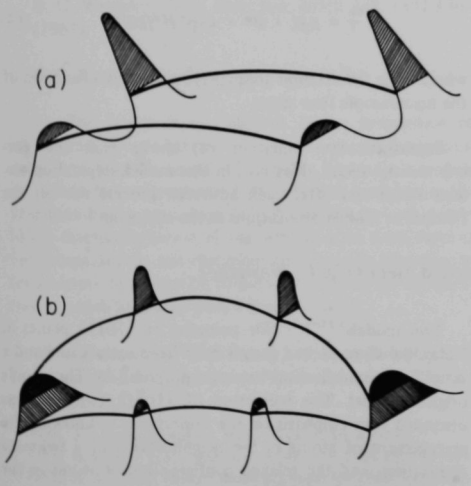

106-9743

Fig. 20. Schematic Force-Distance Curves of Obstacles at Various Locations, and Two Successive Positions of a Dislocation Segment (heavy lines): (a) for two-part obstacles, and (b) for two independent obstacle sets.

Figure 20(b), on the other hand, schematically shows two kinds of obstacles at independent locations, such as forest dislocations and solute atoms. In two successive positions of the dislocation, the included angle at the weak obstacles is acute, while the included angle at the strong obstacles is obtuse. The situation is reversed later. At the same applied stress, the force on the two kinds of obstacles is thus different. The force at the weak obstacles continuously decreases, so that the waiting time increases. The dislocation will remain pinned at the strong obstacles, although the potential waiting time continuously decreases. The critical position is reached when *the waiting time has become the same at both kinds of obstacles*; the dislocation can then break away from both. In other words, the energy H^* to be supplied by thermal fluctuations is the same. Since the number of places at which attempts at breakthrough are made, and the area swept out when an attempt is successful, are not associated with any particular kind of obstacle, there is also a single value of $\dot{\gamma}_0$. Thus, Equation (1) is valid despite the fact that more than one process is involved.

The effective curvature of a dislocation segment pinned at two strong obstacles is, in the example of Figure 20(b), decreased from that due to the applied stress by just the curvature necessary to break through the weak obstacles. The superposition law for the flow stresses of the two processes follows from this argument and is linear, if the two obstacle densities are substantially different.[102] The inverse activation volumes $(-\partial\tau/\partial H^*)_{structure}$ are then also additive, and these two additivity laws together have provided an easy method for separation of the contributions from the two processes.[102]

Finally, the nonregular distribution of obstacles expected in real crystals, which gives rise to a nonuniformity of the force exerted on an obstacle at uniform applied stress, does not lead to a violation of Equation (1). This result was derived[102] from the Statistical Theory of Flow Stress[100,101] and may be illustrated on the random array of obstacle points shown in Figure 21. Imagine that all "neighboring" obstacle points, through which the dislocation must go, were originally connected by lines, and then those links were deleted which are penetrable at or below a given applied stress σ_1. If there were a dislocation source in one of the relatively free areas, it would have emitted one dislocation loop, which, however, would have been stopped at the periphery of this free-slip area. If the stress is now raised so that all the links shown as fine lines become penetrable, the neighboring free-slip areas are separated by only a single link. If the stress were raised such as to make this link penetrable, or if a dislocation source were available in each one of the two neighboring areas, the slip area can suddenly become very large, the back stress on the original source will be relieved, and further loops can thus spread

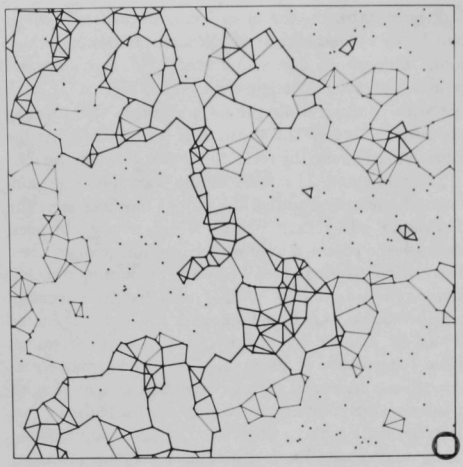

106-9544

Fig. 21. A Diagram of 550 Random Points that Represent Strong Obstacles for which $s_0 = 0.85$. Heavy lines connect all points that cannot be bypassed at an applied stress $0.95 \cdot s_0$, light lines connect those additional points that cannot be bypassed at an applied stress $0.87 \cdot s_0$. These may be overcome by thermal fluctuations. Lower right-hand corner: the square contains one point in the average, the circles indicate the relative stresses.

through a large area. This is the picture we have of the flow stress at 0°K.

If the stress σ_1 is again applied at 0°K, but the temperature, rather than the applied stress, is raised, then, with time, the dislocation may penetrate some of the links (represented by light lines in Figure 21). It is in the nature of the geometry considered here, that the dislocation will progressively encounter harder and harder obstacles so that it will spend more and more waiting time. The obstacle that links the two free-slip areas will be the hardest to overcome.

The area swept out by the dislocation increases very slowly during the easy activation processes, i.e., while it is breaking through the light links, but it increases by the free-slip area a_c when the critical obstacle is overcome. At that point, a sum Σt_i of waiting times has been spent, so that

$$\dot{\gamma} \propto \frac{ba_c}{\Sigma t_i}. \tag{2}$$

As soon as the dislocation has spread into the neighboring area, it will attempt to occupy the old area as well as the other neighboring areas. By this process, a single source will soon make the entire slip plane active. The number of sources per unit volume is thus $1/(a_c d)$ where d is the slip plane spacing, and

$$\dot{\gamma} = \frac{b}{d} \cdot \frac{1}{\Sigma t_i}. \tag{3}$$

Equation (3) is apparently in contradiction with Equation (1). However, the waiting times to be added in Equation (3) are never in competition; their order is determined by geometry and may not change with temperature. The longest waiting time will always occur at the same obstacle that was critical in the determination of the macroscopic flow stress. For all practical purposes, this waiting time is equal to the sum in Equation (3). We can thus write

$$\dot{\gamma} = b/d \cdot \nu^* \cdot \exp(-H^*/kT), \tag{4}$$

where ν^* is the attempt frequency, and H^* is a function of the macroscopic flow stress.

Parenthetically, Equation (4) shows that the pre-exponential factor does not, in this model, depend on the area swept out after each activated process nor on the number of mobile dislocations in the slip plane.

Deformation of Hexagonal Close-Packed Metals *(D. G. Westlake)*

Publications

D. G. Westlake, Scripta Met. *1*, 9-12 (1967).

U. F. Kocks and D. G. Westlake, Trans. Met. Soc. AIME *239*, 1107-1109 (1967).

D. G. Westlake, Acta Met. *15*, 1407-1408 (1967).

D. G. Westlake, Trans. Met. Soc. AIME *239*, 1101-1102 (1967).

Two models[120-122] for twinning on $\{10\bar{1}1\}$ planes in hexagonal close-packed metals have been reevaluated and a simplifying modification has been proposed for Thornton's original model. The prediction of $\{10\bar{1}1\}$ twinning was discussed with emphasis on the importance of knowing the arrangement of atoms in the neighborhood of a twinning dislocation, and the relaxed configuration of atoms in the neighborhood of a $\{10\bar{1}1\}$ "coherent" interface.

[120] P. H. Thornton, Acta Met. *13*, 611 (1965).
[121] P. H. Thornton, Acta Met. *14*, 444 (1966).
[122] D. G. Westlake, Acta Met. *14*, 442 (1966).

The glide and twinning modes responsible for extensive plastic deformation were compiled for 13 hexagonal close-packed metals. The ductilities of these metals were compared with the ductilities predicted by application of the von Mises[123] criterion. We concluded that compatibility can be maintained, for some considerable amount of strain at least, by fewer than five full modes. From a phenomenological point of view, while unlimited ductility is possible only with five full, independent deformation modes, the absence of some modes, especially unidirectional ones, only decreases the *degree* of ductility. In hexagonal close-packed materials about 10% tensile elongation can be obtained with one type of slip (provides two independent modes) plus one type of twinning (provides three additional independent but unidirectional modes). This combination of independent modes is the most restrictive ever observed in any one of the hexagonal close-packed metals at all temperatures. Therefore, fracture, after strains much less than 10% (for example, in polycrystalline zinc or beryllium), cannot be due to a lack of the number of independent deformation modes.

The hydride habit planes, glide planes, and twin planes were determined for zirconium, titanium, hafnium, gadolinium, dysprosium, holmium, erbium, and yttrium. The $\{11\bar{2}1\}$ and $\{10\bar{1}2\}$ planes were either of primary or of secondary importance as twin planes for all of these metals. The $\{10\bar{1}0\}$ prism planes were primary hydride habit planes and primary glide planes for zirconium, titanium, and hafnium; however, for yttrium and the rare earths, while the prism plane was the primary glide plane, hydrides precipitated parallel to the basal plane.

An examination of published experimental results[124] establishes that, in the temperature range 220-300°K, no single thermally activated mechanism for prismatic slip occurs. There is even some doubt in the range 0-220°K. Similarly, the evidence for a single thermally activated mechanism for basal slip is unconvincing.

Hydrogen in Metals *(D. G. Westlake)*

Publications

D. G. Westlake, Trans. Met. Soc. AIME *239*, 1106-1107 (1967).

D. G. Westlake, Trans. Met. Soc. AIME *239*, 1341-1344 (1967).

D. G. Westlake, Phil. Mag. *16*, 905 (1967).

The problems encountered in the preparation of vanadium-hydrogen alloys for transmission electron microscopy have been discussed.[125,126] The problems forced us to initiate the resistometric study of phase equilibria in the vanadium-hydrogen system.[125,127] This approach established that precipitation of the hydride is not suppressed at low temperatures, and that a correlation exists between the temperature for initiation of precipitation and the temperature at which hydrogen embrittlement occurs.

We have discussed,[128] critically, the anomalies that have been reported for the temperature dependence of six physical properties of vanadium: lattice parameters, electrical resistance, thermal expansion, magnetic susceptibility, elastic constants, and thermoelectric power. All of the anomalies were observed between 180 and 250°K. Some investigators explain their observations by invoking a magnetic transition at the anomaly temperature T_A, while others believe that body-centered cubic vanadium assumes a crystal structure of lower symmetry at temperatures below T_A. Our resistometric study[127] of vanadium-hydrogen alloys revealed that phase changes occurred at low temperatures in the alloys, but not in hydrogen-free vanadium. A compilation of the evidence indicates that many of the anomalies reported for vanadium actually may be attributable to hydrogen content.

Habit Planes of the Hydride in Zirconium, Zircaloy-2, and Zircaloy-4: The numerous hydride habit planes reported for zirconium, Zircaloy-2, and Zircaloy-4 have been compiled.[129] The reasons for discrepancies between the results of various researchers were not easily assessed because of the many experimental and analytical techniques. By the use of standardized techniques, we have been able to show that $\{10\bar{1}0\}$ prism planes are the hydride habit planes in zirconium, compared with $\{10\bar{1}7\}$ for both zircaloys.

Niobium-Hydrogen Alloys: A resistometric study of low-temperature phase equilibria in the niobium-hydrogen

[123] R. Z. von Mises, Angew. Math. Mech. *8*, 161 (1928).

[124] E. D. Levine, Trans. Met. Soc. AIME *236*, 1558-1564 (1966).

[125] D. G. Westlake, Annual Progress Report for 1966, Metallurgy Division, ANL-7299, pp. 234-237.

[126] D. G. Westlake, Trans. Met. Soc. AIME *239*, 1106-1107 (1967).

[127] D. G. Westlake, Trans. Met. Soc. AIME *239*, 1341-1344 (1967).

[128] D. G. Westlake, Phil. Mag. *16*, 905 (1967).

[129] D. G. Westlake, *The Habit Planes of Zirconium Hydride in Zirconium and Zircaloy*, J. Nucl. Mater. (to be published).

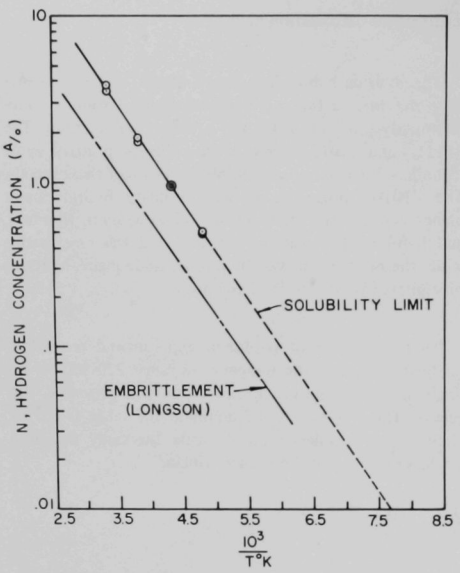

48079

Fig. 22. Log Hydrogen Concentration versus Reciprocal Absolute Temperature.

system has been completed, and the results are shown in Figure 22. The linear plot is described by

$$\ln N = (5.925 \pm 0.012) - \frac{2737 \pm 45}{RT},$$

where N is the solubility limit (expressed as atomic percent). The heat of solution of niobium hydride in saturated niobium-hydrogen solid solution is, therefore, 2.737 kcal/g atom.

This is in good agreement with 3 ±0.3 kcal/mole obtained by Longson[130] when he plotted the logarithm of the hydrogen concentration causing embrittlement versus reciprocal temperature. The plots are nearly parallel, but are not coincident. Thus, some correlation seems to exist between precipitation and embrittlement, but embrittlement occurs at a temperature slightly above the critical temperature for precipitation of the hydride, as indicated by our phase diagram. This seems to be explained by a theory now being developed for hydrogen embrittlement that is based on triaxial stress-inducement of precipitation of the hydride phase during tensile testing.

130B. Longson, TRG Report 1035(c), January 12, 1966.

Ductile-Brittle-Ductile Transition: As is well established,[131,132] hydrogenated vanadium or niobium tensile specimens are ductile at ambient temperature, but become brittle as the temperature is reduced, and regain ductility at temperatures near 77°K. This has been explained in terms of hydrogen mobility at the various temperatures coupled with the interaction between hydrogen atoms and dislocations. The experiments described below indicate that these are not important; instead, it is the substructure resulting from thermal history that influences the mechanical behavior at a given temperature.

We have been able to show, by standard metallographic techniques, that slow-cooled specimens exhibit large hydride particles, while quenched specimens exhibit only very small particles. During quenching, the particles punch prismatic dislocation loops into the matrix. Evidence for this phenomenon is shown in Figure 23. The Nb-1% hydrogen alloy tensile tested at 298°K had a yield point. The load drop is a manifestation of dislocation multiplication by the double cross-glide mechanism. When a similar alloy was cycled between 298 and 77°K before tensile testing, sufficient mobile dislocations were produced so that the yield point was eliminated. Increased numbers of

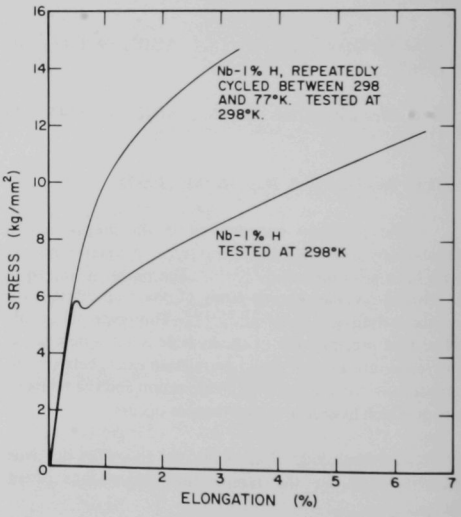

47755

Fig. 23. Effect of Prismatic Dislocation Loops on the Mechanical Behavior of Niobium-Hydrogen Solid Solutions.

131A. L. Eustice and O. N. Carlson, Trans. Met. Soc. AIME *221*, 238 (1961).

132T. W. Wood and R. D. Daniels, Trans. Met. Soc. AIME *233*, 898 (1965).

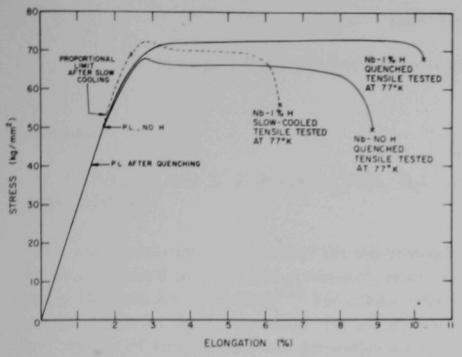

48078

Fig. 24. Effect of Cooling Rate on the Mechanical Behavior of Niobium-Hydrogen Alloys at 77°K.

dislocation interactions produced a marked increase in the rate of strain hardening.

The effect of substructure on the mechanical properties at 77°K is shown in Figure 24. The quenched alloy does not exhibit a yield point for the reason given above. Its proportional limit is actually lower than that of the hydrogen-free niobium because with the increased density of mobile dislocations, macroyielding would occur at a lower stress. The rate of strain hardening was also increased. Both uniform and total elongation were actually greater for the alloy. Necking was observed in both specimens.

The effect of large particle size is also shown in Figure 24. The Nb-1% hydrogen alloy that was slow-cooled to 77°K, did exhibit a yield point, and did neck to failure, but the uniform elongation was greatly reduced. Thus, the so-called "return of the ductility" at 77°K must be attributed to the fact that, in the earlier studies, quenching to this temperature resulted in many mobile dislocations and small particles that probably do not contribute substantially to the initiation of cracks.

Extrapolation of the plot in Figure 22 reveals that below about 140°K the sclubility of hydrogen in niobium is negligible. We observe that below about 140°K niobium-hydrogen alloys neck before failure, but over a large range of T >140 the alloys fail without necking. Thus, the capacity for necking apparently is dependent on complete precipitation of hydrogen from solid solution. When some hydrogen remains in solid solution, the triaxial stress state that occurs at the onset of necking may induce precipitation of hydride particles. Their presence would inhibit glide and lead to fracture without further plastic deformation.

DIFFUSION IN SOLIDS

Isotope Effect for Self-Diffusion in Zinc *(N. L. Peterson and S. J. Rothman)*

Publication

N. L. Peterson and S. J. Rothman, Phys. Rev. *163*, 645-649 (1967).

The experiments on isotope effect for self-diffusion in zinc were discussed in detail and preliminary results were given in the 1966 Annual Report.[133] The cited publication contains results for the isotope effect for self-diffusion in single crystals of zinc, parallel and perpendicular to the *c* axis, at seven temperatures in the range 289-418°C. The conclusions from this study are: (1) diffusion in zinc takes place by the vacancy mechanism, (2) the correction factor for many-body effects at the saddle point ΔK is 0.93 ±0.03, independent of temperature and direction of diffusion, (3) diffusion along dislocations significantly lowers the isotope effect, and (4) self-diffusion in zinc is given by

$$D(\text{parallel to the } c \text{ axis}) = (0.13 \pm 0.01) \exp(-21\,900 \pm 150/RT)\ \text{cm}^2/\text{sec},$$

and

$$D(\text{perpendicular to the } c \text{ axis}) = (0.18 \pm 0.01) \exp(-23\,000 \pm 110/RT)\ \text{cm}^2/\text{sec}.$$

Isotope Effect for Diffusion of Zinc in Silver, Copper, and CuZn *(S. J. Rothman and N. L. Peterson)*

Publications

S. J. Rothman and N. L. Peterson, Phys. Rev. *154*, 552-558 (1967).

N. L. Peterson and S. J. Rothman, Phys. Rev. *154*, 558-560 (1967).

The results of these experiments were reported[133] and the program terminated with the publication cited.

Impurity Diffusion in Aluminum *(N. L. Peterson and S. J. Rothman)*

The background for these experiments, as well as results for the diffusion of zinc, gallium, and cobalt in aluminum have been reported.[133] We have measured the diffusion of ^{71}Ge and ^{64}Cu in aluminum single crystals, and found:

$$D_{Ge} = 0.48 \pm 0.01 \exp(-29\,000 \pm 210/RT)\ \text{cm}^2/\text{sec},$$

and

$$D_{Cu} = 0.65 \pm 0.01 \exp(-32\,270 \pm 270/RT)\ \text{cm}^2/\text{sec}.$$

The activation energies for impurity and self-diffusion in aluminum are shown in Table 14. With the exception of copper, the activation energy for impurity diffusion is the same as the most recently measured value for self-diffusion in aluminum.[134] This indicates that the high impurity-vacancy binding energies in aluminum found in quenching studies[135] are not correct.

TABLE 14. Activation Energies for Diffusion in Aluminum

Impurity	Activation Energy, cal/mole	Impurity	Activation Energy, cal/mole
Self-diffusion[134]	28 750 ±800	Gallium	29 500 ±140
Copper	32 270 ±270	Germanium	29 000 ±200
Zinc	28 850 ±150		

Further evidence for the near-zero impurity-vacancy binding energies in aluminum is obtained from our measurements of the isotope effect for the diffusion of zinc in aluminum. From a measurement of the simultaneous diffusion of two different isotopes (α and β) of the same element, the product of $f\Delta K$ can be obtained, where f is the correlation factor. Although we do not have a value of ΔK for zinc diffusion in aluminum, we can state with reasonable certainty that ΔK is independent of temperature and probably lies between 0.8 and 1.0. If there is a binding energy between the impurity and vacancy, f will vary with temperature. If f is temperature independent, the impurity-vacancy binding energy must be small. Our preliminary measurements of the diffusion of ^{65}Zn and ^{69}Zn in aluminum show f is constant over a fairly wide temperature range, which supports our conclusion that impurity-vacancy binding energies in aluminum are very small.

Measurements of the diffusion of ^{110}Ag and ^{28}Mg in aluminum are now in progress. Quenching studies have

[133] S. Rothman and N. Peterson, Annual Progress Report for 1966, Metallurgy Division, ANL-7299, pp. 246-248.

[134] F. Y. Fradin and T. J. Rowland, Appl. Phys. Letters *11*, 207 (1967).

[135] Reviewed by M. Doyama, Phys. Rev. *148*, 681 (1966).

shown large binding effects for these impurities, but high-temperature equilibrium studies[136] have shown that the impurity-vacancy binding energy in these systems is nearly zero.

Diffusion of Copper in Iron *(N. L. Peterson, S. J. Rothman, and C. M. Walter)*

This study was undertaken to check the highly unusual results of Anand and Agarwala,[137] who found that the Arrhenius plots for diffusion of copper in iron do not show a discontinuity at the alpha-gamma transformation temperature. This result is unusual because most measurements for tracer diffusion in iron show a change of two orders of magnitude in the diffusion coefficient at 910°C and there seems to be no reason why copper should behave differently.

We have measured the diffusion of ^{64}Cu in alpha and gamma iron. Linear penetration plots, representative of lattice diffusion, were obtained at $T > 1250$°C in gamma iron and $T \geq 850$°C in alpha iron. At $T \leq 815$°C in the alpha phase and $T < 1250$°C in the gamma phase, curved penetration plots, indicating the presence of grain-boundary diffusion, were obtained. Autoradiographs of a tapered section of iron samples diffused at 800°C in the alpha phase and at 1000°C in the gamma phase showed preferential penetration along the grain boundaries.

The values of D, taken at temperatures where grain-boundary diffusion is not dominant, are plotted versus $1/T$ in Figure 25 together with the data for self-diffusion in pure iron.[138,139] There is a discontinuity at the alpha-gamma transformation temperature, contrary to the data of Anand and Agarwala.[137] The large values of D, obtained by Anand and Agarwala at low temperatures in the gamma phase, must represent grain-boundary diffusion rather than lattice diffusion.

The low values of D, obtained in Reference 137 at high temperatures in the alpha phase may be explained by the following experiment. We measured the diffusion of ^{64}Cu in an impure Armco iron sample that contained many inclusions. The penetration plot for this sample showed a much steeper slope near $X = 0$ (smaller D) than for the pure iron sample that underwent the same heat treatment. The region of steep slope was followed by a region dominated by dislocation diffusion. We believe that the steep slope is due to the trapping of copper by the inclusions. An autoradiograph of an identical sample had intense "dots" in the diffused zone, thus showing that the ^{64}Cu atoms were trapped at various sites in the iron single crystal.

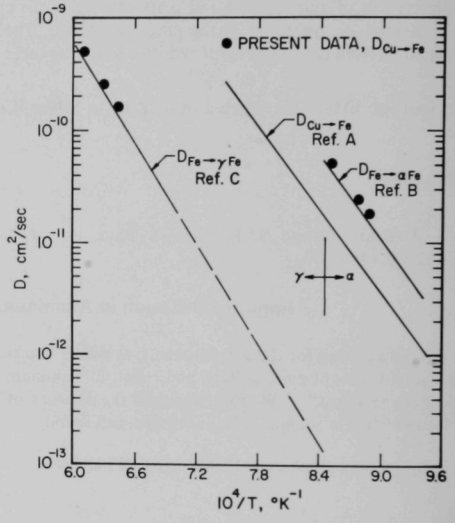

48142

Fig. 25. Plot of log D versus $1/T$ for the Diffusion of Copper and for Self-Diffusion in Iron. Reference A is Reference 137; Reference B is Reference 138; and Reference C is Reference 139.

136D. R. Beaman, R. W. Balluffi, and R. O. Simmons, Phys. Rev. *134*, A532 (1964); ibid. *137*, A917 (1965).

137M. S. Anand and R. P. Agarwala, J. Appl. Phys. *37*, 4248 (1966).

138F. S. Buffington, K. Hirano, and M. Cohen, Acta Met. *9*, 434 (1961).

139T. Heumann and R. Imm (to be published).

Diffusion in Body-Centered Cubic Metals

From measurements of the isotope effect, effect of pressure on diffusion, effect of solutes on self-diffusion, impurity diffusion, Simmons-Balluffi-type experiments, and quenching studies, it is clear that diffusion in face-centered cubic (fcc) metals occurs by the vacancy mechanism. Even though many of these measurements have been made on body-centered cubic (bcc) metals, there is no bcc metal for which we can state unambiguously the mechanism of diffusion. Sodium is probably the simplest and most thoroughly investigated bcc metal. Isotope effect measurements in sodium[140] give $f\Delta K = 0.36$, which is consistent with several diffusion mechanisms. The effect of pressure measurements on self-diffusion in sodium[141] gives a low activation volume suggesting that diffusion occurs by a highly relaxed defect mechanism. Simultaneous measurements of lattice parameter and thermal expansion[142,143] show that an appreciable concentration of vacancies exists in sodium near the melting point. These measurements[143] combined with the self-diffusion measurements[140] suggest that the activation energy for defect formation is at least ten times larger than the activation energy for defect motion in sodium.

Much less data are available for the bcc transition elements and the data that are available cannot be interpreted in terms of a unique diffusion mechanism. Some of the bcc metals have very low (and temperature dependent) values of activation energy for diffusion. In an effort to delineate the diffusion mechanism in the bcc metals, programs have been initiated to study diffusion in the alkali metals and in a transition metal.

DIFFUSION IN ALKALI METALS *(J. N. Mundy)*

The self- and impurity-diffusion coefficients, the isotope effect parameters for self-diffusion and impurity diffusion, and the effects of solute additions on self-diffusion will be measured on a sodium-base alloy system. In view of the very low isotope effect in sodium and the large relaxation around vacancies in this open bcc structure, measurements of the isotope effect for sodium self-diffusion, as a function of temperature and pressure, will be made in sodium single crystals.

The reactive nature of the alkali metals necessitates the building of special equipment to make these experiments. The designs for the apparatus are complete and construction is under way.

DIFFUSION IN DELTA AND GAMMA IRON *(C. M. Walter and N. L. Peterson)*

Iron was selected as the bcc transition metal to be studied because it appeared that a good isotope pair (^{52}Fe and ^{59}Fe) could be developed, and our techniques could be checked in the more readily understood fcc gamma phase. Both isotope-effect experiments and the effect of solutes on self-diffusion are in progress.

Isotope Effect–Experimental Techniques and Results: Isotope ^{59}Fe with a half-life of 45.1 days is purchased, and isotope ^{52}Fe with a half-life of 8.3 hours is produced in the Argonne cyclotron by the reaction ^{50}Cr $(\alpha, 2n)$ ^{52}Fe.* The isotopes are diffused simultaneously into high-purity iron samples. After the diffusion anneal, the samples are sectioned on a lathe, and the concentration of ^{52}Fe (C_{52}) and ^{59}Fe (C_{59}) is determined to 0.1% in each section by the half-life technique.[144] The slope of the plot of ln C_{59}/C_{52} versus ln C_{59} yields a value of $f\Delta K$. Four successful experiments were made in the bcc delta phase. The ln C_{59}/C_{52} versus ln C_{59} plots for these samples are shown in Figure 26, and the results are summarized in

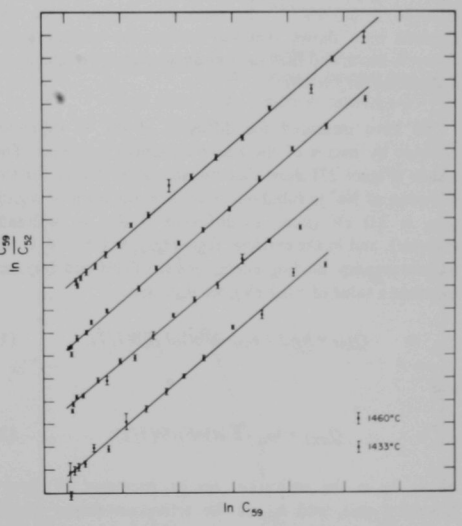

48136

Fig. 26. Plot of ln C_{59}/C_{52} versus ln C_{59} for ^{52}Fe-^{59}Fe Diffusion in Gamma Iron. Each division on the ordinate is 0.01. Each division on the abscissa is 1.0. Log C_{59} decreases from left to right. Log C_{59}/C_{52} is negative and decreases from bottom to top.

[140] J. N. Mundy, L. W. Barr, and F. A. Smith, Phil. Mag. *14*, 785 (1966).

[141] N. H. Nachtrieb, J. A. Weil, E. Catalano, and A. W. Lawson, J. Chem. Phys. *20*, 1189 (1952).

[142] G. A. Sullivan and J. W. Weymouth, Phys. Rev. *136*, A1141 (1964).

[143] R. Feder and H. P. Charbnau, Phys. Rev. *149*, 646 (1966).

*We gratefully acknowledge Mr. M. Oselka and Mr. J. J. Hines for their assistance and cooperation in producing this isotope.

[144] S. J. Rothman and N. L. Peterson, Phys. Rev. *154*, 552 (1967).

TABLE 15. Isotope Effect for Self-Diffusion in Delta Iron (ΔK Calculated Assuming a Vacancy Mechanism)

Temperature, °C	D, cm^2/sec x 10^{-8}	$1 - D_{59}/D_{52}$	ΔK
1433	8.20	0.0208 ±0.0003	0.468 ±0.007
1433	7.95	0.0206 ±0.0003	0.464 ±0.007
1460	1.16	0.0206 ±0.0004	0.464 ±0.009
1460	1.19	0.0201 ±0.0004	0.451 ±0.009

Table 15. Assuming a vacancy mechanism ($f = 0.727$) one obtains the ΔK values listed. Future experiments will be made in the gamma phase and further experiments are planned for the alpha and delta phases.

Assuming a vacancy mechanism, the data to date reproducibly give $\Delta K = 0.46$, which is in good agreement with the results on bcc sodium ($\Delta K = 0.50$), but is much smaller than the ΔK values found for fcc crystals (typically 0.8 to 1.0). The values of $f\Delta K$ obtained for fcc crystals are consistent only with the vacancy mechanism, but the results for delta iron and sodium are consistent with many diffusion mechanisms.

Effect of Solute Additions on Self-Diffusion: From measurements of the effect of solute additions on self-diffusion, one may obtain the correlation factor for solute diffusion f_i.[145] By choosing a solute that diffuses slower than self-diffusion, one limits f_i for the vacancy mechanism to a value outside the range of f_i for some substitutional mechanisms. Since cobalt diffusion in gamma and delta iron is slower than self-diffusion, we have begun experiments using cobalt as the solute. Four iron-cobalt alloys containing 0.75, 1.5, 2.25, and 3.0 at.% cobalt have been prepared. Since the measurement of temperature leads to the largest error, all diffusion anneals at a given temperature will be made simultaneously in a large heat sink. Measurements will be made in the alpha, gamma, and delta phases.

Diffusion of Sodium in Rubidium Chloride *(N. L. Peterson and S. J. Rothman)*

These experiments are an attempt to verify the calculations of Tosi and Doyama[146] who found that the activation energy for the jump of a sodium ion in rubidium chloride is only 0.2 eV, and the activation energy for the diffusion of Na^+ in rubidium chloride is 1.22 eV. The experimental value for the diffusion of Rb^+ in rubidium chloride is 2.0 eV.[147] In these calculations, Tosi and Doyama have shown that the sodium ion-vacancy interaction is small, and they have assumed that the temperature dependence of f is zero.

We have measured the diffusion of Na^+ in rubidium chloride by means of the tracer-sectioning technique. The results (Figure 27) show that the activation energy for the diffusion of Na^+ in rubidium chloride in the intrinsic region Q_{int} is 2.0 eV (same as diffusion of Rb^+ in rubidium chloride), and in the extrinsic region Q_{ext} is 0.61 eV. If the sodium-vacancy binding energy is zero (Tosi and Doyama calculate a value of ~0.1 eV), we may write

$$Q_{int} = h_f/2 + h_m - k\,\partial(\ln F_i)/\partial(1/T), \qquad (1)$$

and

$$Q_{ext} = h_m - k\,\partial(\ln F_i)/\partial(1/T), \qquad (2)$$

where h_f is the activation energy necessary to form a Schottky pair, and h_m is the activation energy of Na^+ motion in rubidium chloride. In order to obtain agreement between the theoretical values of h_f and h_m and the experimental values of Q_{int} and Q_{ext}, the temperature dependence of the correlation factor must be large.

The term $k\,\partial(\ln F_i)/\partial(1/T)$ may be determined experimentally by measuring the isotope effect for Na^+ diffusion in rubidium chloride. We have made five measurements of the diffusion of ^{22}Na and ^{24}Na in rubidium chloride. Since the decay schemes of ^{22}Na and ^{24}Na are qualitatively similar to those of ^{65}Zn and ^{69}Zn, respectively, the

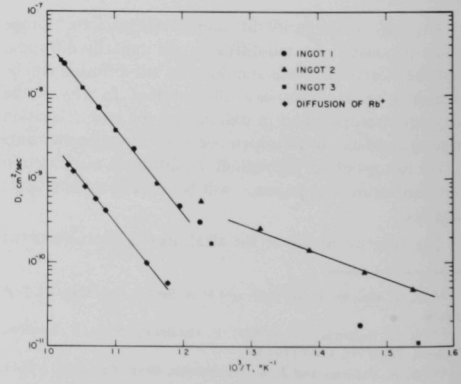

48143

Fig. 27. Plot of log D versus $1/T$ for Diffusion of Na^+ in Rubidium Chloride. The rubidium chloride ingot 2 contains more polyvalent impurities than ingots 1 and 3. Diffusion of Rb^+ in rubidium chloride[147] is also shown.

145A. B. Lidiard, Phil. Mag. *5*, 1171 (1960).
146M. P. Tosi and M. Doyama, Phys. Rev. *151*, 642 (1966).
147G. Arai and J. G. Mullen, Phys. Rev. *143*, 663 (1966).

TABLE 16. Isotope Effect for Na^+ Diffusion in Rubidium Chloride

Measurement Number	Temperature, °C	$f\Delta K'$
1	531.9	0.242 ±0.024
2	587.6	0.280 ±0.014
3	634.7	0.312 ±0.031
4	678.0	0.377 ±0.006
5	707.0	0.362 ±0.022

experimental method used is similar to that for the zinc isotopes.[144] The results (Table 16) yield $k\,\partial(\ln F_i)/\partial(1/T)$ ~0.2 eV. The experimental measurements are not in agreement with the theoretical value of h_m. From the difference Q_{int}-Q_{ext}, the theoretical value of $hf/2$ is too small by 0.4 eV.

In order to specify the impurity content of our rubidium chloride crystals, we have started measurements of the electrical conductivity of rubidium chloride, as a function of temperature, with a standard ac bridge technique. A least-squares program is being developed for analysis of the results.

Oxygen Diffusion in Near-Stoichiometric α-Nb_2O_5 *(W. K. Chen and R. A. Jackson)*

Publication

W. K. Chen and R. A. Jackson, J. Chem. Phys. *47*, 1144 (1967).

Diffusion measurements were used to investigate the nature of the predominant defect in the oxygen-deficient α-Nb_2O_5 in the near-stoichiometric range of composition. The results and conclusions were reported in the cited publication and were summarized in the Annual Progress Report for 1966.[148]

Oxygen Diffusion in Undoped and Doped Cobalt Monoxide *(W. K. Chen and R. A. Jackson)*

Publication

W. K. Chen and R. A. Jackson, Bull. Am. Ceram. Soc. *46*(4), 357 (1967). Abstract

The purpose of the program is to study the type of point defect responsible for the anion transport in oxygen-excess cobalt monoxide.

The diffusion measurements were made on single crystals grown by the Vernuil process in an arc-image furnace. The starting material for undoped crystals was a "Baker analyzed" reagent-grade cobalt oxide powder. The doped cobalt-oxide powders were obtained from decomposition of cobalt oxalate mixed with dopant oxalate. Oxygen diffusion was determined by the gas/solid O-18 isotopic exchange technique. The apparatus and the procedures were similar to those described previously.[149] The oxide specimen used in this experiment was a thin, parallel-faced, crystal wafer cleaved from a crystal boule along the (100) cleavage plane.

Undoped Oxide: The diffusion coefficients were determined for undoped cobalt monoxide at a constant oxygen pressure in the temperature range from 1175 to 1560°C. The results are plotted as log D versus $1/T$ in Figure 28. The

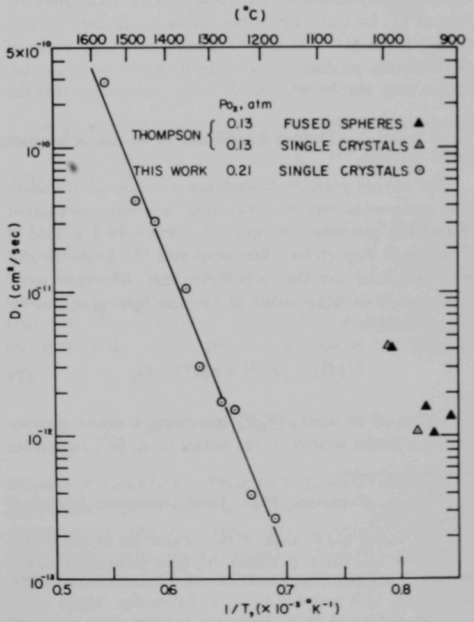

48083

Fig. 28. Oxygen Diffusion Coefficient D in Undoped Cobalt Monoxide Plotted versus Temperature at P_{O_2} = 0.21 atm.

[148] W. K. Chen and R. A. Jackson, Annual Progress Report for 1966, Metallurgy Division, ANL-7299, pp. 276-278.

[149] W. K. Chen and R. A. Jackson, J. Chem. Phys. *47*, 1144 (1967).

best least-squares fit straight line is represented by

$$D = 50 \exp(-95 \pm 5 \text{ kcal}/RT) \text{ cm}^2/\text{sec.} \quad (1)$$

The data previously determined by Thompson[150] at the lower temperatures are also included in Figure 28. From transition-state theory, the preexponential term in Equation (1) gives the entropy of activation to be 14.4 e.u./mole.

Attempts were made to study the influence of oxygen pressure on diffusion with 0-18 enriched oxygen gas as well as 0-18 enriched CO-CO_2 gas mixtures. In CO-CO_2 gas mixtures, a constant CO/CO_2 ratio in the closed system was difficult to maintain throughout the course of the exchange annealing; therefore, the results were inconclusive.

Doped Oxides: At high temperature and moderate oxygen pressure, a singly ionized cobalt vacancy is believed to be the predominant defect for oxygen-excess cobalt monoxide. This is supported by a number of experimental findings, such as the electrical conductivity,[151-153] and the cobalt ion diffusivity[154] are approximately proportional to the one-fourth power of oxygen pressure at a constant temperature. The defect equilibrium can be influenced by the incorporation of aliovalent cations. Thus, substitution of Li^+ for Co^{2+} diminishes the cation vacancy concentration while Al^{3+} increases its concentration. By virtue of the Schottky product relation, the defect in the anion sublattice may also be influenced. If one can assume that the oxygen ions migrate via a random motion of oxygen vacancies, the diffusion coefficient is expected to increase or decrease with increasing concentration of doped Li^+ or Al^{3+} in cobalt monoxide at constant temperature and oxygen pressure. This was experimentally observed, as shown in Figure 29. A tentative conclusion derived from this study is that oxygen ions diffuse via oxygen vacancies in cobalt monoxide.

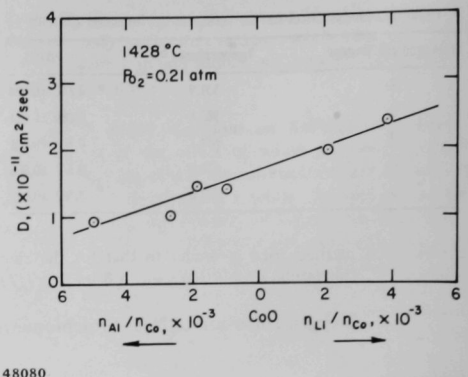

Fig. 29. Oxygen Diffusion Coefficient D in Doped Cobalt Monoxide Plotted versus Concentrations of Dopants at 1428°C and P_{O_2} = 0.21 atm.

Defect Equilibria in Nonstoichiometric Oxides *(M. L. Volpe and J. F. Reddy)*

The oxygen pressure dependence of cation self-diffusion and semiconductivity in nickel oxide has been investigated during the past year. The methods previously described in the Annual Report for 1966 were used.[155] Evidence also was presented for the hypothesis that attributes semiconductivity in nickel oxide to electron holes produced by the reaction:

$$1/2\, O_2 = [V_C^{-a}] + a[h^+] + O_\ell \quad (1)$$

with a equal to unity, $[V_C^{-a}]$ represents a cation vacancy having a charge relative to the lattice of $-a$, $[h^+]$ represents an electron hole, and O_ℓ is an oxygen ion in a normal lattice position. In nickel self-diffusion, a more complicated situation is found; either cation vacancies, other than those arising from Equation (1), must be considered, or some complex defect interactions must be invoked.

Our experiments were conducted on single-crystal wafers grown from a single batch of powder to insure identical impurity concentrations. Prediffusion anneals were used at temperatures below 1450°C to establish the defect concentration. For duplicate diffusion runs, this procedure permitted the standard deviation from the mean at all temperatures to be kept below 4%. Usually, during each diffusion anneal, the electrical conductivity was measured on a crystal held within a few millimeters of the diffusion sample. The oxygen pressure dependence was determined by making runs at a number of temperatures in pure carbon dioxide as well as in pure oxygen. The carbon dioxide atmosphere provided partial pressures of oxygen from about 10^{-4} atm at the lowest temperature to 10^{-2} atm at the highest, and, along with the runs in pure oxygen, permitted measurement of the pressure dependence as a function of temperature. These data are presented in

150B. A. Thompson, Ph.D. Thesis, Rensselaer Polytechnic Institute, 1962.

151C. Wagner and E. Koch, Z. Phys. Chem. (B) *32*, 439 (1936).

152N. G. Eror and J. B. Wagner, Jr., Paper presented at the Fall Meeting of the Met. Soc. AIME, Cleveland, Ohio, October 20-24, 1963.

153B. Fisher and D. S. Tanhauser, J. Chem. Phys. *44*, 1663 (1966).

154R. E. Carter and F. D. Richardson, J. Metals *6*, 1244 (1954).

155M. L. Volpe and J. F. Reddy, Annual Progress Report for 1966, Metallurgy Division, ANL-7299, pp. 272-274.

Figures 30 and 31. The pure carbon dioxide-pure oxygen results are being checked by runs using oxygen-argon mixtures.

The pure carbon dioxide-pure oxygen Arrhenius plots (Figures 30 and 31) are strictly linear; this is especially notable for diffusion where the temperature range extended to 0.9 of the melting point of the oxide (2223°K). The oxygen pressure dependence β was calculated from these plots under the usual assumptions:[156]

$$D_{Ni} \, a P_{O_2}^{\beta D}, \quad \sigma a P_{O_2}^{\beta C}, \tag{2}$$

where D_{Ni} is the nickel self-diffusion coefficient, σ the electrical conductivity, and P_{O_2} the equilibrium partial pressure of oxygen. It was found that β_D was between 1/4 and 1/6 and increased with temperature. On the other hand, β_C did not vary with temperature (or increased only slightly) and the magnitude was between 1/4 and 1/5. For β to be independent of temperature, the activation energy in pure carbon dioxide must be greater than the activation

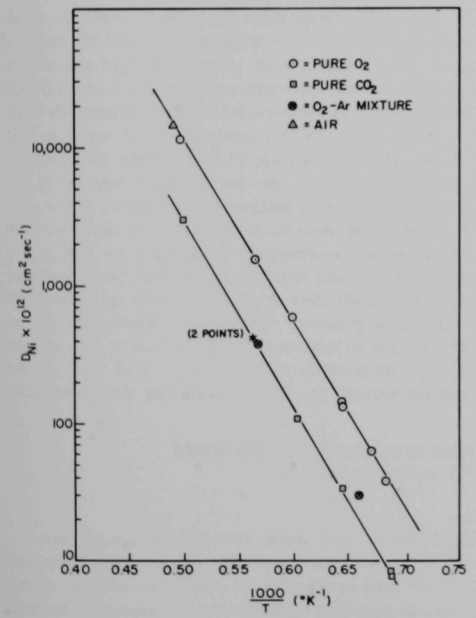

48085

Fig. 30. Arrhenius Plots for Nickel Self-Diffusion in Nickel Oxide. For pure oxygen, $D_{Ni} = 5.60 \times 10^{-2} \exp[-60.8(1000/RT)]$ cm^2/sec. For pure carbon dioxide, $D_{Ni} = 2.26 \times 10^{-2} \exp[-62.5(1000/RT)]$ cm^2/sec. The point made in air was corrected to $P_{O_2} = 1$ atm by using the value of β appropriate to the temperature of the run. The oxygen-argon points are for $P_{O_2} = 1.60 \times 10^{-3}$ atm.

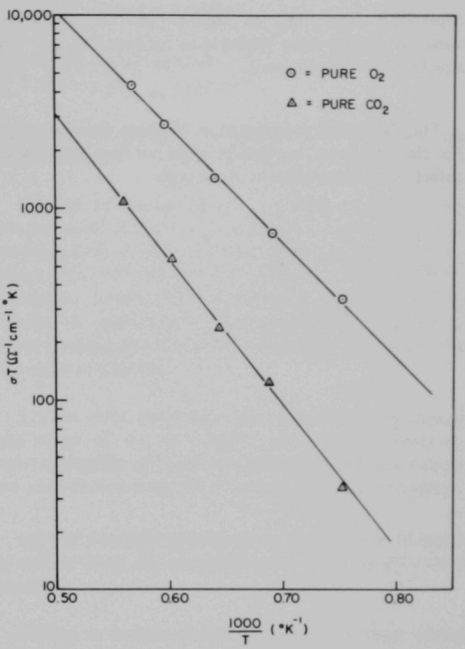

48084

Fig. 31. Arrhenius Plots for Semiconductivity of Nickel Oxide. For pure oxygen, $\sigma T = 1.02 \times 10^7 \exp[-27.4(1000/RT)]$ Ω^{-1} cm^{-1} °K. For pure carbon dioxide, $\sigma T = 1.70 \times 10^7 \exp[-34.4(1000/RT)]$ Ω^{-1} cm^{-1} °K.

energy in pure oxygen by $[3/2\ a]^{-1}\ \Delta H$, ΔH being the standard enthalpy change of the reaction: $1/2\ O_2 + CO = CO_2$. Thus, the activation energy difference for diffusion must be 8.4 kcal/mole instead of only 1.7 kcal/mole, as was observed. The functional relationship derived for the variation of the oxygen pressure dependence for diffusion was:

$$\beta_D = [0.152 + 0.104x]\,[3.51x - 1]^{-1}, \tag{3}$$

where $x = 1000/T(°K)$. These findings were confirmed by experiments performed at constant temperature with oxygen-argon mixtures having different values of P_{O_2}. In these experiments, β_D was found to be 0.197 at 1380°C, and 0.163 at 1245°C, values that compare very well with those calculated from Equation (3), 0.192 and 0.168, respectively. On the other hand, β_C did not vary

156 R. A. Swalin, *Thermodynamics of Solids* (John Wiley and Sons, Inc., New York, 1962), p. 291ff.

appreciably from 1205 to 1056°C, and was about the same for oxygen-argon mixtures as for pure CO_2 (β_C was equal to 0.22 in both cases).

The theoretical interpretation of these observations is not clear. However, our results could not have been due to defect association reactions of the type

$$[V_C^{-2}] + [h^+] = [V_C^-] \tag{4}$$

that have been invoked in other cases of variable pressure dependence.[154] Equation (4) would predict a *decrease* of both β_C and β_D with increasing temperature, whereas in our research an *increase* was observed for β_D alone. The application of the simple Debye-Hükel interactions[157] also predicts that β would decrease with increasing temperature.

[157] F. E. Kröger, *The Chemistry of Imperfect Crystals* (Interscience, New York, 1964), p. 279ff.

ELASTIC PROPERTIES OF METALS AND ALLOYS

Elastic Moduli of Body-Centered Cubic Titanium and Titanium-Chromium Alloys *(E. S. Fisher and D. J. Dever)*

The interaction between closed ionic shells in metals or alloys with the body-centered cubic (bcc) structure leads to a calculated negative contribution to the elastic shear modulus $c' = (c_{11} - c_{12})/2$, for (110) [110] shear. The occurrence of body-centered structures among metals is presumed to be caused by properties that either minimize or oppose the repulsive forces between overlapping ions and produce a positive value for c'. In the bcc alkali metals, the large separation between the ions minimizes the ionic overlap and c' is positive, but still only about 1/10 of c_{44} (i.e., the anisotropy factor, $A = c_{44}/c' \sim 10$). The bcc transition metals, however, are presumed to be rendered stable by attractive forces that accompany the exchange interactions between the overlapping unfilled d electron shells. Thus, vanadium, chromium, molybdenum, niobium, tantalum, and tungsten have A ratios near unity. The A ratios in bcc titanium and zirconium (transition metals with fewer d electrons) have not been measured, but are of considerable interest. Since these structures are stable only at relatively high temperatures, an assumption can be made that the anisotropy ratio is relatively large ($A \sim 10$) and that the d electrons in titanium and zirconium do not contribute the exchange forces necessary for strengthening c'. As proposed, the stability of the β phase at $T > 0.5T_m$ may be due to the high vibrational entropy. An alternative assumption is that an unusual temperature dependence of the d electron exchange interaction exists such that c' becomes nearly zero, or negative, at temperatures just below the structure transformation. In the latter case, the A ratio in the stable range should be nearer to unity than in the alkali metals and should decrease with increasing temperature because of a positive dc'/dT. The assumption ($dc'/dT > 0$) has in fact been invoked as an explanation for the anomalously low activation energies and negative entropy factors for self-diffusion and impurity diffusion in titanium and zirconium.

Because of several obvious difficulties in the direct measurement of the elastic anisotropy in pure β titanium, measurements are being made in single crystals of titanium alloys with ~10, 15, and 30% chromium. The addition of chromium lowers the $\alpha\beta$ transition temperatures and enables the quenching in of the metastable β structure at room temperatures. The results obtained to date lead to the following conclusions:

(1) The shear anisotropy ratio in pure β titanium is in the range of 4:6 at 1000°C, an indication that the nearest-neighbor overlap forces contain a significant attractive contribution from the d electron exchange interaction.

(2) The β stabilizing influence of chromium in titanium is derived from the sensitivity of c' to the number of d electrons.

(3) The ω structure forms as a metastable phase during aging of the dilute alloys at $T < 400$°C, and is very similar to the bcc structure in the relative atomic positions. Because of an extremely large increase of c' in the transformation, the ω structure is more stable and mechanically harder than the bcc structure.

Experiments with single crystals of a 7% chromium alloy are now in progress to determine c' and dc'/dT in pure β titanium with greater numerical accuracy than permitted with the present data. The c_{44} modulus has been obtained from measurements in unalloyed single crystals of titanium at $T > 950$°C.

Electronic Contributions to Elastic Moduli in Rare Earth and Actinide Metals and Alloys *(E. S. Fisher and D. J. Dever)*

Scandium and the rare earth metals have relatively large electronic specific-heat coefficients, which indicates a high density of electronic states near the Fermi level. On the basis of paramagnetic susceptibility data and electron-energy band calculations, apparently the high density of states arises from strong electron-phonon interactions at, or near, 0°K. As the Fermi level increases in energy with temperature, the effect of the strong electron-phonon interaction may be observed in the temperature dependence of the elastic moduli, particularly if the density-of-states curve has a significant slope near the Fermi level. We have observed very clear anomalies in the temperature dependence of ultrasonic wave velocities in scandium (Figure 32) at temperatures as high as 300°K and in gadolinium, dysprosium, and erbium at somewhat higher temperatures. These anomalies are observed only for compressional and transverse waves propagated along the c direction, an indication of a highly anisotropic Fermi surface.

In the case of scandium, the purity of the sample has a very marked effect on the extent of the anomaly, as shown in Figure 32. Chemical analyses suggest that this effect was

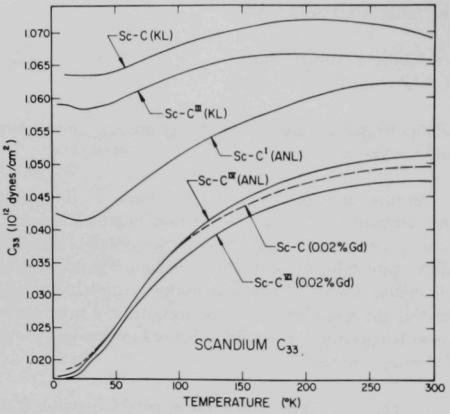

47818

Fig. 32. Temperature Dependence of c_{33} in Each Lot of Single Crystals of Scandium.

caused by variation in thorium content among the samples. Crystals C(KL) and C^{III}(KL),* each contained approximately 500 ppm thorium, and crystal C^{I}(ANL), made by annealing an arc-melted button, contained about 50 ppm thorium. In contrast, crystal C^{IV}(ANL) and the gadolinium alloy crystals, made by annealing levitation-melted buttons, contained <10 ppm thorium. Variations in gadolinium compositions, up to 200 ppm produced only very slight effects. The absence of a pronounced effect of additions of gadolinium is consistent with the similarities of the band structures of scandium and the rare earth metals. The changes in magnetic properties due to localized moments on gadolinium sites is not reflected in the elastic moduli. Thorium, however, has one more *d* electron in the unfilled 6*d* shell of the free atom and could change the density-of-states curve in the alloy. An investigation of this phenomenon will be made in scandium alloyed with thorium and other actinide metals.

In view of the similarities between yttrium and scandium the elastic modulus anomaly also should be observed in yttrium metal, although the measurements stated in the literature are not conclusive. We have obtained a good single crystal from zone-refined yttrium and intend to pursue the study.

*Crystals purchased from Koch-Light Laboratories, Ltd., Poyle Trading Estate, Colnbrook, Bucks, England.

PHYSICAL METALLURGY OF ACTINIDE METALS AND COMPOUNDS

Preparation of High-Purity Plutonium *(G. B. O'Keeffe, J. J. Rechtien, and M. B. Brodsky)*

Electrorefining of plutonium metal was discontinued during the year. In the future, electrorefined metal will be obtained from Los Alamos Scientific Laboratory. A total of 0.70 kilograms of refined metal was produced and was converted to 0.66 kilograms of usable ingots. During 1967, 0.12 kilograms were furnished to other ANL divisions and 0.39 kilograms were transferred to Metallurgy Division researchers. A total of 0.53 kilograms of high-purity plutonium was on hand at the end of 1967, and should satisfy ANL needs until the metal is received from Los Alamos. Existing equipment, which has been in use for the plutonium electrorefining, will be kept intact until the new arrangement has proved satisfactory.

Interest continues in the further purification of electrorefined plutonium. The high vacuum system has been received and has successfully pumped below 10^{-9} Torr. Installation in a glovebox will be made after several nonradioactive metals have been melted or otherwise heated in the system. Low-frequency, horizontal-zone levitation has not proved successful on plutonium. Although high-frequency levitation seems feasible, the electrotransport approach seems to be more easily adapted to plutonium. The recent success of the electrotransport process in purifying thorium[158] has led to the conclusion that this approach should be tried on plutonium.

Preparation of Single Crystals of Uranium Monophosphide *(J. M. Williams, Y. Baskin, and F. P. Campos)*

Small single crystals of a substoichiometric UP_{1-x} were prepared[159] by heating powdered uranium monophosphide above 2000°C in vacuum. At temperatures exceeding 1400°C, UP_{1-x} is formed; however, uranium monophosphide, when vacuum sealed in tungsten, can be melted (m.p. ≅2610°C) without appreciable departure from stoichiometry,[160] but has not yielded single crystals.

Two methods are under investigation for the preparation of single crystals of uranium monophosphide. First, the crystals are grown by sublimation at or below 2000°C. Second, the principle of vapor transport is employed, by using iodine as the carrier, at temperatures of approximately 900-1100°C.

Sublimation Method: Powdered uranium monophosphide was sealed, under vacuum, in tantalum crucibles. After several preliminary experiments, single crystals were formed on the inner side of the crucible top when the powdered sample was heated at 2000°C for 168 hours. A series of x-ray powder photographs established the compound as stoichiometric uranium monophosphide (a_0 = 5.589Å), and the small crystals yielded well-defined, single-crystal diffraction patterns. The maximum crystallite size obtained was approximately 0.5 millimeters on the largest edge, therefore, efforts are being made to grow larger crystals.

Vapor Transport Method: The transport of phosphides that use halogen carriers has been employed in the preparation of single crystals of, for example, boron phosphide,[161] indium phosphide,[162] and gallium phosphide.[163] As an added advantage, crystal growth by the vapor transport method can be achieved at temperatures considerably below the melting point of the pure compound.

Powdered uranium monophosphide and redistilled crystalline iodine were sealed in vacuum ($<10^{-4}$ Torr), in Vycor tubes. Well-formed crystals grew within the hot zone (1000°C), and along the Vycor walls at somewhat reduced temperatures (600-800°C). Multifaceted crystals as large as 2 millimeters on an edge were produced initially, but were multitwinned. Again, x-ray analysis of powdered material determined that the crystals were stoichiometric uranium monophosphide. Further experiments are in progress.

---

158 D. T. Peterson, F. A. Schmidt, and J. D. Verhoeven, Trans. Met. Soc. AIME *236*, 1311-1315 (1966).

159 Y. Baskin and J. T. Dusek, Annual Report for 1963, Metallurgy Division, ANL-6868, pp. 142-148.

160 Y. Baskin, Annual Progress Report for 1965, Metallurgy Division, ANL-7155, pp. 108-109.

161 A. F. Armington, J. Cryst. Growth *1*, 47 (1967).

162 G. R. Antell and D. Effer, J. Electrochem. Soc. *106*, 509 (1959).

163 A. S. Roy, J. Electrochem. Soc. *109*, 750 (1962).

Effects of Pressure on Transformations *(R. G. Liptai and R. J. Friddle)*

Publications

R. G. Liptai and R. J. Friddle, J. Nucl. Mater. *21*, 114-116 (1967). Letter

R. G. Liptai, L. T. Lloyd, and R. J. Friddle, *Crystal Growth* (Supp. to J. Phys. Chem. Solids), Proc. Intl. Conf. on Crystal Growth, Boston, June 20-24, 1966, H. S. Peiser, ed. (Pergamon Press, Oxford, 1967), pp. 573-577.

R. G. Liptai, Abst. Bull. IMD-AIME *2*, 116 (1967).

R. G. Liptai, J. Nucl. Mater. *22*, 117-118 (1967). Letter

M. B. Brodsky, *Plutonium 1965*, Proc. Third Intl. Conf. on Plutonium, London, 1965, A. E. Kay and M. B. Waldron, eds. (Chapman and Hall, London, 1967), pp. 137-139. Discussion

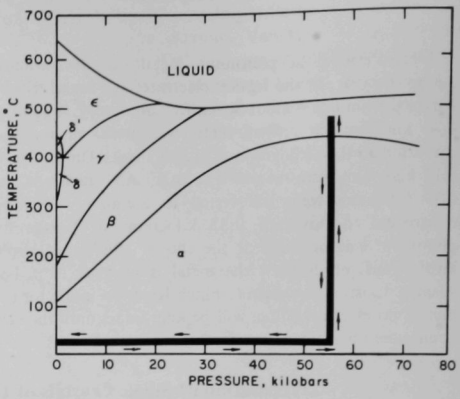

48094

Fig. 33. Pressure-Temperature Phase Diagram of Plutonium. The treatment followed for the preparation of single crystals of alpha plutonium is indicated.

The effort during 1967 has been directed toward the development of techniques for the preparation of large crystals of alpha plutonium that will be used in studies of properties as a function of crystallographic direction. The phase transformation technique for the growth of large crystals has been the most promising. This technique (Figure 33) consists of pressurizing a plutonium sample to 55 kilobars ("belt-type," high-pressure apparatus); heating through the alpha → beta transformation to a temperature of 480°C; holding this temperature for 2 to 3 days; cooling to room temperature at 40°C/hr; and depressurizing. The volume change of the alpha → beta transformation is near zero at a pressure of 55 kilobars. Holding a sample at a temperature of 480°C apparently allows growth of the beta grains, which appears to be beneficial in obtaining large alpha grains. Experiments have shown that cooling rates substantially different than 40°C/hr are detrimental to the formation of large crystals of alpha plutonium. The experiments also established that pressures had to be *truly* hydrostatic during the beta → alpha transformation; hence, samples were surrounded by an annulus of sodium and encapsulated in a stainless steel container.

Subgraining is a problem, but the individual size of the subgrains is large (1-3 mm) and the orientation difference is usually less than 0.3°. The samples are cylindrical (5.0-mm diam by 3.5 mm long). Single crystals are removed from a coarse-grained matrix by grinding. Methods of achieving full control of experimental conditions are being determined for the routine production of crystals.

Deformation Mechanisms of Alpha Plutonium *(R. G. Liptai and R. J. Friddle)*

A program has been initiated to study and to identify quantitatively all deformation elements of alpha plutonium. Two surface analyses will be used, and the initial efforts will be centered on room-temperature measurements. The x-ray apparatus for back-reflection Laue techniques has been installed in a glovebox. Apparatus and procedures for preparing and orienting single crystals of alpha plutonium have been tried, and several single crystals have been oriented.

The rate of progress of this program will depend upon the yield of single-crystal samples that are prepared by high pressure-temperature techniques. Contamination-risk procedures for conducting compression tests on an Instron testing machine have been formulated for the initial experiments. One sample has been strained, and an analysis of the deformation markings is being made. Future tests will be made on an Instron machine in a glovebox.

Elastic Wave Emissions during Martensitic Transformations in Metals and Alloys *(R. G. Liptai)*

Many investigators have noted the high rates of propagation of plate-shape grains, and the autocatalytic features of martensitic transformations in pure metals and alloys.[164,165] A study has begun to determine the quantitative details of low-energy vibrations. The objective is to characterize diffusionless transformations by examining the elastic waves emitted during the transformation and to relate the emitted energy to atomic processes.

An electronic technique has been developed for preliminary experiments in the frequency range between 50 and 300 kilocycles. A lead zirconate-titanate sensing transducer is used to detect the elastic waves. Exploratory experiments have been conducted on the alpha ≒ beta transformation in plutonium, which is presumably martensitic,[166] and the cubic ≒ orthorhombic transformation in gold-47.5 at.% cadmium, which is classically martensitic.[167] These experiments showed that individual events during martensitic transformation can be detected. Preparations are being made to study the systems quantitatively. In addition, the diffusionless phase change in indium-20% thallium will be examined.[168] The Lawrence Radiation Laboratory detection and analysis systems will be used for the early experiments.

An Internal Friction Study of Neptunium *(J. J. Rechtien and J. E. Selle*)*

Sufficient neptunium has been received to permit studies of its physical metallurgy. The first studies of the internal friction of the pure metal have been made on existing equipment at Mound Laboratories.** The goal of this work has been to investigate the nature of the allotropic phase changes of the metal. The choice of technique, namely the measurement of low-frequency, torsional, internal friction, and relative shear modulus, was based upon studies of uranium, cobalt, and plutonium. These studies showed that the mechanism of phase transformation in metals can be inferred from the behavior of the above named properties as a function of time and temperature.[169] The advantage of this technique over others is that a large amount of information can be collected in a short time, and the risk of material loss is minimal.

Specimens were prepared by melting 20 grams of the as-received neptunium under a protective salt and drawing the molten metal into a quartz capillary tube by means of a hypodermic syringe. Five specimens, approximately 7 in. long by 0.030 in. in diameter with a total weight of 13 grams were prepared in this manner.

The internal friction measurements consist of two types: (1) isothermal measurements–the specimen is brought to a temperature and the time dependence of the internal friction is measured; and (2) dynamic measurements–the temperature is slowly varied in the vicinity of a phase transformation and internal friction and shear modulus are measured as a function of time and temperature.

The isothermal measurement gives the internal friction spectrum of the material after the transient effects of the temperature change have subsided. The spectrum of the α phase was uninteresting, but in the β modification a peak was observed at approximately 420°C ($\frac{1}{T} \times 10^3 = 1.34$). As seen in Figure 34, the peak that had a shoulder at a lower temperature did not reappear after the $\beta \rightarrow \gamma \rightarrow \beta$ sequence, although the internal friction remained high. The behavior of this peak with thermal cycling is unusual, and at present we can only suggest that the peak is a result of impurities dissolving rather than an intrinsic property of neptunium. Attempts to find an activation energy for the peak failed. A few equilibrium measurements were made in the γ-phase field but the spectrum was not determined because the phase is apparently very soft and, even under light tension, the wire began to deform.

The dynamic measurement was made to determine the allotropic transformation mechanisms of neptunium. The analysis of the data depends on correlating the changes of internal friction and relative shear modulus with transformations that have known mechanisms. The $\alpha \rightarrow \beta$ transformation was studied in more detail than the other three solid-state transformations and will be discussed first. Figure 35 shows the data obtained near the $\alpha \rightarrow \beta$ transformation. The relative shear modulus goes through an isothermal decrease at the initiation of the transformation accompanied by a nonisothermal rise in the internal

---

[164] R. F. Bunshah and R. F. Mehl, Trans. Met. Soc. AIME *197*, 1251 (1953).

[165] E. S. Machlin and M. Cohen, Trans. Met. Soc. AIME *191*, 746 (1951).

[166] M. Rosen, L. T. Lloyd, and R. G. Peterson, *Plutonium 1965*, Proc. Third Intl. Conf. on Plutonium, London, 1965, A. E. Kay and M. B. Waldron, eds. (Chapman and Hall, London, 1967), pp. 18-38.

[167] D. S. Lieberman and T. A. Read, J. Appl. Phys. *28*, 532 (1957).

[168] Z. S. Basinski and J. W. Christian, Acta Met. *2*, 148 (1954).

*Present address, Monsanto Research Corporation, Miamisburg, Ohio.

**Monsanto Research Corporation, Miamisburg, Ohio.

[169] J. E. Selle, Ph.D. Dissertation, University of Cincinnati, Ohio, June 1967, unpublished data.

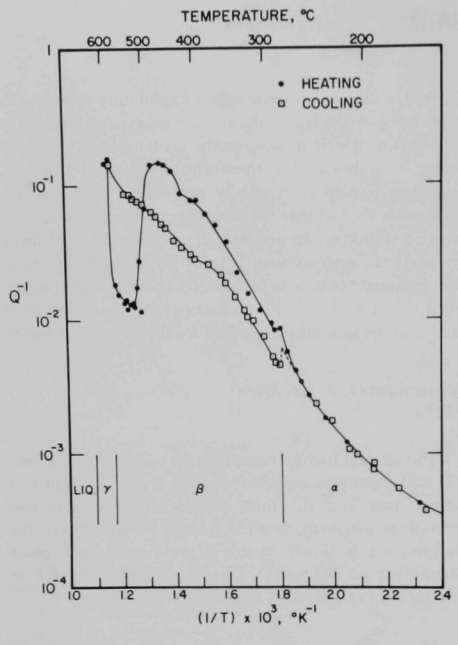

Fig. 34. Internal Friction Spectrum of Neptunium.

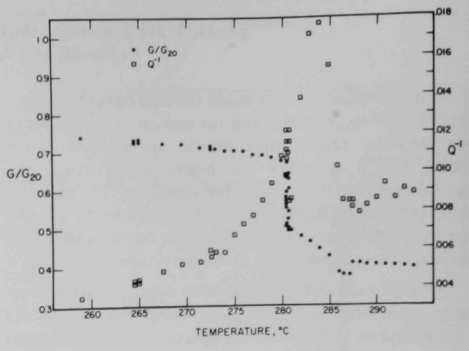

Fig. 35. Internal Friction and Relative Modulus Changes during the $\alpha \rightarrow \beta$ Transformation.

TABLE 17. Summary of Transformation Temperatures and Mechanisms as Determined by Internal Friction

Transformation	Temperature, °C	Mechanism
$\alpha \rightarrow \beta$	280.5	Isothermal shear
$\beta \rightarrow \gamma$	579	Diffusional
$\gamma \rightarrow \beta$	579	Shear
$\beta \rightarrow \alpha$	275	Isothermal shear

friction. This is followed by a more gradual decrease in the modulus over a temperature range during which the internal friction peaks sharply. The heating rates during this experiment were very slow, on the order of 10°C/hr, and the temperature was held constant every 5°C until the reaction was complete for that temperature. This behavior indicates a shear-type transformation, which has been preceded by a diffusion controlled reaction. The data in the reverse direction $\beta \rightarrow \alpha$ are not as detailed but show strong indications that the reaction is the reverse of the $\alpha \rightarrow \beta$. Shear takes place, followed by an isothermal completion of the reaction. The $\beta \rightarrow \gamma$ reaction appears to be a type of diffusion and growth reaction while the $\gamma \rightarrow \beta$ appears to proceed in a shear mode. The nonreversibility of this transformation is unusual but has some precedence in the literature of uranium.[170] The temperatures of transformation and their modes are summarized in Table 17.

Metallographic studies of the wires used in this work are under way. To date only the as-cast starting material has been examined. The following observations have been made: (1) A pattern of precipitates is observed, which may have surrounded the original γ grains, and (2) the α structure appears to be highly twinned with each region of parallel orientation defining what were probably the original β grains. Further metallographic and x-ray studies of the effects of heat treatment on the material, are continuing.

Defect Equilibria in PuO_{2-x} *(L. M. Atlas and G. J. Schlehman)*

Publication

L. M. Atlas and G. J. Schlehman, *Plutonium 1965*, Proc. Third Intl. Conf. on Plutonium, London, 1965, A. E. Kay and M. B. Waldron, eds. (Chapman and Hall, London, 1967), pp. 838-844.

The oxygen pressure in equilibrium with PuO_{2-x} at temperatures above 1500°C must be known to explain the evaporation behavior of plutonium dioxide. For the most

[170] J. Burke and P. H. Dixon, J. Nucl. Mater. 7(1), 38 (1963).

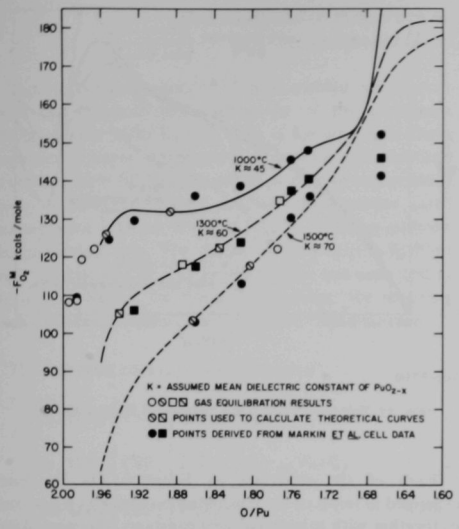

106-9739

Fig. 36. Experimental Data and Theoretical Curves for the Relative Partial Molar Free Energy ($F^M_{O_2}$) of Oxygen in PuO_{2-x}.

part, this information has been obtained by long extrapolations from the galvanic cell data of Markin, Bones, and Gardner,[171] which go no higher than 1100°C. Oxygen activities in PuO_{2-x} have recently been determined between 1000 and 1500°C,[172] but the reported oxygen pressures in the equilibrium gas are open to question because of possible interferences from the alumina walls of the reaction vessel. A new series of equilibration experiments between PuO_{2-x} and O_2 in an H_2/H_2O gas mixture in an all-metal apparatus are in progress. Preliminary results are in good agreement with extrapolations from the galvanic cell data.

Data obtained from these measurements are shown in Figure 36 for 1000, 1300, and 1500°C, and points taken directly or extrapolated from cell experiments by Markin et al. are included for comparison. Agreement between the two sets of free energies is now much closer than when the equilibrations were carried out in alumina.

Figure 36 also includes theoretical free-energy curves calculated from a new statistical model of defects in nonstoichiometric compounds.[173] Each of the curves is based upon two experimental points, designated in the figure by diagonal lines. The curve segments displaying zero or reversing slope are interpreted as marking regions where two phases coexist. Two such regions are shown: one between $PuO_{1.92}$ and $PuO_{1.86}$, and one for oxygen content below ~$PuO_{1.66}$. The first region corresponds approximately to a section near the top of the PuO_{2-x} + PuO_{2-y} field in the phase diagram proposed by Gardner et al.,[174] but the temperature has been displaced upward by about 400°C. The second two-phase region predicted by the model probably corresponds to the field PuO_{2-x} (cubic) + Pu_2O_3 (hexagonal), which the phase diagram locates between $PuO_{1.61}$ and $PuO_{1.5}$. According to the computed curves this field disappears between 1300 and 1500°C, and the composition range of the cubic compound is widened accordingly. However, vapor pressure measurements by Ohse and Ciani[32] show that the phase boundary at $PuO_{1.61}$ persists to temperatures at least as high as 1927°C. The occurrence of a third two-phase field between $PuO_{1.70}$ and $PuO_{1.72}$ at lower temperatures is suggested by an inflection in the 1000°C curve. Although a compound with a composition of $PuO_{1.71}$ has not been identified, an analog has been observed in the cerium-oxygen system.[175]

The statistical model appears to be fairly successful in describing the transformation of PuO_{2-x} into other compounds at certain compositions, but the predictions regarding the temperature ranges of the various phases are, as noted above, not very accurate. To determine these temperature ranges the model relies heavily on the dielectric constant; the discrepancies might, therefore, be lessened if more information were known about this property and its variation with temperature and composition.

Statistical Model of Partially Ordered Defects in UO_{2+x} (*L. M. Atlas*)

A statistical model of UO_{2+x} has been developed that takes into account defect ordering and its variation with temperature. The analysis, which is an extension of an earlier treatment of defects in MO_{2-x} compounds,[173] entails a distribution of the defect ensemble over a series of levels of interaction energy. Although attractive interactions are probably the key factor in defect ordering, the levels are defined solely in terms of differences of repulsion energy. This simplification is made possible by a transformation of the real defect distribution into a negative

[171] T. L. Markin, R. J. Bones, and E. R. Gardner, U.K.A.E.A. Report AERE-R4724, 1964.

[172] L. M. Atlas and G. J. Schlehman, *Plutonium 1965*, Proc. Third Intl. Conf. on Plutonium, London, 1965, A. E. Kay and M. B. Waldron, eds. (Chapman and Hall, London, 1967), pp. 838-844.

[173] L. M. Atlas, J. Phys. Chem. Solids (in press).

[174] E. R. Gardner, T. L. Markin, and R. S. Street, J. Inorg. Nucl. Chem. *27*, 541 (1965).

[175] D.J.M. Bevan and J. Kordis, J. Inorg. Nucl. Chem. *26*, 1509 (1964).

image analog. The magnitude of the repulsion energy corresponding to each level is determined by an integer that controls the defect spacing.

The vibrational contribution of the excess oxygen in UO_{2+x} has been estimated on the basis of the following assumptions: (1) all of the anions have similar oscillator behavior; and (2) the oscillator frequency rises with x, and the increase can be related to the lattice contraction by a variant of the Gruneisen equation.

Two kinds of defect units are assumed to predominate in the hyperstoichiometric solid: (1) clusters[176] consisting of three interstitial anions, two anion vacancies, and a trapped U^{+5} ion; and (2) individual U^{+5} ions, which are considered to be distributed independently of the clusters.

On the assumption that the change of crystal volume with defect concentration has relatively little effect on the total energy, the partition function for the defects in a solid having N_M metal atoms and N_X excess oxygen atoms is given approximately by

$$QD \approx \sum_i \Omega_h(m_j)\Omega_c(n_k)\bar{q}_X^{(2N_M+N_X)}/q_S^{2N_M} \exp[-(N_X\bar{e}_f + \sum_j m_j\epsilon_j + \sum_k n_k u_k + N_{hc}(N_X)\bar{e}_{hc})/\underline{k}T], \quad (1)$$

where $j = 0, 1, ..., L_M$, and $k = 0, 1, ..., L_A$.

In Equation (1), m_j is the number of free U^{+5} ions in the jth energy level; n_k is the number of cluster units in the kth level; $\Omega_h(m_j)$ and $\Omega_c(n_k)$ are the configurational counting functions for the free U^{+5} ions and the cluster units; $\overline{q}_X$ is the mean contribution of an anion to the vibrational partition function of UO_{2+x}; q_S is the corresponding contribution of an anion in $UO_{2.00}$; ϵ_j is the repulsion energy per free U^{+5} ion in level j; u_k is the repulsion energy per cluster in level k; $\bar{e}_f$ is a constant that represents the mean energy required to transfer an oxygen atom from the gas into the solid, forming the various defect units at infinite dilution; $\bar{e}_{hc}$ is a constant representing the mean energy of attraction between a free U^{+5} ion and a cluster; $N_{hc}(N_X)$ is a function that counts the number of pairs of mutually attracting U^{+5} ions and clusters; $\underline{k}$ is the Boltzmann constant; and T is the absolute temperature.

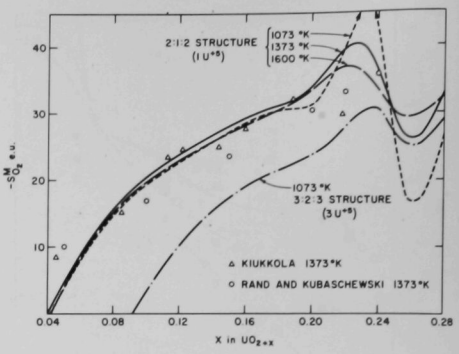

106-9710

Fig. 37. Relative Partial Molar Entropy of Oxygen UO_{2+x}.

Each of the functions in Equation (1) has been expanded in terms of the concentration variables N_X, m, and n, together with certain physical constants (the mean static dielectric constant, the Einstein temperature of the anions in $UO_{2.00}$, the lattice constant of UO_{2+x}, and the Gruneisen constant). The summation over i in Equation (1) may be replaced by its maximum term by setting $\ell n\Omega_h$ and $\ell n\Omega_c$ to conditional maxima for each and every value of j and k. The result is a series of equations that determine the most probable defect populations for all of the energy levels of particular values of N_X and T.

Differentiation of ℓnQ_D with respect to N_X permits the calculation of theoretical values for the relative partial molar entropy ($S^M_{O_2}$), enthalpy ($H^M_{O_2}$), and free energy ($F^M_{O_2}$) of oxygen in UO_{2+x}. Of the three, $S^M_{O_2}$ may be evaluated without prior knowledge of the entropy at any composition. Theoretical curves of $S^M_{O_2}$ as a function of x are compared with Kiukkola's experimental values[177] in Figure 37. In general, the computed entropy and enthalpy results compare favorably with observed values in the range $0.06 \leqslant x \leqslant 0.2$; however, agreement is less satisfactory for the free energy. Many of the curves show reversals of slope that are interpreted as marking two-phase fields in the UO_2-oxygen system. For the enthalpy curves, these slope changes coincide fairly well with the phase fields $UO_{2+x} + U_4O_{9-y}$ and $U_4O_9 + UO_{2.61}$.[178]

[176] *Thermodynamic and Transport Properties of Uranium Dioxide and Related Phases*, IAEA, Tech. Report Series 39, Section II.4, 7-15, Vienna, Austria, 1965.

[177] K. Kiukkola, Acta Cehm. Scand. *16*, 327 (1962).

[178] *Thermodynamic and Transport Properties of Uranium Dioxide and Related Phases*, IAEA, Tech. Report Series 39, Section III.3, 29-40, Vienna, Austria, 1965.

Thermodynamic Properties of Plutonium Carbides from Galvanic Cell Measurements *(L. M. Atlas and G. J. Schlehman)*

Vaporization experiments[179] have yielded information about the thermodynamic properties of the plutonium carbides above 1600°K, but little is known about these properties at lower temperatures, except by extrapolation. In order to help fill this gap and to provide an independent check on the vaporization studies, electromotive force measurements between 900 and 1200°K are being made on electrochemical cells. The design of these cells, which use single crystals of CaF_2 as an electrolyte, was described in the Annual Report for 1966;[180] however, the materials used in the construction of the cells have been changed.

The following cells have been measured:

$Th, ThF_4 \mid CaF_2 \mid PuF_3, Pu_2C_3, C$	Cell 1
$Th, ThF_4 \mid CaF_2 \mid PuF_3, PuC_{1-x}, Pu_2C_3$	Cell 2
$Th, ThF_4 \mid CaF_2 \mid PuF_3, Pu$	Cell 3

Combining the electromotive forces of the cells by standard thermodynamic relationships gives the free energy of formation of the monocarbide. Stable and reproducible voltages were obtained from cells 1 and 3, which were constructed with alumina and fused silica parts. These conditions did not prevail for cell 2; voltage drift was a severe problem until all of the oxide parts in the hot zone were replaced by metal. Experimental free energies, which should be regarded as preliminary, for the formation of the sesquicarbides and monocarbides are presented in Figure 38. The activity of plutonium in Pu_2C_3 and in PuC_{1-x} (in both cases at the high-carbon phase boundaries) may be obtained from the free energies.

Combining these activities with the vapor pressure of plutonium metal[181] gives the partial pressure of plutonium (in atmospheres) in both the sesquicarbides and the monocarbides:

$$\log P(\text{Pu in } Pu_2C_3) = -(24\,500 \pm 226)/T + 6.98 \pm 0.21,$$

and

$$\log P(\text{Pu in } PuC_{1-x}) = -(24\,050 \pm 462)/T + 8.05 \pm 0.43.$$

The pressure results were extrapolated to the lower temperature limit of the vaporization experiments.[179] Agreement is good for both sets of vapor-pressure data, but there are significant differences in the slopes of the respective curves.

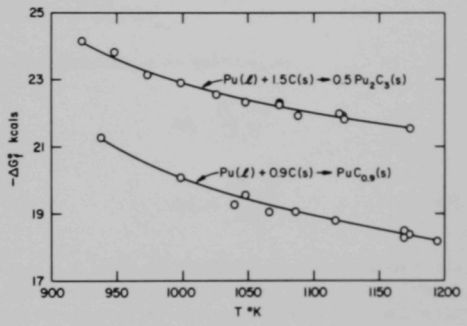

106-9737

Fig. 38. Free Energies of Formation of Plutonium Sesquicarbides and Monocarbides.

[179] W. M. Olson and R.N.R. Mulford, *Thermodynamics of the Plutonium Carbides*, Paper SM 98/40, Symp. on Thermodynamics of Nucl. Mater. with Emphasis on Solution Systems, IAEA, Vienna, Austria, September 4-8, 1967.

[180] L. M. Atlas and G. J. Schlehman, Annual Progress Report for 1966, Metallurgy Division, ANL-7299, pp. 221-222.

[181] R.N.R. Mulford, *Thermodynamics* (IAEA, Vienna, Austria, 1966), Vol. I, p. 231.

Electrochemical Processes in the High-Temperature Oxidation of Metals *(R. H. Spitzer and C. E. Harris)*

Oxidation kinetics are normally determined by rates of transport of charged ionic and electronic defects across the growing oxide layer. The fundamental equation describing the flux J_j of a charged defect, whose mobility, charge, and local concentration are B_j, $z_j\epsilon$, and c_j, respectively, under the influence of chemical and electrical potential gradients $d\mu_j/dx$ and $d\phi/dx$ is

$$J_j = B_j c_j \left(-\frac{d\mu_j}{dx} - z_j\epsilon\frac{d\phi}{dx}\right). \tag{1}$$

An equation of this form is obtained for each diffusing species.

Before steady state is attained, a potential gradient $d\phi/dx$ is created by the rapid movement of the most mobile species such that transport of the less mobile species is enhanced and the transport of the most mobile species is retarded. At steady state, the charge current of positively charged defects must be equal to that of negatively charged defects in order to preserve the steady-state field.

$$\sum z_j J_j = 0. \tag{2}$$

Solution for the potential gradient yields

$$\Delta\phi = \int_0^{x_i}\frac{d\phi}{dx}\,dx = -\frac{1}{\epsilon}\int_0^{x_i}\frac{\sum z_j B_j c_j d\mu_j}{\sum z_j^2 B_j c_j}, \tag{3}$$

where $x = 0$ at the gas/oxide interface, and $x = x_i$ at the metal/oxide interface.

Equation (3) is equivalent to that obtained by Bradhurst, Draley, and Van Drunen.[182] For oxidation limited by the rate of transport of ionic defects, the potential of the metal/oxide interface with respect to the gas/oxide interface is positive. For limitation by electronic defects, the potential is negative.

It is essential, however, to distinguish between the potential influencing transport and the potential measurable by physical contact of inert electronic conductors to the reaction interfaces. For equilibrium of electronic defects between a probe and a reaction interface, the electrochemical potentials are equal. Consequently, the contact potentials at the interfaces are

$$\Delta\phi_i = \frac{\mu_3^i - \mu_3^p}{z_3\epsilon}$$

and

$$\Delta\phi_o = \frac{\mu_3^p - \mu_3^o}{z_3\epsilon}, \tag{4}$$

where p, i, and o refer to the probe, and to the inner and outer interfaces, respectively. Because the chemical potentials for electrons μ_3^p are equal in the platinum probes, the measurable potential is

$$E = \Delta\phi_i + \Delta\phi + \Delta\phi_o = \frac{1}{z_3\epsilon}(\mu_3^i - \mu_3^o)$$

$$-\frac{1}{\epsilon}\int_0^{x_i}\frac{\sum z_j B_j c_j d\mu_j}{\sum z_j^2 B_j c_j}. \tag{5}$$

Local equilibria between defects and atoms on normal sites relate the chemical potentials of these species across a differential element. Equation (5) becomes

$$E = -\frac{1}{\epsilon}\int_0^{x_i}\frac{B_1 c_1|z_1|d\mu_{me} - B_2 c_2|z_2|d\mu_X}{B_1|z_1|^2 c_1 + B_2 c_2|z_2|^2 + B_3 c_3}, \tag{6}$$

where $d\mu_{me}$ and $d\mu_X$ are the chemical potential gradients of metal and oxygen on normal sites, and the subscripts 1, 2, and 3 refer to the cationic, anionic, and electronic defect species, respectively. Application of the Gibbs-Duhem equation gives:

$$E = -\frac{1}{\epsilon}\int_0^{x_i}\frac{B_1 c_1|z_1|^2 + B_2 c_2|z_2|^2}{B_1 c_1|z_1|^2 + B_2 c_2|z_2|^2 + B_3 c_3}\cdot\frac{d\mu_{me}}{|z_1|}$$

$$= -\frac{B_1\bar{c}_1|z_1|^2 + B_2\bar{c}_2|z_2|^2}{B_1\bar{c}_1|z_1|^2 + B_2\bar{c}_2|z_2|^2 + B_3 c_3}\cdot E_o, \tag{7}$$

where $\bar{c}_1$, $\bar{c}_2$, $\bar{c}_3$ are integrated average concentrations, and E_0 is the emf corresponding to the thermodynamic driving force for the reaction.

The final result predicts that the measured potential will always be of negative polarity (metal/oxide interface with respect to gas/oxide interface). Although the above result is similar to that of Wagner,[183] the polarity was not specified in Wagner's derivation and the omission has been a source of confusion to later authors. The result also predicts

[182] D. H. Bradhurst, J. E. Draley, and C. J. Van Drunen, J. Electrochem. Soc. *112*, 1171-1177 (1965).

[183] C. Wagner, Z. Phys. Chem. *21B*, 25-41 (1933).

that the measured potential will approach zero for an electronically conducting oxide (oxidation limited by rate of transport of ions), and E_0 for an ionic conducting oxide (oxidation limited by rate of transport of electrons).

This simple result is certainly modified by complications encountered in real systems. Steady state is assumed. Further, the final result assumes that the total free energy change occurs across the oxide layer. If equilibrium does not exist at the interfaces, the measured potential will be less than predicted.

Electrical Potentials Measured by Physical Contact: Persuasive evidence for the basic validity of Equation (7) is provided by the applicability to experimental results. Dravnieks and McDonald[184] measured potentials across growing oxide and halide layers with electronically conducting probes. For AgCl, AgBr, $PbCl_2$, and $PbBr_2$ (ionic conductors), the measured potential approached the thermodynamic emf. For copper oxide, the measured potential was very small. These results are in agreement with experiments in the present program in which potentials measurable across copper, nickel, chromium, and iron oxides (all are electronic conductors) are either very small negative potentials or are too small to be measurable. (The material reported as chromium by Levitan, Draley, and Van Drunen[185] was apparently Zircaloy.) The magnitude of the negative potentials developed in oxidizing hafnium and zirconium systems suggests that oxidation is under mixed control by transport of both ionic and electronic species.

Positive potentials–in apparent contradiction to the above formulation–were reported by Levitan, Draley, and Van Drunen[185] across growing oxide layers of tantalum and niobium. More recent experiments, however, indicate that these positive potentials were due to extraneous effects and not to oxidation processes. Negative potentials of 0.3 to 0.5 volt at 550 to 700°C, and 0.001 to 0.003 volt at 450°C are observed for tantalum and niobium, respectively.

Volta Potential Measurements: In order to provide additional information to complement potential measurements made by physical contact to the reaction interfaces, Volta potentials (sometimes called contact or surface potentials) will be measured by a noncontacting technique. Construction and preliminary evaluation of a Kelvin-method apparatus have been completed.

A reference electrode is brought into close proximity to the surface whose contact potential difference (cpd), with respect to the reference, is to be measured. When an external circuit is connected, the cpd is established by electron transfer from the surface with the lower work function to the surface with the higher work function. Change of the capacity of the sample-reference couple, by vibration of the reference electrode with an electromagnetic transducer, induces an alternating current in the external circuit, which is observed on an oscilloscope. A potentiometer circuit is adjusted to produce a null.

Measurements will be made at oxidation temperatures. The reference electrode will be prepared by evaporation of a gold film upon a quartz substrate disk. The work function of a gold surface is known and is stable in an oxidizing atmosphere.

Potential Barriers in Growing Zirconium Dioxide Films: Preliminary voltage-current curves observed across growing zirconium dioxide films suggest that the measurable open-circuit potential includes a barrier potential at a depletion layer between the hyper- and hypostoichiometric regions.

Bulk zirconium dioxide ($ZrO_{2\pm x}$) ranges in composition from oxygen deficient (oxygen vacancies and electrons) to oxygen rich (zirconium vacancies and electron holes) as the equilibrium oxygen partial pressure is varied from 1×10^{-28} Torr to atmospheric pressure at about 1000°C.[186] The stoichiometric composition is in equilibrium with an oxygen partial pressure of about 1×10^{-16} Torr. A growing oxide layer is expected to exhibit a similar range of composition, approaching equilibrium with the oxidizing atmosphere at the gas/oxide interface, and equilibrium with metal at the oxide/metal interface. If the Schottky defect equilibrium constant is much greater than that for the intrinsic electronic equilibrium, the stoichiometric portion of the oxide layer will be a region of high electrical resistivity due to the low concentration of mobile charge carriers and will exhibit ionic conductivity. Available evidence indicates that the physical location of the depletion layer is close to the oxide/gas interface.

The resistance to passage of a small external current across the film is inversely proportional to the reaction rate. Larger biases conform to the conventional *p-n* semiconductor-junction expression. The application of a positive bias to the metal side of the growing zirconium dioxide film produces an increased rate of oxidation (iónic flux) and a decreased electronic flux (measured coulometrically) across the film. A negative bias gives the opposite result. Ishikawa et al.[187] have interpreted similar results for tantalum and silicon dioxide films in terms of *p-n* structure.

184A. Dravnieks and H. J. McDonald, J. Electrochem. Soc. *93*, 77-190 (1948).

185J. Levitan, J. E. Draley, and C. J. Van Drunen, Annual Progress Report for 1965, Metallurgy Division, ANL-7155, pp. 282-284.

186R. W. Vest, N. M. Tallan, and W. C. Tripp, J. Am. Ceram. Soc. *47*, 635-640 (1964).

187Y. Ishikawa, Y. Sasaki, Y. Seki, and S. Inowaki, J. Appl. Phys. *34*, 867-874 (1963).

When the oxidizing atmosphere is removed or replaced by an inert gas, the open-circuit potential abruptly decays to zero and the resistance becomes ohmic. Over a period of 2 hours at 700°C, the measured ohmic resistance decays by about four orders of magnitude, approximately as $R \propto 1/[(1 - \exp(-kt^2)]$. A postulation is made that the loss of the open-circuit potential and the change to ohmic resistance corresponds to the loss of the depletion layer close to the gas/oxide interface, and the subsequent decay in ohmic resistance to the readjustment of defect concentrations to the new, lower oxidizing potential.

Research is being continued in conjunction with gravimetric and metallographic studies to test the postulated conduction mechanisms. Possible barrier effects introduced by the external metal contacts must be evaluated. This type of study promises to be very helpful in elucidating transport mechanisms important to oxidation kinetics.

Gravimetric Studies *(R. H. Spitzer and R. E. Loess)*

A proposed model[188] for the high-temperature oxidation of polycrystalline zirconium at oxygen pressures of 10 to 400 Torr suggests that the observed kinetics are due to a suitable average of growth cycles on the individual crystal faces. To provide a critical test of the model and to provide data necessary for application of the model, it is of interest to examine oxidation kinetics on zirconium single-crystal faces having various orientations with a microbalance system that has greater sensitivity than the present Ainsworth system. Preliminary efforts to use a Cahn microbalance in a Varian ultrahigh-vacuum system were unsuccessful due to large thermal-convection currents. A balance system is under construction that will minimize aerodynamic noise by minimizing the system volume and the cross-sectional area of the furnace tube.

Low-Pressure Oxidation *(J. E. Draley, J. Levitan, and C. J. Van Drunen)*

Publication

J. Levitan, J. E. Draley, and C. J. Van Drunen, J. Electrochem. Soc. *114*(11), 1086-1089 (1967).

The low-pressure oxidation of zirconium at high temperatures exhibits a pressure dependence, and several stages of oxidation were distinguished. An initial period was followed by two periods during each of which the oxidation rate remained constant. Transition from the first constant-rate period to the second was accompanied by an approximate doubling of the oxidation rate. Surface reaction control is suggested for these periods.

The amounts of oxygen taken up at the beginning and end of the second constant-rate period were examined, and a comparison of calculated quantities with published rates of diffusion of oxygen in zirconium was made. This led to the proposal that the metal is free of a continuous oxide film during the first constant-rate period, and is covered with such a film during the second constant-rate period.

Finally, a growing oxide film becomes thick enough to significantly impede the oxidation rate. The oxide thickness at this point was deduced to be about 1-1/2 microns at 700°C. In due course, the thicker oxide film almost completely limits the rate; from this time onward, the rate is independent of oxygen pressure.

Aqueous Corrosion of 1100 Aluminum *(J. E. Draley and R. E. Loess)*

Publications

C. A. Youngdahl and R. E. Loess, J. Electrochem. Soc. *114*(5), 489-492 (1967). Note.

J. E. Draley, Shiro Mori, and R. E. Loess, J. Electrochem. Soc. *114*(4), 353-354 (1967).

Shiro Mori and J. E. Draley, J. Electrochem. Soc. *114*(4), 352-353 (1967). Note

Polarized Corrosion: After an initial period, the amount of corrosion of 1100 aluminum in distilled water at 70°C varies as the logarithm of time. According to a previously developed model of the corrosion process, the primary film of corrosion-product oxide cracks when, at each local site on the surface, the thickness reaches a limiting value. The corrosion-rate constant should depend upon the rate constant for the growth of the primary film, and upon the rate constant for penetration of the cracked or secondary product. From corrosion data alone, a determination of the parameters basic to the model (the two rate constants and the limiting thickness) has been impossible.

It has been believed that an important cause of the

[188] J. Levitan, J. E. Draley, R. H. Spitzer, and C. J. Van Drunen, Annual Progress Report for 1966, Metallurgy Division, ANL-7299, pp. 311-316.

cracking of the primary film is the liberation of hydrogen beneath the film. In this case, it should be possible to obtain the growth kinetics of the primary film by determining corrosion rate constants for specimens held at several potentials where hydrogen evolution does not occur, and extrapolating to the normal corrosion potential.

Accordingly, corrosion tests are being run in which specimen potentials are uncontrolled for the first four days, then maintained constant, relative to a reference electrode (Ag/AgCl), by means of an interrupter-type potentiostat. For the specimens polarized anodically, there was a discontinuous increase in the amounts of corrosion between the 14- and 19-day examinations (amounts of corrosion are determined by an eddy-current gage[189]). Subsequently, the logarithmic rate constant was again similar to that before the 14-day exposure. Since unpolarized specimens show a gradual decrease in potential subsequent to the first few days of corrosion, it is likely that artificial maintenance at a constant value led to film breakdown. This type of breakdown has been observed previously, during constant-current anodic polarization.[190]

The effect of potential on logarithmic corrosion-rate constants for the interval of 4 to 14 days is in accord with the theory, since the rate constant decreases as the potential is made more positive (and as the hydrogen evolution rate decreases), reaching an apparent minimum at about -0.68 volt versus the special reference electrode. This should occur close to the reversible potential for hydrogen evolution. Based on the measured potential difference between the reference electrode and a conventional calomel electrode, and assuming that the *pH* of the water at the surface of the corrosion specimen was 6.5, equilibrium for (1 atm) hydrogen evolution would exist at -0.81 volt. The agreement is satisfactory, considering that the potential for minimum corrosion rate is not yet well established, and especially that both *pH* and potential change within the porous exterior corrosion-product oxide.

Oxide Structure: It has been judged that an inner portion of the corrosion-product oxide is predominantly boehmite (AlOOH, 45.0% Al), and the outer portion is predominantly bayerite ($Al(OH)_3$, 34.6% Al). In an earlier publication[191] the amount of boehmite is deduced to have increased with exposure time, while the amount of bayerite remained essentially constant.

To confirm the deduction, microscopic and electron microprobe examinations have been made of corroded specimen cross sections. Two layers could be discerned in the oxide, irregular in thickness and from specimen to specimen. Generally, the ratio of thickness of the inner layer to that of the outer layer increased with exposure time. Composition of the two layers are rather close to those of pure boehmite and bayerite. The irregularity on the sample side probably is the result of an irregular interface between metal and oxide so that some oxide was sampled by the probe.

Low-Pressure Oxidation and Growth Morphology *(R. K. Hart, J. K. Maurin, and D. G. Pilney)*

Publications

R. K. Hart, USAEC Report ANL-7275, Argonne National Laboratory, 1967, p. 71.

R. K. Hart, USAEC Report ANL-7275, Argonne National Laboratory, 1967, p. 96.

R. K. Hart, USAEC Report ANL-7275, Argonne National Laboratory, 1967, p. 140.

R. K. Hart and D. G. Pilney, Trans. Second National Conf. on Electron Microprobe Analysis, Boston, Massachusetts, June 14-16, 1967, p. 31.

R. K. Hart, Twenty-fifth Anniversary Mtg. Electron Microscopy Society of America, Chicago, Illinois, August 29-September 1, 1967, Claude J. Arceneaux, ed. Claitor's Book Store, Baton Rouge, Louisiana, 1967, p. 258.

Oxide nucleation on thin aluminum foils, maintained at a temperature of 440°C, was investigated at oxygen pressures between 10^{-5} and 10^{-8} Torr. The reaction apparatus was an auxiliary pumped Siemens electron microscope[192] in which base pressures in the vicinity of 10^{-8} Torr can be obtained. The system was pumped down to base pressure, the specimen was heated to 440°C, and the oxygen pressure was brought up by means of a controlled leak. During each run a balance was maintained between the pumping speed of the diffusion pumps and the oxygen leak rate.

189S. Mori, R. E. Loess, and J. E. Draley, Corrosion *19*, 269 (1963).

190S. Mori and R. E. Loess, Annual Progress Report for 1964, Metallurgy Division, ANL-7000, pp. 213-215.

191Shiro Mori and J. E. Draley, J. Electrochem. Soc. *114*(4), 352-353 (1967). Note

192R. K. Hart, T. F. Kassner, and J. K. Maurin, Proc. Sixth Intl. Congr. for Electron Microscopy, Kyoto, August 28-September 4, 1966. Maruzen Co., Ltd., Tokyo, Japan, 1966, pp. 161-162.

The areas of individual nuclei increased with the logarithm of time, after an induction period extending from about 5 to 11 minutes for different specimens. Determination of the effect of oxygen pressure on the logarithmic growth rate constant has not proved feasible because of the variation in rate constant between individual nuclei on the same specimen.

Similarly, the number of nuclei that appeared (essentially simultaneously) at the end of the induction period could not be described simply as a function of the oxygen pressure. The variations in density of nuclei on different portions of one grain were sometimes large, and variations between nominally identical experiments obscured any possible effects of oxygen pressure.

Some progress was made in setting-up an ultrahigh vacuum unit that incorporates an electromicrobalance and furnace. When complete, the system will be used to investigate oxygen pickup during the induction period associated with oxide nucleation. While awaiting the construction of some of this equipment, the vacuum apparatus is being used to determine how aluminum specimens react when heated in the pressure range of 10^{-11} Torr. Several specimens have been subjected to this environment at 440°C; grain boundaries became prominent by grooving, or by a change in contiguous grain surface levels. No oxide nuclei were observed after exposure for one week.

Spectral Line Shift in Electron Probe Microanalysis *(R. K. Hart, J. K. Maurin, and D. G. Pilney)*

The $K\alpha_1$ band shifts that occur when probing from metal to compound were recently reported[193] for Al_2O_3, TiO_2, CoO, and Fe_2O_3. The shift can occur in either direction about the Bragg setting; those observed correspond to an energy change in the exit photons of approximately 2 electron volts.

Oxides of tantalum (Ta_2O_5) and bismuth (Bi_2O_3) have been prepared by melting compacted pellets in an arc-image furnace. A portion of each pellet was submitted for wet-chemical analysis and another portion mounted for electron-probe microanalysis in the manner previously described.[193]

With these two oxides, line shifting in the $L\alpha$ emission spectra from each metal was investigated. Shifts were in the negative direction with Ta_2O_3, and in the positive direction with Bi_2O_3. The magnitudes of the shifts were surprisingly large, even considering that they are for *L*-spectra rather than *K*-spectra: 19.6 electron volts for Ta_2O_3, and 12.8 electron volts for Bi_2O_3. Additional data are being obtained to test the validity of these values.

[193] R. K. Hart and D. G. Pilney, Trans. Second National Conf. on Electron Microprobe Analysis, Boston, Massachusetts, June 14-16, 1967, p. 31.

ELECTRONIC AND MAGNETIC STRUCTURES OF METALS AND ALLOYS

Actinide Metals and Compounds

THEORY OF THE ELECTRONIC PROPERTIES OF THE ACTINIDES *(I. Goroff and F. M. Mueller)*

The solid-state properties of the actinides, as well as the properties of lanthanum and several of the other rare earths, are strongly affected by the presence of *f*-bands near the Fermi surface. At low temperatures many of these solids undergo a second-order phase transition to either a magnetic or superconducting state. Often the strong *f*-electron character of the states at the Fermi surface causes anomalous behavior. In particular, the pressure and isotope dependences of the superconducting transition temperature of alpha uranium show anomalous behavior[194,195] as do many of the other properties of alpha uranium.[196,197] Moreover, superconductivity and ferromagnetism have been found to exist simultaneously in some dilute alloys of the actinides.[198]

The anomalous properties make the actinides not only interesting, but also important to many diverse branches of solid-state physics and metallurgy. Few of the effects can be explained without a thorough study of the one-electron structure of these materials.

We are undertaking detailed relativistic band-structure calculations of the actinides. The first stage of the program is a first-principles calculation of the band structure by the K.K.R. method.[199,200] This method has two variations, as a stationary problem,[199] or as a scattering problem.[200] Initially the stationary formulation is used to find an appropriate starting point, a one-electron potential and band structure. This potential is mapped into phase shifts by means of the scattering formalism. In the second stage the phase shifts are adjusted in an unambiguous manner to agree with a few selected points from the experimental evidence. The adjusted calculations will be used to compare a wide range of experimental data, considerably more than originally used to adjust the band structure calculations.

In most analyses of optical data, experimentalists measure the reflectivity over a wide range of energies and then reconstruct the imaginary part of the dielectric constant by means of a Kramers-Kronig transform. The experiments required to perform this transform successfully are very difficult because of the wide range of frequencies required; in the process small errors are magnified. The reason that the experimentalists have been forced to use this technique is that theorists have been unwilling to calculate the reflectivity because of the large computer effort involved. At best, they have been able to calculate the imaginary part of the dielectric function (ϵ_2) by simplified models. We have developed a scheme that performs sums over phase space with great facility and high accuracy. The reflectivity can be calculated directly, and the results of this calculation can be compared with the experimental data in the region of its highest accuracy. This same approach will be applied to many other physical properties currently being studied at Argonne National Laboratory. In each instance, we will predict the result of an experiment rather than leave a gap between the results of theory and experiment.

ELECTRONIC STRUCTURE OF THE ACTINIDE ELEMENTS *(M. B. Brodsky)*

Publications

M. B. Brodsky, *Plutonium 1965*, Proc. Third Intl. Conf. on Plutonium, London, 1965, A. E. Kay and M. B. Waldron, eds. (Chapman and Hall, London, 1967), pp. 286-298.

M. B. Brodsky, *Plutonium 1965*, Proc. Third Intl. Conf. on Plutonium, London, 1965, A. E. Kay and M. B. Waldron, eds. (Chapman and Hall, London, 1967), pp. 210-212. Discussion.

M. Kalvius,* B. Dunlap,* S. Ruby,** and M. Brodsky, Bull. Am. Phys. Soc. *12*, 25 (1967). Abstract

M. B. Brodsky, Bull. Am. Phys. Soc. *12*, 98 (1967). Abstract

Merwyn B. Brodsky, Phys. Rev. *163*, 484-487 (1967).

*Solid State Science Division, Argonne National Laboratory.
**Physics Division, Argonne National Laboratory.

194J. C. Ho, N. E. Phillips, and T. F. Smith, Phys. Rev. Letters *17*, 694 (1966); W. E. Gardner and T. F. Smith, Phys. Rev. *154*, 309 (1967); R. D. Fowler et al., Phys. Rev. Letters *19*, 892 (1967).

195J. W. Garland and F. M. Mueller, Bull. Am. Phys. Soc. (to be published).

196E. Flotow and D. W. Osborne, Phys. Rev. *151*, 564 (1966); E. S. Fisher and H. J. McSkimin, Phys. Rev. *124*, 67 (1961); C. S. Barrett, M. H. Mueller, and R. L. Hitterman, Phys. Rev. *129*, 625 (1963); V. M. Raetsky, J. Nucl. Mater. *21*, 105 (1967).

197F. M. Mueller and I. Goroff, Bull. Am. Phys. Soc. (to be published).

198N. E. Phillips and B. T. Matthias, Phys. Rev. *121*, 105 (1961); D. K. Finnemore, D. C. Hopkins, and P. E. Palmer, Phys. Rev. Letters *15*, 891 (1965).

199W. Kohn and N. Rostker, Phys. Rev. *94*, 111 (1954).

200J. Korringa, Physica *13*, 392 (1947).

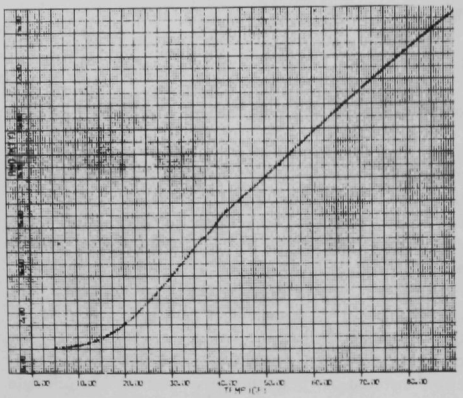

48263

Fig. 39. Resistivity-Temperature Curve for Alpha Uranium in the [100] Direction.

Electrical Resistivity of Uranium: The possibility of first or second order transformations near 42°K in alpha uranium has been the subject of much work (p. 89). Measurements of the electrical resistivity of polycrystalline uranium have not shown the existence of a transition except by plots of ρ/T versus T. A study of the resistivity of oriented, "pseudo-single crystals" of alpha uranium has been started to examine the effects of the transformation in specific lattice directions.

Figure 39 shows the resistivity-temperature for a crystal oriented within 3° of the [100] direction and having subgrain misorientations adding up to 1 to 2°. These results are also similar to those found for crystals oriented in the [010] and [001] directions (i.e., a change in slope on cooling at 42° ±1°K, and a second change in slope at 36° ±1°K). These temperatures may correspond to the initiation and conclusion, respectively, of the transformation. This supposition is not in full agreement with the elastic moduli studies, where it is observed that effects of the 43°K transformation are not found until the sample is cooled to 37°, and that effects continue until the uranium crystals are cooled to 18°K. This study will be extended to a search for hystereses, and to measurements of Hall effect and magnetoresistivity.

Neptunium: The effects of NpC and NpO_2 impurities on the Hall effect and the magnetic susceptibility of neptunium metal were discussed in the 1966 Annual.[201] During the past year, a small sample of very pure neptunium metal was obtained by the reduction of NpO_2 with Mg-Zn alloy. The density of this sample, 20.42 g/cm^3 versus an x-ray density of 20.45, and confirming evidence by metallographic examination showed that the neptunium metal was the purest examined at Argonne, thus far. The electrical resistivity, Hall coefficient, magnetoresistivity, and magnetic susceptibility of this metal have been studied.

The electrical resistivity at 4.2°K was found to be 4.2 $\mu\Omega$cm, which is not very different from metal used earlier. The resistivity-temperature curve was similar to that for less pure neptunium, and no "breaks" were found in the curve. A plot of the Hall coefficient versus temperature was similar to that reported last year. Although some temperature dependence is found, the variation is much smaller than that found in the material containing NpC impurity,[202] and the sign of the Hall coefficient remained positive throughout the temperature range studied.

Figure 40 shows the temperature dependence of the magnetic susceptibility, which is essentially temperature independent. Thus, a conclusion may be made that the susceptibility of neptunium, as for uranium and plutonium, is mainly made up of the Pauli susceptibility and the Van Vleck orbital paramagnetism. Estimates of density of states at the Fermi surface cannot be made because of the large uncertainty in the contribution of the spin-orbit interaction. As in the case of alpha uranium and alpha and delta plutonium, the susceptibility of alpha neptunium gives no indications of localized magnetic moments. "Breaks" reported earlier[203] in the susceptibility-temperature curve at 123 and 273°K are completely absent, and are probably due to impurity effects.

Mössbauer Studies:* Studies of the Mössbauer effect in

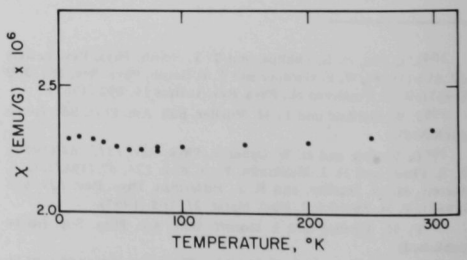

48377

Fig. 40. Magnetic Susceptibility versus Temperature for Alpha Neptunium.

201 M. B. Brodsky, Annual Progress Report for 1966, Metallurgy Division, ANL-7299, pp. 218-219.

202 M. B. Brodsky, Annual Progress Report for 1964, Metallurgy Division, ANL-7000, pp. 174-175.

203 N.A.C. McKay, J. S. Nairn, and M. B. Waldron, Proc. 2nd Intl. Conf. on Peaceful Uses of Atomic Energy, Geneva Paper P/304 (1958).

*Work performed in cooperation with M. Kalvius and B. Dunlap (Solid State Science Division), S. Ruby (Physics Division), and D. Cohen (Chemistry Division).

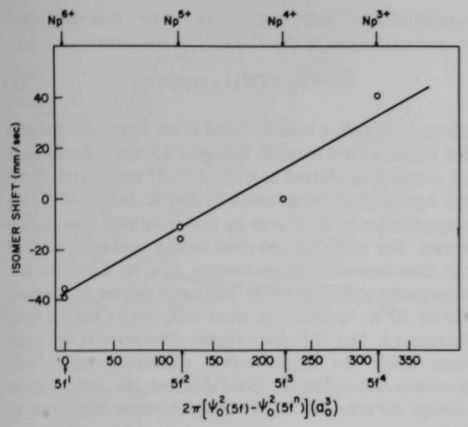

51855

Fig. 41. Isomer Shifts versus Electronic Density at the Nucleus for Free Atom Electronic Configurations. Isomer shifts are given relative to NpO_2.

^{237}Np with ^{241}Am sources is continuing. Figure 41 shows the isomer shifts for various neptunium compounds, relative to NpO_2, plotted versus calculations of the electronic charge density (Ψ^2) at the nucleus. The isomer shifts have been plotted for configuration assignments of, for example, $5f^4$ for Np^{3+} and $5f^3$ for Np^{4+}. Although this plot ignores effects due to covalency or configuration mixing, the points may be fitted by a straight line. This "calibration" of isomer shift will be used to determine the electronic configurations of neptunium alloys, and to compare the results of this method with those of, for example, Hall effect, and resistivity.

The effect has been used to study the antiferromagnetic transition in NpO_2 at 22°K. It is estimated that the magnetic moment is about 0.01 Bohr magneton, which explains the absence of magnetic superlattice lines in neutron diffraction studies having a sensitivity of 0.4 Bohr magneton.[204]

MAGNETIC PROPERTIES OF PLUTONIUM COMPOUNDS *(D. J. Lam and J. W. Ross*)*

Publications

J. W. Ross* and D. J. Lam, J. Appl. Phys. *38*, 1451 (1967).

D. J. Lam, M. V. Nevitt, J. W. Ross,* and A. W. Mitchell, *Plutonium 1965*, Proc. Third Intl. Conf. on Plutonium, London, 1965, A. E. Kay and M. B. Waldron eds. (Chapman and Hall, London, 1967), pp. 274-285.

J. W. Ross* and D. J. Lam, Abst. Bull. IMD-AIME *2*(1), 119 (1967).

A previous study[205] indicated that the "knee" at approximately 100°K in the susceptibility-temperature curve for PuC is probably caused by the presence of the Pu_2C_3 phase in the sample and, hence, the magnetic ordering temperature of PuC, if it exists, is lower than reported by Lallement et al.[206] Recently, Green et al.[207] observed antiferromagnetic ordering just below 100°K in their neutron diffraction study on a two-phase alloy of PuC + Pu_2C_3. Whether antiferromagnetic ordering or a magnetic ordering temperature exists is still uncertain. Since Pu_2C_3 is antiferromagnetically ordered at 120°K, the maximum in the susceptibility-temperature curve at low temperatures could be interpreted in terms of crystal-field splitting of the $5f^4$ ground state.

The low-temperature magnetic properties of PuC are quite difficult to study because of the time-dependent magnetization effect, and the large effect of Pu_2C_3 on the magnetic properties of PuC. The recent magnetic-susceptibility measurements on single-phase PuC alloys were made in a low-temperature facility in which a specified temperature range from 4.2 to 300°K was controlled to ±0.1°K for 4 to 5 hours. Control of the temperature is important since the magnetic susceptibility of PuC changes with time below 40°K.

The magnetic susceptibility of several samples as a function of temperature are shown in Figure 42. The results for samples A ($PuC_{0.887}$) and B ($PuC_{0.786}$) were reported previously.[205] Although an x-ray examination indicated the presence of the Pu_2C_3 phase in sample A but not in sample B, a subsequent optical examination revealed that both contained the Pu_2C_3 phase. Recent magnetic susceptibility results for samples C ($PuC_{0.876}$) and D ($PuC_{0.779}$), which were well-characterized single-phase alloys, do not show a "knee" in the susceptibility-temperature curve as reported by Lallement et al.[206] While the composition of the Lallement sample was not specified, the presence of

---

[204] L. Heaton, M. H. Mueller, and J. M. Williams, J. Phys. Chem. Solids *28*, 1651-1654 (1967).

*Present address: The Physical Laboratories, The University, Manchester, England.

[205] D. J. Lam, M. V. Nevitt, J. W. Ross, and A. W. Mitchell, *Plutonium 1965*, Proc. Third Intl. Conf. on Plutonium, London, 1965, A. E. Kay and M. B. Waldron, eds. (Chapman and Hall, London, 1967), pp. 274-285.

[206] R. Lallement, P. Costa, and R. Pascard, J. Phys. Chem. Solids *26*, 1255 (1965).

[207] J. L. Green, G. P. Arnold, J. A. Leary, and H. C. Neresun, J. Nucl. Mater. *23*, 231 (1967).

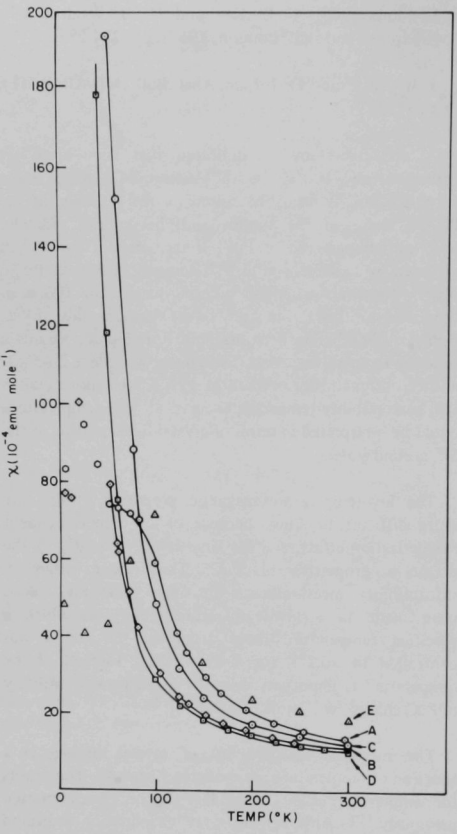

47764

Fig. 42. The Magnetic Susceptibility versus Temperature Curves for the Following PuC Samples: (1) A–$PuC_{0.887}$–two phase; (2) B–$PuC_{0.786}$–two phase; (3) C–$PuC_{0.876}$–single phase; (4) D–$PuC_{0.779}$–single phase; and (5) E–exact composition unknown–two phase.

Pu_2C_3 as a second phase was indicated. The magnetic susceptibility maximum in the vicinity of 100°K for sample E, and the "knee" in the curve between 50 and 100°K for sample A are related to the presence of the Pu_2C_3 phase. Although sample B does not show a pronounced "knee," in spite of the presence of a small amount of the Pu_2C_3 phase, the susceptibility values between 40 and 80°K are lower than those of sample D, which has a slightly smaller carbon concentration.

A comparison of the magnetic susceptibility results for all the samples below 40°K is difficult because the magnetizations vary with time. The time-dependent magnetization can be expressed[205] in the form

$$\sigma(t) = \sigma_0 + CH[1 - \exp(-t/\tau)], \qquad (1)$$

where $\sigma_0 = \chi_0 H$, t is time, τ and C are constants, and H is the magnetic field strength. In Figure 43, the magnetization of sample C is plotted as a function of temperature from the liquid-helium temperature to 300°K. Below 40°K, the magnetization at time zero σ_0 and at infinite time σ_∞ are shown. The values were derived from a least-squares fit of the time-dependent magnetization data to Equation (1). Apparently a magnetization maximum occurs at approximately 30°K; however, the exact temperature has not been determined. The time dependence disappears at temperatures above the magnetization maximum, which substantiates our earlier proposal[205] that the self-radiation damage disturbs the antiferromagnetic spin alignment in PuC.

The magnetization σ_∞ versus temperature curves for sample D at two different magnetic field strengths H are shown in Figure 44. The magnetization is not linearly dependent on H at temperatures below the magnetization maximum. As evidenced from Figures 43 and 44, σ_0 drops sharply below 10 or 20°K, depending upon the carbon concentration of the sample. At present, the cause of the sharp decrease in magnetization is not clear. Possibly, the magnetic ions change ground state below the temperature of 10 or 20°K as proposed earlier, or other complicated mechanisms may exist that affect the low-temperature magnetic behavior of PuC.

Magnetic susceptibility measurements were made on two PuO_2 samples. The stoichiometric PuO_2 sample displayed a temperature-independent susceptibility in the range

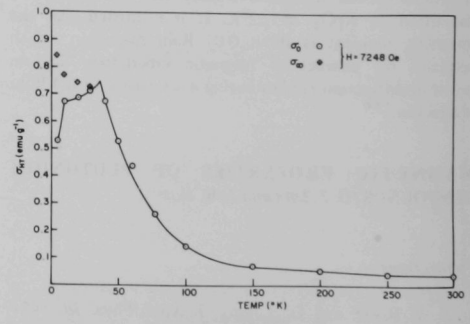

47803

Fig. 43. The Magnetization versus Temperature Curve for the $PuC_{0.876}$ Alloy (Sample C).

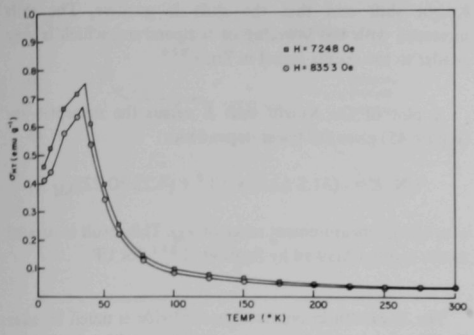

Fig. 44. The Magnetization versus Temperature Curve for the $PuC_{0.779}$ Alloy (Sample D).

4.2-300°K; however, the susceptibility of an oxygen deficient PuO_2 sample varied with temperature and indicated the presence of plutonium ions with valence states different from +4. A study is in progress to determine the relative quantities of plutonium ions with different valence states as a function of oxygen concentration.

THE MAGNETIC SUSCEPTIBILITY OF SINGLE CRYSTAL ALPHA URANIUM *(J. W. Ross* and D. J. Lam)*

Publication

J. W. Ross and D. J. Lam, Bull. Am. Phys. Soc. *12*, 354 (1967).

A preliminary account of the work on the magnetic susceptibility of single crystal alpha uranium was reported previously.[208] The program was completed in 1967 and a complete account will be published.[209]

Magnetic susceptibility measurements on a single crystal of alpha uranium were made within a range of temperatures from 4.2 to 300°K. A different temperature dependence in the susceptibility was found for each of the three principal crystallographic axes, and a plot of the susceptibility as a function of temperature indicated a change in slope at approximately 43°K. The results do not support the suggestion of other investigators[210] that a random arrangement of localized moments is the source of the magnetic anomaly. The measurements, however, cannot differentiate between three other possible sources for the anomaly; ordered magnetic moments, spin-density wave, and/or temperature dependence of the electronic band structure of alpha uranium.

NUCLEAR RESONANCE STUDIES ON THE NaCl-TYPE ACTINIDE COMPOUNDS *(F. Y. Fradin)*

A program was initiated to study the variety of magnetic behavior exhibited by the NaCl-type compounds of uranium, neptunium, and plutonium with the nontransition elements of Groups IV, V, and VI. A systematic investigation of the temperature dependence of the Knight shift of carbon and Group V anions will be combined with susceptibility results on the same compounds in the magnetically disordered state to determine the indirect *s-f* exchange interaction. The indirect interaction is thought to be the mechanism for magnetic coupling of the 5*f* spins in the actinide compounds. Nuclear magnetic resonance measurements will be made on the actinide compounds in the magnetically ordered state to determine the magnetic hyperfine field. The nuclear magnetic resonance results will be combined with Mössbauer, neutron scattering, and macroscopic magnetization measurements to determine the electronic configuration and magnetic moment distribution in the NaCl-type compounds.

SPIN-LATTICE RELAXATION TIME OF ^{31}P IN URANIUM MONOPHOSPHIDE *(Moshe Kuznietz and G. A. Matzkanin)*

The continuous wave nuclear magnetic resonance of ^{31}P in the paramagnetic state of uranium monophosphide was reported first by Scott et al.[211] We used their room-temperature linewidth of about 5 oersteds to calculate a spin-spin relaxation time (T_2) of about 20 microseconds. The resulting decay time should be easily observed. Our results gave a decay time of 20-40 microseconds with 90° pulses. When a 180-90° pulsed series and a box-car integrator was used, the spin-lattice relaxation time (T_1) was 295 ±15 microseconds and 390 ±20 microseconds at 8 and 12 MHz, respectively, at room temperature.

NUCLEAR MAGNETIC RESONANCE STUDY OF ^{14}N IN THE PARAMAGNETIC STATE OF URANIUM MONONITRIDE *(Moshe Kuznietz)*

A nuclear magnetic resonance study of ^{14}N in the paramagnetic state of uranium mononitride was initiated. Magnetic measurements by Trzebiatowski et al.,[212] Allbutt

*Present address: The Physical Laboratories, The University, Manchester, England.

[208] J. W. Ross and D. J. Lam, Annual Progress Report for 1966, Metallurgy Division, ANL-7299, pp. 210-211.

[209] J. W. Ross and D. J. Lam, Phys. Rev. (to be published).

[210] T. H. Geballe, B. T. Matthias, K. Andres, E. S. Fisher, T. F. Smith, and W. H. Zachariasen, Science *152*, 755 (1966).

[211] B. A. Scott, K. A. Gingerich, and R. A. Bernheim, Phys. Rev. *159*, 387 (1967).

[212] W. Trzebiatowski, R. Troc, and J. Leciejewicz, Bull. Acad. Polon. Sci., Ser. Chim. *10*, 395 (1962).

et al.,[213] and Curry[214] showed that uranium mononitride has the Type-I antiferromagnetic ordering below $T_N = 53 \pm 2°K$ with $n_a = 0.75 [\mu_B]$. In the paramagnetic state, the susceptibility measurements obey a Curie-Weiss law.

Very few nuclear magnetic resonance studies of ^{14}N in solids and, to our knowledge, only one such study of nitrides[215] has been reported. Shulman and Wyluda succeeded in detecting the ^{14}N resonance in TbN and TmN but failed to detect the ^{14}N resonance in HoN. All three nitrides have the NaCl structure. Shulman and Wyluda mentioned problems encountered in the ^{14}N nuclear magnetic resonance detection.

Our experimental situation has been very similar. We had to use a large 40-hertz field modulation (about 9 Oe), and were able to detect signals only in the dispersion mode and only by applying *rf* fields as high as 0.3 oersted. Under these conditions we made measurements at 1950, 3077, and 4000 kHz, or in the corresponding ^{14}N resonance fields 6340, 10 000, and 13 000 oersteds, respectively. Measurements were made in the temperature range from 300 to 77°K. At liquid nitrogen temperature, the ^{14}N signal was detected in UN and in N_2 from the liquid hydrogen coolant. As a result, a direct measurement of the Knight shift (+0.94%) was possible. At all other temperatures, runs have been performed separately for uranium mononitride and for an 85% solution of HNO_3 in water, which serves as a reference material, and subsequently the Knight shift was calculated.

Measurements at the three frequencies (1950, 3077, and 4000 kHz) at 300°K showed that the line of ^{14}N in uranium mononitride is shifted toward the lower applied magnetic field with respect to the line of ^{14}N in HNO_3. The fractional shift has been the same (0.5%) indicating a Knight shift and that the shift is positive. The shift increased with the lowering of temperature, which is very similar to the results found in TmN.[215]

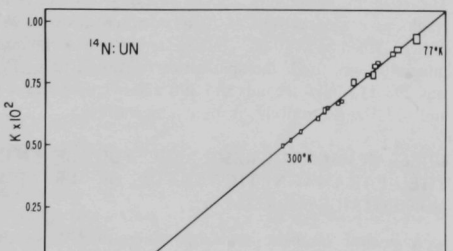

48145

Fig. 45. Knight Shift of ^{14}N in UN versus Susceptibility (with Temperature as an Implicit Variable).

A plot of the Knight shift K versus the susceptibility (Figure 45) gives the linear dependence,

$$UN: K = -(31.5 \pm 3.0) \times 10^{-4} + (4.22 \pm 0.22)\chi_M$$

over all the measurement range of χ_M. This result is parallel to the results obtained by Scott et al.[211] for UP.

The linewidth in uranium mononitride is much broader than the 5-oersted room-temperature linewidth reported for UP.[211]

NEUTRON DIFFRACTION STUDY OF URANIUM MONOPHOSPHIDE *(M. H. Mueller, L. Heaton, and K. D. Anderson)*

Our original neutron investigation of uranium monophosphide[216] was carried out to nitrogen temperatures only; however, Curry[217] carried out his investigation to near helium temperatures and noted an increase in the intensity of the magnetic reflections at approximately 33°K with a width of about 7 Kelvin degrees. Recently, our investigation has been extended to helium temperatures and an increase in the magnetic reflections at the lower temperatures has been noted. The increase of the (110) reflection occurs at approximately 25°K (within 1 Kelvin degree), as shown in Figure 46, with a considerably sharper transition than found by Curry. Both investigations indicate a general increase in all of the magnetic reflections; however, all of the intensities are relatively weak. Single crystals are needed to determine possible changes in the magnetic form factor due to electronic configurations.

NEUTRON DIFFRACTION STUDY OF THE ANTIFERROMAGNETISM OF URANIUM MONOARSENIDE *(J. M. Williams, L. Heaton, and F. P. Campos)*

A neutron diffraction study was carried out at Argonne National Laboratory to investigate the possibility of antiferromagnetic ordering in uranium monoarsenide, since recent

213 M. Allbutt, A. R. Junkison, and R. M. Dell, Proc. Intl. Symp. on Compounds of Interest in Nuclear Reactor Technology, Boulder, Colorado, 1965, pp. 65-81.

214 N. A. Curry, Proc. Phys. Soc. (London) *86*, 1193 (1965).

215 R. G. Shulman and B. J. Wyluda, J. Phys. Chem. Solids *23*, 166 (1962).

216 S. S. Sidhu, W. Vogelsang, and K. D. Anderson, J. Phys. Chem. Solids *27*, 1197 (1966).

217 N. A. Curry, Proc. Phys. Soc. *89*, 427 (1966).

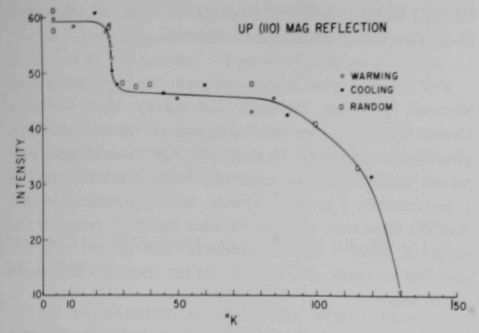

Fig. 46. Neutron Diffraction Intensity of Uranium Monophosphide (110) Reflection versus Temperature.

susceptibility-temperature measurement studies[218] exhibited a minimum at 128°K.

The polycrystalline sample was furnished by Y. Baskin.[219] X-ray and neutron powder patterns showed the presence of a small U(N,O) impurity. While objectionable, the impurity did not prohibit interpretation of the data. Results obtained from chemical analysis and from neutron diffraction indicate that the compound was stoichiometric uranium monoarsenide.

Neutron diffraction powder patterns were taken with a wavelength of 1.00Å, and the scattering amplitudes were b_U = 0.85 and b_{AS} = 0.64 x 10^{-12} cm. All lines of magnetic origin that appeared in the liquid nitrogen diffraction pattern were indexed with mixed indices and could, therefore, be accounted for by a magnetic structure similar to the structure in uranium mononitride and uranium monophosphide.[216,217] The (110) magnetic line was completely free of overlap and was reasonably intense. The ratio of the intensity of the (110) magnetic line to the (200) nuclear line was 1:8.

The form factor curve appeared to be very similar to that of uranium monophosphide;[216] however, no observable magnetic reflections were found in the high sin θ/λ region. The extrapolated value of $|F_m|$ at sin θ/λ = 0.0 is 2.04, and the derived magnetic moment per uranium atom at liquid nitrogen temperature is 1.89 ±0.05 Bohr magnetons. This value compares favorably with the value found below 35°K for uranium monophosphide;[217] but, is significantly higher than the high-temperature form.[216,217]

[218]W. Trzebiatowski, A. Sepichowska, and A. Zygmunt, Bull. Acad. Polon. Sci., Ser. Chim. *12*, 687 (1964).

[219]Y. Baskin, J. Inorg. Nucl. Chem. *29*, 2480 (1967).

NEPTUNIUM DIOXIDE *(L. Heaton, M. H. Mueller, and J. M. Williams)*

Publication

L. Heaton, M. H. Mueller, and J. M. Williams, J. Phys. Chem. Solids *28*, 1651-1654 (1967).

The present neutron diffraction study is fully described in the cited publication. After our investigation was completed, we learned that Brookhaven National Laboratory had made a similar investigation.[220] Cox and Frazer indicated an upper limit of approximately 0.4 Bohr magneton per Np ion, for a possible ordered magnetic moment, in contrast to our value of 0.5 Bohr magneton. Excellent agreement in the coherent scattering amplitude of Np with values of 1.057 ±0.015 and 1.055 ±0.010 x 10^{-12} cm was reported by the two groups.

NEPTUNIUM CARBIDE *(L. Heaton, G. Lander, M. Mueller, K. D. Anderson, and D. Zauberis)*

Magnetic susceptibility measurements by Ross and Lam[221] showed that NpC is paramagnetic at temperatures above 310°K, antiferromagnetic between 310 and 220°K, and ferromagnetic below 220°K. Neutron diffraction patterns in the paramagnetic region (above 310°K) verify that NpC has the face-centered cubic NaCl-type structure. A refinement of the nuclear intensities in the paramagnetic region indicates the composition of the sample to be $NpC_{0.93}$, which is in agreement with chemical analyses.

In the antiferromagnetic region (310-220°K), the additional reflections in the neutron diffraction pattern indicate that the antiferromagnetic structure of NpC consists of ferromagnetic sheets stacked antiferromagnetically along the [001] axis. The spin direction is perpendicular to the sheets. The ordered moment in the antiferromagnetic state is 1.2 Bohr magnetons per neptunium atom.

Below 220°K NpC is ferromagnetic. The transition exhibits no thermal hysteresis (Figure 47), and is apparently complete over 3 Kelvin degrees. The relatively slow decrease in intensity of the antiferromagnetic reflections (for example, (110) in Figure 47) shows that the magnetic scattering is mainly from the tightly bound *f* shell, and the form factor agrees with the theoretical calculations for uranium in the $5f^3$ state.

[220]D. E. Cox and B. D. Frazer, J. Phys. Chem. Solids *28*, 1649-1650 (1967).

[221]J. W. Ross and D. J. Lam, J. Appl. Phys. *38*, 1451-1453 (1967).

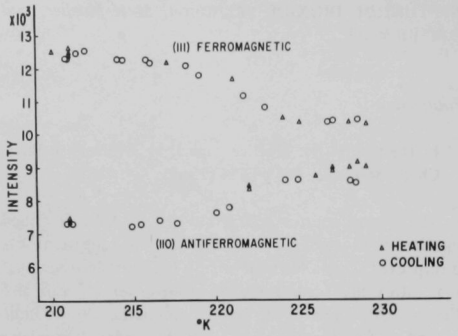

Fig. 47. Peak Intensity of (110) and (111) Reflections versus Temperature for NpC.

The small amount of available sample and the polycrystalline form does not permit an accurate determination of the magnetic intensities, which will influence the description of the magnetic form factor. Preparations are being made to grow single crystals of NpC, which will be used to more accurately describe the ferromagnetic and the antiferromagnetic structures. The magnetic contribution in the ferromagnetic state is superimposed on the strong nuclear reflections; therefore, data from experiments with polarized neutrons on single crystals are essential.

POSITRON ANNIHILATION *(H. G. Hoeve,* D. O. Van Ostenburg, and E. S. Fisher)*

For the past year, a joint program has been under way between Argonne National Laboratory and Northern Illinois University to construct and to use the positron annihilation technique to study the electronic structure of metals and alloys. The apparatus has a resolving time of approximately 2×10^{-8} seconds, which is limited by the NaI(Tℓ) detectors, and has variable scanning times in the range of from 1 to 100 minutes. The output data are punched on cards, and corrections for chance coincidences can be made.

A single crystal of alpha uranium is under investigation in order to study the Fermi surface. Since the crystal structure of alpha uranium can be characterized by an orthorhombic lattice, the Fermi surface is likely to lie in several energy bands. Within the free electron approximation, and, under the assumption that there are six free electrons per atom, the radius k_0 of the Fermi sphere is given by

$$k_0 = \left(\frac{72\pi^2}{abc}\right)^{1/3}$$

where a, b, and c are the edges of the orthorhombic cell. The initial phase of the study will examine the validity of this simple model and will examine deviations from the mean Fermi radius as the crystal is rotated about the three mutually perpendicular axes (a, b, and c).

Transition Metals and Compounds

MAGNETIC PROPERTIES OF DILUTE ALLOYS *(J. W. Ross,** D. J. Lam, and L. L. Isaacs)*

Dilute alloys of gadolinium in scandium form a very interesting system for the study of the onset of magnetism. The host element scandium, the magnetic impurity gadolinium, and their alloys possess the hexagonal close-packed structure. The magnetic properties of the alloys, therefore, are expected to show some anisotropy.

Single crystals of the scandium-gadolinium alloys were prepared by the strain-anneal technique, and the crystals were spark cut to yield specimens with surfaces oriented along the principal crystallographic axes. The gadolinium concentration ranged from 10 to 50 000 parts per million on an atomic percentage basis. Absolute susceptibility was measured by the Faraday method with an accuracy of 5×10^{-8} emu/g, and the susceptibility difference ($\chi\perp_c - \chi\|_c$) was determined with a torque magnetometer that was accurate to 1×10^{-10} emu/g (crystallographic directions are defined with respect to the c axis of the hexagonal cell). Both measurements were determined over the range of temperature from 2 to 300°K.

The data obtained to date show two important effects: (1) the reciprocal susceptibility is not a linear function of temperature over the range investigated, and (2) the susceptibility difference changes sign as the temperature is decreased. Thus, the magnetic moment alignment with respect to the crystallographic axes changes as a function of temperature.

The magnetic fields and temperatures available in our apparatus were too low and too high, respectively, to achieve saturation of the samples. The susceptibility of the 200 parts per million alloy was measured down to 0.3°K in collaboration with scientists in the Physics Department of the University of California at La Jolla. The measurements

*Present address: Northern Illinois University, DeKalb, Illinois.

**Present address: The Physical Laboratories, The University, Manchester, England.

confirmed our data at higher temperatures, and indicated that the paramagnetic Curie temperature extrapolated to -0.35 and -0.5°K parallel and perpendicular, respectively, to the *c* axis.

Further study is in progress to determine the concentration dependence of the magnetic ordering temperatures, and to assess the possibility of polarization effects in the scandium-rich alloys.

MAGNETIC MOMENTS IN BINARY IRON ALLOYS

(A. T. Aldred)

The magnetization measurements were completed on iron-rich solid solution alloys with the transition metals titanium, molybdenum, tungsten, technetium, and rhenium, and the results will be considered in conjunction with the previously reported data.[222] The slope of the magnetic moment versus concentration curve for each alloy system decreases numerically as the group number of the solute increases. The values of the slopes for the alloy systems, where the second- or third-long-period solute is from Group VI (molybdenum and tungsten), agree quite closely. Agreement also occurs where the solute is from Group VII (technetium and rhenium). In both groups the slopes are more negative than those obtained for the alloys with the corresponding first-long-period solutes chromium and manganese.[223]

The apparent relationship between the slope of the mean moment versus concentration curve and the group number of the solute suggests that a band model may be applied to these alloys. The moments have been plotted against electron concentration in Figure 48; the solid line is an extrapolation of the Slater-Pauling curve. Also included are data for alloys of other first-period transition elements with iron.[223,224] The data fit, at least qualitatively, the extrapolated Slater-Pauling curve. The deviations from the line seem to depend systematically on the group number of the solute, i.e., Fe-Ti alloys have the most positive deviation from the extrapolated Slater-Pauling curve, and Fe-Mn alloys the most negative.

Magnetization measurements were also made on a series of iron-rich alloys with nontransition metal solutes. The rate of change of mean magnetic moment with concentration in such alloys has been understood previously in terms of a dilution model. In the model, the solute atoms are assumed to carry no magnetic moments and the presence of such atoms does not affect the moments on the iron atoms.

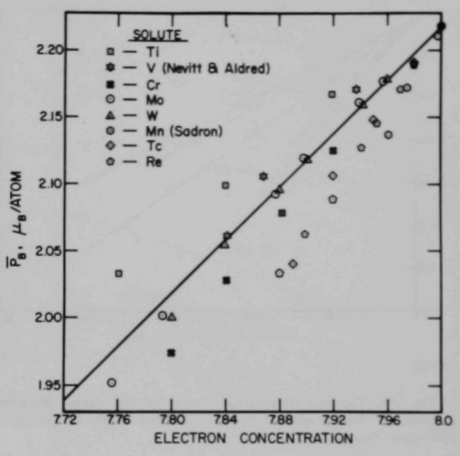

46969

Fig. 48. Mean Atomic Magnetic Moments for Body-Centered Cubic Iron Alloys Plotted as a Function of Electron Concentration. The data for Fe-V alloys are from Nevitt and Aldred;[224] the data for Fe-Mn alloys are from Sadron.[223]

The analysis is based mainly on the magnetization data of Fallot.[225] Recent neutron magnetic scattering experiments[226] on similar alloys indicated that the solute atoms do not have magnetic moments, which gave additional support to the dilution model. Although the results of magnetization measurements on Fe-Be alloys[227] were consistent with dilution, subsequent data from Fe-Ga and Fe-As alloys[228] gave rates of decrease of mean moment with concentration that were substantially less than would be expected from the dilution model. In order to study the applicability of the dilution model over as wide a range of solutes as possible, measurements were made on binary iron-rich Fe-Cu, Fe-Au, Fe-Ge, Fe-Sn, and Fe-Sb alloys. The mean magnetic moments for the various alloys with nontransition solutes are plotted as a function of solute concentration in Figure 49. The magnetic moment values for all the systems fit straight lines and were subjected to least-squares analysis.

The values of the coefficient *C* for body-centered cubic iron alloys with nontransition elements are listed in Table 18. When the values are arranged relative to the position of the solute in the periodic table, several trends become evident. First, only the solutes with the lowest atomic

[222] A. T. Aldred and D. I. Bardos, Annual Progress Report for 1966, Metallurgy Division, ANL-7299, pp. 251-253.

[223] C. Sadron, Ann. Phys. *17*, 371-451 (1932).

[224] M. V. Nevitt and A. T. Aldred, J. Appl. Phys. *34*, 463-468 (1963).

[225] M. Fallot, Ann. Phys. (Paris) *6*, 305-387 (1936).

[226] T. M. Holden, J. B. Comly, and G. G. Low, Proc. Phys. Soc. *92*, 726-730 (1967).

[227] A. T. Aldred, J. Appl. Phys. *37*, 671-674 (1966).

[228] A. T. Aldred, J. Appl. Phys. *37*, 1344-1346 (1966).

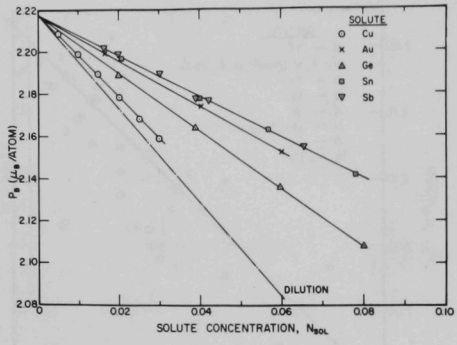

47796

Fig. 49. Concentration Dependence of the Mean Magnetic Moment for Body-Centered Cubic Iron Alloys with Various Nontransition Element Solutes.

numbers (namely, beryllium, aluminum, and silicon) are in reasonable agreement with the dilution model. Significantly, these are the only solute elements in Table 18 that have no *d* electrons. The *d*-electron shells of the other solutes, however, are all filled, and there is little possibility of interactions between electrons in these shells and the electrons in the unfilled *d* levels of iron. Second, in periods 3 to 5, the values of *C* for solutes within a given period agree closely. Third, in Groups III to V, the values of *C* for solutes from a given group show a steady decrease with increasing period number. A pattern emerged from these relationships with regard to the value of *C* and the position of the solute in the periodic table. Unfortunately, the lack of solid solubility of other nontransition elements in iron prohibits any further attempts at systematization.

TABLE 18. Values of *C* for Nontransition Metal Solutes in Iron Shown as a Function of the Position of the Solute in the Periodic Table

Period \ Group →	I	II	III	IV	V
2		Be[b] 2.26			
3			Al 2.27[a]	Si 2.28[a]	
4	Cu 2.00	Zn 2.01[a]	Ga[c] 1.43	Ge 1.36	As[c] 1.40
5				Sn 0.97	Sb 0.97
6	Au 1.09				

[a]Calculated from the data of Fallot.[225]
[b]Reference 227.
[c]Reference 228.

Since most of these systems do not fit the dilution model, the location of the extra magnetic moment becomes important. Conceivably the solute atoms possess aligned magnetic moments, but the neutron scattering results of Holden et al.[226] show that this does not occur, at least in dilute alloys of aluminum, silicon, gallium, germanium, tin, or antimony in iron. By analogy, an inference could be made that none of the nontransition metal solutes have a magnetic moment when dissolved in iron. Therefore, the present data were recalculated to express the data in terms of moment per iron atom. All the solutes produce a small increase in the average moment per iron atom; the maximum value is ~2.35 Bohr magnetons. The precise nature of, and reasons for, the increase in iron moment is unresolved.

NEUTRON SCATTERING EXPERIMENTS ON FERROMAGNETIC ALLOYS *(A. T. Aldred)*

The magnetization data for iron-rich alloys with transition metals, described on page 93, are satisfactorily understood in terms of a nearly rigid-band model; however, the location of the magnetic moments on an atomic scale is not known in any detail. Such information is required for a complete interpretation of the data.

The best method to study the distribution of magnetic moments in concentrated alloys is the diffuse magnetic neutron scattering technique, which yields the difference in moments on the two atomic species in a binary ferromagnetic alloy. When the magnitude of the difference in moments is combined with the magnetization data, the moments on the individual species can be obtained. Such neutron scattering experiments were first performed by Shull and Wilkinson,[229] and more recently by Collins and Forsyth.[230] The technique is valid for concentrated alloys; in dilute alloys, other neutron scattering experiments[231] yield more detailed results but, unfortunately, cannot be applied to concentrated alloys.

In the iron-rich alloys with transition metals, for which magnetization data have been obtained, the magnetic moments on the individual species should vary strongly with concentration. The concentration variation cannot be confirmed until neutron scattering information is available; therefore, experiments of the Shull and Wilkinson type will be attempted on certain alloy systems. The modification of an existing neutron diffractometer* is almost complete and calibration experiments will be under way in the near future.

[229]C. G. Shull and M. K. Wilkinson, Phys. Rev. 97, 304-310 (1955).

[230]M. F. Collins and J. B. Forsyth, Phil. Mag. *8*, 401-409 (1963).

[231]G.G.E. Low and M. F. Collins, J. Appl. Phys. *34*, 1195-1199 (1963).

*Modification is in collaboration with M. H. Mueller and L. Heaton.

MAGNETIC MOMENTS IN TERNARY ALLOYS

(D. I. Bardos and A. T. Aldred)

Publication

D. I. Bardos, A. T. Aldred, and P. A. Beck,* J. Appl. Phys. *38*, 1260-1262 (1967).

The determination of atomic magnetic moments in ternary alloys, from saturation magnetization measurements, was extended to body-centered cubic alloys in the Fe-Ni-Al and the Fe-Co-Al systems. The results for face-centered cubic alloys in the Fe-Ni-Al system were reported previously.[222]

In Figure 50, the average atomic moments $\bar{p}$ are plotted versus the ratios of the transition-element components for several series of alloys, each with a constant aluminum concentration. The initial rates of decrease of the average atomic moment with aluminum concentration were determined for ternary alloys at fixed nickel-to-iron ratios. The results may be rationalized in terms of a molecular-field theory in which the mean moment at a given atomic site is determined by the moments present elsewhere in the alloy. In this model, the presence of aluminum atoms, which have no magnetic moments, does not affect the iron moments; an identical behavior is observed for dilute Fe-Al alloys.[226] The broad maximum in the curve for the binary Fe-Ni alloys (Figure 50) is the result of an enhancement of the iron moments by near-neighbor nickel atoms. As aluminum is added to the binary alloys, the substitution of aluminum for the nickel near neighbors of an iron atom reduces the magnitude of the enhancement of the average iron moment. A quantitative version of the semiempirical model is under investigation[232] to confirm the interpretation of the experimental results on the Fe-Ni-Al system.

The mean atomic moments in the binary Fe-Co system were redetermined, since an earlier investigation[233] was made prior to the discovery of a CsCl-type ordered structure.[234] The previous measurements on alloys near the equiatomic composition may have been carried out on alloys that were chemically ordered. In the present investigation, alloys were quenched at various rates from a temperature of 850°C. A maximum difference of 3% in the mean moment for the equiatomic alloy is observed for the two extremes in quenching rates. In Figure 51, the dash-line curve, which shows $\bar{p}$ for ordered alloys, agrees very well with the earlier determination;[233] however, the curve does not represent the variation of the mean moment with

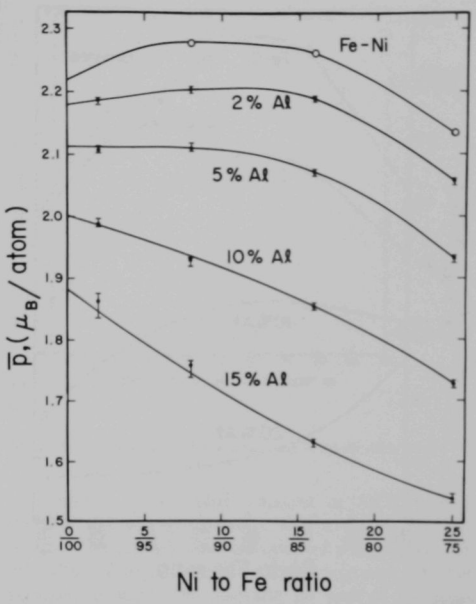

Fig. 50. Average Magnetic Moment per Atom $\bar{p}$ versus Nickel-to-Iron Ratios for the Binary Fe-Ni Alloys and Several Series of Ternary Fe-Ni-Al Alloys with Constant Aluminum Concentration.

electron concentration for a random distribution of atomic species,* as summarized for binary alloys by the Slater-Pauling curve. The contribution to the mean moment as a result of ordering is reduced by quenching; therefore, the curve labeled Fe-Co quenched, is the correct Slater-Pauling curve in the electron-concentration range between iron and cobalt.

The average magnetic moments for the body-centered cubic Fe-Co-Al alloys, subjected to the fastest cooling rate, are shown in Figure 51. The rate of decrease of $\bar{p}$ with aluminum concentration, is similar to that observed for Fe-Ni-Al alloys. The curves for ternary Fe-Co-Al alloys in Figure 51 are not parallel to the binary Fe-Co curve, an indication that the previously proposed[235] rigid-band approximation is not valid. A semirigid band model, where the variation of bandwidth and exchange interaction with aluminum concentration is considered, might be applicable but the model cannot be determined solely on the basis of saturation moment data. An effort is being made to rationalize the results by a model similar to that employed for the Fe-Ni-Al alloys.

*Present address: University of Illinois, Urbana, Illinois.

[232] J. L. Beeby, AERE, Harwell, England.

[233] P. Weiss and R. Forrer, Ann. Phys. *12*, 279 (1929).

[234] C. G. Shull and S. Seigel, Phys. Rev. *75*, 1008 (1949).

[235] B. R. Coles and W. R. Bitler, Phil. Mag. *8*, 477 (1956).

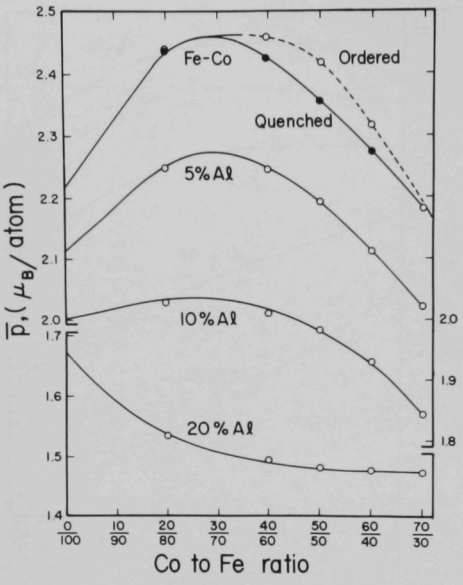

Fig. 51. The Average Magnetic Moment per Atom $\bar{p}$ versus Cobalt-to-Iron Ratios for the Binary Fe-Co Alloys and Several Series of Ternary Fe-Co-Al Alloys with Constant Aluminum Concentration.

NUCLEAR RESONANCE STUDIES ON TRANSITION-METAL ALLOYS *(F. Y. Fradin)*

Publication

F. Y. Fradin and T. J. Rowland,* Appl. Phys. Letters *11*, 297 (1967). [Work performed at the University of Illinois.]

A program was initiated to study the effect of magnetic and nonmagnetic impurities on the electronic structure of the transition metals. Nuclear magnetic resonance measurements of ^{195}Pt Knight shift and of the indirect coupling between ^{195}Pt nuclear spins via the conduction electrons as well as resistivity measurements will be made on the same samples of platinum-base alloys with small concentrations of nonmagnetic solutes. The concentration dependence of the results will be analyzed to determine the variation of *s*-electrons and *d*-holes in platinum alloys. Knight shift, resistivity, and susceptibility measurements also will be made on Pt-Rh alloys doped with small concentrations of dissolved magnetic impurities. The Pt-Rh system has complete solid solubility, and evidence indicates that iron and cobalt have localized moments in platinum but not in rhodium. The dependence of the hyperfine field on the composition of the Pt-Rh host and on temperature will be related to the average magnetic moment and to the resistivity in order to explore further the relationship between the occurrence of localized moments and the electronic structure of the host.

*Present address: University of Illinois, Urbana, Illinois.

VANADIUM-NIOBIUM ALLOYS *(D. O. Van Ostenburg, J. J. Spokas,** and D. J. Lam)*

Publication

D. J. Lam, J. J. Spokas,** and D. O. Van Ostenburg, Phys. Rev. *156*, 735-739 (1967).

The nuclear-magnetic-resonance properties of the ^{51}V and ^{93}Nb isotopes and magnetic susceptibilities were measured in the body-centered cubic VNb alloy system from pure vanadium to pure niobium. In these alloys, the electronic character at the vanadium and niobium sites is not the same, and the simple rigid-band picture cannot account for the composition dependence of the nuclear-magnetic-resonance and susceptibility data. A more detailed account of this work is found in the cited publication.

BETA MANGANESE *(G. A. Matzkanin and C. H. Sowers)*

Publication

G. A. Matzkanin and C. H. Sowers, Bull. Am. Phys. Soc. *12*, 291 (1967). Abstract

The spin-lattice relaxation time T_1 in beta manganese exhibits unusual behavior compared with that generally observed in metals. As previously reported,[236] the temperature dependence of the relaxation rate is quite different from that expected for relaxation by conduction electrons. Analysis of the data indicates that within experimental error T_1T is practically independent of temperature from 300 to 180°K. A possible source of the strong temperature dependence T_1T at lower temperatures below 180°K is the influence of the density of states and of the amplitude of the electronic wave function on the relaxation time; however, attempts to interpret the results in this manner are not satisfactory.

Additional measurements revealed that T_1 is not dependent on magnetic field, at least at temperatures below

**Present address: St. Procopius College, Lisle, Illinois.

[236] G. A. Matzkanin and D. O. Van Ostenburg, Annual Progress Report for 1966, Metallurgy Division, ANL-7299, p. 264.

about 200°K. A possibility exists that some field dependence occurs at higher temperatures, although experimental error precludes a definite conclusion. Measurements are in progress at other fields that use signal enhancing techniques to reduce error.

MÖSSBAUER EFFECT STUDIES IN SOLID SOLUTION ALLOYS AND INTERMEDIATE PHASES

(C. W. Kimball, H. Montgomery,** A. T. Aldred, and J. B. Darby, Jr.)*

Publications

C. W. Kimball,* J. K. Tison,† and M. V. Nevitt, J. Appl. Phys. *38*, 1153-1154 (1967).

B. D. Dunlap,†† A. E. Dwight, G. M. Kalvius,†† and C. W. Kimball,* Proc. 6th Rare Earth Research Conf., Gatlinburg, Tennessee, May 3-5, 1967. Oak Ridge National Laboratory, Oak Ridge, Tennessee, 1967, pp. 506-509.

B. D. Dunlap,†† J. B. Darby, Jr., and C. W. Kimball,* Phys. Letters *25*, 431 (1967).

C. W. Kimball,* *Mössbauer Technology*, E. Gruverman, ed. (Plenum Press, New York, 1967), Vol. 3.

R. H. Hannon,† C. W. Kimball,* and A. E. Dwight, Illinois State Acad. of Sci., April 1967. Abstract

Magnetic susceptibility measurements[237] and isomer shift data from the Mössbauer spectra[238] of palladium-rich Pd-Sn alloys suggest that the host *d* band is filled at a rate roughly proportional to the solute valence, and that there is a charge transfer from the solute to the neighboring solvent atoms. In the case of dilute alloys, the charge transfer hypothesis is contrary to Friedel's theory, which assumes that each solute atom is almost perfectly screened by conduction electrons within the atomic volume. Mössbauer studies were made on Pd-Sb alloys to determine the extent of charge transfer.

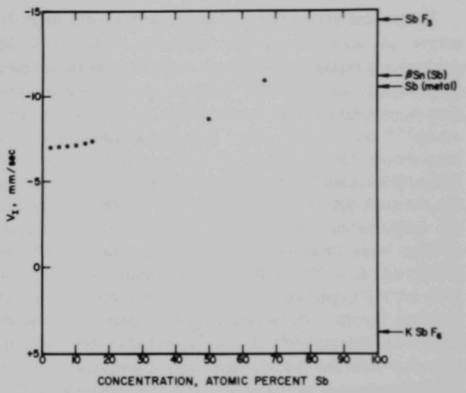

48184

Fig. 52. Isomer Shifts of Antimony in Pd-Sb Alloys.

Mössbauer spectra were obtained at 80°K with a standard transmission geometry and a $CaSnO_3(^{121}Sb)$ source.[239] Each spectrum consisted of a single line; the linewidth for the solid solution alloys increased with the antimony content. The linewidth for each of the compounds PdSb and $PdSb_2$ was somewhat broader and probably represent unresolved quadrupole spectra as a result of the locations of the antimony atoms at noncubic sites.[240] The linewidth of the solid solution alloys probably arises partly from a spread of isomer shifts over the various solute sites and partly from a spread in electric field gradients, which makes a quantitative analysis of the linewidths impossible. The isomer shifts, however, were determined fairly accurately by a least-squares analysis and the results are shown in Figure 52. The shift measurements are relative to the $CaSnO_3$(Sb) source and should be compared with the values of -14.4 mm/sec for the trivalent ionic compounds SbF_3 and +3.8 mm/sec for the pentavalent compounds $KSbF_6$.[241] The electron density at the antimony nucleus is intermediate between the values for the two ionic states and increases with the antimony concentration. The isomer shifts for the Pd-Sb and Pd-Sn alloys can be interpreted with the Friedel model[242] but with less conviction, since the isomer shifts are extremely sensitive to the relative *s*- and *p*-character of the screening electrons. The isomer shifts for the Pd-Sb and Pd-Sn alloys suggest that the electrons screening the solute atoms have somewhat greater *p*-character in the alloys than in pure antimony or tin.

*Consultant, Visiting Scientist; Northern Illinois University, DeKalb, Illinois.

**Formerly Research Associate in the Metallurgy Division, now at the Department of Physics, University of Edinburgh, Scotland.

†Present address: Northern Illinois University, DeKalb, Illinois.

††Solid State Science Division, Argonne National Laboratory.

237D. J. Lam and K. M. Myles, J. Phys. Soc. Japan *21*, 1603 (1966).

238M. Cordey-Hayes and I. R. Harris, Phys. Letters *24A*, 80 (1967).

239S. L. Ruby et al., Phys. Rev. *148*, 176 (1966).

240R.W.G. Wyckoff, *Crystal Structures* (Interscience, New York, 1963), Vol. 1, p. 124.

241S. L. Ruby et al., Phys. Rev. *159*, 239 (1967).

242H. Montgomery et al., Proc. Roy. Soc. *A301*, 261 (1967).

Theoretical attempts to relate hyperfine field measurements to atomic magnetic moments, determined by neutron scattering or saturation magnetization techniques, have been unsuccessful;[243] however, several clues suggest that a correlation may be possible. Mössbauer measurements[244] on iron-rich alloys with transition-metal solutes have shown that the hyperfine field on a given iron atom is critically affected by the local environment (to at least the third-nearest neighbors). Qualitatively, similar variations in the magnetic moments on iron atoms in the same alloy systems were observed in neutron scattering studies by Collins and Low.[245] In the iron-aluminum and iron-silicon systems, the hyperfine field at an iron site without a solute atom in the first three near-neighbor shells is also unaffected by alloying.[244] If the correlation between the hyperfine field and the atomic moments could be extended, a useful technique would be available to obtain information on the magnetic moments on iron atoms in alloys.

Mössbauer studies have been initiated to measure the magnetic hyperfine field in iron-rich Fe-Ga and Fe-Sn solid solution alloys with a solute concentration of from 2 to 10 at.%. Saturation magnetization studies show that the average moment on the iron atoms increases with an increase in solute concentration. While preliminary Mössbauer results indicate that the hyperfine field decreases with the addition of gallium or tin, measurements with greater resolution are in progress to distinguish more clearly the hyperfine field of an iron site in a given environment.

THE ELECTRONIC STRUCTURE OF HEXAGONAL ALLOYS BETWEEN SECOND-LONG-PERIOD TRANSITION ELEMENTS *(L. L. Isaacs and D. J. Lam)*

Publication

T. B. Massalski,* G. A. Sargent,* and L. L. Isaacs, *Phase Stability in Metals and Alloys*, P. S. Rudman, J. Stringer, and R. J. Jaffee, eds. (McGraw-Hill Book Co., New York, 1967), pp. 291-305.

A systematic investigation is under way to acquire the experimental data that is required to calculate the density of states for the binary hexagonal solid solutions formed between the elements molybdenum, technetium, ruthenium, or rhodium of the second long period. The experiments in progress include the low-temperature specific heat and the magnetic susceptibility.

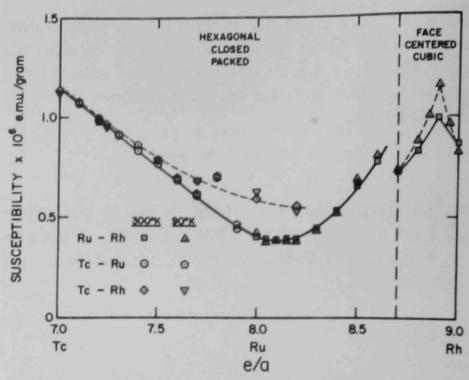

Fig. 53. Magnetic Susceptibility versus *e/a* Ratio for the Hexagonal Close Packed and Face-Centered Cubic Alloys of Transition Metals from the Second Long Period.

Low-Temperature Specific-Heat Measurements: The design of a helium-three cryostat was described previously.[246] The construction and assembly of the cryostat and the electronic recording system were completed. Preliminary operation of the facility has indicated that the low-temperature design limit of 0.3°K can be achieved. As soon as the calorimeter has been calibrated, the low-temperature specific-heat determinations will begin on the alloys of interest.

Magnetic Susceptibility Measurements: The magnetic susceptibility and the electronic specific heat of an alloy are directly proportional to the density of states. Magnetic susceptibility measurements were made at 300 and 90°K on the binary hexagonal and face-centered cubic alloys in the Ru-Rh, Tc-Ru, and Tc-Rh systems. A plot of susceptibility (emu per gram) as a function of electron concentration (*e/a*) is shown in Figure 53. (The electron concentration is defined as the number of electrons outside of the filled krypton shell for each of the component elements.) A well-defined minimum in the susceptibility values is observed at an electron concentration of 8.1, which corresponds to the alloy 90 at.% Ru-10 at.% Rh, and a maximum occurs for a face-centered cubic alloy at an *e/a* value of 8.9 (10 at.% Ru-90 at.% Rh). A corresponding minimum and maximum, respectively, is anticipated in the density-of-states curve at the two respective *e/a* values. A variation is observed in the susceptibility values for a given value of electron concentration; for example, the values for elemental ruthenium are lower than for an alloy, with the same *e/a* value, that consists of equiatomic amounts of

[243] W. Marshall and C. E. Johnson, J. Phys. Radium *23*, 733 (1962).

[244] M. B. Stearns, Phys. Rev. *147*, 439 (1966).

[245] M. F. Collins and G. G. Low, Proc. Phys. Soc. *86*, 535 (1965).

*Carnegie-Mellon University, Pittsburgh, Pennsylvania.

[246] L. L. Isaacs, Annual Progress Report for 1966, Metallurgy Division, ANL-7299, pp. 257-259.

technetium and rhodium. Thus, either the rigid-band approximation is not applicable, or, the enhancement effects for a given *e/a* value vary with the component elements. Measurements of the temperature dependence of the susceptibility, down to liquid helium temperatures, are in progress.

THE HEATS OF FORMATION OF TRANSITION-METAL ALLOYS *(J. B. Darby, Jr.)*

Publication

J. B. Darby, Jr., Ind. Eng. Chem. *59*, 13 (1967). Abstract

The heats of formation were reported previously[247] for binary palladium-rich alloys that contain the polyvalent solutes cadmium, indium, tin, or antimony. The heat-of-formation values for all the systems, except Pd-Sb, fall essentially on a common curve when the values are plotted as a function of electron concentration (assuming the effective valence of the solute to be the number of electrons outside of the filled 4*d* shell). Paramagnetic susceptibility data for the Pd-Ag, and for the palladium-rich Pd-Cd and Pd-Sb alloys display a similar behavior when plotted as a function of electron concentration. The atypical behavior of the two bulk properties of the Pd-Sb system, and the limited information on the electronic structure of the system prompted measurements of the isomer shift in the Mössbauer spectrum of the antimony atoms, and of the low-temperature specific heat.

The details of the Mössbauer study are presented on pages 97-98. The isomer-shift measurements can be interpreted in terms of a charge transfer from antimony to palladium on the basis of the simple rigid-band model, as proposed earlier for the Pd-Sn alloys.[238] An alternate interpretation of the results can be based on the Friedel screening model, which assumes that each solute atom is almost perfectly screened by the conduction electrons within the atomic volume.

Low-temperature specific-heat studies on palladium-rich Pd-Sb alloys were carried out in collaboration with Paul Tsang.* The measurements were made on four alloys that contained 3, 6, 9, and 12 at.% antimony, respectively, in palladium. Approximately 40 low-temperature specific-heat determinations were made for each alloy between 1.4 and 4.2°K. The heat capacities of the alloys were fitted to the equation

$$C_v/T = \gamma + \beta T^2 .$$

The experimental C_v/T versus T^2 curves were extrapolated to absolute zero to obtain the electronic specific-heat coefficient γ; the Debye temperatures were calculated from the slopes of the curves.

The electronic specific heats of Pd-Ag alloys have frequently been interpreted in terms of a rigid-band model, in which the *d* band of palladium is progressively filled without a change in shape. The present results for Pd-Sb were plotted together with the γ values for the Pd-Ag system;[248] the 5*s* and 5*p* electrons of antimony were assumed to contribute 5 electrons to the *d* band of palladium. The specific-heat curve for the Pd-Sb alloys did not superimpose on the Pd-Ag curve (the γ values for the antimony alloys are slightly higher than the corresponding silver alloys); the γ values for the Pd-Sb alloys decreased as the antimony content increased and leveled off at a limiting composition of approximately 16 at.% antimony, the approximate solid solubility limit of antimony in palladium. If the rigid-band model is assumed to be valid for the Pd-Ag and Pd-Sb systems, the effective number of electrons outside the filled *d* shell of antimony that participate in filling the *d* band of palladium may be obtained by superimposing the experimental γ values for the Pd-Sb system on the γ versus *e/a* curve for the Pd-Ag alloys. The effective number of electrons, obtained from the abscissa of the plot, varies between 3.0 and 4.0 as the concentration of antimony increases.

Recent theoretical calculations[249] show that hybridization and spin-orbit splitting may broaden the combined energy bands in alloys and the perturbations may well be expected in the Pd-Sb alloys. Other arguments[242] could be presented to rationalize the present results in terms of shifts in the energy bands of the alloys with electron concentration. The rigid-band model is not, therefore, a unique explanation for the specific heat or Mössbauer results obtained for the Pd-Sb or, for that matter, many other palladium-base alloys.[238]

Preliminary results were obtained for the heats of formation of the complete series of solid solutions that exist at elevated temperatures in the Pd-Pt and Pt-Ni systems. The heat-of-formation values at 298°K are negative (exothermic reaction) for both systems with a maximum negative value at the equiatomic composition of -2250 and -900 cal/g-atom for the Pt-Ni and Pt-Pd systems, respectively. A significant difference is observed in the composition dependence of the heats of formation between the Pt-Ni and Pd-Ni systems. The heat-of-formation values

[247] K. M. Myles and J. B. Darby, Jr., Annual Progress Report for 1966, Metallurgy Division, ANL-7299, pp. 259-262.

*Michigan State University, East Lansing, Michigan.

[248] F. E. Hoare and B. Yates, Proc. Roy. Soc. *A240*, 42 (1957).

[249] L. Hodges, E. Ehrenreich, and N. D. Lang, Phys. Rev. *152*, 505 (1966).

of the Pt-Ni system are negative, and show a symmetrical composition dependence about the equiatomic composition. Heats of formation for the Pd-Ni system are negative for the palladium-rich alloys, but become positive when the nickel content exceeds 70 at.%. An independent investigation[250] confirms our results. A recent investigation[251] of the thermodynamic properties of the Pd-Co system found the heats of formation to have a similar composition dependence, i.e., negative values for the palladium-rich alloys and positive values for the cobalt-rich alloys.

The elements with aligned magnetic moments appear to have an interaction in alloys with low-to-moderate concentrations of palladium, but in the equivalent platinum alloys the interaction is absent. An investigation of palladium or platinum binary systems with elements that have aligned magnetic moments, such as chromium, iron, or cobalt, will be carried out to determine whether magnetic or chemical interactions are responsible for the positive contributions to the heats of formation.

THERMODYNAMIC PROPERTIES OF Pd-Rh ALLOYS

(K. M. Myles)

The thermodynamic properties of the complete series of solid solutions in the Pd-Rh system were investigated. The alloys, prepared from 99.99% pure elements, were homogenized above 1500°K. The lattice parameters were determined from x-ray powder patterns, which indicated that the alloys were homogeneous. The thermodynamic properties were calculated from measurements of the vapor pressure of palladium over the alloys. The vapor pressures were measured by means of the torsion-effusion apparatus described previously.[252,253]

The activities of palladium were computed from the vapor pressure data at temperatures of 1525, 1575, and 1625°K. The activities of rhodium were determined by means of the Gibbs-Duhem relation, and the pure solid metals were defined as having unit activity. The activities of palladium and rhodium at 1575°K exhibit large positive deviations from Raoult's law, and become almost independent of composition near the equiatomic composition. The positive deviations are consistent with the miscibility gap that occurs in the Pd-Rh system below 1118°K, and the near constancy of the activities suggests that the tendencies toward clustering are still extremely strong at 1575°K. The partial and integral free energies, enthalpies, and entropies of formation at 1575°K were computed from the activities; the results are assembled in Figure 54. By analogy with other palladium-base systems,[254,255] the major factors that influence the enthalpies are assumed to be electronic, vibrational, and configurational in origin. The electronic contribution which arises from alternations in the electronic structure of the pure elements upon formation of an alloy, was evaluated for the Pd-Rh system by the method described by Pratt,[254]

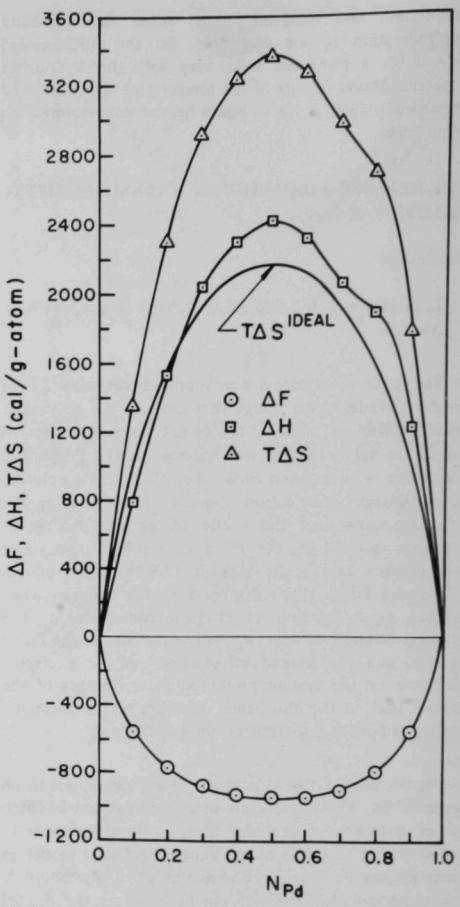

Fig. 54. The Integral Free Energies (○), Enthalpies (□), and Entropies (△), of Formation of Pd-Rh Alloys at 1575°K.

250 L. R. Bidwell and R. Speiser, Acta Met. 13, 61 (1965).

251 L. R. Bidwell, private communication, 1967.

252 K. M. Myles, USAEC Report ANL-6657, Argonne National Laboratory, 1963.

253 A. T. Aldred and K. M. Myles, Trans. Met. Soc. AIME *230*, 736 (1964).

254 J. N. Pratt, Trans. Faraday Soc. *56*, 975 (1960).

255 J. B. Darby, Jr., Acta Met. *14*, 265 (1966).

and was exothermic with a maximum value of approximately 1000 cal/g atom. The vibrational contribution at room temperature estimated from the low-temperature electronic heat coefficients[256] and the Debye theory of lattice heat capacity, was endothermic and less than 100 cal/g atom. Since the experimentally determined enthalpies are endothermic with a maximum value of about 2400 cal/g atom, the dominating contribution must be configurational in origin. Palladium and rhodium have equal valences, nearly equal atomic sizes, and, therefore, provide only minor contributions to the configurational enthalpy.

The entropy values for the Pd-Rh system primarily reflect the configurational and vibrational contributions. The configurational contribution, although perhaps substantial, cannot be the dominant contribution since the experimental entropies are larger than the ideal entropy of mixing. The Pd-Rh alloy system is highly clustered at 1575°K, and, therefore, the strength of the bonds between the atoms of unlike kind is reduced and manifested by an overall increase in the thermal excitation of the lattice. The heat capacities of the Pd-Rh alloys at 298°K exhibit positive deviations from Neumann-Kopp behavior and yield a vibrational entropy that is more than one-half of the total entropy found in the present work.

In summary, the activities and the free energies at 1575°K for the Pd-Rh system reflect the clustering associated with the miscibility gap at lower temperatures. While the dominant contribution to the entropy is related to the thermal energy of the system and is vibrational in origin, the nonrandomness of the alloys also makes a substantial contribution.

THE STRUCTURE AND OCCURRENCE OF INTERMEDIATE PHASES *(A. E. Dwight)*

Publications

A. E. Dwight, *Intermetallic Compounds*, J. H. Westbrook, ed. (John Wiley and Sons, New York, 1967).

A. E. Dwight, Abst. Bull. IMD-AIME *2*(1), 42 (1967).

A. E. Dwight, Proc. 6th Rare Earth Research Conf., Gatlinburg, Tennessee, May 3-5, 1967. Oak Ridge National Laboratory, Oak Ridge, Tennessee, 1967, pp. 156-165.

A. E. Dwight, J. W. Downey, and R. A. Conner, Jr., Acta Cryst. *22*, 745 (1967).

A. E. Dwight, J. W. Downey, and R. A. Conner, Jr., Acta Cryst. *23*, 860 (1967).

An investigation of the Fe_2P-type compounds[257] has been completed. A total of 63 examples of such compounds are known to exist, including the eight compounds discovered in 1967 (Table 19). The Fe_2P-type compounds comprise one of the larger families of intermediate phases. The elements that can occupy the two phosphorus sites in the prototype compound Fe_2P are: iron, ruthenium, cobalt, rhodium, iridium, nickel, palladium, platinum, or copper. One of the iron sites 3(*f*) is preferentially occupied by aluminum, gallium, or indium, while the other site 3(*g*) may be occupied by zirconium, hafnium, thorium, or uranium. Not all possible combinations of the elements listed will yield the Fe_2P-type structure, since other combinations in the same ratio are known to stabilize competing structure types, e.g., $MgCu_2$, $MgZn_2$, Ni_2In, $CeCu_2$, and perhaps others. At least three factors appear to control the stability of the ternary Fe_2P-type compounds; the relative atomic size, the nonequivalence of 3(*f*) and 3(*g*) sites, and the electron concentration. The size factor requires the presence of three species: one with a large, one with a medium, and one with a small atomic size. The nonequivalence of the 3(*f*) and 3(*g*) sites is evident since the large atom occupies the 3(*f*) site and the medium-size atom occupies the 3(*g*) site. The electron-concentration factor is indicated by the selective grouping of the three component elements of a compound in the periodic table. The position of the participating elements in the periodic table indicates that plutonium may replace uranium and thallium may replace gallium, although the proposed substitutions have not been verified.

TABLE 19. Representative Fe_2P- and $MoSi_2$-Type Compounds

Compound	Unit-Cell Constants, Å			Structure Type	V/M[a] Å^3
	a	*c*	*c/a*		
ThPdAl	7.265	4.181	0.57	Fe_2P	63.60
ThNiIn	7.367	4.117	0.56	Fe_2P	64.50
ThPdIn	7.541	4.190	0.56	Fe_2P	68.79
ThPtIn	7.535	4.166	0.55	Fe_2P	68.28
UPdIn	7.415	4.096	0.55	Fe_2P	65.01
UPtIn	7.413	4.058	0.55	Fe_2P	64.38
URuAl	6.895	4.029	0.58	Fe_2P	55.29
URuGa	7.076	3.818	0.54	Fe_2P	55.17
TiNiCu	3.122	7.965	2.55	$MoSi_2$	38.81
TiPdCu	3.24	8.21	2.54	$MoSi_2$	43.0

[a]Volume per formula weight.

[256]D. W. Budworth, F. E. Hoare, and J. Preston, Proc. Roy. Soc. *A257*, 250 (1960).

[257]A. E. Dwight, Annual Progress Report for 1966, Metallurgy Division, ANL-7299, pp. 254-257.

The compounds TiNiCu and TiPdCu (Table 19) are the first ternary examples of the $MoSi_2$-type structure to be discovered. The $MoSi_2$ family of compounds includes 48 known binary examples and is the seventh most frequent structure type. In the prototype compound $MoSi_2$ (D_{4h}^{17}, I4/mmm), molybdenum atoms occupy the 2(*a*) sites, and silicon atoms occupy the 4(*e*) sites. In TiNiCu, the nickel and copper atoms may be either randomly distributed, or may be ordered on 4(*e*) sites. If an ordered structure is present, a lower symmetry and a different space group would be necessary. X-ray diffraction patterns for TiNiCu do not show any lines indicative of an ordered structure, but the observation is inconclusive because of the small difference in atomic scattering factor between nickel and copper. Neutron diffraction studies are under way and preliminary results indicate that an ordered structure is probable.

Alkali and Noble Metal Alloys

PREASYMPTOTIC FORM OF IMPURITY SCREENING IN A METAL *(L.C.R. Alfred and D. O. Van Ostenburg)*

Publication

L.C.R. Alfred and D. O. Van Ostenburg, Phys. Letters *26A*, 27-28 (1967).

The expression usually adopted for the long-range electron density change around an impurity atom in a free electron metal is that of Blandin and Friedel,[258] *viz*,

$$\delta n(R) = A \cos(2k_F R + \phi)/R^3, \qquad (1)$$

where

$$A \cos\phi = -\sum_{\ell=0}^{\infty} (2\ell + 1)(-1)^{\ell} \sin(2\eta_{\ell}^{k_F})/4\pi^2,$$

$$A \sin\phi = -\sum_{\ell=0}^{\infty} (2\ell + 1)(-1)^{\ell} \sin^2(\eta_{\ell}^{k_F})/2\pi^2,$$

and $\eta_{\ell}^{k_F}$ is the ℓth order phase shift at the Fermi level $k_F^2/2$.* Since the expression of Blandin and Friedel is derived from an asymptotic form that is characteristic (to four decimal places) of the scattered wave at $k_F R > 100$, i.e., well beyond the 50th nearest neighbor in the common metals, the expression could be seriously in error at the first few atomic shells where the interaction with the matrix is strong.

An estimate of the error is made by deriving $\delta n(R)$ from the preasymptotic form of the outgoing wave, i.e.,[259]

$$\Psi = \sum_{\ell=0}^{\infty} (2\ell + 1) i^{\ell} e^{i\eta_{\ell}^{k}} [\cos\eta_{\ell}^{k} j_{\ell}(kR) - \sin\eta_{\ell}^{k} n_{\ell}(kR)] P_{\ell}[\cos(k, R)], \qquad (2)$$

where k is the wave number, j_{ℓ} and n_{ℓ} are the spherical Bessel and Neumann functions, respectively, and P_{ℓ} is a Legendre polynomial. Utilization of the free electron result:

$$\delta n(R) = \frac{1}{4\pi^3} \int^{k_F} dk\, (\Psi\Psi - 1), \qquad (3)$$

and following Blandin and Friedel,[258] and others,[260] then

$$\delta n(R) = A \cos(2k_F R + \phi)/R^3 + B \cos(2k_F R + \xi)/R^4, \qquad (4)$$

where A and ϕ are defined in Equation (1),

$$B \cos\xi = \sum_{\ell=0}^{\infty} (2\ell + 1)(-1)^{\ell} \left[\frac{2\ell(\ell + 1)}{k_F} \sin^2\left(\eta_{\ell}^{k_F}\right) + \left(\frac{\partial\eta_{\ell}}{\partial k}^{k}\right)_{k_F} \sin\left(2\eta_{\ell}^{k_F}\right)\right] \Big/ 4\pi^2,$$

and

$$B \sin\xi = -\sum_{\ell=0}^{\infty} (2\ell + 1)(-1)^{\ell} \left[\frac{\ell(\ell + 1)}{k_F} \sin\left(2\eta_{\ell}^{k_F}\right) + \left(\frac{\partial\eta_{\ell}}{\partial k}^{k}\right)_{k_F} \cos\left(2\eta_{\ell}^{k_F}\right)\right] \Big/ 4\pi^2.$$

The corresponding self-consistent screening potential to order R^{-4} is

$$V(R) = \frac{\pi}{k_F^2} [\delta n(R) + 2A \sin(2k_F R + \phi)/k_F R^4]. \qquad (5)$$

We have evaluated A, B, ϕ, and ξ by utilization of the semiempirical phase shifts of Kohn and Vosko[260] for copper-base alloys, and by rough estimates of $\partial\eta_{\ell}^{k}/\partial k$ derived from the approximation[261] $\eta_{\ell}^{k} \sim a_{\ell} k^{2\ell+1}$. In all cases considered, B was much larger than A, an indication

258 A. Blandin and J. Friedel, J. Phys. Radium *21*, 689 (1960).

*Atomic units are used throughout.

259 N. F. Mott and H.S.W. Massey, *The Theory of Atomic Collisions* (Clarendon Press, 1965), 3rd ed., p. 35.

260 W. Kohn and S. H. Vosko, Phys. Rev. *119*, 912 (1960).

261 P. M. Morse and H. Feshbach, *Methods of Theoretical Physics* (McGraw-Hill Book Co., New York, 1953), p. 1694.

that (within the error limits of our estimates of $\partial n_0^k/\partial k$) the correction terms can very significantly change the field at the first few neighboring shells. The corresponding wipe-out numbers also change. The work will continue with the use of the more realistic phase shifts derived recently by the authors.

A NEW SCHEME FOR THE CONSTRUCTION OF PHASE SHIFTS WITH APPLICATION TO NMR *(L.C.R. Alfred and D. O. Van Ostenburg)*

Publications

D. O. Van Ostenburg and L.C.R. Alfred, Bull Am. Phys. Soc. *12*, 59 (1967). Abstract

D. O. Van Ostenburg and L.C.R. Alfred, Bull. Am. Phys. Soc. *12*, 349 (1967). Abstract

L.C.R. Alfred and D. O. Van Ostenburg, Phys. Rev. *161*, 569-570 (1967).

D. O. Van Ostenburg and L.C.R. Alfred, Indian J. Pure Appl. Phys. *5*, 556 (1967).

A semiempirical scheme was developed for the construction of phase shifts of unlimited order to investigate properties that depend on electron redistribution in alloys. The method utilizes a generalized free-electron potential around the solute atom, residual-resistivity data, and the Friedel sum rule. Application to the Knight shifts, in a series of dilute alloys with liquid copper and solid silver as hosts, leads to much better agreement with experiment than obtained previously. Further details are found in the publications cited.

SCREENING OF IMPURITIES IN METALS AND SEMICONDUCTORS *(L.C.R. Alfred)*

Approximate analytical solutions have been derived for the self-consistent field around an impurity atom in a free electron metal and semiconductor. For metals, the screening potential for an impurity atom with residual nuclear charge Z is given by the expression

$$V(r) = -\frac{Z}{2r}\left\{e^{-qr}\left[1 + \frac{1+q^2/4k^2}{q/2k}\tan^{-1}\frac{q}{2k}\right] + \cos(2kr) + 2kr\,si(2kr) + \frac{1+q^2/4k^2}{q/k}\left[e^{-qr}\,ImE_1(-qr+i2kr) - e^{qr}\,ImE_1(qr+i2kr)\right]\right\}, \quad (1)$$

where k is the Fermi wave number of the metal, $q^2 = 4k/\pi$, si denotes a sine integral,[262] and E_1 an exponential integral.[262] This potential agrees closely with that of Mott ($Z\exp(-qr)/r$) for small values of r, and assumes the oscillating form of Friedel ($\sim\cos(2kr)/r^3$) asymptotically. Our analytical expression for V is also in good agreement with the numerical solutions of March and Murray[263] and Langer and Vosko,[264] which were obtained by tedious computations.

For semiconductors, the long-range oscillations are absent, and the Yukawa form is a good approximation for the screening potential over all space. Again good agreement is evident with the available numerical solutions.[265]

The utilization of our analytical forms for the impurity screening field (instead of the available numerical tables) should facilitate considerably the investigation of defect problems. This method is particularly applicable when an order of accuracy greater than three decimal places is required, or when an explicit functional dependence of the field on the Fermi energy is required.

MAGNETIC RESONANCE AND POSITRON ANNIHILATION RESEARCH IN DILUTE ALLOYS *(D. O. Van Ostenburg, G. A. Matzkanin, J. J. Spokas,* C. H. Sowers, and H. G. Hoeve**)*

Publication

G. A. Matzkanin, D. O. Van Ostenburg, J. J. Spokas,* and C. H. Sowers, Bull. Am. Phys. Soc. *12*, 911 (1967). Abstract

Measurements in dilute gold and silver alloys represent the beginning of a broad study of the interactions between solute and solvent atoms in dilute alloys using wide-line and pulsed nuclear-magnetic-resonance techniques.

In a series of gold-base alloys, the concentration dependence of the solute Knight shift K has been determined for the solutes copper, indium, and gallium in the concentration range from 1 to 5 at.%. For indium and gallium, a slight concentration dependence is observed; for copper, the shift is independent of concentration within experimental error.

In silver alloys, the solute Knight shift has been measured for the solutes copper, indium, and aluminum.

---

[262] *Handbook of Mathematical Functions*, U. S. Department of Commerce, National Bureau of Standards, Applied Mathematics Series, 55 (1965).

[263] N. H. March and A. M. Murray, Proc. Roy. Soc. *A261*, 119 (1961).

[264] J. S. Langer and S. H. Vosko, J. Phys. Chem. Solids *12*, 196 (1960).

[265] N. H. March and A. M. Murray, Proc. Phys. Soc. *79*, 1001 (1962).

*Present address: St. Procopius College, Lisle, Illinois.

**Present address: Northern Illinois University, DeKalb, Illinois.

The concentration dependence has been determined only for the copper solute where, as in the case of *Au*Cu, K is independent of concentration. The indium Knight shift has approximately the same value in both the silver and gold alloys; whereas, the copper Knight shift differs by about 25% between the two alloy systems.

The concentration dependences of the solute Knight shifts in the gold alloys correspond roughly to those observed by Rowland[266] for the silver host resonance in dilute *Ag*Ga, *Ag*In, and *Ag*Cu alloys. Silver, which has a spin of one-half, is not affected by quadrupole interactions. This leads to the conclusion that in these dilute alloys the changes with concentration expected for the solute resonance, on the basis of the Daniel theory,[267] are not completely masked by quadrupole effects. The solute linewidths decrease with decreasing field, an indication that quadrupole effects are not the dominant contribution to the linewidth.

The solute spin-lattice relaxation time T_1 has been measured in the gold and silver alloys. For all solutes studied, T_1 is longer than that for the corresponding pure metal. In alloys that contain gallium and indium as solutes, the relaxation rate is an order of magnitude larger than for alloys that contain copper. The increase in the relaxation rate is attributed to the charge buildup around the impurity atoms in the host. In all cases, the experimental Korringa constant (K^2T_1T) is larger than that calculated for free electrons. The discrepancy, however, is less for the non-noble metal solutes (indium, gallium, and aluminum) than for the noble metal solutes, and the discrepancy is generally greater by about a factor of two for the silver-base alloys as compared with the gold-base alloys. Work will continue on other transition and nontransition metal impurities in platinum, palladium, iridium, and rhodium as hosts.

ELECTRON-SPIN RESONANCE IN $CdCl_2$ *(H. G. Hoeve* and D. O. Van Ostenburg)*

The crystal structure of $CdCl_2$ is a layer structure of the type $|Cl^-Cd^{2+}Cl^-|Cl^-Cd^{2+}Cl^-|$ with rhombohedral symmetry and belongs to the space group D_{3d}^5. The Cl^- ions are cubic close packed if the c/a ratio is $\sqrt{6/3}$. The Cd^{2+} ions are located in the octahedral holes between the neighboring Cl^- layers. The c/a ratio is temperature dependent and differs in general from the value of $\sqrt{6/3}$, which produces a slight trigonal distortion of the positions of the octahedral interstices in the Cl^- lattice.

The electron-spin resonance measurements were made in the temperature range from 96 to 710°K. The spin Hamiltonian parameter D varied appreciably in this temperature range. The variance of D can be explained by considering the influence of the temperature on the magnitude of the trigonal lattice distortion of the octahedral Mn^{2+} sites in the Cl^- lattice of $MnCl_2$. At room temperature, the c/a ratio is 0.755 for $CdCl_2$ and 0.790 for $MnCl_2$. In order for the cation sites to be octahedrally surrounded by nearest neighbors, a c/a ratio of $\sqrt{6/3}$ is required. The Cl^- octahedra are slightly compressed along the c direction at room temperature and below. The Mn^{2+} site has a cubic arrangement for nearest neighbors only at a temperature slightly above room temperature. The increase in the c/a ratio with increasing temperature is to be expected for a lattice, where the "sandwiches" $Cl^-Mn^{2+}Cl^-$ are held together by van der Walls' forces. The anisotropic lattice expansion is confirmed by an x-ray analysis of $CdCl_2$, where the lattice expansion with increasing temperatures was predominantly along the c direction. Thus, the temperature variation of D is related to an anisotropic expansion of the host lattice.

No satisfactory theory exists that predicts the temperature dependence nor the variation of D with atomic bond length. The measurements will continue on similar crystals so that a systematic set of experimental data will be available to test various theoretical ideas.

---

[266] T. J. Rowland, Phys. Rev. *125*, 459 (1962).

[267] E. Daniel, Phys. Chem. Solids *10*, 174 (1959).

*Present address: Northern Illinois University, DeKalb, Illinois.

STRUCTURES OF LIQUID AND SOLID METALS

A Diffraction Study of HoNiAl and CeNiAl *(H. W. Knott and M. H. Mueller)*

A number of intermetallic compounds have been reported to have the Fe_2P-type structure.[268] Two of these compounds (HoNiAl and CeNiAl) were chosen for x-ray and neutron diffraction studies to refine the position parameters and to identify the types of atoms in various sites.

In Fe_2P, nine atoms are in the unit cell of the space group $P\bar{6}2m$; three iron in (*g*) sites, three iron in (*f*) sites, two phosphorus in (*c*) sites, and one phosphorus in the (*b*) site. The integrated intensity results of each of the samples, HoNiAl and CeNiAl, were refined by a least-squares program adapted to handle overlapped data of powder samples. Each of the four diffractometer patterns was treated in space group $P\bar{6}2m$ with each kind of atom in each site, or six permutations for each pattern. The best result for each of the four patterns is the permutation shown in Table 20. Since the *R* value in each case is a fairly large number, and would be even larger if the data could be treated in a completely resolved manner, it is evident that a lack of agreement exists between the calculated and observed intensities. This suggests that the structure of these compounds is not exactly correct. A further x-ray investigation and an investigation of possible magnetic properties will be made with a single crystal.

TABLE 20. Summary of Neutron and X-ray Diffraction Results on HoNiAl and CeNiAl

	HoNiAl		CeNiAl	
Sites	Neutron	X-ray	Neutron	X-ray
3(*g*)				
$x, 0, \frac{1}{2}$	Ho (x = 0.597)	Ho (x = 0.584)	Ce (x = 0.580)	Ce (x = 0.578)
3(*f*)				
$x, 0, 0$	Al (x = 0.201)	Al (x = 0.236)	Al (x = 0.219)	Al (x = 0.280)
2(*c*)				
$\frac{1}{3}, \frac{2}{3}, 0$	Ni	Ni	Ni	Ni
1(*b*)				
$0, 0, \frac{1}{2}$	Ni	Ni	Ni	Ni
R value	0.077	0.169	0.043	0.136

Structure Determination of Manganese Silicide *(H. W. Knott, M. H. Mueller, and L. Heaton)*

Publication

H. W. Knott, M. H. Mueller, and L. Heaton, Acta Cryst. *23*, 549-555 (1967).

The crystal structure of manganese silicide was discussed in the cited publication. Results of an examination of over 2000 reflections from a single crystal of $MnSi_{1.75}$ composition were used in Patterson, Fourier, and least-squares techniques to establish the structure. The $Mn_{15}Si_{26}$ compound is tetragonal a = 5.531, c = 65.11Å; space group $I\bar{4}2d$, with Z = 4, and 8 manganese and 7 silicon atoms in the unit cell. The unit cell consists of 15 stacked, small manganese subcells with 52 silicon atom pairs oriented alternately in opposite quadrants about the central axis in the *c* direction. The structure may also be described as pseudohexagonal sheets along and parallel to {110}.

Neutron Diffraction Study of Potassium Ferrocyanide Trideuterate *(M. H. Mueller, J. C. Taylor,* and R. L. Hitterman)*

Publication

J. C. Taylor, M. H. Mueller, and R. L. Hitterman, Amer. Cryst. Assoc. Symp. on Thermal Neutron Scattering Applied to Chemical and Solid State Physics, Atlanta, Georgia, January 25-28, 1967, Paper J6, p. 70.

As reported in the 1966 Annual,[269] potassium ferrocyanide trideuterate has two types of disordered water molecules at room temperature. The least-squares method could not be used to refine the disordered water molecules in the general position; however, Fourier techniques have now given very reasonable oxygen-to-deuterium distances

[268] A. E. Dwight, M. H. Mueller, R. A. Conner, J. W. Downey, and H. Knott, Trans. Met. Soc. AIME (to be published).

*Present address: Australian AERE, Sutherland, N.S.W., Australia.

[269] M. H. Mueller, J. C. Taylor, and R. L. Hitterman, Annual Progress Report for 1966, Metallurgy Division, ANL-7299, pp. 288-289.

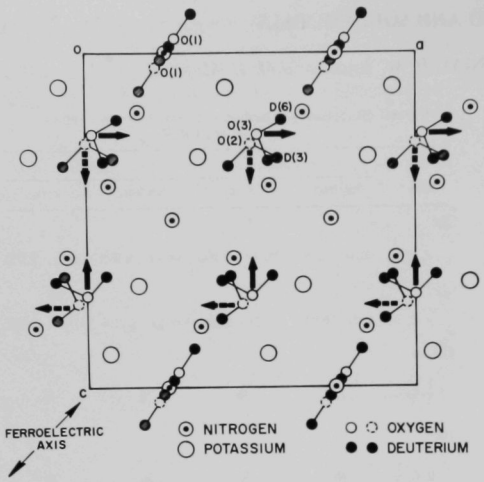

48106

Fig. 55. Potassium Ferrocyanide Trideuterate Water Molecule Layer at $y = 1/2$ Showing the Electrical Dipole Moments Determined by Neutron Diffraction.

and angles for the water molecules. Based on nuclear magnetic resonance data, investigators have agreed that the ferroelectric behavior is connected with an ordering of the hydrogen-bonded water molecules (or deuterium, in the present crystal); however, the exact atomic structures that have been proposed are all different.

If the neutron diffraction results in the paraelectric disordered phase are combined with the nuclear magnetic resonance study by Kiriyama et al.[270] (carried out at -170°C where the water molecules are rigid), the role of the water molecules becomes evident. Water disordering apparently occurs at the ferroelectric transition, and, at room temperature, one of the water molecules (near the center of Figure 55) splits into two nonequivalent molecules associated with O(2) and O(3). The O(1) water molecule (shown near the top and bottom of Figure 55), which is disordered about the two-fold axis at room temperature, loses this symmetry in the ferroelectric state. Although the water disordering goes through a sudden increase in reorientation frequency near the Curie point, no large shifts of the heavier atoms are apparent. These diffraction results are in agreement with previous proposals of structural changes and with the present interpretation of the nuclear magnetic resonance data by O'Reilly and Tsang.[271]

In the ferroelectric state, the crystal possesses a permanent electrical dipole moment along the $[\bar{1}01]$ direction, as shown in Figure 55, which can be accounted for by the dipole moment of the water molecules. The dipole moment of the water molecule bisects the *D-O-D* angle in the plane of the molecule. Moments associated with the O(2) and O(3) water molecules are directed parallel and antiparallel to the *a* and *c* axes. The resultant moment is along the $[\bar{1}01]$, which is the ferroelectric axis of the crystal.

The Neutron Diffraction Study of $[UO_2(H_2O)\{CO(NH_2)_2\}_4](NO_3)_2$

(N. K. Dalley, M. H. Mueller, and S. H. Simonsen**)*

Publications

N. Kent Dalley and M. H. Mueller, Amer. Cryst. Symp. on Crystal Growth, Minneapolis, Minnesota, August 20-25, 1967, Paper T6, p. 97.

M. H. Mueller and N. Kent Dalley, 2nd Materials Research Symp. on Molecular Dynamics and Structure of Solids, Gaithersburg, Maryland, October 16-19, 1967, NBS, Paper C4, p. 2.

A neutron diffraction study of $[UO_2(H_2O)\{CO(NH_2)_2\}_4](NO_3)_2$ was of interest because one could study (1) the coordination of the uranyl ion, and (2) the hydrogen bonding scheme of a material in which approximately 40% of the atoms are hydrogen and most of the hydrogen bonds would involve N-H ... O linkage. This material is monoclinic, with $a = 0.99$Å, $c = 13.18$Å, and $\beta = 100.18°$; space group $P2_1/c$, with four formula weights per unit cell. An x-ray investigation of this crystal structure would be of limited value since the scattering power of a hydrogen atom is only 0.01% of that of a uranium atom and, therefore, could not be detected.

Interpretations of infrared studies[272] suggested a six-fold coordination about the uranium with four carbonyl oxygen atoms of urea ligands, one water oxygen atom, and one oxygen atom of a monodentate nitrato ligand; another

---

[270] R. Kiriyama, H. Kiriyama, T. Wada, N. Niisiki, and H. Hirabayashi, J. Phys. Soc. Japan *19*, 540 (1964).

[271] D. E. O'Reilly and Tung Tsang, J. Chem. Phys. *47*, 4072 (1967).

*Resident Student Associate, The University of Texas at Austin.

**Faculty Associate, The University of Texas at Austin.

[272] L. S. Campisi, Ph.D. Thesis, Fordham University, New York, 1965.

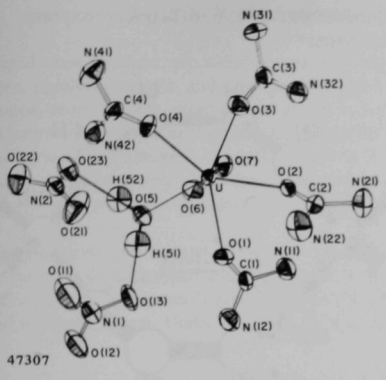

Fig. 56. Arrangement of Atoms about the Uranyl Ion in $[UO_2(H_2O)\{CO(NH_2)_2\}_4](NO_3)_2$.

investigator[273] suggested that instead of the nitrato oxygen atom, a uranyl oxygen atom of another molecule occupied the sixth position. Another possibility is a five-fold coordination about the uranium.

About 3800 reflections were measured at the CP-5 reactor using the ARCADE computer-controlled diffractometer. The results established that the linear uranyl ion had a coordination of five oxygen atoms from the four ligands, and one oxygen atom from the water ligand, as shown in Figure 56. The five oxygen atoms form a planar pentagon, which is nearly regular and perpendicular to the *O-U-O* group. The nitrate ions do not participate in the primary coordination sphere of the uranium and are tied into the complex ion by hydrogen bonds from the water ligand. All of the nitrate oxygen atoms are involved in N-H . . . O hydrogen bonds, which form a network by joining the independent ions.

The Diaquohydrogen Ion $(H_5O_2)^+$ *(J. M. Williams)*

Publications

J. M. Williams, Inorg. Nucl. Chem. Letters *3*, 297-302 (1967).

J. M. Williams, Amer. Cryst. Symp. on Crystal Growth, Minneapolis, Minnesota, August 20-25, 1967, Paper K2, p. 51.

J. M. Williams, 2nd Materials Research Symp. on Molecular Dynamics and Structure of Solids, Gaithersburg, Maryland, October 16-19, 1967, NBS, Paper C2, p. 1.

While hydrates of the type $H^+(H_2O)_n$, with n = 1-8, have been observed in the gas phase, only compounds that contain the oxonium ion $(H_3O)^+$ have been extensively studied in the crystalline state. The diaquohydrogen ion $(H_2O{\cdot}H{\cdot}OH_2)^+$, first postulated by Huggins as a component of acid solutions, has been positively identified in a current three-dimensional neutron diffraction study of *trans* $[Co(H_2NCH_2CH_2NH_2)_2Cl_2]^+Cl^-(H_5O_2)^+Cl^-$.

The compound is monoclinic, space group $P2_1/c$, with a = 10.686 ±0.010Å, b = 7.886 ±0.007Å, c = 9.084 ±0.009Å, and β = 110.76 ±0.03°, and the unit cell contains two molecules.

The most interesting feature of the structure is the *trans*-diaquohydrogen ion $(H_2O{\cdot}H{\cdot}OH_2)^+$, which lies outside the primary coordination sphere of the cobalt atom. The details of the angles, distances, and orientation of the $(H_5O_2)^+$ ion have been discussed.[274] The water-molecule configurations are *trans* with respect to the central hydrogen atom H(3) of $(H_5O_2)^+$, having *apparent* site symmetry $\bar{1}$ and involving a short hydrogen bond (O-O), which is equal to 2.50 ±0.03Å. All water molecules are bonded through O-H . . . Cl hydrogen bonds. For the *diaquo*-species this *trans* form of $(H_2O{\cdot}H{\cdot}OH_2)^+$ minimizes both H-H repulsion and lone-pair electron repulsion by the oxygen atoms.

[273] P. S. Gentile, private communication, 1967.

[274] J. M. Williams, Inorg. Nucl. Chem. Letters *3*, 297 (1967).

The Crystal Structure of Tetramethyl-*cis*, *Cis*-3, 8-Cyclodecadiene-1, 1, 6, 6-Tetracarboxylate

(N. K. Dalley and S. H. Simonsen**)*

The crystal structure investigation of tetraethyl *cis*, *cis*-3, 8-cyclodecadiene-1, 1, 6, 6-tetracarboxylate by x-ray diffraction was initiated to determine the reason for the unreactive nature of the double bonds of the decadiene ring toward hydrogenation. As proposed,[275] this could be caused by orbital interactions that required the ring configuration indicated by the dotted-line locations for *C*(8) and *C*(9) in Figure 57.

The material is monoclinic, space group $P2_1$, with a = 8.556Å, b = 10.858Å, c = 12.723Å, β = 90.68°, and two formula weights per unit cell. The systematic extinctions OkO, $k = 2n + 1$, do not uniquely determine the space group. The intensity data were treated by graphical and statistical techniques to distinguish the noncentrosymmetric space group $P2_1$ from the centrosymmetric space group $P2_1/m$.

The structure was partially determined by symbolic addition methods for the noncentrosymmetric space groups developed by Karle and Karle.[276] Fourier methods were used to complete the structure, and the results were confirmed by the partial structure method of Karle.[277] Apparently this method has definite advantages over the conventional Fourier methods, and may have considerable value in solving structures of intermetallic compounds using either x-ray or neutron diffraction data.

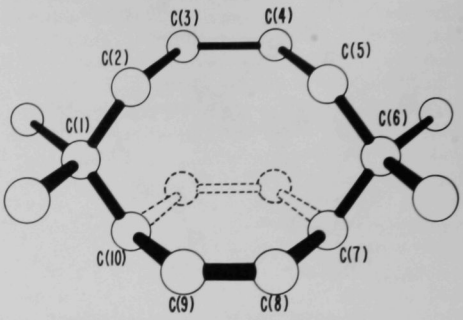

48164

Fig. 57. The Structure of the Decadiene Ring Determined in This Study Is Indicated by the Solid Lines. The previously proposed structure, in which atoms *C*(8) and *C*(9) are replaced by the atoms shown by dotted lines, would have allowed overlap of *pi* orbitals of *C*(3) with *C*(9), and *C*(4) with *C*(8).

The ring structure shown in Figure 57 differs considerably from the previously proposed dotted location of *C*(8) and *C*(9). This presently determined atomic arrangement does not allow any orbital interactions; therefore, other effects, such as steric hinderance of hydrogen atoms, must cause the added stability of the double bonds.

Scattering of Neutrons by Liquids *(L. Heaton)*

Publications

E. H. Henninger,† R. C. Buschert,† and Leroy Heaton, J. Chem. Phys. *46*, 586-591 (1967).

E. H. Henninger,† R. C. Buschert,† and Leroy Heaton, J. Phys. Chem. Solids *28*, 423-432 (1967).

A method was proposed for the direct determination of the complete structure of a binary liquid by neutron diffraction techniques. Three distribution functions are necessary to fully characterize the structure of a binary liquid–two distributions of like atoms (*A-A*, *B-B*) and one distribution of unlike atoms (*A-B*). In principle, the distributions can be derived from three independent scattering curves. Since the neutron scattering amplitude is a nuclear property, chemically identical samples of different isotopic compositions may be used to produce three different and independent neutron scattering curves.

The fused salt Cu_2Cl_2 was chosen initially to demonstrate this method because isotopes ^{63}Cu and ^{65}Cu were available in sufficient quantities for neutron diffraction samples, and because the values of the scattering amplitude of these isotopes differ considerably. Samples of $^{63}Cu_2Cl_2$, $^{65}Cu_2Cl_2$, and a normal isotopic mixture have been prepared for the determination of the three independent scattering curves. Neutron diffraction patterns of the fused salt will be obtained at temperatures above 430°C, and attempts will be made to make other isotopic samples as required.

*Resident Student Associate, The University of Texas at Austin.

**Faculty Associate, The University of Texas at Austin.

275R. M. Gipson, H. W. Guin, S. H. Simonsen, C. G. Skinner, and W. Shive, J. Am. Chem. Soc. *88*, 5366 (1966).

276J. Karle and I. L. Karle, Acta Cryst. *21*, 849 (1966).

277J. Karle, Amer. Cryst. Symp. on Crystal Growth, Minneapolis, Minnesota, August 20-25, 1967, Paper Q3, p. 81.

†Purdue University, Lafayette, Indiana.

Neutron Monochromator Studies *(S. W. Peterson* and J. M. Williams)*

Several new neutron monochromators (pressed germanium, pyrolytic graphite, and deformed zinc) have been developed recently. An extensive series of reflectivity measurements were made so that the highest possible beam intensities would be obtained at AARR as well as at CP-5. Included in the tests were a number of monochromators obtained from several sources as detailed in Table 21.

Rocking curves and integrated reflectivities were determined using a double crystal spectrometer with the first crystal a "perfect" (unpressed) germanium crystal and the second a sample crystal. Under these conditions, absolute values of crystal reflectivities and mosaic spreads were obtained. Some representative values are given in Table 21.

The monochromators in use at several different laboratories are reasonably comparable in efficiency. Unusually high integrated reflectivity is usually accompanied by a large rocking curve width or mosaic spread, as is evident for zinc and pyrolytic graphite. Beryllium is somewhat unique with high integrated reflectivity and a narrow peak width. One result of the study has been an increase in neutron flux by a factor of approximately 2.5 at Diffractometer I.

TABLE 21. Brief Summary of Measured Monochromator Parameters

	Source[a]	*hkl*[b]	$B_{1/2}$[c]	Peak Intensity, 10^3 counts	Integrated Intensity, 10^3 counts	Integrated Reflectivity $R(\theta)$, 10^{-3} radians
Germanium-Pressed	(1)	111 *T*	0.30°	15	142	1.24
		220 *R*	0.25	34	189	1.65
Germanium-Pressed	(2)	220 *T*	0.21	24	135	1.18
		220 *R*	0.21	38	232	2.02
Germanium-Pressed	(3)	111 *T*	0.36	16	124	1.08
		220 *T*	0.60	14	170	1.49
Beryllium	(1)	002 *R*	0.14	51	188	1.64
		002 *R*[d]	0.27	75	475	4.14
		110 *T*	0.30	21	150	1.31
Pyrolytic Graphite	(4)	002 *R*	0.92	34	654	5.70
Copper	(1)	111 *R*	0.34	46	281	2.44
		222 *R*	0.42	18	166	1.45
Copper	(2)	200 *T*	0.15	27	99	0.86
		200 *R*	0.20	32	168	1.46
Zinc	(5)	002 *R*	0.90	22	438	3.81
		110 *T*	0.92	9	152	1.32

[a]The sources are as follows: (1) Argonne, (2) Brookhaven, (3) Oak Ridge, (4) National Carbon, (5) Ames.

[b]*R*--reflection; *T*--transmission.

[c]Full peak width at peak half-maximum intensity.

[d]Values obtained from the same face of the same crystal but in a different orientation and after reduction to half thickness.

*Chemistry Division, Argonne National Laboratory.

Computer Controlled Neutron Diffraction Units *(M. H. Mueller, L. Heaton, J. M. Williams, and R. L. Hitterman)*

Publication

M. H. Mueller, L. Heaton, R. A. Aschenbrenner, and L. Amiot, Amer. Cryst. Assoc. Symp. on Crystal Growth, Minneapolis, Minnesota, August 20-25, 1967, Paper E8, p. 35.

The tremendous advantage of computer control for diffraction equipment has been evident in many of our current investigations. The computer method was developed as a cooperative effort with the Applied Mathematics Division, as briefly described in the 1966 Annual.[278] Two IBM-1130 computers are in use on the neutron four-circle Diffractometer I, and on the heavy-duty Spectrometer II.

Although the computers and interfacing are the same for the two units, considerable variation in programming exists to fit the needs of the individual instrument. To date, the ARCADE system has a collection of approximately 50 diffraction programs with some 200 subroutines. Experience has shown that this method of control is extremely flexible and reliable. We anticipate that considerable programming effort will be required to (1) vary data collection, (2) control experimental conditions (for example, magnetic field, high and low temperatures, and flipping of a polarized neutron beam), and (3) incorporate preliminary data processing routines.

AUXILIARY INSTRUMENTATION *(L. Heaton, M. H. Mueller, G. H. Lander, K. D. Anderson, and D. Zauberis)*

In order to expand our neutron diffraction studies of magnetic materials (especially antiferromagnetic), a cryo-orienter has been constructed.[279] Three-dimensional magnetic or crystallographic data can be obtained at any given temperature, from liquid helium to room temperature. We believe this is the first such operating unit. The cryo-orienter will permit a thorough investigation of possible structural changes in alpha uranium at low temperatures, especially in the 45°K region where a number of anomalous changes have been reported. This instrument will also be an asset in the determination of the magnetic structures of the actinide single-crystal compounds.

An electromagnet (20 kg) has been purchased for use on the heavy-duty neutron instrument, and control will be incorporated in the computer operation. The addition of this auxiliary device will permit magnetic studies of diffuse elastic magnetic scattering from polycrystalline alloy samples. Data will be collected with the magnetic field both on and off. The initial experiments will attempt to determine the deviations of the atomic magnetic moments in iron- and nickel-base alloys as a function of composition.

A modification of Neutron Spectrometer I will provide a *polarized beam* for use in the study of ferromagnetic materials. These studies require that the sample be contained in the neutron beam in a high magnetic field and often at low temperatures. A specially designed 20 kg magnet and helium cryostat with a tail section extending through the iron core is being constructed. This spectrometer will still be able to function as a powder diffractometer with a nonpolarized neutron beam.

Crystallographic Computer Programming *(J. M. Williams, N. K. Dalley, L. Heaton, H. W. Knott, and K. D. Anderson)*

All of the computer programs are being integrated and placed on one magnetic tape in order to completely automate crystallographic computations and minimize card deck handling. The various programs* may be "called" individually from the tape, or used sequentially by certain specified control cards.

The CDC-3600 programs are being converted to the IBM-360-75 because of an overall average gain of three in computation speed. A number of additions have been made to the Least-Squares Refinement Program ANL FLS(14E7043) to increase the number of variable parameters, to permit correction for anomalous dispersion, and to permit full or fractional parameter shifts based on each cycle. A program was written for rapid interpretation of Fourier computations for location of peaks (17E7057). Considerable flexibility was built into the powder diffraction plotting program to allow averaging and subtraction of the nuclear from the magnetic component, for example.

[278] M. H. Mueller, L. Heaton, J. Williams, and H. Knott, Annual Progress Report for 1966, Metallurgy Division, ANL-7299, pp. 280-281.

[279] M. H. Mueller, L. Heaton, and R. L. Hitterman, Annual Progress Report for 1965, Metallurgy Division, ANL-7155, p. 248.

*We are greatly indebted to Mr. Joe Gvildys of the Applied Mathematics Division for programming most of the work described.

IRRADIATION EFFECTS AND DEFECTS

Theory of Atomic Collision Cascades *(P. Sigmund*)*

Studies[280-282] of the spatial extension of atomic collision cascades in the kiloelectron-volt range have continued. In the previous work the following assumptions were made: (1) the medium is random and infinite, (2) the collisions are elastic, and (3) the cross section is approximated by the Lindhard power-law formula.[283]

Assumptions (2) and (3) are no longer used since inelastic energy loss has been included in accordance with the Lindhard scheme,[283] and arbitrary scattering cross sections are now taken into consideration. The relevant integral equations can now be solved numerically. Coding of a computer program is in progress to determine (1) spatial distribution of energy deposited by ion bombardment, (2) distribution of Frenkel pairs in recoil cascades, (3) sputtering efficiency of heavy ions, and (4) calculation of the energy emitted by secondary electron emission.

Irradiation Hardening *(C. A. Arenberg and T. H. Blewitt)*

Publications

C. A. Arenberg and T. H. Blewitt, Bull. Am. Phys. Soc. *12*, 390 (1967). Abstract

T. H. Blewitt and M. W. Lucas,** Bull. Am. Phys. Soc. *12*, 302 (1967).

R. Benaroya,† T. H. Blewitt, J. M. Brooks,†† and C. Laverick,†† IEEE Trans. NS-14(3), 383-385 (1967).

R. Benaroya,† T. H. Blewitt, J. M. Brooks,†† and C. Laverick,†† Bull. Am. Phys. Soc. *12*, 949 (1967). Abstract

T. H. Blewitt, Proc. Symp. on Pulsed High Intensity Fission Neutron Sources, USAEC, Washington, D. C., February 1965, CONF-650217, pp. 108-110.

A. C. Klank, T. H. Blewitt, J. J. Minarik,§ and T. L. Scott, Proc. Intl. Inst. Refrigeration Commission I Symp., University of Colorado, Boulder, Colorado, June 16-18, 1966, pp. 373-381 (1967).

James A. Horak§§ and T. H. Blewitt, Bull. Am. Phys. Soc. *12*, 303 (1967). Abstract

Studies of the effect of fast neutron bombardment of face-centered cubic single crystal metals have been continued. Although the controversy relating to the dose dependence of the yield stress has been essentially resolved[284] and a model presented that agreed with the one-third power relationship down to about 4×10^{13} n/cm^2, experiments were made to obtain data at smaller doses. Consequently, the macroyield stress was determined *in situ* before the reactor went to power. For doses lower than 6×10^{13} n/cm^2 (about two minutes full-power operating time), the initial yield stress σ_0 is of the same order of magnitude as the radiation-induced yield stress, and attempts were made to prepare crystals with as low an initial macroyield stress as possible. A critically resolved shear stress of less than 200 g/mm^2 would be reasonable. One of the greatest problems in this regard has been the attachment of grips to the crystal. A technique for performing the welding in a reducing atmosphere has evolved, and fairly low yield stress crystals are now possible. Several runs with crystals whose σ_0 were about 400 g/mm^2 verify the preceding thesis and indicate the desirability of attaining crystals with a σ_0 as low as 100 g/mm^2.

Experimental investigation of the microyield stress region was also continued by means of pulse annealing techniques on previously unstressed irradiated crystals. The microyield stress appears to disappear in the region of

*Visiting scientist from Kernforschungsanlage, Jülich, Germany.

280P. Sigmund and J. B. Sanders, *Spatial Distribution of Energy Deposited by Ion Bombardment*, Proc. Conf. on Application of Ion Beams to Semiconductor Technology, Grenoble, France, 1967 (in press).

281P. Sigmund, G. P. Schneidler, and G. Roth, *Spatial Distribution of Defects in Cascades. Black Spot Defects in Electron Bombarded Copper*, Proc. Conf. on Solid State Research with Accelerators, Brookhaven National Laboratory, Long Island, New York, 1967 (in press).

282P. Sigmund, *Sputtering Efficiency of Amorphous Substances*, Can. J. Phys. (in press).

283J. Lindhard, V. Nielsen, M. Scharff, and P. V. Thomsen, Mat. Fys. Medd. Dan Vid. Selsk. *33*, 10 (1967).

**University of Sussex, England.

†Chemistry Division, Argonne National Laboratory.

††High Energy Physics Division, Argonne National Laboratory.

§Central Shops Department, Argonne National Laboratory.

§§Los Alamos Scientific Laboratory, Los Alamos, New Mexico.

284C. Arne Arenberg and T. H. Blewitt, Annual Progress Report for 1966, Metallurgy Division, ANL-7299, pp. 305-308.

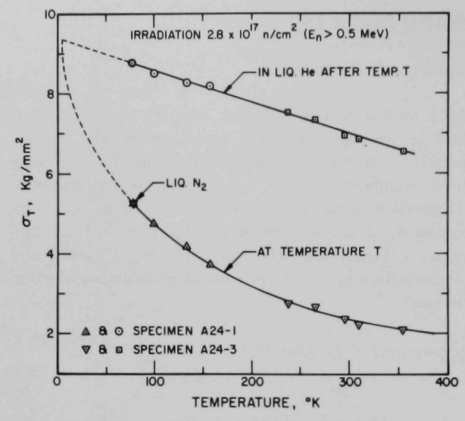

48340

Fig. 58. Isochronal Annealing of Copper Single Crystals.

160-180°K but the temperature seems to be somewhat dependent on the total radiation dose. Many more determinations will have to be made before this important phenomenon can be elucidated.

Isochronal annealing has been carried out to about 400°K. The results for two simultaneously irradiated crystals are shown in Figures 58 and 59. One can see that the effect of radiation damage on mechanical properties is quite different from the effect of electrical resistivity. Apparently there is a continual diffusion of barriers to sinks, i.e., the annealing is diffusion controlled (Figure 59 indicates $\sigma_T \propto 1/T^{1/2}$).

The present status of the program can be stated in terms of the summary presented at the International Conference on The Strength of Metals and Alloys:[285]

> In summary, the fact that there are two yield points clearly establishes that hardening at 4.2°K is the result of radiation-induced barriers that impede the motion of the dislocation line. The macroyield stress data from a large number of crystals clearly show that the stress varies as the one-third power of the neutron dose for doses ranging from 6 x 10^{13} neutrons/cm^2 through 3 x 10^{17} neutrons/cm^2. At doses less than 6 x 10^{13} the initial shear stress will dominate the radiation-induced hardness and obscure the dose dependence. Estimates of the radiation-induced yield stress can be made from a friction hardening model that yields self-consistent values.

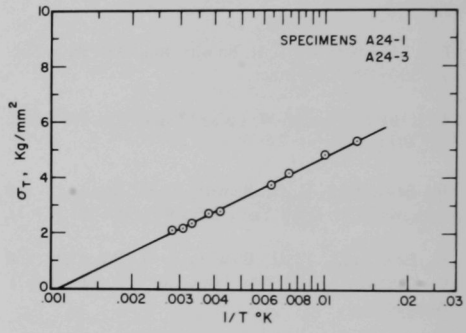

48339

Fig. 59. Annealing of Copper Single Crystals.

Electrical Resistivity of Neutron-Irradiated Uranium *(B. A. Loomis)*

Publication

B. A. Loomis, Bull. Am. Phys. Soc. *12*, 391 (1967). Abstract

The temperature dependence for the mobility of vacancy and interstitial defects in neutron-irradiated uranium crystals was determined from experiments on the recovery of the irradiation-induced electrical resistivity. These results were used to obtain an understanding for the temperature dependence of the irradiation-induced length changes of uranium crystals that was discussed in the 1966 Annual.[286]

Pseudosingle crystals[287] with a rod axis parallel to either the [100], [010], or [001] crystallographic direction were irradiated at temperatures of 4.5 and 20°K in the VT-44 and VT-53 cryogenic facilities in the CP-5 reactor.[288] The neutron flux in the VT-44 facility was approximately 1 x 10^{12} thermal neutrons/cm^2-sec with a cadmium ratio of 260. The neutron flux in the VT-53 facility was approximately 2 x 10^{12} neutrons/cm^2-sec with

---

[285] T. H. Blewitt and C. Arne Arenberg, *Irradiation Hardness in Copper*, Proc. Intl. Conf. on The Strength of Metals and Alloys, Tokyo, Japan, September 4-8, 1967, Supp. Trans. Japan Inst. of Metals (to be published).

[286] B. Loomis, Annual Progress Report for 1966, Metallurgy Division, ANL-7299, pp. 206-210.

[287] E. S. Fisher, USAEC Report ANL-5159, Argonne National Laboratory, 1953.

[288] A. C. Klank, T. H. Blewitt, J. J. Minarik, and T. L. Scott, Proc. Intl. Inst. Refrigeration Commission I Symp., University of Colorado, Boulder, Colorado, June 16-18, 1966, pp. 373-381 (1967).

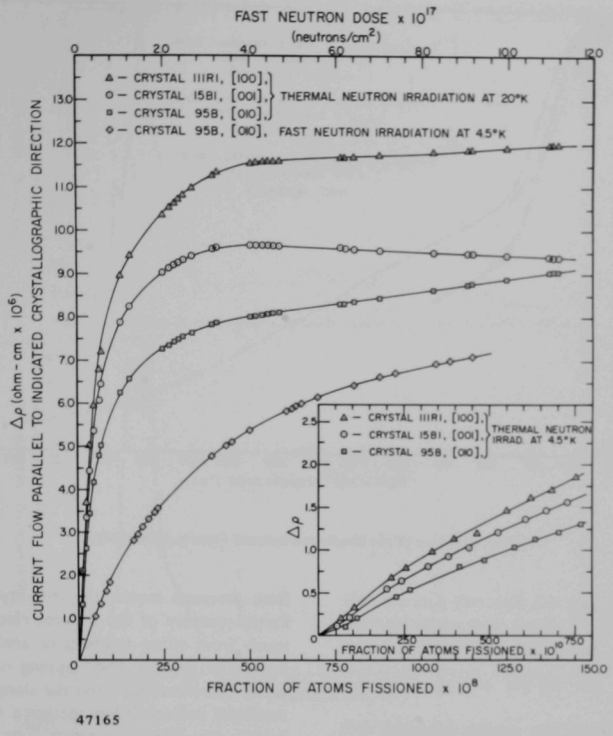

Fig. 60. The Effect of Thermal and Fast Neutron Irradiation on the Electrical Resistivity of Uranium Pseudosingle Crystals.

an energy greater than 0.1 million electron volts and 1 x 10^8 neutrons/cm^2-sec with an energy less than 0.14 electron volts.

The electrical resistance of the crystals was measured during irradiation by the potentiometric method with a precision of 0.02 $\mu\Omega$. Silver wires (0.5-mm diameter) were welded to the crystals to provide electrical contact. The irradiation-induced electrical resistivity was calculated from the resistance data with appropriate correction for the dimensional changes of the crystals that occurred during irradiation. The temperature of the crystals during irradiation was determined by the use of calibrated carbon resistors and copper-constantan thermocouples.

The recovery of the irradiation-induced electrical resistivity was determined by isolation of the liquid-helium reservoir from the capsule containing the irradiated specimens and by heating the capsule with a resistance heater to the desired annealing temperature. The duration of the heat pulse was 5 minutes. The specimens were cooled to 4.2°K following the heat pulse to determine the extent of recovery.

The effect of thermal neutron irradiation at 4.5 and 20°K on the electrical resistivity of the single crystals is shown in Figure 60. The increase of the electrical resistivity $\Delta\rho$ as the result of irradiation is plotted against the fraction of total atoms fissioned τ. The curves for each of the crystal orientations exhibit a negative curvature up to approximately 45 x $10^{-8}\tau$, and, on further irradiation, the $\Delta\rho$ values change at a constant rate. The curves for the [100] and [010] oriented crystals have a positive slope after approximately 45 x 10^{-8} τ, whereas the curve for the [001] oriented crystal has a negative slope.

Following thermal neutron irradiation of the crystals at 4.5°K, the crystals were pulse annealed at temperatures up to 100°K and, following the 20°K irradiation, the crystals were pulse annealed up to 570°K. The recovery of the irradiation-induced electrical resistivity is shown in Figure 61, and the differential of the recovery curve for the 20°K

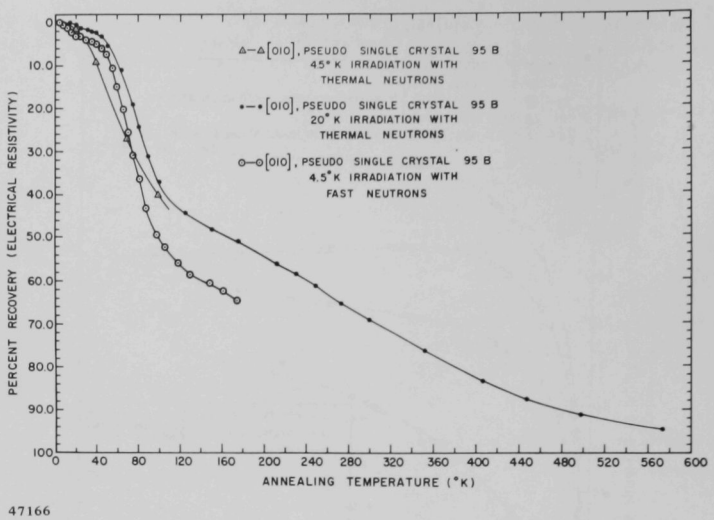

47166

Fig. 61. Recovery of the Irradiation-Induced Electrical Resistivity.

irradiation is shown in Figure 62. Recovery data are only shown for the [010] oriented crystal, since nearly identical data were obtained for the [100] and [001] oriented crystals.

Following the annealing of the crystals irradiated with thermal neutrons, the [010] oriented crystal was irradiated at 4.5°K with fast neutrons. The increase of the electrical resistivity for this crystal is plotted against the fast neutron dose in Figure 60. The $\Delta\rho$ curve shows negative curvature throughout the irradiation up to 9.4×10^{17} fast neutrons/cm^2, whereas during thermal neutron irradiation of this crystal at 20°K, the $\Delta\rho$ curve was linear from 2×10^{17} to 6×10^{17} neutrons/cm^2. The recovery of the electrical resistivity induced in this crystal by fast neutron irradiation is shown in Figure 61 and the differential of the recovery curve is shown in Figure 62. The electrical resistivity recovery data for the crystals, after thermal neutron irradiation or fast neutron irradiation, show that a major stage for recovery occurs between 40 and 140°K, and a minor stage of recovery exists below 40°K. Stages for recovery of the irradiation-induced length changes in uranium crystals also occur in these temperature ranges.[286]

We attribute the recovery of the irradiation-induced electrical resistivity and dimensional changes at temperatures below 40 to 50°K to trapping of single interstitial defects at interstitial clusters, and to annihilation of single interstitial defects at single vacancies or vacancy clusters. Both processes require the mobility of interstitial defects. Partial recovery of the induced electrical resistivity would result from either trapping or annihilation of the single interstitial defects. The trapping of interstitials at interstitial clusters would cause the elongation observed for the irradiated polycrystalline specimen and the [010] oriented crystal, i.e., "inverse recovery," on annealing at temperatures up to 50°K.[286] The annihilation of interstitials at vacancy clusters would cause the elongation observed for the [100] oriented crystal, i.e., recovery of the irradiation-induced contraction.[286] The recovery between ~5 and ~30°K of the additional electrical resistivity that results from quenching uranium to 4.2°K[289] or electron irradiation of uranium at 7°K[290] has been ascribed also to interstitial mobility at temperatures above 5°K.

The recovery stage between 40 and 140°K is attributed to the release of interstitial defects from unstable, small diameter interstitial clusters. The interstitials are subsequently trapped at stable, large diameter interstitial clusters or annihilated at vacancy clusters. Both of these processes would result in further recovery of the induced electrical resistivity for the [100], [010], and [001] oriented crystals (Figure 61). The annihilation of interstitials at vacancy clusters would cause recovery of the

289J. C. Jousset, Acta Met. *14*, 193 (1966).

290J. C. Jousset, A. Lucasson, and P. Lucasson, Phil. Mag. *13*, 887 (1966).

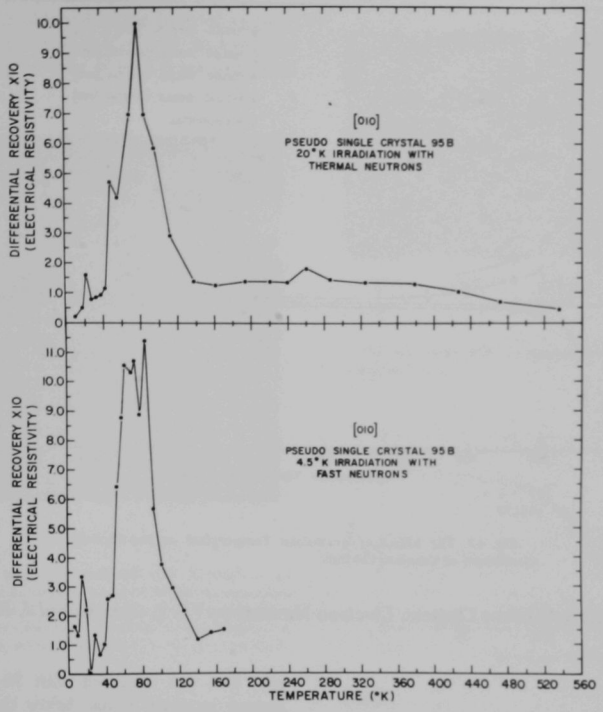

Fig. 62. Differential of the Recovery Curves Shown in Figure 61.

irradiation-induced contraction of the [100] oriented crystal.[286] To agree with the experimental observations, the result of the dissociation of unstable, small diameter interstitial clusters is a recovery of the irradiation-induced elongation in the [010] oriented crystal.[286] Burger et al.[291,292] have also determined the recovery of the electrical resistivity induced by irradiation of uranium with neutrons at 4.2°K. They interpreted their results to show that vacancies are mobile in uranium at 60°K. However, previous data[290] show that $G[010]/G[100]$ increases from 1.5 at 20°K to 4.4 at 70°K and then decreases to 1.0 at higher irradiation temperatures. A value for $G[010]/G[100]$ greater than unity at a given irradiation temperature can be expected, if interstitials are the mobile defects. Although the mobility of interstitials can result in annihilation of vacancies, the mobility of these defects can also result in their being trapped at more stable interstitial clusters. The result of these processes is that $G[010]/G[100]$ is greater than unity.

Approximately 50% of the electrical resistivity induced during irradiation at 20°K is recovered on annealing at temperatures up to 140°K (Figure 61). Also, the irradiation-induced length changes of uranium crystals decrease substantially in magnitude on increasing the irradiation temperature from 20 to 140°K (Figure 63). Therefore, we attribute the temperature dependence of the irradiation-induced length changes, on the basis of the preceding discussion, to increased annihilation of single interstitials at vacancy defects. With increasing irradiation temperature a larger fraction of the small diameter interstitial clusters formed by the fission event dissociate to yield single interstitials before the small clusters can aggregate into thermally stable clusters.

[291] G. Burger, K. Isebeck, H. Wenzl, J. C. Jousset, and Y. Quere, Phil. Mag. *11*, 621 (1965).

[292] G. Burger, K. Isebeck, H. Wenzl, J. C. Jousset, and Y. Quere, 10th Metallurgical Colloquium, Saclay, France (1966).

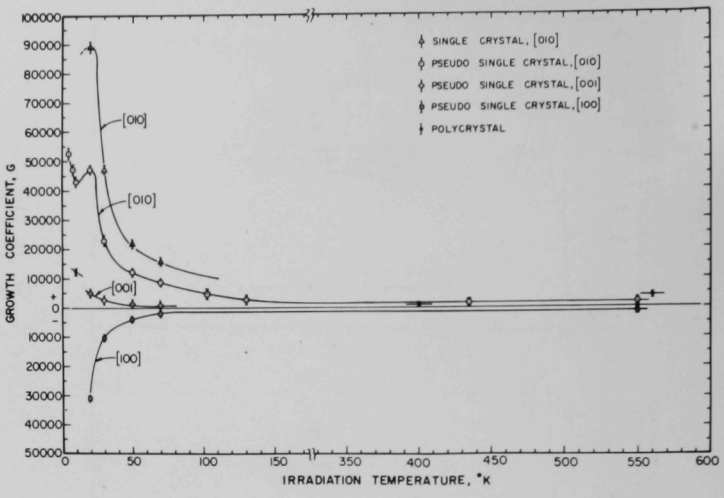

Fig. 63. The Effect of Irradiation Temperature on the Growth Coefficient of Uranium Crystals.

Radiation-Induced Defect Clusters. Electron Microscopy *(K. L. Merkle and J. R. Wrobel)*

Publications

K. L. Merkle, J. Appl. Phys. *38*(1), 301-309 (1967).

K. L. Merkle and L. R. Singer, Bull. Am. Phys. Soc. *13*, 390 (1967). Abstract

K. L. Merkle and L. R. Singer, Appl. Phys. Letters *11*(2), 35-37 (1967).

We have firmly established in recent years that the defect clusters in gold, produced in energetic collision cascades, are of the vacancy type and are associated with a cascade energy of the order of 30 keV. During the past year some of the finer details of the cascade process have been observed by transmission electron microscopy. One of the features of very energetic cascades is the observation of multiple defect clusters at the site of a single cascade. This phenomenon was observed in the early fission fragment irradiations of gold. During the past year, this effect has been investigated by means of xenon-ion bombardment, where the cascade is initiated just below the surface of the monocrystals. The occurrence of double defects starts at fairly low energy, an order of ~50 to 100 keV.

Another phenomenon is illustrated in Figure 64. The gold film was irradiated with 50 keV xenon-ions. The damage produced is just below the surface of the film, because the range of the ions is about 100Å. If, however, the ions enter a (100) channel, they can travel much farther and actually penetrate the film without producing damage. However, if the channeled ion encounters an atom that is not exactly on a lattice site (due to thermal vibrations and lattice defects), the ion can be dechanneled and the entire energy deposited in a cascade, which results in a defect cluster that can be directly observed. A stacking fault can almost completely stop the channeled beam, as can be seen in Figure 64. The heavily damaged top layer has been etched away after irradiation in order to expose the underlying part of the crystal. The stacking fault originally extended across the denuded zone and prevented the channeled ions from reaching this region.

One of the important questions regarding the cascade cluster is whether submicroscopic, interstitial clusters are associated with the observable vacancy clusters, or whether all of the interstitials have gone to insaturable sinks, leaving a pure vacancy defect structure. The latter situation is more likely in irradiations where only low-energy primaries are produced, and the visible defect clusters occur when the migrating small defects merge. The well-known tetrahedral

form of defects can be observed in the form of vacancy tetrahedra in quenching experiments of gold. We have now compared the annealing behavior of both types of defects,

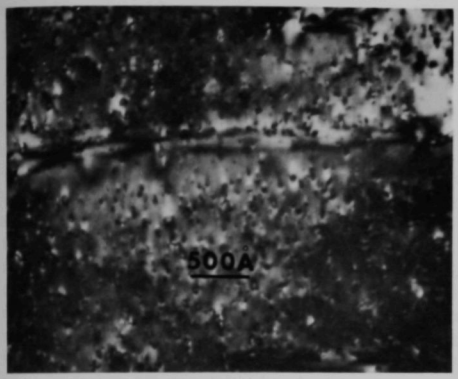

141620

Fig. 64. Gold Film Irradiated with 50 keV Xenon-Ions to 7.2 x 10^{13} Xe/cm^2. The irradiation top half of the specimen has been etched away. Note the stacking fault that originally extended over the denuded region. Channeled xenon ions have penetrated deep into the crystal, but were dechanneled at the stacking fault.

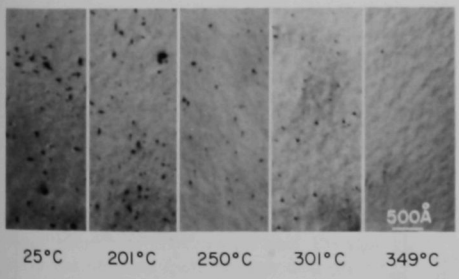

49421

Fig. 65. Isochronal Anneal of Black Spot Defects.

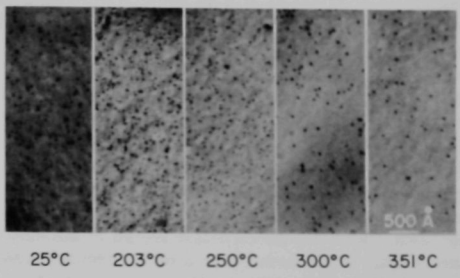

49422

Fig. 66. Isochronal Anneal of Radiation-Induced Tetrahedra of Stacking Faults.

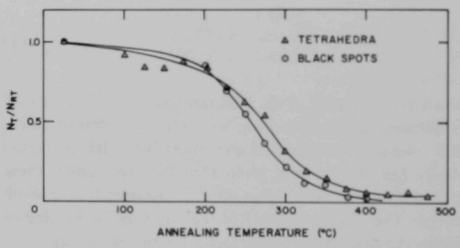

49423

Fig. 67. Isochronal Annealing Curves for Tetrahedra and Black Spot Defects.

the tetrahedra and the black spot defects, which are spontaneously produced in collision cascades. A difference in the isochronal annealing behavior has been observed (Figures 65-67). Further analysis of the annealing data is necessary in order to decide whether the breakup of interstitial clusters plays a significant role in the annealing behavior of the black spot vacancy clusters. Figure 67 indicates that the black spots anneal at a somewhat lower temperature than the tetrahedral defects. Future plans should include an investigation of this annealing behavior by measurements of electrical resistivity on thin films.

Low-Temperature Charged-Particle Irradiations of Thin Metal Films *(K. L. Merkle and L. R. Singer)*

The scattering behavior of the conduction electrons at the film surface must be considered in the investigation of radiation-induced defects by means of electrical resistivity measurements.[293] The corrections that must be applied are evaluated by means of the Fuchs-Sondheimer theory. The specimens studied to date indicate partial specular scattering, and the degree of specularity varies from specimen to specimen. Therefore, the correction applied to the measured damage rate does not depend on the film thickness alone. An independent measurement is necessary to determine the correction factors. The temperature dependence of the thin film resistivity is used to determine the correction factors for any given thin specimen. If Matthiesson's rule is applicable, we obtain

$$\frac{d\rho_\infty^{(1)}}{dT} = \frac{d\rho_\infty^{(2)}}{dT}, \qquad (1)$$

where the derivative of the bulk resistivity with respect to T is the same in two specimens with slightly different defect and impurity concentrations. Therefore, the corrected values $(d\rho_\infty/dT)$ of any given thin film are, under these assumptions, equal to the $d\rho_\infty/dT$ measured in a bulk sample. The measured $d\rho/dT$ of the thin film can be used to obtain the desired correction factor for the damage rate

$$\frac{d\rho_\infty}{d\rho} = \frac{d\rho_\infty}{dT}\frac{dT}{d\rho}. \qquad (2)$$

The set of values $d\rho_\infty/d\rho$, ρ can be used to determine the parameters of ρ and γ of the Sondheimer theory that give the best fit to this set of data. The resistivity values that are measured upon irradiation at 4.2°K are then corrected for the size effect by means of the Sondheimer theory. Sufficiently accurate data have not been collected to determine if deviations from the Sondheimer theory must be considered. In first approximation the Sondheimer theory should be well suited for the extrapolation from thin film measurements to bulk values of the resistivity. Figure 68 shows $d\rho/dT$ of a copper film of a = 3200Å prior to irradiation with 1 MeV protons, and the values corrected for the size effect using p = 0.5 and $\gamma = 5.38 \cdot 10^6\ \Omega^{-1}\ \text{cm}^{-1}$. By using the same values of p and γ, the corrections to the damage rates can be obtained (Figure 68). At high defect densities the correction becomes smaller than the experimental scatter. After a thorough test of the Sondheimer theory, hopefully, reliable extrapolations to the bulk resistivity and extrapolations at low defect densities can be obtained.

Apart from the necessary corrections due to the size effect, the electrical resistivity can also be used very advantageously in the measurement of low defect densities in thin films. In the case of diffuse scattering at the surface and low defect densities in the film, the electrical conductivity is essentially determined by those electrons that travel almost parallel to the film surface. A small-angle scattering event that normally would not cause a large change in the momentum of the electron will bring the electron to the film surface where the drift velocity component will be completely lost if the specularity coefficient $p = 0$. This has some important consequences for the study of defects in thin films. At small defect concentrations, the change in electrical resistivity per defect is larger than in the bulk. In single crystalline films the anisotropy of the electronic scattering cross section of the defects will be reflected in different resistivity changes for different orientations of the films. Finally, a large defect concentration introduced just below the surface of a film with $p = 0$ will not affect the resistivity of the film as long as the thickness of this surface damage is small compared with the film thickness. The resistivity of the film will increase if the defects near the surface start migrating into the bulk of the crystal. A sensitive means for the detection of long-range migration of defects is provided in this way.

Preliminary preparations are under way to investigate the areas discussed in this report. An important tool is the

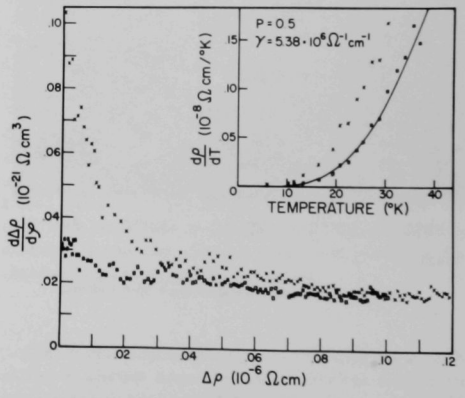

47644

Fig. 68. The Damage Rate Curve for a Copper Film Irradiated at 4.2°K with 1 MeV Proton. The measured values are represented by x. The squares represent values corrected for the size effect with p = 0.5 and $\gamma = 5.38 \cdot 10^6\ \Omega^{-1}\ \text{cm}^{-1}$. The insert shows $d\rho/dT$ as a function of T before irradiation. The solid curve is $d\rho/dT$ of a bulk specimen.

[293] K. L. Merkle and L. R. Singer, Annual Progress Report for 1966, Metallurgy Division, ANL-7299, pp. 291-293.

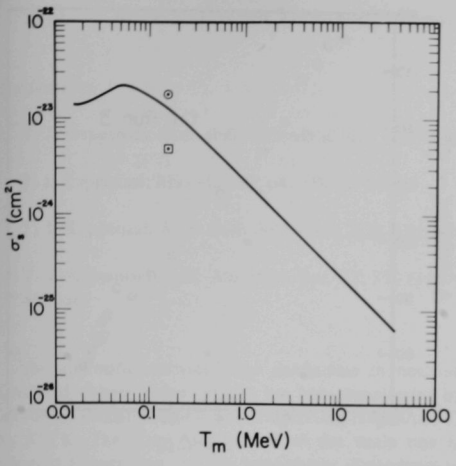

47457

Fig. 69. Reduced Black Spot Cross Section in Gold σ_s' as a Function of T_m. The solid curve is a best fit to the data from room temperature experiments. The two data points are from the present low-temperature irradiations. The high dose experiment is indicated by ⊡; the low dose experiment is indicated by ⊙.

new data acquisition system that was first used in some irradiations late in 1967.

As previously reported,[293] defect clusters were observed, by transmission electron microscopy, in a specimen that had been irradiated to a very high defect density at 4.2°K. The density of black spot defect clusters has been determined in this experiment and also in an additional experiment with a much lower dose. The results are shown in Figure 69, where the reduced cross section σ_s' for black spot formation versus maximum recoil energy T_m is plotted. The reduced black spot cross section of the low dose and the high dose experiments are compared with the solid black line, which represents a fit to our data from the room temperature irradiations of gold. The point below the curve was obtained from the high dose experiment. Here the average distance between clusters is of the order of their diameter. Saturation effects due to overlapping cascades are expected to reduce the observed number of spots. The low dose experiment, however, gives a value of σ_s', which is within the experimental error in agreement with the room temperature value. Thus, the temperature of irradiation does not influence the number of spots formed and is in agreement with our earlier result which indicated that the spots are formed in energetic displacement cascades. It is of considerable interest to compare the resistivity associated with the observed black spot defect clusters with the resistivity increase that one would expect from the visible defects. By using the size distribution and assuming that all of the clusters are planar loops, we find that the resistivity per percent atom in a cluster is $\Delta\rho = 1.53 \times 10^{-6}$ Ωcm. We are left with the surprising result that those cascades, which leave a visible cluster, can completely account for the observed resistivity increase that remains at room temperature.

A rough estimate shows that the submicroscopic clusters should contribute to the resistivity at least as much as the visible clusters. Therefore, unless the resistivity per defect in a cluster is widely different from that of the isolated defect, almost all of the clusters in gold that are present at room temperature can be seen by transmission electron microscopy. This is difficult to understand in terms of the stability of vacancy clusters, because, certainly, small clusters with 10-20 atoms are still expected to be stable. The reason for a lower limit in the size of the clusters probably lies in the following: the vacancy cluster produced in the center of a displacement cascade is stable only if the interstitials at the periphery also form stable clusters; otherwise, the interstitials recombine with the vacancy cluster and no stable configuration evolves. The criterion for the survival of the large vacancy cluster, therefore, is the stability of the much smaller interstitial clusters. If, below a certain recoil energy, the size of the cascade becomes too small, the probability for the formation of interstitial clusters also becomes very small. However, because of the uncertainties in the absolute values of the resistivity contributions an experiment more sensitive to submicroscopic defects must be performed. An irradiation with T_m of the order of the threshold energy for black spot formation should give more information on the submicroscopic defects.

Recovery of Lattice Parameter and Electrical Resistivity in Low-Temperature Neutron-Irradiated Copper *(E. E. Gruber and J. A. Tesk*)*

Publication

E. E. Gruber, J. Appl. Phys. *38*, 243-250 (1967).

*Formerly at the University of Illinois, Chicago Circle, Consultant to ANL, Metallurgy Division; presently with the Applied Research Section of ANL, Metallurgy Division.

The purpose of this experiment, which was initiated in 1964, is to investigate the nature of the defects that are present in the various annealing stages of neutron-irradiated copper by measuring simultaneously the changes that occur in electrical resistivity and lattice parameter during isochronal annealing.

Four specimens have been irradiated and annealed. Although none of the runs was a complete success, each lead to modifications and improvements in equipment and technique. The first run yielded no useful recovery data because of equipment and alignment problems. For example, the x-ray counting equipment was completely inadequate to measure the lattice parameter of a radioactive sample. The use of a single-channel pulse-height analyzer has effectively eliminated background radioactivity.

Run 2 provided the first significant data; after the transfer of the sample from the reactor to the storage Dewar and finally to the cryostat without warming the sample, the isochronal annealing was conducted successfully to a temperature of 130°K. A leak in a vacuum seal caused temporary postponement of further measurements. Measurements were continued after seal repair, but the necessary realignment was not sufficiently accurate to give a continuous curve. The precision of the measurement of the lattice parameter varied from about ±2 ppm at temperatures below 50°K to ±10 ppm at temperatures above 195°K, which is comparable to the 15 ppm precision obtained by Himmler et al.,[294] and the 10 ppm obtained by Simmons and Balluffi.[295]

Optimization of the collimating system and application of a constant torque to the cryostat, to minimize backlash effects, lead to a consistently good precision of <3 ppm in run 3. A trimmer heater was added to the capsule design to eliminate the small thermal gradient observed in run 2. Run 3 was only a partial success, however, because the sample warmed above liquid-nitrogen temperature when a pumping stem on the storage Dewar was accidently broken during a helium transfer; thus, essentially all data below 150°K were lost.

The data obtained in run 3 is plotted in Figure 70 as irradiation-induced lattice parameter change in parts per million versus the residual resistivity change.

The glass storage Dewar was enclosed in a protective metal case before run 4. Run 4 was similarly limited in the useful temperature range by warmup to about 77°K when a glass Miller gage on the cryostat was broken, and alignment problems forced abandoning the annealing above 105°K. The Miller gage has been replaced by a metal Hughes ionization gage, and significant improvements have been

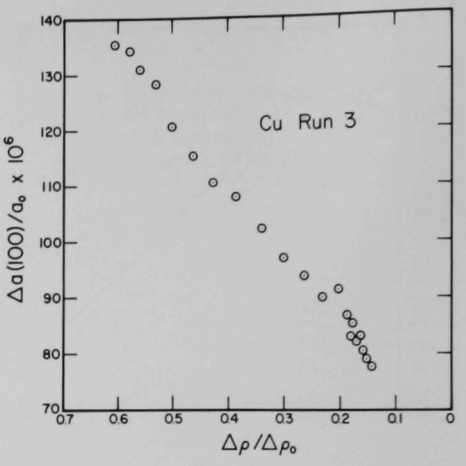

48205

Fig. 70. Residual Lattice Parameter Increase as a Function of Residual Resistivity after 10-min Isochronal Annealing Pulses at Temperatures from 150°K to 348°K.

made in the cryostat mounting and tilting hardware. The new cryostat mount is more rigid, allows finer tilt adjustment, and adds the capability for independent vertical movement.

Some very accurate and useful resistivity data were obtained during irradiation of the specimen for run 4. The specimen was in liquid helium at 4.5°K throughout the irradiation, and the resistivity was measured with newly operational automatic equipment. The results show a linear dependence of rate of resistivity increase on resistivity. Comparison with other data taken at 28.5°K on an identical sample indicates that some characteristics of the damage curve may be determined by the irradiation temperature, rather than resulting from the detailed mechanics of the irradiation damage. Further work is being done on this problem. The work on copper will be completed in the near future. The experiment will be continued with aluminum because of its higher damage rate, which will increase the change in lattice parameter relative to the sensitivity of measurement.

294U. Himmler, H. Peisl, A. Sepp, W. Waidelich, and H. Wenzl (to be published).

295R. O. Simmons and R. W. Balluffi, Phys. Rev. *109*, 1142-1152 (1958).

Stress Relaxation in Neutron Irradiated Copper Single Crystals *(T. J. Koppenaal*)*

Publications

T. J. Koppenaal, Abst. Bull. IMD-AIME *2*(1), 77 (1967).

T. J. Koppenaal, Acta Met. *15*, 681-690 (1967).

T. J. Koppenaal, Abst. Bull. IMD-AIME *2*(2), 6 (1967).

T. J. Koppenaal, Bull. Am. Phys. Soc. *12*, 390 (1967). Abstract

The thermally activated slip mechanism in neutron-irradiated copper single crystals has been investigated by measuring stress-relaxation in a temperature range from 77 to 420°K. The stress dependence of the strain rate at constant temperature and the temperature dependence of the flow stress at constant strain rate have been established. With the use of these two quantities, the activation enthalpy and activation volume are calculated as a function of effective stress. The experimental observations of these activation parameters are in good agreement with the theoretical stress dependencies predicted by the Fleischer theory for strengthening by tetragonal distortions. An experimental force-distance curve for the dislocation-defect interaction responsible for neutron-irradiation strengthening is also in excellent agreement with the Fleischer theory. The results indicate that the thermally activated, rate controlling mechanism for slip in these crystals can be expressed entirely through the relationship

$$\dot{\gamma} = \dot{\gamma}_0 \exp -\frac{H_0}{kT}\left[1 - \left(\frac{\tau^*}{\tau_0^*}\right)^{1/2}\right],$$

where $\dot{\gamma}$ is the strain rate, $\dot{\gamma}_0$ a constant, H_0 (= 3.0 eV) the activation enthalpy at zero effective stress, τ^* the effective stress, τ_0^* the effective stress at 0°K, and kT has the usual meaning.

Irradiation-Induced Resistivity in Pure Metals *(James A. Horak)*

Publication

James A. Horak and T. H. Blewitt, Bull. Am. Phys. Soc. *12*, 303 (1967). Abstract

For nine high-purity metals the irradiation-induced resistivity rate $d\rho_i/dt$ was determined as a function of the induced-point defect concentration (indicated by the induced-residual resistivity ρ_i). The residual resistivities of the metals are given in Table 22. The table also provides the total resistivity induced by a dose of 2×10^{18} n/cm^2 of $E > 0.1$ MeV at an irradiation temperature of 4.5°K.

Since $d\rho_i/dt$ is not a linear function of ρ_i for any of the metals tested, the production of defects is not a simple function of the defect concentration. Figures 71 through 79 show the resistivity data; the solid line is the time derivative of the expression $\rho_i = A_1(1 - e^{-\alpha t}) + B_1(1 - e^{-\beta t})$, which was reported previously.[296] The line gives a good fit for aluminum, copper, silver, nickel, cobalt, and molybdenum but does not fit the data for iron. Because of the scatter in the data for gold and platinum a valid fit cannot be ascertained.

TABLE 22. Residual Resistivity and Irradiation-Induced Resistivity in Metals

Element	ρ_0, 10^{-9} Ω-cm	ρ_{i_0}, 10^{-8} Ω-cm	Element	ρ_0, 10^{-9} Ω-cm	ρ_{i_0}, 10^{-8} Ω-cm
Aluminum	1.02	38.23	Iron	53.70	113.72
Copper	0.82	11.62	Nickel	11.60	36.39
Silver	1.64	8.79	Cobalt	89.60	79.46
Gold	2.54	10.27	Molybdenum	4.19	59.33
Platinum	5.58	26.46			

The dashed line (Figures 73-75 and 77-79) represents a fit of the data to the expression suggested by Balarin and Hauser.[297] They modified the expression of Lück and Sizmann[298] by utilizing a concentration dependent recombination volume (V_r) for interstitials and vacancies, yielding the expression $d\rho_i/dt = A(1 - V_{r_0}\,\rho_i)^2$, which is represented by the dashed line. A data comparison with both lines indicates that aluminum, copper, and silver fit both lines; the dashed line is the better fit for iron, but is not as good a fit for nickel, molybdenum, and cobalt.

A large change in slope for cobalt, molybdenum, and nickel occurs at a point-defect concentration of 10^{-4} atomic fraction. For silver, gold, and platinum, the change in slope occurs more gradually and an extrapolation of two straight lines (initial slope and final slope), gives an

*Present address: Applied Research Laboratory, Aeronutronic Division of Philco-Ford Corporation, Newport Beach, California.

[296] James A. Horak, USAEC Report ANL-7185, Argonne National Laboratory, 1967.

[297] M. Balarin and O. Hauser, phys. stat. solidi *10*, 475 (1965).

[298] G. Lück and R. Sizmann, phys. stat. solidi *5*, 683 (1964).

intersection also at 10^{-4} atomic fraction. The data were obtained during almost two days of irradiation in a flux of 1.3×10^{12} n/cm^2 of $E > 0.1$ MeV. Hence, the initial slope is not due to a transient but is a real physical effect.

The "saturation" value of the resistivity (ρ_S) and the recombination volume (V_r) for each metal have been calculated by several methods, as shown in Table 23; recombination volumes obtained by the author are compared with those of other investigators.[299-301] Note that the ρ_S values obtained in the present work are significantly different from those obtained by Burger and co-workers[302] who suggest that the plot of $d\rho_i/dt$ versus ρ_i is linear. Nonlinearity in $d\rho_i/dt$ versus ρ_i has also been observed by Wollenberger and co-workers.[303]

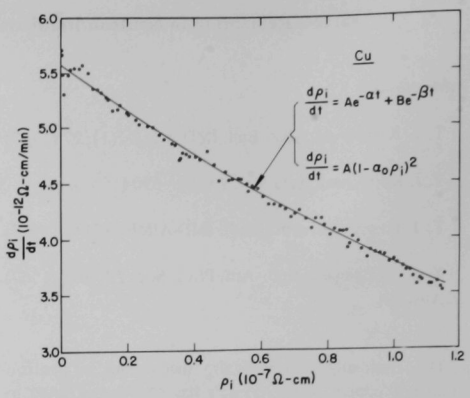

47857

Fig. 72. Resistivity Increase Rate as a Function of Induced Resistivity for Copper.

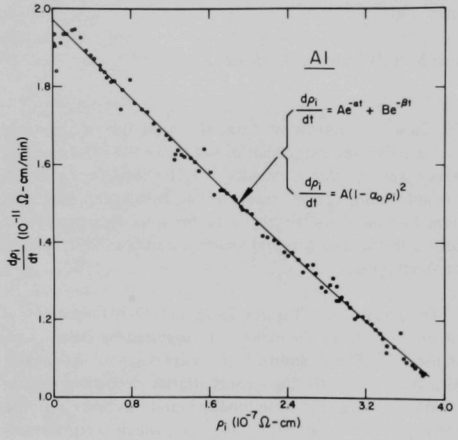

47861

Fig. 71. Resistivity Increase Rate as a Function of Induced Resistivity for Aluminum.

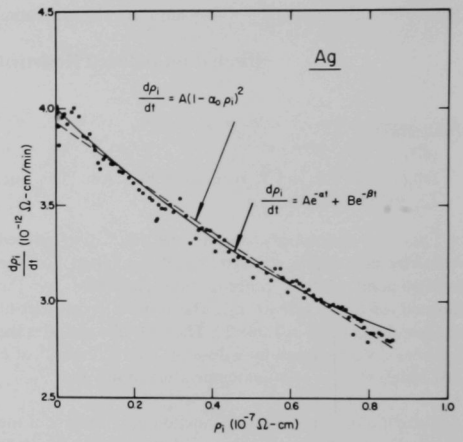

47932

Fig. 73. Resistivity Increase Rate as a Function of Induced Resistivity for Silver.

299K. Dettmann, G. Leibfried, and K. Schroeder, phys. stat. solidi *22*, 433 (1967).

300E. A. Burke, private communication, 1967.

301P. G. Lucasson and R. M. Walker, Phys. Rev. *127*, 1130 (1967).

302G. Burger, H. Meissner, and W. Schilling, phys. stat. solidi *4*, 281 (1964).

303H. Wollenberger, private communication, 1967.

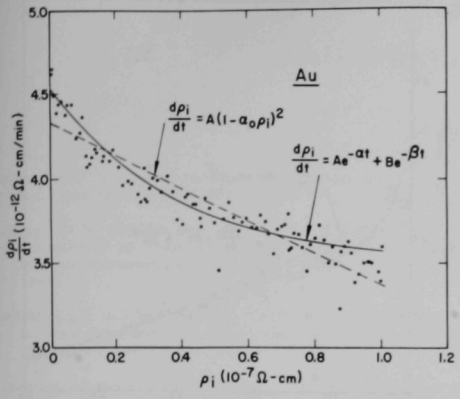

47860

Fig. 74. Resistivity Increase Rate as a Function of Induced Resistivity for Gold.

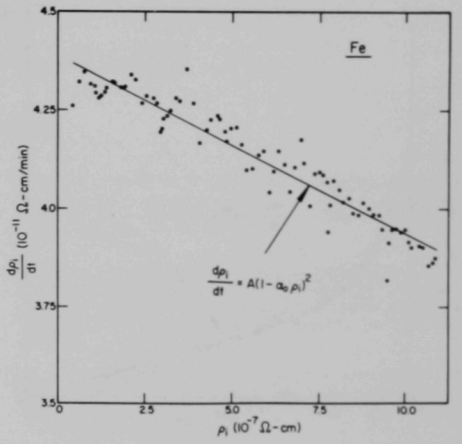

47931

Fig. 76. Resistivity Increase Rate as a Function of Induced Resistivity for Iron.

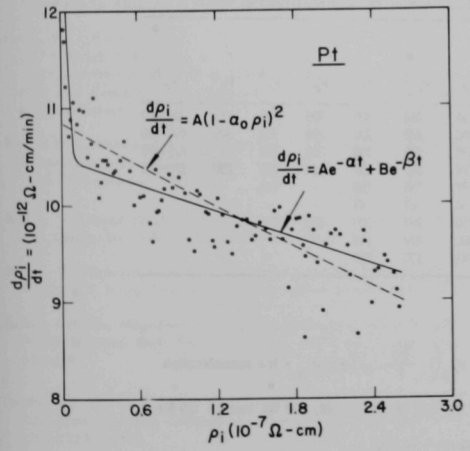

47858

Fig. 75. Resistivity Increase Rate as a Function of Induced Resistivity for Platinum.

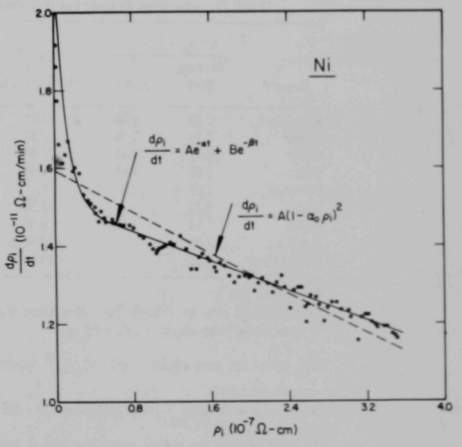

47930

Fig. 77. Resistivity Increase as a Function of Induced Resistivity for Nickel.

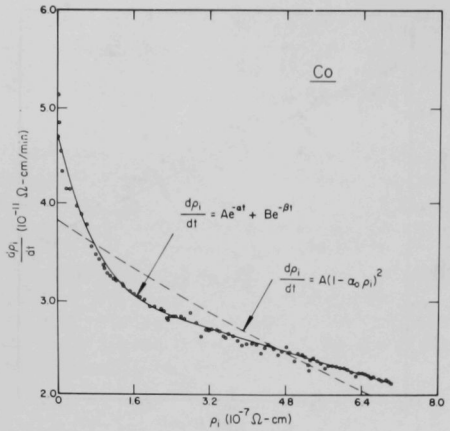

Fig. 78. Resistivity Increase Rate as a Function of Induced Resistivity for Cobalt.

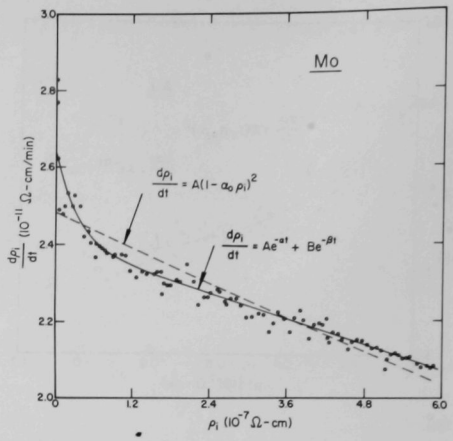

Fig. 79. Resistivity Increase Rate as a Function of Induced Resistivity for Molybdenum.

TABLE 23. Saturation Resistivities and Recombination Volumes for Neutron-Irradiated Metals

Element	ρ_s, μΩ-cm: Present Work	ρ_s, μΩ-cm: Burger[a]	ρ_{fp}[b] (10^{-4} Ω-cm/af)	V_r[c]	V_{r_0}[d]	V_r[e]	V_r[a]	V_r[f]	V_r[g]	V_r[h]
Aluminum	0.80	0.86	6.8[a]	416	468	300	300	400	270	200–400
Copper	0.33	0.34	2.5[a]	400	442	300	300	370	370	490–700
Silver	0.31	0.40	2.5[a]	438	432	360	260	310	-	425–605
Gold	0.82	0.65	2.5[a]	274	285	135	190	190	250	370–385
Platinum	1.82	2.1	7.5[i]	237	255	180	-	180	-	
Iron	9.23	-	12.5[j]	54	67	43	-	-	-	
Nickel	1.14	1.42	6.4[a]	250	284	220	150	230	-	
Cobalt	2.11	-	10 (est)	300	418	190	-	-	-	
Molybdenum	3.83	-	10 (est)	141	155	120	-	-	-	

[a]Reference 302.
[b]Abbreviations are: fp--Frenkel pair, af--atomic fraction.
[c]V_r calculated from $d\rho_i/dt = A(1 - 2V_r \cdot \rho_i)$.
[d]V_{r_0} calculated from $d\rho_i/dt = A(1 - V_{r_0} \cdot \rho_i)^2$, where $V_r = V_{r_0}\left(1 - \frac{V_{r_0}}{2} \cdot \rho_i\right)$ and V_{r_0} = the recombination volume at $\rho_i = 0$.
[e]V_r calculated from $V_r = (\rho_{fp}/2\rho_s)f$, where $f = 0.7$ for Al, $f = 0.8$ for Cu, Fe, Ni, and Co, and $f = 0.9$ for Ag, Mo, Au, and Pt.[299]
[f]V_r calculated by the author using the data of Burger and $V_r = \rho_{fp}/2\rho_s$.
[g]Reference 303.
[h]Reference 299.
[i]Reference 300.
[j]Reference 301.

APPENDIX

PUBLICATIONS, REPORTS, AND PATENT

PUBLICATIONS

Aldred, A. T., *Thermoelectric Powers of Palladium Alloys*, J. Phys. Soc. Japan *22*(3), 762-766 (March 1967).

Alfred, L.C.R. and Van Ostenburg, D. O., *New Scheme for the Construction of Phase Shifts with Application to Nuclear Magnetic Resonance*, Phys. Rev. *161*(3), 569-570 (September 15, 1967).

Alfred, L.C.R. and Van Ostenburg, D. O., *Preasymptotic Form of Impurity Screening in a Metal*, Phys. Letters *26A*(1), 27-28 (December 4, 1967).

Arenberg, C. Arne and Blewitt, T. H., *Radiation Hardening in Copper Crystals*, Bull. Am. Phys. Soc. *12*(3), 390-391 (March 1967). Abstract

Atlas, L. M. and Schlehman, G. J., "Defect Equilibria of PuO_{2-x}, 1045°C to 1505°C," *Plutonium 1965*, Proc. Third Intl. Conf. on Plutonium, London, England, 1965, A. E. Kay and M. B. Waldron, eds. Chapman and Hall, London, 1967, pp. 838-844.

Atlas, L. M. and Schlehman, G. J., *Thermodynamic Properties of Plutonium Trifluoride and Plutonium Carbides From Solid Electrolyte Cell Measurements*, Bull. Am. Ceram. Soc. *46*(4), 419 (April 1967). Abstract

Bailey, W. J.,* Cohn, P. D.,* Aase, D. T.,* Foote, F. G., Heck, F. M.,** Kittel, J. H., Last, G. A.,* McHugh, W. E.,† Strasser, A. A.,†† and Wheelock, C. W.,§ *Potential of Advanced Fuels for a Fast Test Reactor*, Trans. Am. Nucl. Soc. *10*(1), 108-109 (June 1967). Abstract

Bardos, D. I., Aldred, A. T., and Beck, P. A.,§§ *Effect of Aluminum on the Saturation Moments of Fe-Ni Alloys*, J. Appl. Phys. *38*(3), 1260-1262 (March 1, 1967).

Baskin, Y., *Phase Studies in the Pseudobinary System UN-UP*, J. Am. Ceram. Soc. *50*(2), 74-76 (February 1967).

Baskin, Y., *Preparation and Properties of Uranium Metaphosphate, $U(PO_3)_4$*, J. Inorg. Nucl. Chem. *29*(2), 383-391 (February 1967).

Baskin, Yehuda, *Properties of Uranium Monoarsenide and Related Binary Systems*, Bull. Am. Ceram. Soc. *46*(4), 417 (April 1967). Abstract

Baskin, Y., *Solid-Solubility Relationships and Atomic Size in NaCl-Type Uranium Compounds*, Trans. Met. Soc. AIME *239*, 1708-1712 (1967).

Baskin, Y., *Synthesis of Uranium Monoarsenide (UAs)*, J. Inorg. Nucl. Chem. *29*(9), 2480-2482 (September 1967). Note

Beals, R. J. and Kern, R. S.,‡ *Irradiation Testing (Pulse Conditions) of the Clad-Insulator-Ternary Fuel System for the Power Burst Facility*, Bull. Am. Ceram. Soc. *46*(9), 901 (September 1967). Abstract

Beck, W. N., *A Design of a Flux Positioning Capsule for Use in the Vertical Thimbles of the CP-5 Reactor*, Intl. Symp. on Developments in Irradiation Capsule Technology, Pleasanton, California, May 3-5, 1966. USAEC Report CONF-660511, pp. 4.7.1-4.7.9 (1967).

Beck, W. N., Brown, F. L., Koprowski, B. J., and Kittel, J. H., *Performance of Advanced U-Pu-Zr Alloy Fuel Elements Under Fast-Reactor Conditions*, Trans. Am. Nucl. Soc. *10*(1), 106-107 (June 1967). Abstract

Beck, W. N., Murphy, W. F., Kittel, J. H., and Foote, F. G., "Irradiation Behavior of Plutonium Alloy Fuels for Fast Reactors," *Plutonium 1965*, Proc. Third Intl. Conf. on Plutonium, London, England, 1965, A. E. Kay and M. B. Waldron, eds. Chapman and Hall, London, 1967, pp. 933-948.

Benaroya, R., Blewitt, T. H., Brooks, J. M., and Laverick, C., *Effect of Fast Neutron Irradiation at Low Temperature on NbZr Coil Performance*, IEEE Trans. on Nucl. Sci. *14*(3), 383-385 (1967).

Benaroya, R., Blewitt, T. H., Brooks, J. M., and Laverick, C., *Effects of Neutron Radiation on Superconducting Solenoids*, Bull. Am. Phys. Soc. *12*, 949 (1967). Abstract

Berger, Harold, *Applications of Neutron Radiography*, Proc. 15th Conf. on Remote Systems Technology, Am. Nucl. Soc., Hinsdale, Illinois, 1967, pp. 95-96; Trans. Am. Nucl. Soc. *10*(2), 441-442 (November 1967). Abstract

Berger, H., *An Ultrasonic Imaging Lamb-Wave System for Reactor-Fuel-Plate Inspection*, Ultrasonics *5*(1), 39-41 (January 1967).

Berger, Harold, *Radiography with Reactor Neutron Beams*, Symp. on Research Reactor Applications, General Atomic, Div. of General Dynamics Corp., San Diego, California, June 16, 1967, Paper No. 4. Abstract

Berger, Harold, *Ultrasonic Image Systems for Nondestructive Testing*, J. Acoust. Soc. Am. *42*(5), 1185 (November 1967). Abstract

Berger, Harold, Dolon, Paul,‡‡ and Niklas, Wilfrid F.,‡‡ *An Improved Neutron Image Intensifier Tube*, IEEE Trans. on Nucl. Sci. *14*(1), 428-432 (February 1967).

Berger, Harold and Drexelius, V. W.,¶ *Neutron Radiographic Inspection of Ordnance Components*, Proc. Fifth Symp. on Electroexplosive Devices, The Franklin Institute, Philadelphia, Pennsylvania, June 13-14, 1967, pp. 1-2.1 to 1-2.13.

Berger, Harold and Kraska, I. R., *A Track-Etch Plastic-Film Technique for Neutron Imaging*, Trans. Am. Nucl. Soc. *10*(1), 72-73 (June 1967). Abstract

*Battelle Northwest Laboratory, Richland, Washington.

**Westinghouse Atomic Power Division, Pittsburgh, Pennsylvania.

†Atomic Power Development Associates, Detroit, Michigan.

††United Nuclear Corporation, Elmsford, New York.

§Atomics International, Canoga Park, California.

§§University of Illinois, Urbana, Illinois.

‡Phillips Petroleum Company, Idaho Falls, Idaho.

‡‡The Rauland Corporation, Chicago, Illinois.

¶McDonnell-Douglas Corporation, St. Louis, Missouri.

Blewitt, T. H. and Koppenaal, T. J., "Irradiation Hardening in Copper and Copper Alloys," *Radiation Effects*, IMD-AIME Symp. on Radiation Effects, Asheville, North Carolina, September 8-10, 1965, W. F. Sheely, ed. Gordon and Breach, Science Publishers, New York, 37, 561-625 (1967).

Blewitt, T. H. and Lucas, M. W., *Energy Release in Irradiated Copper*, Bull. Am. Phys. Soc. *12*(3), 302 (March 1967). Abstract

Blumenthal, B. and Sanecki, J. E., *The Lattice Parameter of High-Purity Thorium with Reference to Impurity Content and Heat Treatment*, J. Nucl. Mater. *22*, 100-102 (April 1967).

Brodsky, M. B., "Hall Effect and Electronic Structure of Various Actinide Metals," *Plutonium 1965*, Proc. Third Intl. Conf. on Plutonium, London, England, 1965, A. E. Kay and M. B. Waldron, eds. Chapman and Hall, London, 1967, pp. 286-298.

Brodsky, M. B., *Magnetoresistivity of Alpha Plutonium*, Bull. Am. Phys. Soc. *12*(1), 98 (January 1967). Abstract

Brodsky, M. B., "The Pressure/Temperature Behavior of Pure Plutonium," *Plutonium 1965*, Proc. Third Intl. Conf. on Plutonium, London, England, 1965, A. E. Kay and M. B. Waldron, eds. Chapman and Hall, London, 1967, pp. 137-139. Discussion

Brodsky, M. B., "Thermoelectric Power of Delta Plutonium, and Resistivity of Americium and Their Relevance to Magnetism in the Actinide Elements," *Plutonium 1965*, Proc. Third Intl. Conf. on Plutonium, London, England, 1965, A. E. Kay and M. B. Waldron, eds. Chapman and Hall, London, 1967, pp. 210-212. Discussion

Brodsky, Merwyn B., *Transverse Magnetoresistivity of α and β Plutonium*, Phys. Rev. *163*(2), 484-487 (November 10, 1967).

Brown, F. L., Neimark, L. A., Koprowski, B. J., Ayer, J. E., and Kittel, J. H., *Performance of Vibratorily Compacted Mixed-Oxide Fuel Rods Under Fast-Reactor Conditions*, Trans. Am. Nucl. Soc. *10*(1), 101-102 (June 1967). Summary

Brown, F. L., Neimark, L. A., Koprowski, B. J., Kittel, J. H., Ayer, J. E., and Kruger, O. L., *Performance of Mixed-Carbide Fuel Rods Under Fast-Reactor Conditions*, Trans. Am. Nucl. Soc. *10*(2), 473-474 (November 1967). Abstract

Chen, W. K. and Jackson, R. A., *Diffusion of Oxygen in Cobaltous Oxide*, Bull. Am. Ceram. Soc. *46*(4), 357 (April 1967). Abstract

Chen, W. K. and Jackson, R. A., *Diffusion of Oxygen in Near-Stoichiometric α-Nb_2O_5*, J. Chem. Phys. *47*(3), 1144-1148 (August 1967).

Cotterill, R.M.J., *The Role of Lattice Vacancies in Phase Transformations of Binary Alloys*, Phys. Letters *24A*(4), 216-217 (February 13, 1967).

Cotterill, R.M.J. and Doyama, M., *Atomistic Calculations of Complete and Dissociated Edge Dislocations in Solid Krypton*, Bull. Am. Phys. Soc. *12*(3), 370 (March 1967). Abstract

Cotterill, R.M.J. and Doyama, M., "Energies and Atomic Configurations of Line Defects and Plane Defects in F.C.C. Metals," *Lattice Defects and Their Interactions*, R. R. Hasiguti, ed. Gordon and Breach, Science Publishers, New York, 1967, pp. 1-78.

Cotterill, R.M.J. and Doyama, M., *Formation Energies of Vacancies and Interstitials in Solid Krypton*, Phys. Letters *25A*(1), 35-36 (July 1967).

Cotterill, R.M.J. and Doyama, M., "Morse Potential Calculations of Vacancy and Vacancy-Type Defect Properties in F.C.C. Metals," *Calculation of the Properties of Vacancies and Interstitials*, Proc. Conf., Shenandoah National Park, Virginia, May 1-5, 1966. NBS Misc. Publ. 287, pp. 47-51 (1967).

Cotterill, R.M.J. and Doyama, M., *Vacancies and Interstitials in Solid Krypton*, Bull. Am. Phys. Soc. *12*, 117 (January 1967). Abstract

Dalley, N. Kent, Mueller, M. H., and Simonsen, S. H.,* *A Neutron Diffraction Study of Uranyl Nitrate Dihydrate*, Am. Cryst. Assoc. Symp. on Thermal Neutron Scattering Applied to Chemical and Solid State Physics, Atlanta, Georgia, January 25-28, 1967, Paper J9, p. 71.

Dalley, N. Kent and Mueller, M. H., *A Neutron Diffraction Study of* $[UO_2(H_2O)\{CO(NH_2)_2\}_4](NO_3)_2$, Am. Cryst. Assoc. Symp. on Crystal Growth, Minneapolis, Minnesota, August 20-25, 1967, Paper T6, p. 97.

Darby, J. B., *The Thermodynamics of Alloys*, Ind. Eng. Chem. *59*(5), 13 (May 1967). Abstract

Dickerman, C. E., Robinson, L. E., Blumenthal, B., and Stewart, R., *Behavior of Th-20 wt% U Fast-Reactor Fuel under Transient Heating to Failure*, Nucl. Appl. *3*, 9-17 (January 1967).

di Novi, R. A., *Postirradiation Thermal Properties of a Uranium-Fissium Alloy as a Function of Burnup*, Trans. Am. Nucl. Soc. *10*(2), 476-477 (November 1967). Abstract

Doyama, M. and Cotterill, R.M.J., *Atomistic Calculations of Complete and Dissociated Screw Dislocations in Solid Krypton*, Bull. Am. Phys. Soc. *12*(3), 424 (March 1967). Abstract

Doyama, M. and Cotterill, R.M.J., "Atomistic Calculations of Interstitials in F.C.C. Metals," *Calculation of the Properties of Vacancies and Interstitials*, Proc. Conf. Shenandoah National Park, Virginia, May 1-5, 1966. NBS Misc. Publ. 287, pp. 43-45 (1967).

Doyama, M. and Cotterill, R.M.J., "Energies and Atomic Configurations of Point Defects in F.C.C. Metals," *Lattice Defects and Their Interactions*, R. R. Hasiguti, ed. Gordon and Breach, Science Publishers, New York, 1967, pp. 79-165.

Doyama, M. and Cotterill, R.M.J., *Vacancies and Interstitials in Solid Xenon*, Bull. Am. Phys. Soc. *12*(1), 117 (January 1967). Abstract

Draley, J. E., Mori, Shiro, and Loess, R. E., *The Corrosion of 1100 Aluminum in Water from 50° to 95°C*, J. Electrochem. Soc. *114*(4), 353-354 (April 1967). Note

Dunlap, B. D., Darby, J. B., Jr., and Kimball, C. W., *Hyperfine Field of* ^{197}Au *in Ferromagnetic* Au_4V, Phys. Letters *25A*(6), 431-432 (September 1967).

Dunlap, B. D., Dwight, A. E., Kalvius, G. M., and Kimball, C. W., *Temperature Dependence of the Hyperfine Field in Rare Earth-Gold Compounds*, Proc. 6th Rare Earth Research Conf., Gatlinburg, Tennessee, May 3-5, 1967. Oak Ridge National Laboratory, Oak Ridge, Tennessee, 1967, pp. 506-509.

Dwight, A. E., *Ternary Compounds having the* $CeCu_2$*-type Structure*, Proc. 6th Rare Earth Research Conf., Gatlinburg, Tennessee, May 3-5, 1967. Oak Ridge National Laboratory, Oak Ridge, Tennessee, 1967, pp. 156-165.

*The University of Texas at Austin.

Dwight, A. E., *ZrNiAl and Related Compounds*, Abst. Bull. IMD-AIME *2*(1), 42 (1967).

Dwight, Austin E., "Body-Centered Cubic Derivative Structures," *Intermetallic Compounds*, J. H. Westbrook, ed. John Wiley and Sons, Inc., New York, 1967, Chapter 10, pp. 166-179.

Dwight, A. E., Downey, J. W., and Conner, R. A., Jr., *Equiatomic Compounds of Y and the Lanthanide Elements with Ga*, Acta Cryst. *23*, 860-862 (November 10, 1967). Letter

Dwight, A. E., Downey, J. W., and Conner, R. A., *Some C11b-type Compounds of Sc, Y and the Lanthanides with Cu, Ag and Au*, Acta Cryst. *22*, 745-747 (May 1967). Letter

Eggenberger, D. N. and Shuck, A. B., *Remote Balance for Accurate Weighing in High Radiation Environment*, Nucl. Instr. Methods *57*, 89-92 (1967).

Falicov, L. M.* and Penn, David R., *Concentration Dependence of the Spin-Density-Wave Periodicity in Antiferromagnetic Chromium Alloys*, Phys. Rev. *158*(2), 476-482 (June 10, 1967).

Fisher, E. S. and Dever, D., *Elastic Moduli of Gd Metal*, Proc. 6th Rare Earth Research Conf., Gatlinburg, Tennessee, May 3-5, 1967. Oak Ridge National Laboratory, Oak Ridge, Tennessee, 1967, pp. 522-533.

Fisher, E. S. and Dever, D., *Temperature Dependence of Elastic Moduli of Ruthenium, Rhenium, Cobalt, Dysprosium, and Erbium; a Study of the Elastic Anisotropy-Phase Transformation Relationship*, Trans. Met. Soc. AIME *239*, 48-57 (January 1967).

Flinn, J. E. and Rechtien, J. J., *Stress and Strain Considerations for Composite Rod Drawing*, Nucl. Eng. Design *6*(3), 217-222 (October 1967).

Forlano, Roberto J., Allen, A. W.,** and Beals, R. J., *Elasticity and Anelasticity of Uranium Oxides at Room Temperature: I, Stoichiometric Oxide*, J. Am. Ceram. Soc. *50*(2), 93-96 (February 1967).

Greenberg, S., Ruther, W. E., and Levin, H. A., *Corrosion of Vanadium-Base Alloys in Sodium at 550° to 750°C*, Proc. IAEA Symp. on Alkali Metal Coolants - Corrosion Studies and System Operating Experience, Vienna, Austria, November 28-December 2, 1966. IAEA, Vienna, 1967, pp. 63-84.

Gruber, E. E., "Analysis of the Effect of an Energy Gradient on Bubble Coalescence in Solids," *Radiation Effects*, IMD-AIME Symp. on Radiation Effects, Asheville, North Carolina, September 8-10, 1965, W. F. Sheely, ed. Gordon and Breach, Science Publishers, New York, 37, 269-274 (1967).

Gruber, E. E., *Calculated Size Distributions for Gas Bubble Migration and Coalescence in Solids*, J. Appl. Phys. *38*(1), 243-250 (January 1967).

Handwerk, J. H., Kruger, O. L., and Moser, J. B., "Preparation and Properties of Some Groups V and VI Compounds of Plutonium," *Plutonium 1965*, Proc. Third Intl. Conf. on Plutonium, London, England, 1965, A. E. Kay and M. B. Waldron, eds. Chapman and Hall, London, 1967, pp. 739-750.

Hart, Raymond K., *Electron Microscopy: The High Voltage Approach*, Twenty-fifth Anniversary Mtg. Electron Microscopy Society of America, Chicago, Illinois, August 29-September 1, 1967, Claude J. Arceneaux, ed. Claitor's Book Store, Baton Rouge, Louisiana, 1967, p. 258.

*Cambridge University, Cambridge, England.
**University of Illinois, Urbana, Illinois.

Hart, R. K. and Pilney, D. G., *Effect of Spectral Line Shift on Microprobe Data*, Trans. Second Natl. Conf. on Electron Microprobe Analysis, Boston, Massachusetts, June 14-16, 1967, p. 31.

Heaton, L., Mueller, M. H., and Williams, J. M., *A Neutron Diffraction Determination of the Coherent Scattering Amplitude of Np and the Possible Antiferromagnetism of Neptunium Dioxide*, J. Phys. Chem. Solids *28*, 1651-1654 (September 1967).

Henninger, E. H.,† Buschert, R. C.,† and Heaton, Leroy, *Atomic Radial Distribution in Amorphous Selenium by X-Ray and Neutron Diffraction*, J. Chem. Phys. *46*(2), 586-591 (January 1967).

Henninger, E. H.,† Buschert, R. C.,† and Heaton, Leroy, *Atomic Structure and Correlation in Vitreous Silica by X-Ray and Neutron Diffraction*, J. Phys. Chem. Solids *28*(3), 423-432 (March 1967).

Henninger, E. H.,† Buschert, R. C.,† and Heaton, Leroy, *Structure and Correlation in Liquid Alloys by X-ray and Neutron Diffraction*, Advan. Phys. *16*, 177-188 (1967).

Henriksen, L.,†† Johansen, A.,†† Koch, J.,†† Anderson, H. H.,§ and Cotterill, R.M.J., *Rows of Dislocation Loops in Aluminum Irradiated by Aluminum Ions*, Appl. Phys. Letters *11*(4), 136-138 (August 15, 1967).

Holloway, J. A.,§§ Stuhrke, W. F.,§§ and Berger, H., *Low-Voltage and Neutron-Radiographic Techniques for Evaluating Boron-Filament Metal-Matrix Composites*, Proc. 15th Conf. on Remote Systems Technology. Am. Nucl. Soc., Hinsdale, Illinois, 1967, pp. 105-106; Trans. Am. Nucl. Soc. *10*(2), 445 (November 1967). Abstract

Horak, J. A. and Blewitt, T. H., *Irradiation-Induced Resistivity in Pure Metals*, Bull. Am. Phys. Soc. *12*(3), 303 (March 1967). Abstract

Jacoby, W. R.,‡ Palm, R. G.,‡ and Latimer, T. W., *Compatibility of Stabilized Hypostoichiometric Uranium-Plutonium-Monocarbide Fuels with Stainless Steel*, Trans. Am. Nucl. Soc. *10*(1), 108 and 110 June 1967). Abstract

Kalvius, M., Dunlap, B., Ruby, S., and Brodsky, M., *Temperature Dependence of the Hyperfine Field in $NpAl_2$ by the Mössbauer Effect in Np^{237}*, Bull. Am. Phys. Soc. 12(1), *25* (January 1967). Abstract

Kassner, T. F., *A Convective-Diffusion Study of the Dissolution Kinetics of Type 304 Stainless Steel in the Bismuth-Tin Eutectic Alloy*, Trans. Met. Soc. AIME *239*, 1643-1651 (October 1967).

Kassner, T. F., *Rate of Solution of Rotating Tantalum Disks in Liquid Tin*, J. Electrochem. Soc. *114*(7), 689-694 (July 1967).

Kelman, L. R., "Further Work on ANL on Fast Reactor Fuels," *Plutonium 1965*, Proc. Third Intl. Conf. on Plutonium, London, England, 1965, A. E. Kay and M. B. Waldron, eds. Chapman and Hall, London, 1967, pp. 525-526.

Kelman, L. R., Rhude, H. V., Schnizlein, J. G., and Savage, H., "Metallic Plutonium Alloys for Fast Critical Experiments," *Plutonium 1965*, Proc. Third Intl. Conf. on Plutonium, London, England, 1965, A. E. Kay and M. B. Waldron, eds. Chapman and Hall, London, 1967, pp. 510-524.

†Purdue University, Lafayette, Indiana.
††University of Copenhagen, Denmark.
§The Technical University, Lyngby, Denmark.
§§Wright-Patterson Air Force Base, Ohio.
‡Westinghouse Materials Systems Laboratory, Cheswick, Pennsylvania.

Kelman, L. R., Savage, H., Walter, C. M., Blumenthal, B., Dunworth, R. J., and Rhude, H. V., "Status of Metallic Plutonium Fast Power-Breeder Fuels," *Plutonium 1965*, Proc. Third Intl. Conf. on Plutonium, London, England, 1965, A. E. Kay and M. B. Waldron, eds. Chapman and Hall, London, 1967, pp. 458-484.

Kern, R. S.* and Beals, R. J., *Thermal Properties of Compositions in the System UO_2-ZrO_2-CaO*, Bull. Am. Ceram. Soc. *46*(12), 1154-1159 (December 1967).

Kettunen, Pentti O., *Comparison of Fatigue Properties of Single Crystals and Polycrystals*, Phil. Mag. *16*(140), 253-259 (August 1967).

Kettunen, P. O., *Influence of Carbide Precipitation on the Fatigue of Armco Iron*, Abst. Bull. IMD-AIME *2*(2), 3 (1967).

Kettunen, P. O. and Kocks, U. F., *On a Possible Relation between Work Hardening and Fatigue Failure*, Scripta Met. *1*, 13-17 (1967).

Kettunen, P. O. and Kocks, U. F., *Speculation Concerning Dislocation Movement During Fatigue*, Bull. Am. Phys. Soc. *12*(3), 413 (March 1967). Abstract

Kimball, C. W., Tison, J. K., and Nevitt, M. V., *Hyperfine Interactions at ^{57}Fe Nuclei in Intermetallic Compounds of the Fe-Mn System with the β-Manganese Structure*, J. Appl. Phys. *38*(3), 1153-1154 (March 1, 1967).

Kittel, J. H., "Book Review: Thorium Utilization," *Utilization of Thorium in Power Reactors*, IAEA, 1966, Nucl. Appl. *3*, 263 (April 1967).

Kittel, J. H., *Irradiation Effects on Reactor Structural Materials, Argonne National Laboratory*, Proc. AEC-Industry Mtg. on Irradiation Effects on Reactor Structural Materials, USAEC HQ, Germantown, Maryland, July 18, 1967, BNWL-609, pp. 22-26 (1967).

Knott, H. W., Mueller, M. H., and Heaton, L., *The Crystal Structure of $Mn_{15}Si_{26}$*, Acta Cryst. *23*, 549-555 (October 1967).

Kocks, U. F., *On the Importance of Twinning in Polycrystal Plasticity*, Abst. Bull. IMD-AIME *2*(1), 27 (1967).

Kocks, U. F., *On the Internal Stresses due to a Quasiuniform Distribution of Dislocations*, Acta Met. *15*, 1415-1417 (August 1967). Letter

Kocks, U. F., *On Stress Relaxation and Dislocation Structure Observations*, Bull. Am. Phys. Soc. *12*(3), 413 (March 1967). Abstract

Kocks, U. F., *Statistical Treatment of Penetrable Obstacles*, Can. J. Phys. *45*, 737-755 (February 1967).

Kocks, U. F. and Kettunen, P. O., *Contribution to a Statistical Theory of Fatigue Life*, Abst. Bull. IMD-AIME *2*(2), 4 (1967).

Kocks, U. F. and Westlake, D. G., *The Importance of Twinning for the Ductility of CPH Polycrystals*, Trans. Met. Soc. AIME *239*(7), 1107-1109 (July 1967). Letter

Koppenaal, T. J., *Effect of Mild Annealing on the Strength of Neutron Irradiated Copper Single Crystals*, Abst. Bull. IMD-AIME *2*(2), 6 (1967).

Koppenaal, T. J., *Stress Relaxation in Neutron Irradiated Copper Single Crystals*, Abst. Bull. IMD-AIME *2*(1), 77 (1967).

Koppenaal, T. J., *Stress Relaxation in Neutron Irradiated Copper Single Crystals*, Acta Met. *15*, 681-690 (May 1967).

Koppenaal, T. J., *Thermally Activated Slip in Neutron Irradiated Copper Single Crystals*, Bull. Am. Phys. Soc. *12*(3), 390-391 (March 1967). Abstract

Koprowski, B. J. and Brown, F. L., *Examination Techniques for High Burnup U-Pu Fuel Elements for Fast-Breeder Reactors*, Proc. 15th Conf. on Remote Systems Technology, Am. Nucl. Soc., Hinsdale, Illinois, 1967, pp. 63-67; Trans. Am. Nucl. Soc. *10*(2), 671-672 (November 1967). Abstract

Kruger, Owen L., *Fluid Resins for Mounting Metallographic Samples. Part I: Selection of Polyester Resins and Review of Chemical Reactions*, Praktische Metallographie *4*(3), 125-137 (1967).

Kruger, Owen L., *Fluid Resins for Mounting Metallographic Samples. Part II: Experimental Results and Discussion of Curing Process*, Praktische Metallographie *4*(3), 181-191 (1967).

Kruger, O. L. and Moser, J. B., *Electrical Properties and Electronic Configuration of the Monocarbide, Monophosphide, and Monosulfide of Plutonium*, J. Chem. Phys. *46*(3), 891-900 (February 1, 1967).

Kruger, O. L. and Moser, J. B., *Lattice Constants and Melting Points of Actinide-Group IVA-VIA Compounds with NaCl-type Structures*, J. Phys. Chem. Solids *28*, 2321-2325 (November 1967).

Kruger, O. L. and Moser, J. B., *Preparation, Electronic Structure, and Conduction Processes of Actinide IVA-VIA Compounds*, Chem. Eng. Prog. (Symp. Series) *63*(80), 1-10 (1967).

Kruger, O. L. and Moser, J. B., *Uranium Monosulfide-Plutonium Monosulfide System*, Bull. Am. Ceram. Soc. *46*(4), 417 (1967). Abstract

Lam, D. J., Darby, J. B., Jr., Downey, J. W., and Norton, L. J., *Equiatomic Ternary Compounds of Uranium and Aluminum with Group VIII Transition Elements*, J. Nucl. Mater. *22*(1), 22-27 (April 1967).

Lam, D. J., Nevitt, M. V., Ross, J. W., and Mitchell, A. W., "The Magnetic Susceptibility of the Monocarbides of Uranium and Plutonium," *Plutonium 1965*, Proc. Third Intl. Conf. on Plutonium, London, England, 1965, A. E. Kay and M. B. Waldron, eds. Chapman and Hall, London, 1967, pp. 274-285.

Lam, D. J., Spokas, J. J.,** and Van Ostenburg, D. O., *Nuclear Magnetic Resonance and Magnetic Susceptibilities of V-Nb Alloys*, Phys. Rev. *156*(3), 735-739 (April 15, 1967).

Lapinski, Norman P., *A Shortened Processing Time Technique for Color Industrial Radiography*, Mater. Eval. *25*(2), 33-35 (February 1967).

Latimer, T. W., *Compatibility of (U,Pu) Carbides with Iron- and Nickel-Base Alloys Below 900°C*, Bull. Am. Ceram. Soc. *46*(4), 417 (April 1967). Abstract

Legault, R. A. and Draley, J. E., *An Electrochemical Study of Aluminum Corrosion in Boiling High Purity Water*, Corrosion *23*, 365-370 (December 1967).

Levitan, J., Draley, J. E., and Van Drunen, C. J., *Low-Pressure Oxidation of Zirconium*, J. Electrochem. Soc. *114*(11), 1086-1089 (November 1967).

*Phillips Petroleum Company, Idaho Falls, Idaho.

**St. Procopius College, Lisle, Illinois.

Liptai, R. G., *Another Comment on the Pre-α→β Transformation in Plutonium*, J. Nucl. Mater. *22*, 117-118 (April 1967). Letter

Liptai, R. G., *On the Substructure of Alpha Plutonium*, Abst. Bull. IMD-AIME 2(1), 116 (1967).

Liptai, R. G. and Friddle, R. J., *The Effects of High Pressure on the Phase Equilibria of Some Plutonium Alloys*, J. Nucl. Mater. *21*(1), 114-116 (January 1967). Letter

Liptai, R. G. and Friddle, R. J., *On the Formation of Substructure in Alpha Plutonium at High Pressures*, J. Nucl. Mater. *24*, 316-322 (December 1967).

Liptai, R. G., Lloyd, L. T., and Friddle, R. J., "On the Use of High Pressure as a Parameter in Crystal Growth," *Crystal Growth* (Supp. to J. Phys. Chem. Solids), Proc. Intl. Conf. on Crystal Growth, Boston, Massachusetts, June 20-24, 1966, H. S. Peiser, ed. Pergamon Press, Oxford, England 1967, pp. 573-577.

Loomis, B. A., *Length Changes of Uranium Crystals During Thermal Neutron Irradiation*, Bull. Am. Phys. Soc. *12*(3), 391 (March 1967). Abstract

Loomis, B. A., "Swelling of Uranium on Postirradiation Annealing," *Radiation Effects*, IMD-AIME Symp. on Radiation Effects, Asheville, North Carolina, September 8-10, 1965, W. F. Sheely, ed. Gordon and Breach, Science Publishers, New York, 37, 403-409 (1967).

Matzkanin, G. A. and Sowers, C. H., *Nuclear Spin-Lattice Relaxation in β Manganese*, Bull. Am. Phys. Soc. *12*(3), 291 (March 1967). Abstract

Matzkanin, G. A., Van Ostenburg, D. O., Spokas, J. J.,* and Sowers, C. H., *Study of the Solute NMR in Dilute Gold Alloys*, Bull. Am. Phys. Soc. *12*(6), 911 (August 1967). Abstract

Mayfield, R. M. and Karasek, F. J., *Fabrication of V-Ti-Cr Alloy Fuel Cladding for LMFBR Applications*, Trans. Am. Nucl. Soc. *10*(2), 475 (November 1967). Abstract

Merkle, K. L., *Energy Dependence of Fission-Fragment Damage in Gold Films*, J. Appl. Phys. *38*(1), 301-309 (January 1967).

Merkle, K. L., "Energetic Displacement Cascades in Gold," *Radiation Effects*, IMD-AIME Symp. on Radiation Effects, Asheville, North Carolina, September 8-10, 1965, W. F. Sheely, ed. Gordon and Breach, Science Publishers, New York, 37, 173-182 (1967).

Merkle, K. L. and Singer, L. R., *Charged-Particle Irradiation Damage in Thin Metal Films*, Bull. Am. Phys. Soc. *12*(3), 390 (March 1967). Abstract

Merkle, K. L. and Singer, L. R., *Radiation Damage in Thin Metal Films at 4.2°K*, Appl. Phys. Letters *11*(2), 35-37 (July 1967).

Messier, D. R., *Evaporation of PuO_2 From 1900° to 2100°K*, Bull. Am. Ceram. Soc. *46*(4), 421 (April 1967). Abstract

Messier, D. R., *Vapor Pressure of Gd_2O_3 from 2350° to 2590°K*, J. Am. Ceram. Soc. *50*(12), 665-668 (December 1967).

Mori, Shiro and Draley, J. E., *Oxide Dissolution and Its Effect on the Corrosion of 1100 Aluminum in Water at 70°C*, J. Electrochem. Soc. *114*(4), 352-353 (April 1967). Note

Moser, J. B. and Kruger, O. L., *Thermal Conductivity and Heat Capacity of the Monocarbide, Monophosphide, and Monosulfide of Uranium*, J. Appl. Phys. *38*(8), 3215-3222 (July 1967).

Moser, J. B. and Kruger, O. L., *Thermal Conductivity and Heat Capacity of Plutonium Compounds*, Bull. Am. Ceram. Soc. *46*(4), 419 (April 1967). Abstract

Mueller, M. H. and Dalley, N. Kent, *The Structure of Several Uranyl Nitrate Compounds As Determined by Neutron Diffraction*, 2nd Materials Research Symp. on Molecular Dynamics and Structure of Solids, Gaithersburg, Maryland, October 16-19, 1967, NBS, Paper C4, p. 2.

Mueller, M. H., Heaton, L., Aschenbrenner, R. A., and Amiot, L., *Argonne Computer Aided Diffraction Equipment*, Am. Cryst. Assoc. Symp. on Crystal Growth, Minneapolis, Minnesota, August 20-25, 1967, Paper E8, p. 35.

Nevitt, M. V., "Atomic-Size Criteria in Certain Intermediate Phases of Silver and Gold," *Phase Stability of Metals and Alloys*, Proc. Battelle Colloquium, Geneva, Switzerland, March 7-12, 1966, P. S. Rudman, John Stringer, and R. I. Jaffee, eds. McGraw-Hill Book Co., New York, 1967, pp. 281-290.

Nevitt, M. V., "Miscellaneous Structures of Fixed Stoichiometry," *Intermetallic Compounds*, J. H. Westbrook, ed. John Wiley and Sons, Inc., New York, 1967, Chapter 13, pp. 217-229.

O'Boyle, D. R., "Discussion on Alloy Systems - 2," *Plutonium 1965*, Proc. Third Intl. Conf. on Plutonium, London, England, 1965, A. E. Kay and M. B. Waldron, eds. Chapman and Hall, London, 1967, pp. 532-534.

O'Boyle, D. R., Brown, F. L., and Sanecki, J. E., *Microanalysis of Solid Fission Products in Mixed-Oxide Fuel Irradiated in EBR-II*, Trans. Am. Nucl. Soc. *10*(2), 462-463 (November 1967).

Penn, David R. and Cohen, Morrel H., *Antiferromagnetism in Simple Metals*, Phys. Rev. *155*(2), 468-477 (March 10, 1967).

Peterson, Norman L. and Rothman, Steven J., *Impurity Diffusion in Aluminum*, Bull. Am. Phys. Soc. *12*(3), 324 (March 1967). Abstract

Peterson, N. L. and Rothman, S. J., *Isotope Effect for the Diffusion of Zinc in Copper, and Ordered and Disordered CuZn*, Phys. Rev. *154*(3), 558-560 (February 15, 1967).

Peterson, N. L. and Rothman, S. J., *Isotope Effect in Self-Diffusion in Zinc*, Phys. Rev. *163*(3), 645-649 (November 15, 1967).

Peterson, Ronald G. and Rosen, Moshe, *Use of Thick Transducers to Generate Short-Duration Stress Pulses in Thin Specimens*, J. Acoust. Soc. Am. *41*(2), 336-345 (February 1967).

Philofsky, E. M.** and Flinn, J. E., "A New Method for Measuring Strain Distribution," *Stereology*, Proc. Second Intl. Congr. for Stereology, Chicago, Illinois, April 8-13, 1967, Hans Elias, ed. Springer-Verlag, New York, 1967, pp. 110-111.

Podhradsky, W. R. and Smith, S. V., *EDM Sparks Research at Argonne Lab*, Steel - The Metalworking Weekly *160*, 70-71 (June 26, 1967).

Readey, D. W. and Handwerk, J. H., *Nuclear Fuel Materials*, Proc. Am. Ceram. Soc. Symp., Washington, D. C., April 7-12, 1966. NBS Misc. Publ. 285, Washington, D. C., 1967, pp. 45-60.

Readey, D. W. and Jech, R. E., *Etch-Pit Observations on Nickel Oxide*, J. Appl. Phys. *38*(9), 3795-3796 (August 1967).

Readey, D. W. and Jech, R. E., *Grain Boundary Energies and Grooving Kinetics of NiO Bicrystals*, Bull. Am. Ceram. Soc. *46*(4), 358 (April 1967). Abstract

*St. Procopius College, Lisle, Illinois.

**Northwestern University, Evanston, Illinois.

Reinke, Charles F., *Computer Program for Determining Specimen and Irradiation Capsule Component Temperature Distribution*, Intl. Symp. on Developments in Irradiation Capsule Technology, Pleasanton, California, May 3-5, 1966. USAEC Report CONF-660511, pp. 2.1.1-2.1.10 (1967).

Rosen, M., Lloyd, L. T., and Peterson, R. G., "The β-α Phase Transformation in High Purity Plutonium," *Plutonium 1965*, Proc. Third Intl. Conf. on Plutonium, London, England, 1965, A. E. Kay and M. B. Waldron, eds. Chapman and Hall, London, 1967, pp. 18-38.

Ross, J. W. and Lam, D. J., *Electronic Configuration of Actinide Ions in Their Monocarbides*, Abst. Bull. IMD-AIME *2*(1), 119 (1967).

Ross, J. W. and Lam, D. J., *Magnetic Susceptibility of α-Uranium*, Bull. Am. Phys. Soc. *12*(3), 354 (March 1967). Abstract

Ross, J. W. and Lam, D. J., *The Magnetic Susceptibility of Neptunium Oxide and Carbide between 4.2° and 350°K*, J. Appl. Phys. *38*(3), 1451-1453 (March 1, 1967).

Rossin, A. D., Blewitt, T. H., and Troiano, A. R.,* *Hydrogen Embrittlement in Irradiated Steels*, Nucl. Eng. Design *4*, 446-458 (1966).

Rossin, A. David, *Hydrogen Embrittlement: A Reactor Safety Problem?*, Power Reactor Technology and Reactor Fuel Processing *10*(2), 102-110 (1967).

Rossin, A. David, "Reporting Neutron Exposure for Radiation Damage," *Interaction of Radiation with Solids*, Proc. Cairo Solid State Conf., Cairo, Egypt, September 3-8, 1966, A. Bishay, ed. Plenum Press, New York, 1967, pp. 553-562.

Rossin, A. D., Kirn, F. S., Armani, R. J., and Smith, D. M., *Fast-Neutron Spectra and Radiation Damage Rates in EBR-II*, Trans. Am. Nucl. Soc. *10*(1), 129 (June 1967). Abstract

Rothman, S. J. and Peterson, N. L., *Correlation Coefficient and the Isotope Effect for the Diffusion of Zinc in Silver*, Phys. Rev. *154*(3), 552-558 (February 15, 1967).

Rothman, Steven J. and Peterson, N. L., *Isotope Effect for Self-Diffusion in Zinc*, Bull. Am. Phys. Soc. *12*(3), 325 (March 1967). Abstract

Selner, R. H. and Berger, Harold, *Comparison Between Ultrasonic Inspection Systems--Mechanical Scan Versus Television Imaging*, Mater. Eval. *25*, 91-95 (April 1967).

Shuck, A. B., *The Fabrication of Plutonium from Highly Irradiated Reactor Fuel*, Proc. IAEA Symp. on the Use of Plutonium as a Reactor Fuel, Brussels, Belgium, March 13-17, 1967. IAEA, Vienna, Austria, 1967, pp. 221-235.

Sidhu, S. S. and Anderson, K. D., *Thermal-Neutron Coherent Scattering Amplitudes and Cross Sections of Nickel-61 and Nickel-64*, Phys. Rev. *156*(4), 1225-1228 (April 20, 1967).

Simmons, J. M.,** Astley, E. R.,† Evans, E. A.,†† Kittel, J. H., Moss, D. A.,** and Strasser, A.,§ "Technology of Sodium Cooled Fast Reactor Fuels in the U. S.," *Fast Breeder Reactors*, Proc. London Conf. on Fast Breeder Reactors, London, England, May 17-19, 1966, P. V. Evans, ed. Pergamon Press, Oxford, England, 1967, pp. 615-630.

Taylor, John C.,§§ Mueller, M. H., and Hitterman, R. L., *A Neutron Diffraction Study of Ferroelectric KFCT $[K_4Fe(CN)_6{\cdot}3D_2O]$ above the Curie Temperature*, Am. Cryst. Assoc. Symp. on Thermal Neutron Scattering Applied to Chemical and Solid State Physics, Atlanta, Georgia, January 25-28, 1967, Paper J6, p. 70.

Van Ostenburg, D. O. and Alfred, L.C.R., *A Note on Phase Shifts for an Inverse Power of R Force Field*, Indian J. Pure Appl. Phys. *5*(11), 556 (1967).

Van Ostenburg, D. O. and Alfred, L.C.R., *Determination of Phase Shifts from the Friedel Sum Rule, Resistivity, and Knight Shift Equations*, Bull. Am. Phys. Soc. *12*(3), 349 (March 1967). Abstract

Van Ostenburg, D. O. and Alfred, L.C.R., *New Scheme for the Construction of Phase Shifts with Application to NMR*, Bull. Am. Phys. Soc. *12*(1), 59 (January 1967). Abstract

Volpe, Milton L. and Reddy, John F., *The Catalytic Decomposition of Nitrous Oxide on Single Crystals of Cobalt Oxide and Cobalt Magnesium Oxide*, J. Catalysis *7*(1), 76-84 (January 1967).

Wang, James Y. N., *Compatibility of Two Ni-Ti Alloys with Mercury*, Corrosion *23*(5), 149-150 (May 1967). Note

Walter, C. M. and Kelman, L. R., *The Interaction of Iron with Molten Uranium*, J. Nucl. Mater. *20*(3), 314-322 (1966).

Westlake, D. G., *Anomalies in the Physical Properties of Vanadium. The Role of Hydrogen*, Phil. Mag. *16*(143), 905-908 (November 1967).

Westlake, D. G., *Discussion of "Deformation Mechanisms in Titanium at Low Temperatures,"* Trans. Met. Soc. AIME *239*(7), 1101-1102 (July 1967).

Westlake, D. G., *Hydride Habit Planes and Deformation Planes of h.c.p. Metals*, Acta Met. *15*(8), 1407-1408 (August 1967). Note

Westlake, D. G., *Models and Prediction of $\{10\bar{1}1\}$ Twinning*, Scripta Met. *1*(1), 9-12 (1967).

Westlake, D. G., *Problems in the Preparation of Vanadium-Hydrogen Alloys for Transmission Electron Microscopy*, Trans. Met. Soc. AIME *239*(7), 1106-1107 (July 1967). Note

Westlake, D. G., *A Resistometric Study of Phase Equilibria at Low Temperatures in the Vanadium-Hydrogen System*, Abst. Bull. IMD-AIME 2(2), 104 (1967); Trans. Met. Soc. AIME *239*, 1341-1344 (September 1967).

Williams, Jack M., *The Aquated Hydrogen Ion: Single Crystal Diffraction Investigations of Compounds Containing the $[H_2O{\cdot}H{\cdot}H_2O]^+$ Ion*, 2nd Materials Research Symp. on Molecular Dynamics and Structure of Solids, Gaithersburg, Maryland, October 16-19, 1967, NBS, Paper C2, p. 1.

Williams, Jack M., *The Diaquohydrogen Ion $(H_5O_2)^+$: A Neutron Diffraction Structure Investigation of trans-$[Co(en)_2Cl_2]^+Cl^-(H_5O_2)^+Cl^-$*, Inorg. Nucl. Chem. Letters *3*(8), 297-302 (1967).

Williams, Jack M., *The $[H_2O{\cdot}H{\cdot}H_2O]^+$ Ion: A Neutron Diffraction Study of trans-$[Co(en)_2Cl_2]^+Cl^-[H_5O_2]^+Cl^-$*, Am. Cryst. Assoc. Symp. on Crystal Growth, Minneapolis, Minnesota, August 20-25, 1967, Paper K2, p. 51.

*Case Institute of Technology, Cleveland, Ohio.
**AEC, Washington, D. C.
†Battelle Northwest Laboratory, Richland, Washington.
††GE Vallecitos Atomic Laboratory, Vallecitos, California.
§United Nuclear Corporation, Elmsford, New York.

§§A.A.E.C. Research Establishment, Sutherland, N.S.W., Australia.

Williams, Jack M., Hitterman, R. L., and Mueller, M. H., *A Neutron Diffraction Investigation of Selenious Acid*, Am Cryst. Assoc. Symp. on Thermal Neutron Scattering Applied to Chemical and Solid State Physics, Atlanta, Georgia, January 25-28, 1967, Paper J8, p. 71.

Yaggee, F. L. and Gilbert, E. R., *Effect of Sodium Exposure on the Mechanical Properties of Potential Fuel Jacket Alloys at 550-700°C*, Proc. IAEA Symp. on Alkali Metal Coolants - Corrosion Studies and System Operating Experience, Vienna, Austria, November 28-December 2, 1966. IAEA, Vienna, 1967, pp. 215-229.

Yoon, Y. K., Watanabe, H., and Kittel, J. H., "Electron Microscopic Studies of Structural Changes in High Burn-up UC-PuC," *Plutonium as a Reactor Fuel*, Proc. IAEA Symp. on the Use of Plutonium as a Reactor Fuel, Brussels, Belgium, March 13-17, 1967. IAEA, Vienna, Austria, 1967, pp. 455-466.

Youngdahl, C. A. and Loess, R. E., *Instrumentation for Potentiostatic Corrosion Studies in Distilled Water*, J. Electrochem. Soc. *114*(5), 489-492 (May 1967). Note

Zebroski, E. L.,* Kittel, Howard, and Moss, DeWitt,** *Reviews of Status of Technology of Fast Reactor Fuels*, Am. Nucl. Soc. Topical Mtg. on Fast Reactors, San Francisco, California, April 10-12, 1967, ANS-*101*, pp. 2-63 - 2-80 (1967).

Zegler, S. T. and Hehemann, R. F., *Superconductivity in Body-Centered Cubic Nb-Zr-V and Nb-Zr-Rh Alloys*, Abst. Bull. IMD-AIME 2(1), 16 (1967).

REPORTS

ANL-7151 Burt, W. R., Jr., Brillhart, D. C., and Mayfield, R. M., *Development of Techniques for Fabrication of Small-Diameter, Thin-Wall Tungsten and Tungsten-Alloy Tubing* (July 1966).

ANL-7185 Horak, James A., *Neutron Irradiation of Pure Metals and Aluminum-Zinc Alloys* (October 1966).

ANL-7206 Kramer, W. C., Burt, W. R., Jr., Karasek, F. J., Flinn, J. E., and Mayfield, R. M., *Vanadium Alloy Screening Studies and Fabrication of V-15w/oTi-7.5w/oCr Tubing for Nuclear Fuel Cladding* (August 1966).

ANL-7229 Messier, Donald R., *Construction of a Glovebox Thermogravimetric Analysis Apparatus; Langmuir and Knudsen Experiments on the Evaporation of Gd_2O_3 from 2140° to 2600°K* (November 1966).

ANL-7252 Levitan, J., Draley, J. E., and Van Drunen, C. J., *Studies in Zirconium Oxidation* (December 1966).

ANL-7227 Draley, J. E. and Ruther, W. E., *Corrosion of Aluminum Alloys by Flowing High-Temperature Water* (January 1967).

ANL-7266 Rossin, A. D., *Hydrogen Embrittlement in Irradiated Steels* (February 1967).

ANL-7272 Peterson, Ronald G., *Elastic Moduli and Ultrasound Velocities of Tungsten as a Function of Temperature* (December 1967).

ANL-7299 *Annual Progress Report for 1966, Metallurgy Division.*

ANL-7313 Shuck, A. B., Jelinek, H. F., Hins, A. G., Carson, N. J., Jr., Denst, A. A., and Steele, T. A., *The Development of a Design and Fabrication Method for Plutonium-Bearing Zero-Power Reactor Fuel Elements* (August 1967).

ANL-7335 Kassner, T. F. and Smith, D. L., *Calculations on the Kinetics of Oxygen Solution in Tantalum and Niobium in a Liquid-Sodium Environment* (September 1967).

ANL-7398 Downey, J. W., *Levitation Melting of Metals and Alloys* (December 1967).

PATENT

Kastner, Jacob and Berger, Harold, *Radiographic Nondestructive Testing Method*, Patent No. 3,359,419 (December 19, 1967).

*General Electric Co., Advanced Products Operation, Sunnyvale, California.

**AEC-DRDT, Brookhaven National Laboratory, Upton, L. I., New York.